The basement geology of the Porcupine High – a key transatlantic link between the Caledonides and Appalachians

Master of Science

Geology

2023

Shannon Raftery Dennehy

Trinity College Dublin
Coláiste na Tríonóide, Baile Átha Cliath
The University of Dublin

Declaration

I declare that this thesis has not been submitted as an exercise for a degree at this or any other university and it is entirely my own work.

I agree to deposit this thesis in the University's open access institutional repository or allow the Library to do so on my behalf, subject to Irish Copyright Legislation and Trinity College Library conditions of use and acknowledgement.

I consent to the examiner retaining a copy of the thesis beyond the examining period, should they so wish (EU GDPR May 2018).

Shannon Dennehy

Summary

The Precambrian geology of the western Irish offshore remains poorly constrained. The Porcupine High, located 200 km west of Ireland, is a key underexplored link between the circum-Iapetus basement geology of north-western Europe and eastern North America. This thesis presents geochronological data and potassium-feldspar Pb isotope (Pb-in-Kfsp) data of dredge and core samples from three marine sampling campaigns conducted in 2006, 2011, and 2014.

Most dredge samples are likely near in-situ; outcrop ridges were targeted by side-scan sonar while the predominance of metamorphic clasts recovered is inconsistent with ice-rafted debris (IRD) derived from the Irish massif.

All samples were collected north of the inferred trace of the Iapetus suture. The southernmost samples come from a core of foliated gneiss boulders which yield U-Pb zircon ages of c. 500-478 Ma. A 385 Ma apatite U-Pb age records its post-Caledonian exhumation; Pb-in-Kfsp isotope data imply a Caledonian affinity. These rocks were recovered adjacent to a E-W trending magnetic boundary, which I correlate with the Fair Head – Clew Bay line. These rocks are assigned to the ophiolitic rocks of the Clew Bay Complex.

Dredge samples, yielding >90% lower greenschist-facies psammite cobbles, were recovered to the north in a region characterized by a magnetic anomaly low. U-Pb detrital zircon data imply a Moine or Grampian Group Dalradian affinity, with the youngest population at c. 950 Ma. U-Pb detrital apatite ages of c. 900 - 1800 Ma are unaffected by Caledonian orogenesis which is atypical of Tonian successions in the Caledonides.

A granitic orthogneiss, recovered north of the aforementioned dredge samples, yields a 1314 Ma U-Pb zircon crystallization age. Granulite-facies metamorphism is interpreted to be of Grenville age and is supported by a 875 Ma apatite U-Pb cooling age. Zircon Hf isotopic and Pb-Kfsp data suggest an affinity with the Rockall Bank Palaeoproterozoic, delimiting the offshore extent of the Annagh Gneiss Complex (AGC) of NW Ireland.

U-Pb detrital zircon ages from two low-grade metasediments imply a Moine/Grampian Group and an Upper Dalradian affinity respectively; Caledonian apatite U-Pb ages are prevalent. The high-grade rocks (orthogneisses and amphibolites) can be divided into three groups: clasts with 2750 Ma U-Pb zircon crystallization ages, 1750 Ma apatite U-Pb ages and a Lewisian Pb-in-Kfsp signature; clasts with 1830-1940 Ma U-Pb zircon ages, 1750 Ma apatite U-Pb ages and an Annagh Gneiss Complex Pb-in-Kfsp affinity, and AGC clasts with 1550-1650 Ma U-Pb zircon ages and U-Pb apatite ages recording post-Grenville cooling. All three groups were found at one dredge site and a component of Quaternary glacial transport is invoked for these dredged clasts.

Acknowledgements

Above all, I want to thank Prof. David Chew, for his unending support and guidance. As my supervisor, he has always been there to point me in the right direction. Thanks for everything, Dave.

I could not have completed this thesis without the help of the technical staff in the Museum Building and the Centre for Microscopy and Analysis (CMA), including Frank, Cora, Colin, Foteini, and Maura.

I also wish to thank Dr. Shane Tyrrell, of NUIG, for his help and contribution.

The Geology Department and Wellesley College Graduate Fellowships made my research possible with their generous funding and financial support.

My parents, John Dennehy and Trish Hunter-Dennehy, and my sisters, Erin and Jackie, who supported my move to Dublin and everything that I have done before and since, deserve all of my gratitude and more.

I am also thankful for my partner, Samuel Carthy, who has heard me talk about this thesis since the day we met and is still interested when I bring it up.

And a very special thank you to Nuala Birthistle, who shared her home with me throughout the Covid-19 pandemic, and the writing of this thesis.

With gratitude,

Shannon Dennehy

Table of Contents

Chapter 1: Introduction

This study seeks to better constrain the geological evolution of the Porcupine High (Fig. 1.1), 200 km west of Ireland. Situated in the North Atlantic, it is surrounded to the southeast by the Porcupine Basin, south by the Goban Spur, to the northwest by the Rockall High, and to the north by the Rockall Basin (Fig. 1.1). There is currently a void in the literature pertaining to this region. While conference abstracts and unpublished reports exist, the data is not readily available to the public. Understanding the geology of near offshore highs is especially pertinent during the transition to renewable energy, which includes the installation of offshore wind turbines.

Chapter 2 will present an overview of the methodology employed in this study, providing in-depth explanations of the theory of the techniques and their practical application. Chapter 3 describes the U-Pb system, which is the basis of the U-Pb zircon and apatite geochronological analysis presented in Chapter 4. Chapter 4 is formatted as a standalone paper (complete with its own reference list) and is intended to be submitted to *Precambrian Research*. It begins with a geological history of the North Atlantic, and then transitions to methodology, which includes LA-ICPMS U-Pb analysis of zircon and apatite and Pb-in-kfsp isotope analysis and their results, followed by a discussion section. Samples from multiple expeditions are included in this study and these expeditions are discussed in detail in section 3 of Chapter 4, along with the start of Chapter 2. While some data has been presented before in reports and conference abstracts, this is the first time it has all been compiled for publication and these data are augmented by LA-ICP-MS U-Pb dating in this study.

The location of the Porcupine High (Fig. 1.1) means that it is a key area to constrain the offshore geology of Ireland and its continuation across the Atlantic to Eastern Canada. The geological evolution of the broader North Atlantic, and the Laurentian margin specifically, is complex and is comprised of a diverse suite of terranes each with unique geological histories. Archean basement rocks of the Lewisian Complex in NW Scotland, Greenland and likely underlying the northern Rockall Basin, and the Paleoproterozoic rocks of the Annagh Gneiss Complex in NW Ireland and the Rhinns Complex off the northern Irish coast and in SW Scotland, comprise the oldest rock found in the North Atlantic region, yielding a U-Pb zircon date of 1779 ± 3 Ma (Daly et al., 1991). Remnants of the c. 1300 – 1000 Ma Mesoproterozoic Grenville Orogeny in the Appalachians of Newfoundland (Cawood and Nemchin, 2001) and the Annagh Gneiss Complex of Ireland point to a shared history between the two regions. The Iapetus Suture, a vestige of the ancient Iapetus Ocean, can be traced from northern Britain through Ireland to the Shannon Estuary. Different phases of the Caledonian Orogeny on the Laurentian margin have been documented in the geology of the Irish mainland. The extent of the effects and evolution of the Caledonian orogen is expanded upon through the analysis of samples recovered from the research sites on the Porcupine High.

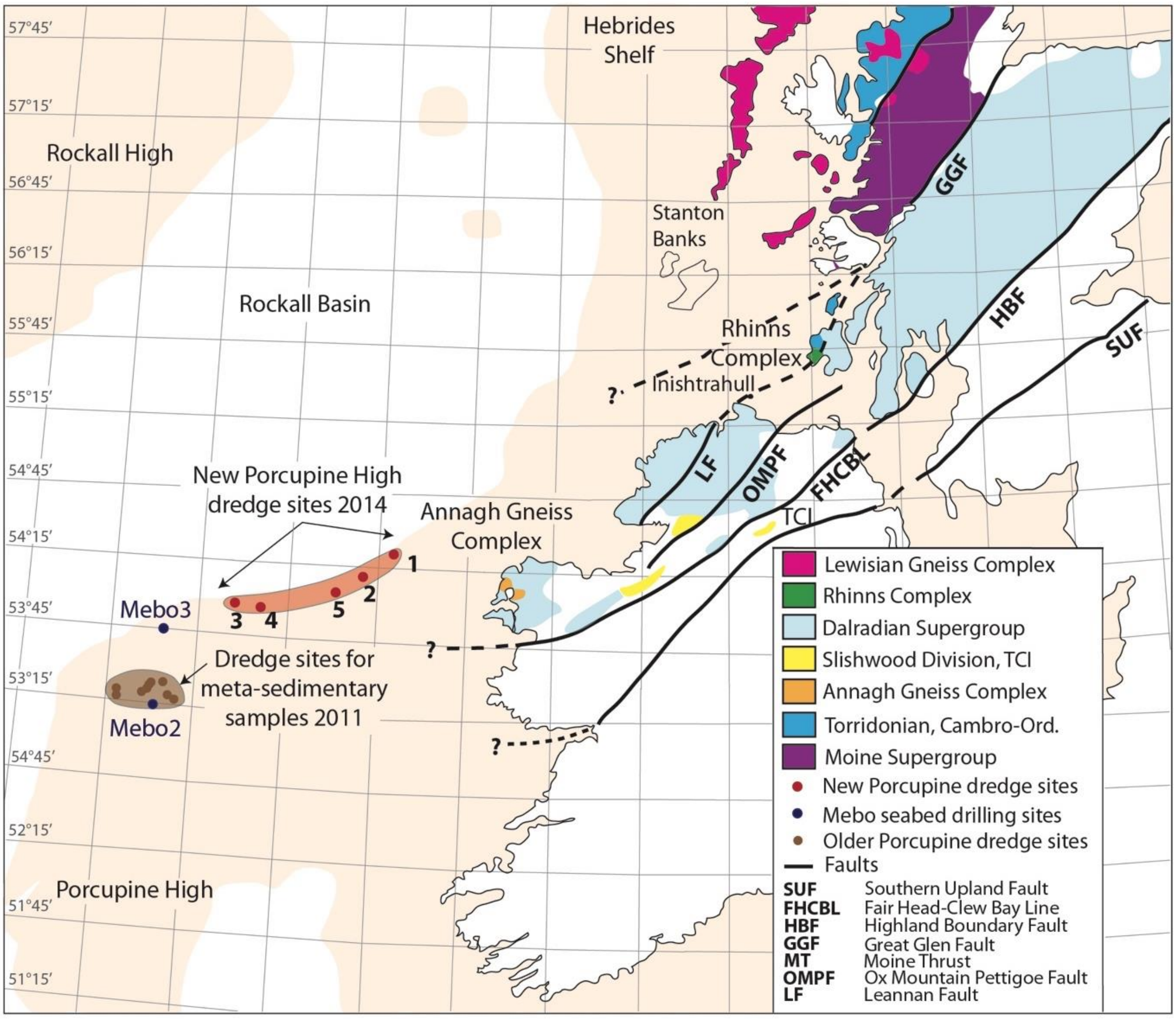

Figure 1.1. Map of the Precambrian geology of the North Atlantic adjacent to the sampling. In 2006, the R/V Celtic Explorer collected the MeBo cores. In 2011, dredge samples were collectd by the Celtic Explorer and a further suite of dredge samples was collected in 2014 by the Celtic Voyager.

Chapter 2: Methodology

The data presented in this thesis incorporates previously unpublished data in addition to my own results which are summarised in Table 2.1. For the 2011 sample suite and for the MeBo3 core (that had been presented in reports and conferences), I compiled the raw data and reprocessed them using Iolite and Isoplot, as described in section 2.5. Thus, all of the U-Pb data figures in Chapter 4 have been processed personally.

Samples	**Sample processing**		**Sample post-processing**	
	Methodology	**Researcher**	**Methodology**	**Researcher**
MeBo2 core	Sample preparation	*S. Dennehy*	Vizual Age (Iolite)	*S. Dennehy*
	U-Pb LA-ICPMS analyses	*S. Dennehy*	Isoplot	*S. Dennehy*
	CL/SEM imaging	*S. Dennehy*		
MeBo 3 core	Sample preparation	*TCD, UoG*	Isoplot	*S. Dennehy*
	U-Pb LA-ICPMS analyses	*TCD*	Pb-in-kfsp analysis	*S. Tyrrell, S. Dennehy*
	U-Pb LA-ICPMS analyses	*TCD*	Vizual Age (Iolite)	*S. Dennehy*
2011 Dredge samples	Sample preparation	*TCD, UoG*		
	U-Pb LA-ICPMS analyses	*TCD, UoG*	Isoplot	*S. Dennehy*
	Pb-in-kfsp LA-ICPMS analyses	*TCD, UoG*	Pb-in-kfsp analysis	*S. Tyrrell, S. Dennehy*
2014 Dredge samples	Sample preparation	*S. Dennehy*	Vizual Age (Iolite)	*S. Dennehy*
	U-Pb LA-ICPMS analyses	*S. Dennehy*	Isoplot	*S. Dennehy*
	Pb-in-kfsp LA-ICPMS analyses	*UoG*	Pb-in-kfsp analysis	*S. Tyrrell, S. Dennehy*
	CL/SEM imaging	*S. Dennehy*		

Table 2.1. List of sample suites, sample processing methods, and sample post-processing methods. TCD refers to Trinity College Dublin, and UoG refers to University of Galway.

2.1 Sample collection and processing

2.1.1 Sample cruises

Seabed drilling in 2006 (Fig. 1.1) yielded two cores, termed MeBo2 and MeBo3 (Table 2.2). This drilling campaign was funded by the Petroleum Infrastructure Programme and the Marine Institute and was carried out by the Center for Marine Environmental Sciences of the University of Bremen and the Petroleum Affairs Division, Ireland.

In 2011, metasedimentary dredge samples were obtained by the Celtic Explorer in a dredging campaign funded by the National Development Plan, Geological Survey Ireland and the Marine Institute. In 2014, the Celtic Voyager recovered samples from four sites are the samples from furthest north in this study (Fig 1.1). more details on the sampling expeditions are provided in Chapter 4, section 3.1.

2006 Cores	
Sample	**Lithology**
7.02	Foliated gneiss
7.13	Amphibolite
7.58	Foliated gneiss
8.08	Foliated gneiss
MeBo3	Orthogneiss
2011 Dredge Samples	
Sample	**Lithology**
PH1	Psammite
PH4	Psammite
PH5	Psammite
PH 9	Psammite
PH10	Psammite
PH 11	Psammite
PH12	Psammite
PH 14	Psammite
PH 15	Psammite
2014 Dredge Samples	
Sample	**Lithology**
204-1	Mica schist replete with K-fsp
302-1	Psammite
303-1	Amphibolite
402-1	Banded gneiss
402-2	Lineated granite
402-3	Foliated, banded gneisss
402-4	Banded pink gneiss
402-8	Banded grey gneiss
402-9	Banded pink-grey gneiss
402-11	Crystalline metamorphic rock, likely gneiss
402-13	Lineated amphibolite

Table 2.2. List of the samples recovered by the 2006, 2011, and 2014 cruises.

2.1.2 Initial preparation

Rock samples were cut into small pieces (typically golf-ball sized, 30 – 50 cm^3) suitable for the jaw crusher. Once crushed, samples were drum sieved using a 300 μm mesh to separate fine material from coarser components. The coarse fraction was set aside for potential future analysis. To prevent cross-contamination, the jaw crusher was thoroughly cleaned after every sample. Similarly, the sieve was also cleaned after every sample using a steel brush, a pin (to remove grains stuck in the steel mesh) and pressurized air.

Water was added to the < 300 μm fraction in a gold pan, and the water (which is dirty due to the suspension of clay-sized components) was decanted. This procedure was repeated until the water was clear. The samples were then placed in the oven for at least 24 hours at 160°C to dry out completely. Once fully dried, the samples were ready for further processing.

2.1.3 Magnetic Separation

A Frantz magnetic separator was used to magnetically separate non-magnetic minerals like zircon from their (para)magnetic counterparts. Prior to processing with the Frantz separator, a strong Nd-alloy hand magnet placed in a plastic bag was used to remove magnetic minerals. Magnetic and paramagnetic minerals were collected and stored for potential analysis in the future. Non-magnetic minerals were collected for further separation using heavy liquids.

2.1.4 Heavy Liquid Separation

Separation by heaving liquids is the last step in the mineral separation process prior to picking grains for analysis. Methylene iodide with a specific gravity of 3.32 was employed. Glass sample collection funnels lined with paper filters (similar to coffee filters) were fitted in a wire ring set above a collection beaker. Above the sample collection funnel, a separation funnel was affixed, with the stopcock closed.

Once set-up is complete, the heavy liquid was poured into the separation funnel followed by pouring in of the sample. The sample – heavy liquid mixture was then agitated / stirred. After fifteen minutes have elapsed the stopcock was then turned, allowing the dense grains to pass through and be collected in the paper filter. This process (stirring, a 15-minute pause, collection of dense minerals) was repeated until no more material sank. The filter paper with the heavy minerals (‘heavies’) was removed and put aside and replaced with another filter in its stead. This filter collected the remaining sample (the 'lights'). The filter papers (heavies and lights) were properly labelled and put aside. The heavy liquid separation apparatus the heavy and lights minerals, and their respective filter papers were thoroughly cleaned with acetone, and the acetone-methylene iodide waste collected for recycling. The heavyand light minerals were left to dry under the hood overnight.

2.2 Sample Imaging

Prior to LA-ICPMS analysis, samples were imaged using cathodoluminescence (CL) and scattered electron (SE) imaging; CL imaging allows for a detailed examination of the internal structures of the crystal (Appendix C).

CL emission is caused when the excitation levels of CL are met by the generation of secondary electrons from a primary electron beam. The primary electron beam, which is characteristic of energies exceeding 20 keV, transfers much of its energy, which forms the secondary electrons (Nasdala et al., 2003). After occupying this higher energy state, these electrons drop once more to a lower energy state, emitting photons in a radiative process. The energy difference between the two bands, known as the band gap, varies for every mineral.

CL emission in REE is most often the result of transitions of 4f electrons, and, in zircon, the emission spectra is characterized by elements Dy^{3+}, Sm^{3+}, Eu^{2+}, and Tb^{3+} (Hanchar and Rudnick, 1995; Yang et al., 1992). Based on the inverse correlation between CL signal brightness and the concentrations of uranium and hafnium, Poller et al. (2001) suggests that these two elements, rather than the [REE] or other trace elements, have greater potential to influence CL signals.

The CL signal can be suppressed or diminished by a variety of factors, including crystallinity of the sample material. When the crystallinity of a sample decreases, so too does the CL emission signal (Nasdala et al., 2003). This relationship is observed in Nasdala et al. (2002), which found that the total CL signal of annealed sample fragments is characterized by higher intensities than their non-treated, metamict counterparts.

2.3 LA-ICPMS Analysis

2.3.1 Theory

2.3.1.1 Background

The use of laser ablation inductively coupled plasma mass spectrometry (LA-ICPMS) in geochronology has allowed for the dating of mineral grains exceeding 4 billion years old. LA-ICPMS analysis, though precise, does not possess the same spatial resolution as SIMS (secondary ion mass spectrometry) analysis. However, due to its less expensive cost and shorter analysis times, it is gaining traction in use and in popularity (Sylvester and Jackson, 2016).

A stream of aerosol is produced when a laser ablates the surface of a sample, and the stream is then transported by He gas into the ICP. The particles are converted into ions, which are discriminated using either a magnet or quadrupole filter and then counted using detector(s).

2.3.1.2 Principles of LA ICP-MS analysis

The first step of the ICP-MS is sample introduction, which, in this case, is undertaken by laser ablation. A pulsed UV laser ablates the sample, creating an aerosol which is then transported to the plasma. The ablated material is atomized and ionized in the plasma and accelerated into the high vacuum part of the ICP mass spectrometer. Either single collector, multiple collector (both of which are sector field instruments), or quadruple collectors are used for U-Pb dating studies. Sector field instruments have higher sensitivity due to the higher extraction voltages employed. However, changing the magnetic field to analyse different elements is slow due to the settling times involved, and so single collector instruments are not well suited for rapid and large peak jumps across the periodic table, while multi-collector instruments are best suited for analysing isotopes which fall with the mass range of the fanning detector array (typically a relative spread of 20% in atomic mass units). The simultaneous isotopic detection afforded by multi-collector (MC) ICPMS yields the best precision in isotopic ratio analysis of single elements (e.g., Pb, Hf, Sr). A quadrupole detector is a sequential analyser capable of analysing over 40 elements in one ablation and is an efficient and cost-effective technique (Sylvester and Jackson, 2016).

2.3.2 Evolution of LA-ICP-MS

The coupling of mass spectrometry with laser ablation did not occur until 1985 and was demonstrated when Gray (1985) employed LA-ICP-MS for *in situ* analysis of solid rock samples and although though there were issues with saturation of the detection system, reasonable results were yielded (Gray, 1985). However, it was not until ten years later in 1995 that laser ablation was first applied to a studies of zircon U-Pb geochronology (Hirata and Nesbitt, 1995). Over the next two decades, it has been applied to U-Pb dating studies of other minerals including titanite, apatite, and calcite (Woodhead et al., 2016).

While it is used for a myriad of applications, this chapter focuses on applications in the realm of U-Pb geochronology. One major development has been the transition from either long wavelength or infrared lasers to ultraviolet light lasers. Gray (1985) employed the use of a long wavelength laser, which caused fragmentation of the ablation site (Gray, 1985; Sylvester and Jackson, 2016). A UV laser, with a wavelength of 213 nm (or increasing 193 nm) is most commonly used, though it, like its longer wavelength predecessor, is not without its shortcomings. The UV laser is less sensitive, since a lesser volume of material is transported (Nesbitt et al., 1997).

Prior to Eggins et al. (1998), only Ar was used in the sample gas chamber. The use of both Ar and He gas ensures that ablation aerosols are carried to the ICP and that ablation yield is sufficient. The presence of He in the sample cell causes a reduction in condensation build-up and increases the signal intensities of the analyzed material (Fig. 2.1; Eggins et al., 1998). By the end of the 2010s, two-volume chambers were developed (e.g., Eggins et al., 2005; Woodhead et al., 2007; Sylvester and Jackson, 2016). These allow for a greater number of samples to be placed in the laser cell while maintaining aerosol transport efficiency and minimizing washout by employing a 'cup' (the effective ablation volume of the system) along with improved control of the sample

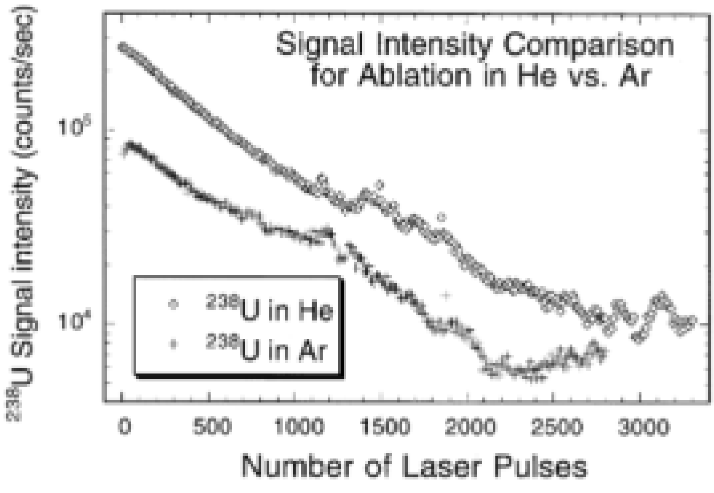

stage.

Figure 2.1. Signal intensity remains consistently elevated in the presence of He instead over Ar. Figure modified from Eggins et al. (1998).

2.4 Correction factors employed in LA-ICP-MS analysis

In LA-ICP-MS analysis, the isotopic ratios yielded by an analysis typically deviates from the true isotopic value of the sample due a variety of factors including mass bias and fractionation. This is typically resolved by a sample-bracketing approach, wherein several unknowns are interspersed between analysis of reference materials whose isotopic and / or elemental abundances are well known.

2.4.1 Fractionation

Fractionation is the total of static and time-dependent fractionation, changes as the session progresses resulting from volatile elements being released as condensation builds up (Chang et al., 2006), or during an ablation (downhole fractionation). Static fractionation, on the other hand, can be explained by several factors, including non-stoichiometric processes, differing ionization efficiencies, or space-charge effects (e.g., Chang et al., 2006; Tanner et al., 2004).

Reducing the effects of downhole fractionation is one of the biggest challenges in U-Pb zircon geochronology. Reference materials, such as the reference 91500 zircon, establish a time-based downhole Pb/U correction factor that is applied to zircon crystals of unknown zircons and standards alike (Ver Hoeve et al., 2017).

Chemical abrasion of zircon, which includes annealing followed by chemical abrasion of the unknown and sample materials, reduces the effects of downhole fractionation and increase the degree of concordance (Crowley et al., 2014). This method was first developed for use in TIMS analysis (Mattinson, 2005), but is increasingly applied to SIMS and LA-ICP-MS analysis due to its effective reduction of Pb loss (e.g., Kryza et al., 2012; Watts et al., 2016; Crowley et al., 2014). The chemical abrasion process anneals lattice radiation damage in zircon grains between 800 – 1000 °C. Samples are then exposed to a treatment of partial dissolution at increasing temperatures (Mattinson, 2005). This process, of annealing unknown samples and reference materials to the same state, offers a significant minimization of the impact of downhole fraction (Allen and Campbell, 2012).

2.4.2 Mass bias

Mass bias refers to the deviation of measured isotopic ratios from their true value; in other words, it is fractionation caused by a mass spectrometer. Different laws can be used to describe mass fractionation, but not all adequately illustrate the effects in an ICP-MS. However, in the interest of diligence, the power and exponential laws will be discussed here. For a more in-depth review of the various laws regarding mass fractionation, see Maréchal et al. (1999) and Albaréde et al. (2004).

The power law of mass fractionation, though not as adequate a descriptor as the exponential law, is useful when examining and constructing the exponential law. It assumes that logarithmic fractionation $\beta=\ln(r/R)$, where R is the true isotopic ratio of two isotopes of mass M_1 and M_2 and r is the ratio measured through mass spectrometry, is expressed as a function of mass difference $\Delta M=M_2-M_1$ (Maréchal et al., 1999). As discussed in Maréchal et al. (1999), the power law illustrates that, when adding a second isotopic ratio, mass fractionation produces a linear array. The exponential law of mass fractionation is more applicable to analysis conducted by ICP-MS, and has proven to provide more consistent results (e.g., Maréchal et al., 1999; Chu et al., 2002). It assumes that logarithmic fractionation, instead of acting as a function of mass difference, acts as a function of mass log-difference $\Delta(\ln M)=\ln(M_2/M_1)$ (Maréchal et al., 1999).

Components of the instruments, such as the ion transport system and the nebulizer, all add to the total mass bias, and their potential contributing factors are discussed in the following paragraphs. The space-charge effect, which describes an electrostatic shield resulting from a polarity imbalance, during ion transport likely causes preferential movement of heavier ions (e.g., Tanner, 1992; Malinovsky et al., 2003; Tanner et al., 2004); in an ICP-MS, space charge is most likely felt in the ion optics (Tanner et al., 1994). The magnitude of this effect increases as the critical radius increases, causing heavier ions to be favoured during sampling (Vanhaecke et al., 1993). The preference of heavier ions from the space-charge effect, this tendency is thought to be a significant cause of mass bias (Andrén et al., 2004) in an ICP-MS (Heumann et al., 1998; Andrén et al., 2004).

It is likely that the effects of mass bias derive from the ICP and during ion transport through the mass spectrometer (Andrén et al., 2004). However, dependence on time is also a large contributing factor to mass bias; for one sample, the difference in isotope ratio can be greater than 0.15% (Malinovsky et al., 2003). Another cause of mass bias occurs during extraction from the plasma (Andrén et al., 2004) and immediately thereafter in the interface region.

In some isotopic systems, correcting for mass bias can be achieved using invariant isotopes. This technique, though not applicable to the Pb system, is used in other isotopic studies. In the Sr isotope system, the $^{88}Sr/^{86}Sr$ ratio is used to correct for mass bias of the $^{87}Sr/^{86}Sr$ ratio and the $^{146}Nd/^{144}Nd$ ratio is used to correct for the $^{143}Nd/^{144}Nd$ ratio (Yang, 2009).

2.5 Post-processing stage

2.5.1 VizualAge software

The raw U-Pb isotope data in this study were reduced using the 'VizualAge' data reduction scheme of Petrus and Kamber (2012) within the freeware IOLITE package of Paton et al. (Paton et al., 2011). User-defined time intervals are established for the baseline correction procedure to calculate session-wide baseline-corrected values for each isotope. The time-resolved fractionation response of individual standard analyses is then characterized using a user-specified down-hole correction model (such as an exponential curve, a linear fit or a smoothed cubic spline). The data reduction scheme then fits this appropriate session-wide 'model' U–Th–Pb fractionation curve to the time-resolved standard data and the unknowns. Sample-standard bracketing is applied after the correction of down-hole fractionation to account for long-term drift in isotopic or elemental ratios by normalizing all ratios to those of the U–Pb reference standards.

2.5.2 Isoplot

Concordia plots using the processed data from Iolite were constructed using the Isoplot 4.15 Excel macro. Uncertainties, either Monte Carlo or first-order, were also calculated for concordia plots and isochrons. Wetherwill and Tera-Wasseburg concordia diagrams are used to display the results of U-Pb zircon and apatite analysis respectively. For the U-Pb zircon analyses, weighted mean $^{206}Pb/^{238}U$ ages are employed due to analytical ellipses that are slightly dispersed along concordia, meaning concordia as can sometimes not be calculated.

For a detailed explanation of the many functions of Isoplot, see the Isoplot User's Manual (Ludwig, 2012).

Chapter 3: The U-Pb System

3.1 Background

3.1.1 Introduction to the U-Pb system

The U-Pb system refers to the radioactive decay of uranium to stable isotopes of lead. It relies on the α decay of ^{238}U, with a half-life of 4.468 billion years, and ^{235}U, with a half-life of 703.8 million years. Equation 3.1 illustrates this relationship, where *dN/dt* refers to the decay rate, and λ refers to the decay constant. When a mineral that preferentially incorporates uranium and rejects common leads crystallizes and becomes a closed system, all lead found in a crystal is the result of subsequent radioactive decay.

$$\frac{dN}{dt} = -\lambda N \tag{3.1}$$

Uranium, which possesses two primary oxidation states, occupies different forms depending on its environment. In reducing conditions, U is found in a tetravalent U(IV) state while in oxidizing conditions, it is most often found as the hexavalent form in UO_2^{2+}(e.g., Frondel, 1957; Hiess et al., 2012). This contrast becomes significant when examining the effect of lattice diffusion of actinides in minerals like zircon, which contain tetravalent uranium (Cherniak and Watson, 2003). Processes like diffusion are dependent on the valency of the present elements; thus, a tetravalent uranium will behave differently than its hexavalent cousin and calculating the activation energies for diffusion of tetravalent uranium provides insight into the different ways diffusion may occur (Cherniak et al., 1997; Meis and Gale, 1998; Cherniak and Watson, 2003). In this case, a likely explanation would be an intrinsic vacancy mechanism (Cherniak and Watson, 2003).

Valency is also significant in terms of understanding the presence of lead in a crystal. Pb^{2+} while too large to occupy the place of tetravalent uranium (or tetravalent hafnium, another common substitute for Zr^{4+}) is still found in zircon grains (Andersen et al., 2019). Therefore, a likely explanation for the presence of Pb^{2+} would be incorporation during alteration processes (Pidgeon et al., 2017).

3.1.2 Concordia diagrams

In order to plot data yielded by U-Pb analysis, a concordia diagram is used, of which there are different types. A Wetherill concordia diagram (Wetherill, 1956) plots $^{206}Pb/^{238}U$ against $^{207}Pb/^{235}U$, with each point on the resultant curve representing the locus of points where both ratios yield the same date (Fig. 3.1a). An analysis is discordant when the ratios yield different dates. When a sample yields multiple discordant dates, they may lie on a discordia chord (Fig. 3.1b). Causes of discordance, such as Pb loss, are discussed in more detail in section 3.2. Another type of concordia diagram is the Tera-Wasserburg concordia, in which $^{207}Pb/^{206}Pb$ ratios are plotted against $^{238}U/^{206}Pb$ ratios (Fig. 3.2).

a.

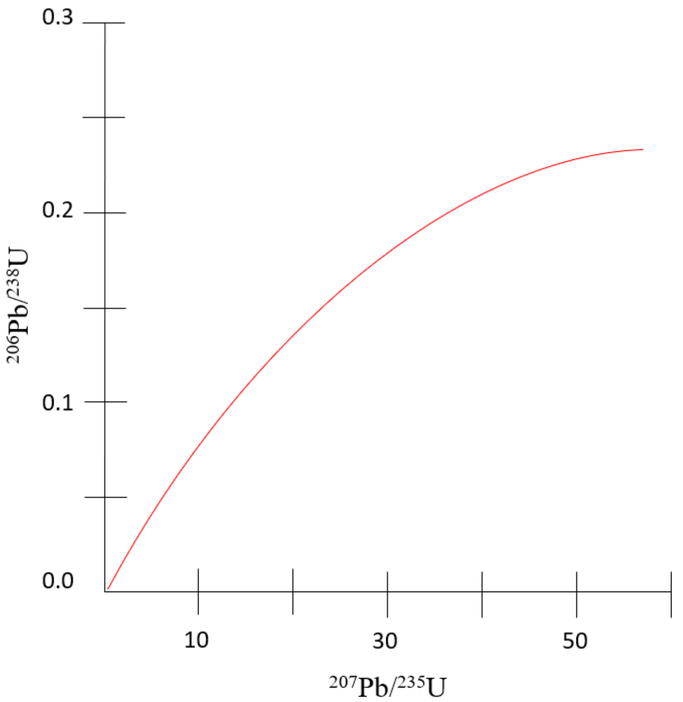

Figure 3.1a. Conventional Wetherill Concordia.

b.

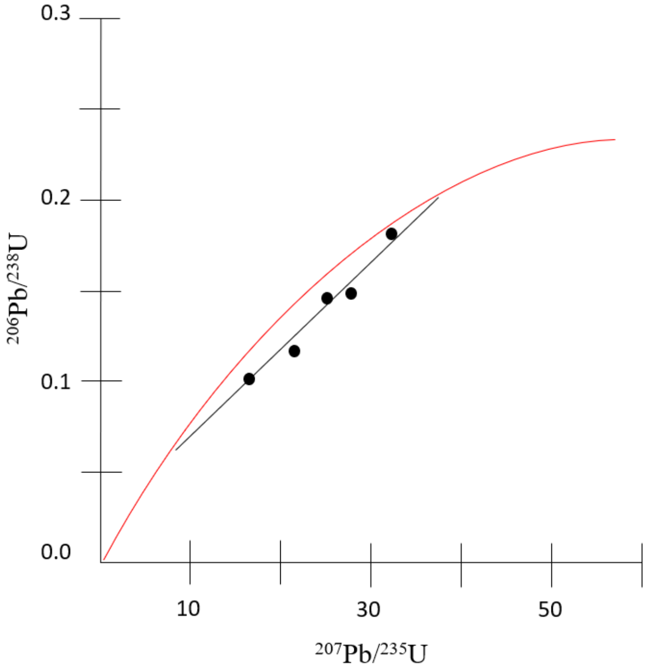

Figure 3.1b. Wetherill Concordia with Discordia intercept

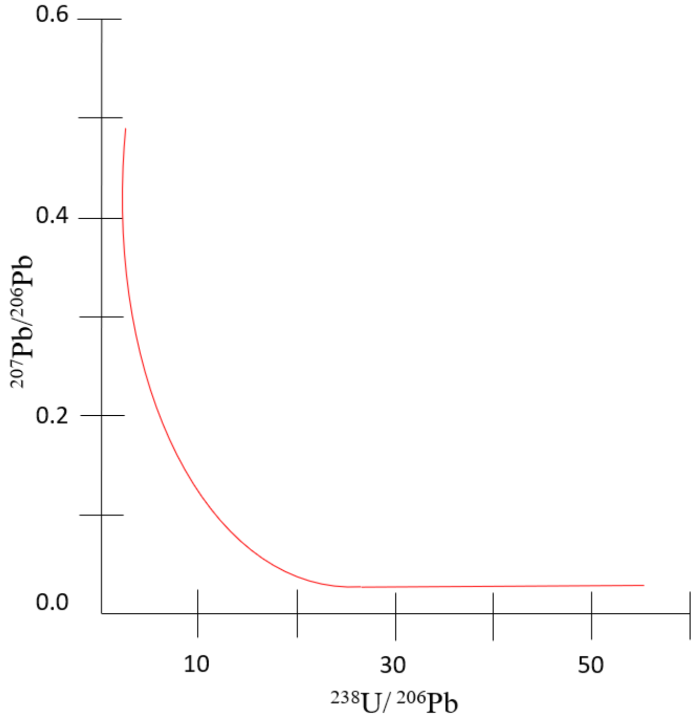

Figure 3.2. Example of a Tera-Wasserburg plot.

The concordia line of the Tera-Wasserburg plot (Tera and Wasserburg, 1972) is based on Equation 3.2 which incorporates both time *t*, the decay constant λ, and the concentrations of ^{235}U, ^{238}U, ^{206}Pb, and ^{207}Pb. In practise, particularly for *in situ* microbeam studies, ^{235}U is calculated directly from the abundance of ^{238}U and the natural $^{235}U/^{238}U$ isotopic abundance (e.g., Stirling et al., 2007; Amelin et al., 2010; Hiess et al., 2012). While a value of 137.88 (Steiger and Jäger, 1977) has commonly been employed in the literature, recent studies suggest a value of 137.818 more closely represents the average isotopic composition of $^{238}U/^{235}U$ in zircon (e.g., Hiess et al., 2012).

$$\frac{207Pb}{206Pb} = \frac{\left(e^{\lambda_{235}t} - 1\right)}{137.818\left(\frac{238U}{206\mathrm{Pb}}\right)} \qquad (3.2)$$

This equation describes the relationship of the $^{207}Pb/^{206}Pb$ ratio with time.

3.2 Causes of discordance and complexity in U-Pb geochronology

Pb loss, incorporation of common Pb, metamictization and new growth/dissolution are sources of complexity in U-Pb geochronology, often resulting in discordant analyses.

3.2.1. Lead loss

One of the most common sources of discordance is Pb loss (Lee et al., 1997). After a mineral (e.g. zircon) crystallizes, lead loss can occur as a result of metamorphism, both contact and regional, and through metamictization (e.g., Orejana et al., 2015; Andersen et al., 2019; see section 3.2.3 for more on metamictization). Lead can also be lost through interaction of a mineral with an aqueous fluid (Rubatto, 2017), though the most common culprits are either recrystallization or diffusion in metamict grains (Cherniak and Watson, 2001).

While the U-Pb system in zircon has a closure temperature exceeding 900 °C, Pb is lost through diffusion at a faster rate than uranium, by several orders of magnitude (Lee et al., 1997). As a result, in radiation-damaged grains, the ratio of lead to uranium can be unrepresentative of the original value. Elemental diffusion is aided by mineral surfaces, which often possess dislocations, cracks, and other disfigurations that will increase the surface area for transport exchange (Cherniak and Watson, 2003). However, Pb loss may also be enhanced by processes that occur at a faster rate than diffusion (Cochrane et al., 2014).

When a mineral grain experiences lead loss, the age discordance pattern can be represented by the following: $t_{208} < t_{206} < t_{207} < t_{7/6} < t_c$, where t_c is the age of crystallization (Andersen, 2002). Numerous studies (e.g. Knudsen et al., 1997) show that detrital zircon grains that have experienced substantial lead loss may plot within the analytical uncertainty of concordia, thus appearing concordant but with younger ages.

On a concordia plot, when a grain plots within 10% of the discordance limit of the curve, the lead loss is said to be concealed; and the age yielded by U-Pb dating may not reflect the true age of crystallization (Fig. 3.3; Andersen et al., 2019). These zircon grains may have experienced an ancient Pb loss event, which could occur before or after deposition in sedimentary samples (Andersen et al., 2019). However, since the lead loss is within acceptable limits, the points remain included in the final data set.

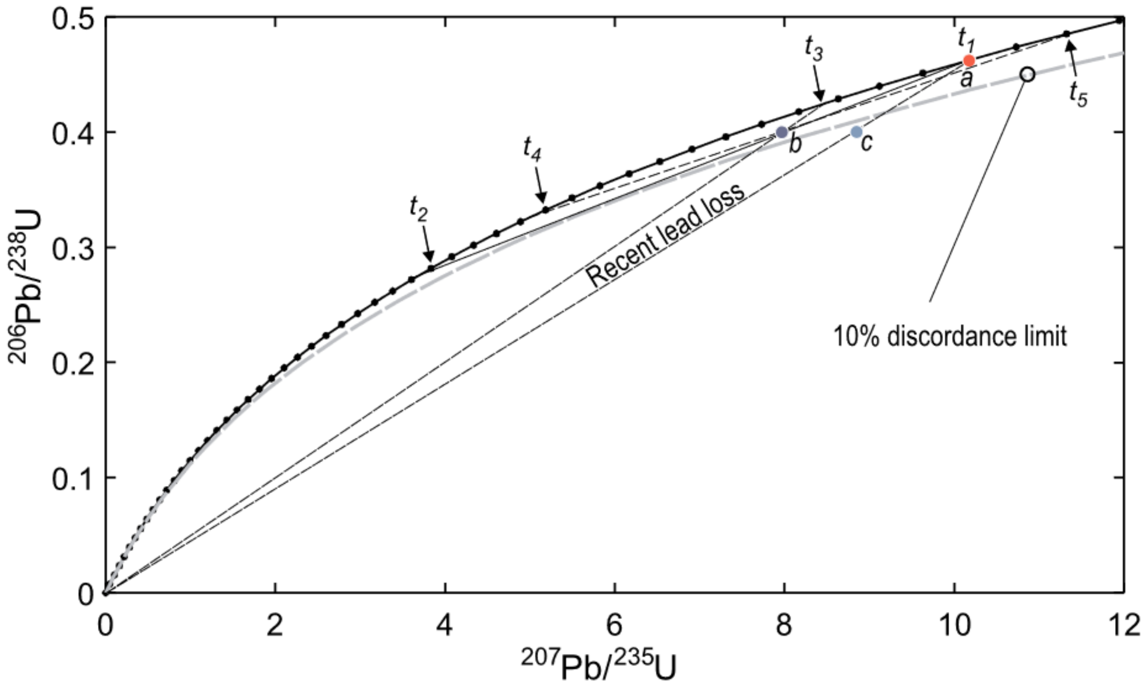

Figure 3.3. A concordia curve from Andersen et al. (2019), which features a limit indicating 10% discordance. In this case, points that fall beyond the 10% limit are excluded, with the assumption that the value of the analytical error falls below that of the discordance limit.

3.2.2 Common lead

The presence of common lead in grains of zircon, titanite, apatite etc. must be corrected in order to determine a concordant age, since common lead can artificially raise a calculated age. Common lead can be incorporated into a mineral grain through different factors: within the mineral lattice, as an inclusion or in laboratory settings (i.e. on the surface of the sample).

Numerical methods (Andersen, 2002) can take into consideration both the presence of common lead and lead loss when analysing the concentration of lead of radiogenic origin in a mineral (i.e., zircon or apatite) against total lead content and the isotopic composition of common lead, among other variables. These models assume that discordance is the result of the presence of common lead or lead loss.

Two methods frequently used to correct for common Pb are the ^{204}Pb- and ^{207}Pb-based methods. The ^{204}Pb correction method requires the measurement of the ^{206}Pb/^{204}Pb ratio. The corresponding amounts of ^{206}Pb, ^{207}Pb, and ^{208}Pb (based on a measurement of a co-genetic U-poor phase such as K-feldspar or a terrestrial Pb evolution model such as Stacey and Kramers, 1975) are then subtracted from the raw data, leading to the ^{204}Pb/^{206}Pb ratio of the Pb-corrected sample to be zero (Andersen et al., 2019).

The ^{207}Pb correction method relies on the assumption that the observed composition of lead is a mixture of radiogenic lead and common lead (Ludwig, 2012; Andersen et al., 2019). It involves projecting on Tera-Wasserburg concordia from the common Pb constraint (the initial ^{207}Pb/^{206}Pb ratio determined from a co-genetic U-poor phase such as K-feldspar or a terrestrial Pb evolution model) through the analysis, resulting in a lower intercept (the ^{207}Pb-corrected age) onto concordia. Common Pb isotopic compositions of minerals such as K-feldspar are often used in provenance studies; K-feldspar tends to exclude U and Th, so its Pb isotopic composition is a reliable measurement of the Pb isotopic composition at the time of crystallization (Hemming et al., 1998; Tyrrell et al., 2006). The Pb-in-Kfsp signatures of detrital K-feldspar can be matched with distinct basement terranes, allowing for the determination of source material (Fig. 3.4; e.g., Hemming et al., 1998; Tyrrell; Johnson et al., 2018) .

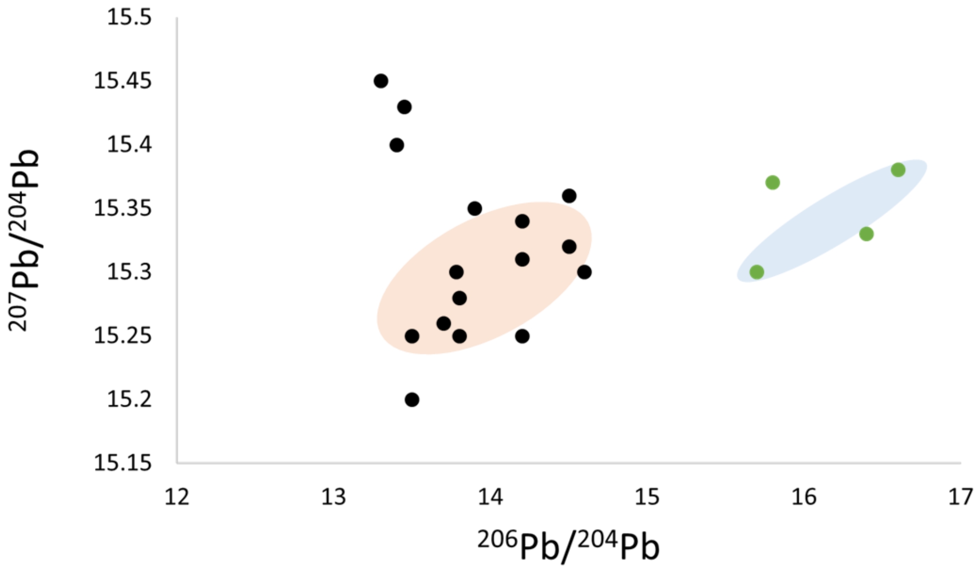

Figure 3.4. Plot of the Pb isotopic composition of detrital K-feldspar for an example sample suite. The light orange and blue ovals represent the Pb-in-kfsp signatures of two isotopically distinct basement terranes. The black dots represent one hypothetical detrital which broadly correlates with the Pb-in-kfsp signature of the light orange oval, and the green dots represent another sample which correlates with the Pb-in-kfsp signature of the light blue oval.

Once a ^{204}Pb- or ^{207}Pb-correction has been chosen, it can be either applied to time-resolved U-Pb data (Jackson et al., 2004; Petrus and Kamber, 2012) or alternatively, selective integration of time-resolved signals (e.g. in Iolite) can remove portions of the signal with common lead. Since common lead (and lead loss) most often occurs in regions like a rim or at fractures, they are more readily recognizable within time-resolved signals (Jackson et al., 2004).

3.2.3 Metamictization

Metamictization renders a mineral amorphous as its crystal structure is affected by radiation damage. Metamict minerals can be susceptible to Pb loss, resulting in discordance in U-Pb dating studies. However, it is important to note that zircon is a very durable mineral that is resistant to many forms of alteration; for this reason, it is even suggested that zircon be the main component to host radioactive waste material, both from nuclear power stations and from weaponry (Trachenko et al., 2002).

As U decays, it emits α radiation, which can cause damage to the crystal structure; as more time passes, the degree of metamictization increases (Mezger and Krogstad, 1997). In the process of α-decay, an α particle displaces atoms, with the number of collisions increasing with the α particle's trajectory. Depending on the energy of recoil, up to 2000 atoms can be displaced permanently during an α-decay event (Ewing et al., 2003). As these atoms are displaced, they cause a cascade of collisions (Ewing et al., 2003). Once the α-decay event is complete, evidence of the damage can be seen in a low-density core within a halo of interstitials (e.g., Trachenko et al., 2002). It is suggested that the transition from a crystalline state to metamict state occurs at an α-decay dosage range of 0.2 $x10^{16}$ to 0.8 x 10^{16} (Chakoumakos et al., 1987).

Radiation damage caused by α-decay is well-studied, with over 65 years of experimental data (e.g., Pabst, 1952; Hurley and Fairbairn, 1952; Headley et al., 1981a; Headley et al., 1981b; Greegor et al., 1990; Malczewski et al., 2018); however, questions remain regarding the recovery process following radiation damage, and how different variables, such as ion energy and temperature affect the cascade formation (Ewing et al., 2003). Further questions involve how rates of diffusion could potentially be intensified (Lee et al., 1997).

3.2.4 New growth and dissolution

Another reason for discordance is simply new growth, or overgrowths, around older cores. In zircon, rim overgrowths occur during the later stages of crystallization during a melting event (Watson, 1996), so these zircons are typically recovered in systems that are rich in melt or fluid (Rubatto, 2017). Cores are more likely to survive such melting events when the melt reservoir is smaller (Bea, 1996; Watson, 1996).

Dissolution of zircon (typically in melt) also needs to be considered for magmatic systems. Whether or not minerals dissolve or survive is dependent on a variety of factors, including the zirconium saturation and spatial distribution of the melt, the heating rate, and the individual characteristics of the grain itself. As time passes under a constant temperature, the dissolution rate tends to operate at an initial high rate, and then becomes steadier and more constant; however, once the radius of the crystal nears zero, the rate increases (Watson, 1996; Fig. 3.4).

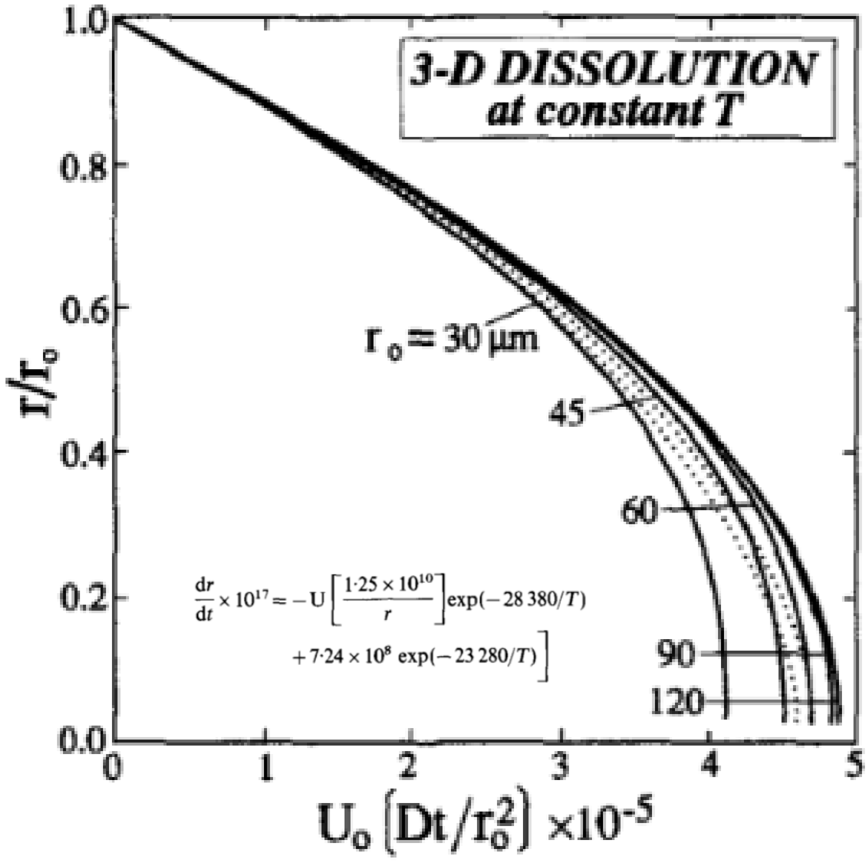

Figure 3.4. Modified plot of constant temperature dissolution of zircon from Watson (1996). The solid curves represent full scale" finite difference simulations while the dotted curves represent the results of step-wise solving the equation on the figure.

3.3 Accessory minerals commonly employed in U-Pb geochronology

3.3.1 Zircon

3.3.1.1 Chemical composition and structure

Zircon ($ZrSiO_4$) is ideally suited for U-Pb geochronology as it incorporates trace (typically tens to thousands of ppm) uranium and minimal lead at the time of crystallization and has a closure temperature exceeding 900 °C (Layer et al., 1989; Cherniak and Watson, 2001). Zircon commonly contains P, Y, Hf and REE in trace amounts (O'Hara et al., 2001; Hoskin and Schaltegger, 2003). Zircon can exert a significant control on the concentration of REE in magmas (Thomas et al., 2003), and its REE systematics can be used as an indicator of the geotectonic environments in which the crystals formed (Rubatto and Hermann, 2007).

Igneous zircons and metamorphic zircons have different morphologies, as metamorphism can modify the surface of the zircon as the grain is exposed to changing temperatures and pressures (e.g., grains can be corroded, leaving a smooth surface; Parrish and Noble, 2003). Metamorphic zircon morphologies are also typically rounded or ovoid (Hoskin and Schaltegger, 2003). While many zircons recovered in low-grade metamorphic rocks are inherited from a protolith or have thin (micron-scale) rims, those recovered in high-grade metamorphic rocks may have formed or been altered during prograde and retrograde metamorphism (Fraser et al., 1997; Hay and Dempster, 2009; Watson 1996; Schaltegger et al., 1999; Hoskin and Schaltegger, 2003).

3.3.1.2 Zoning

Zircons in igneous rocks typically exhibit oscillatory zoning, which is likely the result of either the degree of zircon saturation or the presence of trace elements in granitoids (Hoskin and Schaltegger, 2003). Zoning in zircon is typically imaged using cathodoluminescence (CL) imaging (Fig. 2.7). Secondary election (SE) and back scattered electron (BSE) imaging is also used to detail the surface textures of individual zircon grains (e.g. cracks, inclusions), though internal structures are not rendered visible.

3.3.1.3 Use in detrital U-Pb provenance analysis

Several studies have demonstrated selection bias in detrital zircon U-Pb geochronological analysis, which is capable of yielding statistically significant differences in age distributions (e.g., Chew et al., 2020; Dröllner et al., 2021; Ibañez-Mejia et al., 2018; Hietpas et al., 2011). However, this bias can be minimized by certain practices, such as transferring an unpicked aliquot of target phases to the mount and then measuring all of those grains systematically (Chew et al., 2020). It is also important to consider that sediment transport may cause statistically significant differences in ages of detrital zircons sourced from the same region. Mineral characteristics such as density and shape influence hydraulic sorting (Resentini et al., 2013). Appropriate sampling strategies can be adopted, and the effects of hydraulic sorting can be modelled mathematically.

3.3.2 Apatite

3.3.2.1 Chemical composition and structure

Apatite [$Ca_5(PO_4)_3(F, OH, Cl)$] is another mineral commonly used in U-Pb geochronology. With a closure temperature of 350-550 °C, apatite is an ideal chronometer for garnering geochronological data in this medium temperature range (Cochrane et al., 2014; Chew and Spikings, 2015). Its chemical structure allows for the incorporation of a wide range of trace elements, including the REE (Rakovan and Reeder, 1996; Rakovan et al., 1997).

In thin section, apatite has moderately high positive relief and is usually colourless. Most apatite grains are elongate euhedral to subhedral, though it is not uncommon to find anhedral grains. Apatite is very commonly found in all grades of metamorphic rock and is also found in clastic sedimentary rocks and igneous rocks (e.g., Spear and Pyle, 2002).

3.3.2.2 History of use in geochronology

One drawback to the use of apatite in U-Pb dating is the typically low concentrations of U and Th, coupled with high common Pb to radiogenic Pb ratios (e.g., Chew et al., 2011; Chew and Spikings, 2015). As a result, it is important to employ precise common Pb corrections (section 3.2.2). The effects of Th disequilibrium are an important constraint in samples with high Th/U ratios. However, in silicate melts, increasing the SiO_2 content does not drastically alter the partition coefficients of for either U or Th, thus removing disequilibrium of ^{230T}h as a significant influence (Prowatke and Klemme, 2006) except for very young, Th-rich apatites.

3.3.3 Titanite

3.3.3.1 Chemical composition and structure

Titanite [$CaTiSiO_5$], formerly known as sphene, is common in metamorphic and felsic rocks, making it useful in U-Pb geochronology studies. Titanite is composed of chains of Ti octahedrons which are bonded with Si tetrahedrons, sharing the oxygen (Fig. 3.5). In the Ca site, REEs, U, T, Mn, and Pb can be present (e.g., Higgins and Ribbe, 1977; Frost et al., 2000). High valence ions, including Al, Fe^{3+}, and Zr, may be found occupying the Ti site. In thin section, titanite occurs in varying shades of brown, though it can also be yellow or lacking colour.

The form of titanite also varies, and can be euhedral to subhedral, in addition to anhedral. Twinning is most likely on the {100} face, though lamellar twinning on {221} can be found as a result of deformation. Titanite is commonly found in nepheline syenites and pegmatites; in the latter, titanite can account for up to 50% of the rock (Wenk and Bulakh, 2016). It is also prevalent in hydrothermal mineral deposits, rendering titanite an important mineral in detailing the evolution of such geologic bodies (Li et al., 2010).

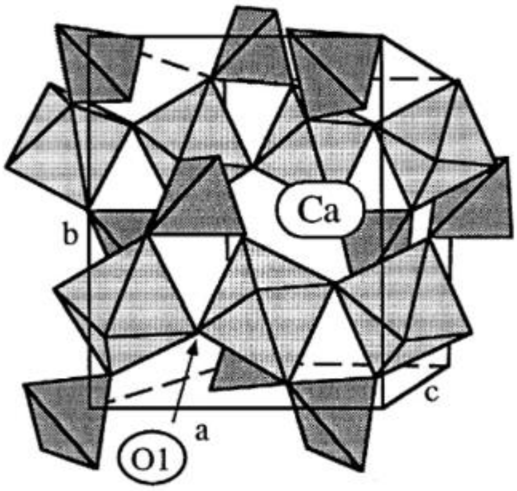

Figure 3.5: Modified depiction of the structure of titanite from Frost et al., 2000. Four sites are capable of hosting substitutions, which include the octahedral Ti site, the tetrahedral Si site, the 7x Ca site, and the O1 site.

Laboratory studies have placed the closure temperature of Pb diffusion to be ~ 660-700 °C (e.g., Frost et al., 2000), thus establishing it as an ideal geochronometer in the U-Pb system. With its high Pb closure temperature, a characteristic not shared among other mineral phases in hydrothermal ore deposits, titanite provides valuable age constraints on such mineral systems (e.g., Li et al., 2010).

In calcium-rich metamorphic rocks, titanite is limited by the reaction Qtz + Cc +Rut = Titanite + CO_2 (Frost et al., 2000). While this reaction prevents titanite from forming in environments with high pressures or high molar volumes of X_{CO2}, titanite is capable of forming in marbles in the eclogite-facies due to stabilization by high concentrations of Al and F (Carswell et al., 1996).

3.3.3.2 U-Pb systematics

Metamorphic or hydrothermal events occurring at temperatures ~660-700 °C can be recorded in titanite, as it possesses a lower T_c than both zircon and monazite (Olierook et al., 2019). However, the incorporation of common Pb during crystallization must be considered in U-Pb geochronology studies, which is further complicated if crystals record more than one event (Olierook et al., 2019).

3.3.4 Rutile

Rutile (TiO_2) often forms in high-pressure metamorphic rocks (Zack et al., 2011). For this reason, U-Pb dating of rutile provides important age constraints on metamorphic processes (Franz et al., 2001). Rutile can crystallize across a wide spectrum of pressures and temperatures, a characteristic it shares with a number of other minerals employed in U-Pb geochronologic studies, including zircon and apatite (e.g. Watson et al., 2006; Chew et al., 2020). Also like zircon, rutile is stable during diagenesis (Chew et al., 2020).

U-Pb ages derived from rutile are also useful in constraining the cooling path of a host rock, since Pb diffusion in rutile occurs rapidly compared to zircon and monazite at temperatures greater than 500 °C (Cherniak 2000; Zack et al., 2011). Rutile is also assumed to be unstable during polycyclic tectonothermal events implying that rutile will not yield evidence of previous metamorphic events (e.g. older cores) (Zack et al., 2011).

The faces of rutile are generally tetragonal-bipyramidal and prismatic, with either a black or reddish-brown colour.

3.3.5. Orthophosphates

3.3.5.1. Monazite

The orthophosphates monazite [(Ce, La, Nd, Th) PO_4] is also a common mineral employed in U-Pb geochronological studies. The structure of monazite is similar to the structure of zircon, wherein PO_4 tetrahedra share edges and corners with CeO_9 (Finch and Hanchar, 2003). This bonding is lateral through 9-fold coordination with oxygen molecules (of the REE, Ce is the most commonly found). Monazite is characterized by tabular and isometric crystals and is often found in granite pegmatites and gneisses. Concentric chemical zoning is observed in monazite, both simple and complex (Spear and Pyle, 2002).

In thin section, monazite has high positive relief and is most often a light green or yellow but can be grey or colourless as well. Though cleavage can be hard to distinguish in some samples, a single cleavage on {100} is most likely to be clear, and simple twins can often be found on {100} as well.

With a closure temperature exceeding 1000 °C (Cherniak and Watson, 2001), monazite is commonly employed in U-Pb dating studies because crystals can preserve the crystallization ages of prograde and retrograde metamorphism (Hawkins and Bowring, 1997).

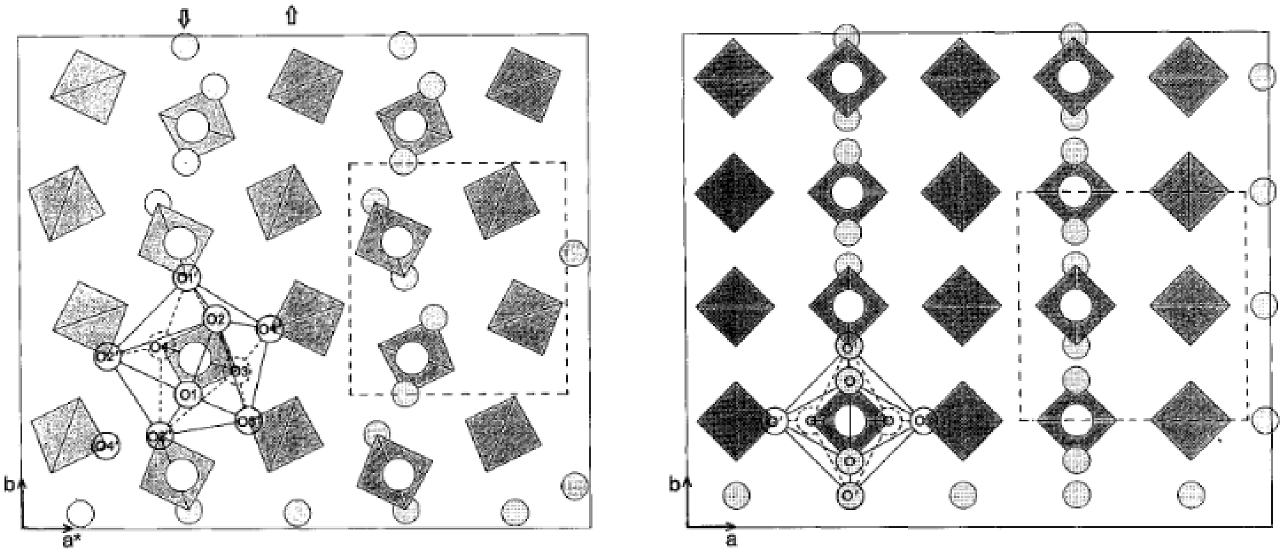

Figure 3.6: Perspective of phases projected downwards [001]. Dashed lines indicate unit cells of monazite and xenotime respectively. Unfilled circles represent RE atoms while smaller, shaded circles indicate O atoms. Figure modified from Ni et al. (1995).

3.3.5.2 Xenotime

Xenotime is commonly found in gneisses and igneous rocks, with HREE cations often substituting for Y. Studies (e.g., Fletcher et al., 2000; Hetherington et al., 2008) have proven that, due to its high uranium concentrations (>1000 ppm) and lack of initial lead, xenotime is well suited to U-Pb geochronological analysis (Rasmussen, 2005). Moreover, diagenetic xenotime is found to resist chemical 're-setting' up to lower amphibolite facies in sandstone, and to mid-upper greenschist facies in pelites (Rasmussen, 2005).

Though xenotime is a phosphate, it crystallizes with the same structure as zircon, with Y occupying the place Zr holds in the ZrO_8 dodecahedra (Ireland and Williams, 2003). Like monazite, xenotime crystals tend to increase in size with increasing metamorphic grade (Pyle et al., 2001). The HREE Gd, Dy, Er, and Yb can comprise 15-25% of the total composition of xenotime (Spear and Pyle, 2002).

In thin section, xenotime, like monazite, has high positive relief. Unlike monazite, it is most likely yellow or brown, though it can be colourless. On {100}, cleavage tends to be distinct, and twinning is uncommon. In slates, xenotime is also associated with low-temperature zircon, as either inclusions or overgrowths (e.g., Hay and Dempster, 2009).

Chapter 4: The basement geology of the Porcupine High – a key transatlantic link between the Caledonides and Appalachians

Shannon Dennehy[1], David Chew[1], Shane Tyrrell[2], and Rémi Rateau[1]

(1) Department of Geology, Trinity College Dublin, Dublin, Dublin 2, Ireland
(2) Earth and Ocean Sciences (EOS), University of Galway, Galway, H91 TK33, Ireland

Abstract

The Porcupine High, 200 km W of Ireland, is a key underexplored link between the circum-Iapetus basement geology of NW Europe and Atlantic Canada. We present geochronological data from basement sampling campaigns (dredging, shallow drill cores) undertaken in the last two decades. The majority of the dredge samples are likely near in-situ; outcrop ridges were targeted by side-scan sonar while the predominance of metamorphic clasts recovered is inconsistent with ice-rafted debris (IRD) derived from the Irish massif. All samples were collected north of the inferred trace of the Iapetus suture. The southernmost samples come from a core of foliated gneiss boulders which yield U-Pb zircon ages of c. 500-478 Ma. A 385 Ma apatite U-Pb age records post-Caledonian exhumation; K-feldspar Pb isotope data (Pb-in-Kfsp) imply a Caledonian affinity. These rocks are assigned to the ophiolitic rocks of the Clew Bay Complex and were sampled adjacent to a E-W trending magnetic boundary across the Porcupine High that we correlate with the Fair Head–- Clew Bay line. To the north dredging recovered >90% lower greenschist-facies psammite cobbles in a region characterized by a magnetic anomaly low. U-Pb detrital zircon data imply a Moine or Grampian Group Dalradian affinity with the youngest population at 950 Ma. U-Pb detrital apatite ages (900–- 1800 Ma) are unaffected by Caledonian orogenesis which is atypical for Tonian successions in the Caledonides. Farther north, drilled granitic orthogneiss yields a 1314 Ma U-Pb zircon crystallization age. Granulite-facies metamorphism (12 kbar, 740°C) is interpreted to be of Grenville age, supported by a 875 Ma apatite U-Pb cooling age. Zircon Hf isotopic and Pb-Kfsp data suggest an affinity with the Rockall Bank Palaeoproterozoic, delimiting the offshore extent of the Annagh Gneiss Complex (AGC) of NW Ireland. Northernmost dredging recovered >98% metamorphic clasts.

U-Pb detrital zircon ages from two low-grade metasediments imply a Moine/Grampian Group and an Upper Dalradian affinity respectively; Caledonian apatite U-Pb ages are prevalent. The high-grade rocks (orthogneisses and amphibolites) can be divided into three groups: clasts with 2750 Ma U-Pb zircon crystallization ages, 1750 Ma apatite U-Pb ages and a Lewisian Pb-in-Kfsp signature; clasts with 1830-1940 Ma U-Pb zircon ages, 1750 Ma apatite U-Pb ages and an AGC Pb-in-Kfsp affinity, and AGC clasts with 1550-1650 Ma U-Pb zircon ages and U-Pb apatite ages recording post-Grenville cooling. All three groups were found at one dredge site and a component of Quaternary glacial transport is invoked for these dredged clasts.

1. Introduction

The Porcupine High is a NNE-trending bathymetric high located 200 km west of the Irish mainland. It is over c. 100 km across at its maximum extent in an ESE-WSW direction, and its seabed expression is referred to as the Porcupine Bank, which was discovered in 1862 by the British survey ship *HMS Porcupine*. The Porcupine High is adjacent to the Porcupine Basin (or Seabight) to the southeast (Fig.1), reaching south to the Goban Spur Basin. The Rockall Basin and Rockall High (whose seabed expressions are referred to as the Rockall Trough and the Rockall Bank respectively) neighbour the Porcupine region to the north and northwest (Fig. 1). Water depths above the Porcupine High are between 300 and 400 m, though at its shallowest point on the SW-NE Porcupine Ridge (Fig. 1), it is only 200 m deep (Thébaudeau et al., 2016). Porcupine High covers an area of more than 40,700 km^2, and is approximately 65,000 km^2 at 500 m depth (Thébaudeau et al., 2016); for comparison the areal extent of the Irish mainland is c. 84,400 km^2.

Constraining the geologic evolution of the Porcupine High region is key to reconstructing the basement geology of the Irish offshore and the North Atlantic as it is a key underexplored link between the circum-Iapetus basement geology of NW Europe and Atlantic Canada. While the surrounding basins have been the site of petroleum exploration since the 1970s, the geological evolution of Porcupine High remains poorly constrained. We present geochronological data from sampling campaigns (dredging, shallow drill cores) in the last two decades, which to date have only been presented in reports or conference abstracts (e.g. Daly et al., 2007; Daly et al., 2008; Hollis et al., 2013; Tyrell, 2013; Barry et al., 2017; Chew et al., 2019). The dredge samples are likely near in-situ; outcrop ridges were targeted by side-scan sonar while the predominance of metamorphic clasts recovered is inconsistent with IRD derived from the Irish massif or nearby. All samples were collected north of the inferred trace of the Iapetus suture (Fig. 1).

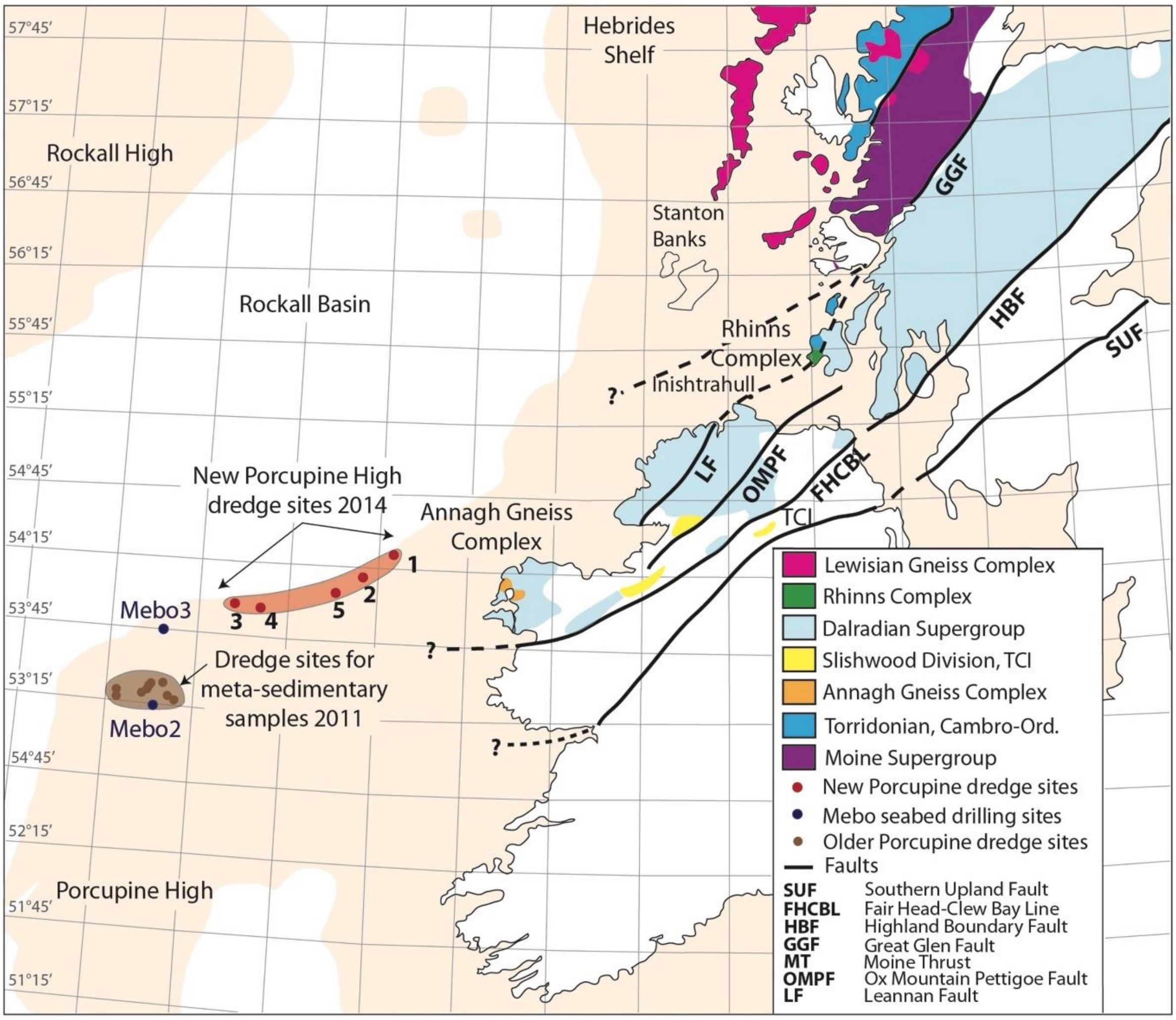

Figure 1. Map of the sampling sites on the Porcupine High along with the Precambrian geology of adjacent areas. In 2006, the R/V Celtic Explorer collected the MeBo cores. Dredge samples were collected by the Celtic Explorer in 2011 and a further suite of dredge samples were collected in 2014 by the Celtic Voyager.

2. Geological Background

The geological evolution of Laurentia proximal to the Iapetus suture is complex, with multiple geological terranes that have experienced differing geological histories.

Hence the geological framework of this complex sector of the North Atlantic is reviewed below for comparison with the tectonothermal histories derived from the samples collected from the Porcupine High basement (Fig. 2).

2.1 Archean Basement Geology

Rocks of Archean age are not found onshore mainland Ireland, with the nearest occurrences in Scotland, Greenland, and the Irish offshore basement highs. Several studies suggest that Archean crust is absent south of the Great Glen Fault (Fig. 1), a NE-SW trending strike-slip fault that runs through Scotland and into northwestern Ireland (e.g. Fitches et al., 1990; Daly et al., 1991). However, Hf isotope analysis of zircon rims from Early Caledonian (Grampian) granitoids cutting the Tyrone Central Inlier (Fig. 2) in NW Ireland (a presumed upper Dalradian Supergroup correlative) indicates that crystalline basement of Archean age may be present at depth (Flowerdew et al., 2009).

The largest areal extent of Archean rocks in the North Atlantic region is in Greenland (Fig. 2). These include the rocks of the North Atlantic Craton (NAC) in southern West Greenland which extend into the Nain Province in Labrador (Buchan et al., 2000). The NAC is bounded by the c. 1910 to 1770 Ma Nagssugtoqidian orogen to the north and the 1800–1870 Ma Ketilidian–Makkovik mobile belt to the south (Fig. 2). The latter can be correlated with the Rhinns Complex in Scotland, which in turn can be linked to the Trans Scandinavian Igneous Belt in Baltica (Buchan et al., 2000).

2.1.1 The Lewisian Complex

Tonalite gneisses of the Lewisian Complex, which extends to the Outer Hebrides, is divided into the northern, central, and southern regions, and includes outcrops adjacent to the Moine thrust zone (e.g., Peach, 1907; Friend and Kinny, 2001) in northwestern Scotland provide evidence of late Archean to early Proterozoic metamorphism and magmatism (e.g. based on U-Pb zircon and titanite geochronology, Corfu et al., 1994). The Lewisian Complex can be divided into three regions, each with unique histories: the northern region (Rhiconich block), central region (Assynt and Gruinard blocks) and southern region (Gairloch and Loch Maree) (e.g., Heaman and Tarney, 1989; Crowley et al., 2014), which are separated from each other by major shear zones.

Protolith ages of the Lewisian TTG (tonalite-trondhjemite-granodiorite) gneisses span the Paleo-, Meso- and Neo-Archean (Corfu et al., 1998; Friend and Kinny, 2001, Goodenough et al., 2013). Protolith ages of c. 2860–2840 Ma have since been found across the mainland outcrop of the Lewisian Gneiss Complex (Crowley et al., 2014) which does question one of the tenets of the multi-terrane models for the Lewisian Gneiss Complex (e.g. Friend and Kinny, 2001; Kinny et al., 2005). Late Archean Badcallian (c. 2700-2500 Ma or 2490 - 2480 Ma) granulite-facies metamorphism affected the Gruniard and Assynt terranes respectively (Cartwright and Barnicoat, 1987) and is associated with partial melting (e.g., Johnson et al., 2012; Rollinson, 2012). The Inverian (2490 – 2480 Ma) event followed the Badcallian and is characterized by amphibolite-facies retrogression (Evans, 1965). After these metamorphic events, the intrusion of the Scourie Dyke Swarm began c. 2400 Ma (Davies and Heaman, 2014) in the Assynt region. The Scourie dyke suite is found in many parts of the Lewisian Complex and was originally considered to represent one magmatic episode and was thus useful in distinguishing Archean (Badcallian and Inverian) versus Proterozoic (Laxfordian) events. However U-Pb baddeleyite dates (Heaman and Tarney, 1989) from the Scourie dyke suite in the Assynt terrane of c. 2418 ± 7 Ma (bronzite-picrite Beannach dyke) and 1992 ± 3 Ma (olivine microgabbro Strathan dyke) show that the dykes can only be used as broad divisors of Archaean and Proterozoic events.

Units with a c. 1900 Ma (volcano)-sedimentary protolith include the Loch Maree Group of the mainland and Roineabhal Terrane (Friend and Kinny, 2001) of the Outer Hebrides and are cut by marginally younger TTG rocks. The Roineabhal rocks in South Harris also experienced a UHT granulite-facies event at c. 1880 Ma (Whitehouse and Bridgwater 2001). The Laxfordian metamorphic event typically comprises amphibolite-facies metamorphism with variable reworking localized within shear zones (Cartwright and Barnicoat, 1987). In the Rhiconich block, Laxfordian metamorphism and deformation is most easily distinguished in the c. 1855 Ma Rubha Ruadh Granites where c. 1740 Ma U-Pb titanite ages are reported (Corfu et al., 1994). A further reworking episode at c. 1670 Ma is seen on the mainland in the Rhiconich and Assynt blocks based on U-Pb ages from a later generation of titanite and rutile (Corfu et al. 1994) and in the Gairloch block by U-Pb titanite dating (Love et al., 2004).

2.1.2 Stanton Bank and Rockall High

In general terms, the geological evolution of the offshore basement highs in the Irish and British sectors of the North Atlantic remains poorly constrained. Two of these banks, the Rockall High and the Stanton Banks (Fig. 1), contain Archean basement. While the southern Rockall Bank exhibits a late Paleoproterozoic (Ketilidian) affinity (Fig. 2; Dicken, 1992), Archean (Lewisian-like) Pb isotope contamination of lavas and tuffs from the George Bligh Bank and Hebrides Shelf indicate that this terrane underlies the northern Rockall Basin (Fig. 2; Hitchen et al., 1997).

Based on U-Pb zircon protolith ages of c. 1790-1830 Ma and Sm-Nd isotopic analysis on gneisses (T_{DM} ages of c. 1900 Ma), it has been suggested that Stanton Banks is a Paleoproterozoic terrane with an alkali-calcic, intermediate composition of gneisses comparable to those of the Rhinns Complex and the Annagh Gneiss Complex (Scanlon et al., 2003). The Paleoproterozoic portion of the Stanton Banks is bounded to the south by an older (c. 2650 Ma) trachyandesite sampled within the Stanton Banks with Sm-Nd T_{DM} ages of 2800 Ma (Scanlon et al., 2003).

2.2 Paleoproterozoic and Mesoproterozoic

The oldest exposed crystalline basement in northwestern Ireland is Paleoproterozoic (c. 1750 Ma) in age and crops out in Mayo and offshore northern Donegal. The Paleoproterozoic Annagh Gneiss Complex structurally underlies the Dalradian Supergroup of the North Mayo Inlier, while the Rhinns Complex is found on islands off the coast of Donegal and SW Scotland (Daly, 1996).

2.2.1 The Annagh Gneiss Complex

Within the Annagh Gneiss Complex (AGC), three distinct gneiss units are recognized: the Mullet, the Cross Point, and the Doolough gneisses. The Mullet gneiss is comprised of metaluminous I-type quartz monzodiorites, granodiorites and granites with granodiorite predominating (Flowerdew et al., 2009) and is dated at 1753 ± 3 Ma by U-Pb zircon TIMS dating (Daly, 1996). The Mullet gneiss contains boudins of coarse amphibolite, now generally concordant but originally emplaced as dykes because in low strain zones they are locally cross-cutting.

The Cross Point gneiss is found on the Mullet peninsula, south of Erris Head, close to the tectonic contact with the Dalradian Supergroup, and is dated at 1271 ± 6 Ma. It is comprised of syenite and granite, with banding controlled by both magmatic development and deformation state (Daly, 1996). The juvenile 1177 ± 4 Ma Doolough gneiss (comprised mainly of sub-alkaline granite and trondhjemite with subordinate amounts of amphibolite) is cut by the c. 1015 Ma Doolough granite (Daly, 1996; McAteer et al., 2010).

The 1753 + 3 Ma Mullet gneiss protoliths, with a Sm-Nd model age of 1800-2000 Ma, exhibit a juvenile crustal origin similar to the alkaline gneisses of the Rhinns Complex on the islands of Islay and Inishtrahull (Daly, 1996). The 1271 ± 6 Ma Cross Point gneiss, with an A-type within-plate signature and Sm-Nd model age of 1700-1800 Ma, is likely the result of melting of crust akin to the Mullet gneiss (Daly, 1996). It is thought that the 1177 ± 4 Ma Doolough gneiss was either intruded into the AGC or deformed along with the AGC during Grenville deformation (Daly, 1996). The Sm-Nd isotopic composition of the Doolough gneisses suggest a juvenile origin, based on its model age range of 1758 to 1450 Ma (Daly, 1996). The AGC is also the locus of Grenville deformation, which is apparent in field relationships observed at Annagh Head and Doolough (Daly, 1996).

2.2.2 Rhinns Complex

The Rhinns Complex, poorly represented in Ireland, consists of c. 1800 Ma Paleoproterozoic juvenile alkaline crust which underwent extensive Paleoproterozoic metamorphism (Muir et al., 1994; Flowerdew et al., 2009). Like the AGC in Mayo, the Rhinns Complex is composed of juvenile orthogneisses (Daly, 1996). Syenite and gabbro dominate the complex, though other intrusions are also noted (Muir et al., 1994).

Large basement inliers of the Rhinns Complex are found on the Scottish islands of Islay and Colonsay, both located in the Inner Hebrides (Muir et al., 1992; Muir et al., 1994). A Sm-Nd model age of c. 1900 Ma indicates the Rhinns Complex on Islay shares similar juvenile mantle extraction ages to the Rhinns Complex on the island of Inishtrahull off the coast of northern Donegal (Dickin and Bowes, 1991). The rocks on Inishtrahull represent the oldest rocks known in Ireland, yielding a U-Pb zircon date of 1779 ± 3 Ma (Daly et al., 1991). Nearly all the exposed rock on Inishtrahull is a coarse-grained syenitic gneiss, with a composite foliation. Gabbro sheets represent a minor component observed in the field.

2.3 Grenville Orogeny

During the Mesoproterozoic at c. 1300-1000 Ma, the Grenville orogen (*sensu stricto*) was a period of convergent orogenesis along the southern and eastern margin of Laurentia. Remnants of the Grenville orogen (*sensu lato*) can be found throughout the world as a result of the subsequent breakup of the Rodinian supercontinent (Fig. 2). In Ireland and Scotland, the effects of the Grenville Orogeny are especially apparent in the Annagh Gneiss Complex in the NW Mayo inlier, which pervasively deformed and metamorphosed the Proterozoic basement rocks (Fig. 2; Daly, 1996). At least three episodes of Grenville deformation are postulated based on field observations of cross-cutting pegmatites at Annagh Head and Doolough (Daly, 1996). Grenville orogenesis, however, is not seen in the Rhinns Complex (Flowerdew et al., 2009).

2.4 Post-Grenvillian sequences and Neoproterozoic deformation

The clastic metasedimentary rocks of the Colonsay Group are exposed on the islands of Colonsay and Oronsay, and share a sheared, tectonic contact with the Rhinns Complex (McAteer et al., 2010b). While the sequence experienced deformation during the Grampian phase of the Caledonian orogeny, the stratigraphic age of the Colonsay Group remains to be precisely constrained (Fitches and Maltman, 1984; McAteer et al., 2010). The basal Colonsay Group (Octofad Sandstone Formation) structurally overlies the Rhinns Complex on Islay and is interpreted to represent a sequence derived from erosion of Grenville belt and is also correlated with the basal units of the Dalradian Supergroup (McAteer et al., 2010b). Late Grenville titanite grains (c. 980-940 Ma) were likely sourced from the Annagh Gneiss Complex or equivalents, while older zircon grains at c. 1750 Ma have a likely Rhinns Complex affinity (McAteer et al., 2010b).

The Moine Supergroup of NW Scotland structurally overlies basement inliers closely resembling the Lewisian Complex (‘Lewisianoid’ basement). It is composed of three lithostratigraphical groups (the Morar, the Glenfinnan, and the Loch Eil; Soper et al., 1998) of metamorphosed psammite and pelite sequences (Friend et al., 2003; Tanner and Evans, 2003). The Moine Supergroup was deposited in a Neoproterozoic basin from c. 950 Ma to c. 870 Ma, with significant input from erosion of the Grenville belt (Friend et al., 2003). Lu-Hf LA-ICP-MS analysis of garnet cores and rims in the Morar Group suggests a phase of prograde garnet growth at c. 950 Ma (Walker et al., 2019).

Post-Grenvillian (Knoydartian) tectonic activity (garnet-grade metamorphism and the intrusion of pegmatites) in the Moine is dated at c. 800 Ma (Vance et al., 1998; Rogers et al., 1998) with P-T constraints implying a minor phase of crustal thickening possibly following a period of extension (Cutts et al., 2009). However, while evidence of Early Neoproterozoic deformation (e.g., the Valhalla orogeny of Cawood et al., 2010) is found in the Moine Supergroup of the Scottish Highlands and in the North Atlantic 'borderlands' (Shetland, Northern Norway, East Greenland), there is currently no unequivocal evidence for Neoproterozoic deformation in Ireland (Daly and Flowerdew, 2005).

The Dalradian Supergroup of Scotland and Ireland is mainly composed of metamorphosed siliciclastic sediments, limestones and basic volcanics. It structurally overlies the Annagh Gneiss Complex and contains no evidence of Grenvillian orogenesis; combined with maximum depositional ages derived from U-Pb detrital zircon data, this suggests it was deposited during the Neoproterozoic on the margin of Laurentia (Harris et al., 1994; Cawood et al., 2003). The Dalradian has been subdivided into the Grampian, Appin, Argyll, and Southern Highland groups. The quartzofeldspathic meta-arkoses of the Grampian Group represent the earliest observed example of rifting in the sequence (Soper and England, 1995) and it has a maximum thickness of up to c. 7 km. The overlying Appin Group has a maximum thickness of up to 4 km and mainly consists of black shales with quartzite units and is believed to represent a thermal subsidence sequence. The base of the Argyll Group is marked by the Cryogenian Port Askaig Tillite, while volcanics (such as the Tayvallich volcanic sequence) become more prominent near the top of the Argyll Group. The Argyll Group has a maximum thickness of 9 km and is comprised of a diverse suite of lithologies including polycyclic quartzite, turbidites, limestone and volcanics deposited during a renewed phase of rifting (Soper and England, 1995). The overlying Southern Highland Group is comprised of turbiditic grits, sandstones and shales (Soper and England, 1995).

2.5 The Caledonian Orogenic cycle

A key feature of the basement geology of this portion of the North Atlantic region is the Iapetus Suture, which marks the locus of closure of the Iapetus Ocean during the Caledonian Orogeny. The Caledonian Orogeny in the North Atlantic involved the collision of three plates: Laurentia, Baltica, and Ganderia-Avalonia, with NW Ireland and Scotland forming part of the Laurentian continent and SE Ireland and England representing part of the Ganderia-Avalonia continent. Seismic reflection profiles and geological evidence place the Iapetus Suture running along the northern Irish Sea through onshore northern England and the Southern Uplands of Scotland (Fig. 2; Beamish and Smythe, 1986; Soper et al., 1992). In the Irish offshore, it is thought to run through the southern portion of the Porcupine High (e.g., Readman et al., 2005).

The Caledonian orogeny, rather than consisting of a single orogenic pulse, is instead divided into phases each associated with variable P-T conditions (Oliver et al., 2008). The peak of the Grampian Orogenic phase occurred c. 475-460 Ma, as Laurentia collided with an intra-oceanic arc, resulting in medium- to high-grade metamorphism and deformation of the Laurentian margin (Dewey and Shackleton, 1984). In Ireland and Britain, the closure of Iapetus in the Late Ordovician to the Early Silurian did not lead to widespread orogenesis; the Acadian Orogeny, the last phase during the early Devonian, significantly post-dates ocean closure (McKerrow et al., 2000). Sinistral strike-slip movement (several hundred km) along the Great Glen Fault is also associated with the end of the Caledonian orogeny (Dewey and Strachan, 2003; Cawood et al., 2012).

2.5.1 The Grampian orogeny

The Grampian Orogeny is a regional (Barrovian) metamorphic event which affected the Laurentian margin, including the Dalradian Supergroup. Evidence for the onset of the Grampian Orogeny can be found from c. 510 – 490 Ma ophiolitic rocks in the Clew Bay Complex of Western Ireland and Highland Border Complex in Scotland (Chew et al., 2010). By c. 490 Ma, an intra-oceanic arc was well developed and started to collide and obduct over the Laurentian margin by c. 480 Ma (Chew et al., 2010). U-Pb zircon ages of anatectic migmatites in the Dalradian Supergroup of NE Scotland yield peak metamorphic ages of 472.2 ± 5.8 Ma and 471.2 ± 5.9 Ma, indicating that the Barrovian metamorphism characteristic of the Grampian episode occurred within a short window (Viete et al., 2013). In Connemara in western Ireland, syn-D2 to early D3 basic intrusions in the Dalradian Supergroup yielded U-Pb zircon ages of 470.1 ± 1.4 Ma and 474. 5± 1 Ma (Friedrich et al. 1999). Late D3 quartz-diorite gneisses in the migmatite zone in south Connemara yield U –Pb zircon ages of 463 + 4 Ma (Cliff et al. 1996) and 467 ± 2 Ma (Friedrich et al. 1999). The post-tectonic Oughterard granite in Connemara has yielded a 462.5 ± 1.2 Ma U-Pb xenotime age (Friedrich et al. 1999a). Granitoid magmatism in the Slishwood Division (Flowerdew et al., 2005) and the Tyrone Central Inlier (Chew et al., 2008) along orogenic strike to the NE also yield ages consistent with c. 470 Ma orogenesis.

2.5.2 Caledonian granites

The late Caledonian granite suite is suggested to have resulted from slab break-off following the closure of the Iapetus Ocean (Atherton and Ghani, 2002). This includes a voluminous suite of c. 430 Ma I-type granites and diorites intruded into the Grampian terrane (Oliver et al., 2008). These granitoids are predominantly granodioritic with a calc-alkaline character implying a subduction zone source (Atherton and Ghani, 2002), but with a significant crustal component based on Nd, Sr and O isotopic evidence (Halliday, 1984). The very last stages (Acadian) of Caledonian magmatism are associated with the emplacement of granites into active sinistral fault zones (Oliver et al., 2008).

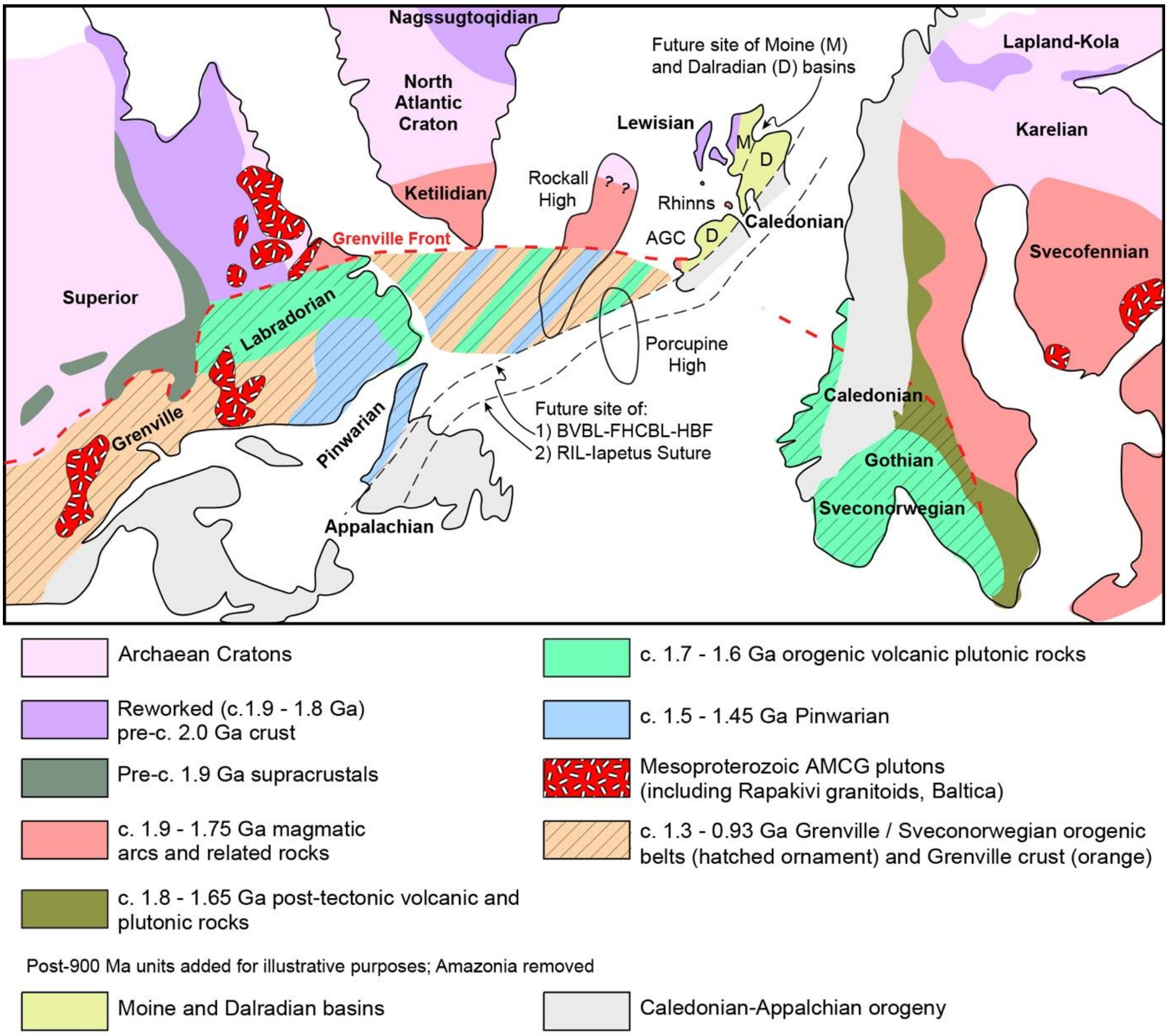

Figure 2. Schematic palaeogeographic reconstruction of the North Atlantic region at ca. 900 Ma adapted from McAteer et al. (2010). Post-900 Ma Laurentian basins (Moine and Dalradian Supergroups) and Caledonian sutures (BVBL-FHCBL-HBF = Baie Verte Brompton Line – Fair Head Clew Bay Line – Highland Boundary Fault; RIL = Red Indian Line) are added for clarity; Amazonia is removed.

3. Methods

3.1 Sample collection

This study incorporates samples from three different expeditions to the Porcupine High region of the western Irish offshore which are presented in chronological order below.

3.1.1 2006 MeBo seabed drilling

Two short drill cores (Fig. 3) were acquired from the Porcupine High using the University of Bremen MeBo seabed drilling rig deployed on R/V Celtic Explorer in July 2006, in a survey funded by the Irish Shelf Petroleum Study Group (ISPSG) of the Petroleum Affairs Division (PAD) and the Marine Institute. Although other boreholes were drilled in this expedition, the two cores discussed here are they are interpreted to represent *in-situ* bedrock. The first core (borehole 25/27-sbMeBo2, Fig. 3B) was collected along the southern region of the Porcupine High (hereafter referred to 'MeBo2'; Fig. 1). The core is tentatively interpreted as representing a rocky shoreline deposit of uncertain age. The core recovered rock from 8.58 to 5.66 m depth and comprises a possible *in situ* fossiliferous limestone with diverse fauna comprising foraminifera, bivalves, fish teeth, algae, bryozoans, echinoderms and large boulders of various metamorphic rocks.

The second core (25/7-sb(MeBo)3 (hereafter referred to as 'MeBo3'; Fig. 1), recovered 0.85 m of *in situ* granitic orthogneiss (Fig. 3A). Ion microprobe U-Pb zircon dating indicates a crystallization age of 1314 ± 6 Ma, signifying a period of magmatism not previously recognized in the region (Daly et al., 2008a). Granulite-facies metamorphism (12 kbar, 740°C) is of likely Grenville age, while zircon Hf isotope and Pb-in-K feldspar data suggest an affinity with the Paleoproterozoic Rockall High, thus delimiting the offshore extent of the Annagh Gneiss Complex (AGC) in NW Ireland (Daly et al., 2008a). Apatite U-Pb data from this short drill core are presented later in this study.

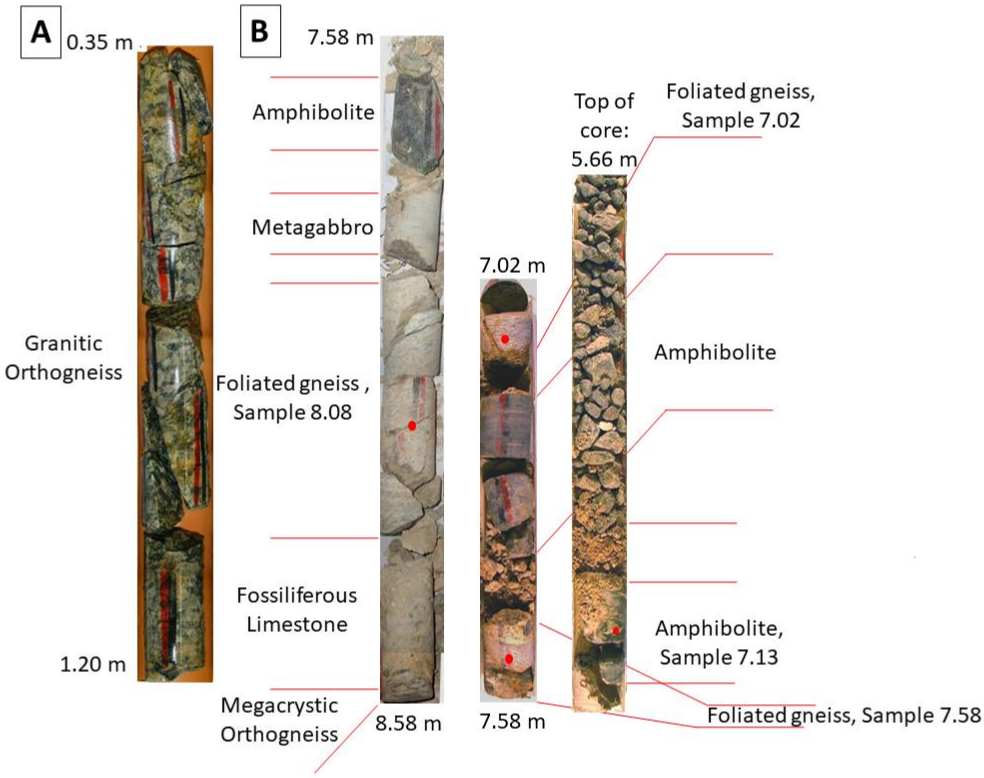

Figure 3. A) MeBo3 core (0.85 m of granitic orthogneiss). B) MeBo2 core. Red circles indicate samples taken in this study.

3.1.2 2011 Dredge sampling campaign

The May 2011 (CE11-017) Celtic Explorer metasedimentary dredge samples were recovered along an E-W transect on Porcupine High (Fig. 1). Over 85% of the samples are quartzo-feldspathic psammites, described as green-reddish metasandstones (Tyrrell, 2013). The samples exhibit a weak lower greenschist-facies foliation with recrystallized quartz, and contain abundant accessory minerals including zircon, titanite, and epidote (Tyrrell, 2013).

3.1.3 2014 Dredge sampling campaign

The October 2014 (CV14-021) Celtic Voyager crystalline basement dredge samples are the most northern samples recovered from Porcupine High, with over 98% metamorphic clasts recovered at some localities. Although the majority of analyzed samples were collected from site 402, two other sites were also sampled. Together, the three sites yielded gneisses (main clast type), quartzite, amphibolite, igneous clasts, and, to a lesser extent, sedimentary rocks (Barry et al., 2017). The dominant mineralogy of the gneiss samples consists of K-feldspar, biotite, quartz, and epidote but garnet is absent (Barry et al., 2017).

3.2 Analytical Methods

Zircon and apatite crystals were separated using standard separation and concentration procedures (jaw crushing, Wilfley table, heavy liquids, and magnetic separation) at the Department of Geology, Trinity College Dublin (TCD). Zircon and apatite were picked under a binocular microscope in ethanol, mounted in 2.5cm epoxy mounts and polished to approximately half thickness prior to analysis. Cathodoluminescence (CL) images of zircon grains were acquired at the Centre for Microscopy and Analysis at TCD using a Tescan MIRA3 FEG-SEM with a KE Developments Centaurus Cathodoluminescence Detector (Appendix C).

3.2.1 U-Pb LA-ICPMS analyses

All U-Pb data were acquired using a Photon Machines Analyte Exite 193 nm ArF Excimer laser-ablation system with a Helex 2-volume ablation cell coupled to either a Thermo Scientific iCAP Q or an Agilent 7900 at TCD. 0.65 l/min He carrier gas was split between the large outer sample chamber and the small inner volume (the 'cup') where ablation occurs. A small volume of N_2 (6 – 10 ml/min) to enhance signal sensitivity and reduce oxide formation and 0.6 - 0.7 l/min Ar nebulizer gas was then introduced to the sample-gas mixture via an in-house smoothing device. ^{202}Hg, $^{204,206,207,208}Pb$, ^{232}Th and ^{238}U were acquired for all U-Pb analyses. ^{91}Zr and ^{43}Ca were employed as the internal standards for zircon and apatite respectively. Zircon analyses employed either a 25 or 30 µm laser spot, a 5 - 10 Hz laser repetition rate and a fluence of c 2.5 – 3.5 J/cm^2. Apatite analyses were acquired using either a 30, 47 or 60µm laser spot, a 5 Hz laser repetition rate and a fluence of 2.5 – 3.5 J/cm^2. All analytical parameters (e.g. gas flows, laser spot size, repetition rate and fluence) were kept constant for a given analytical session.

The raw isotope data were reduced using the "Vizual Age" data reduction scheme of Petrus & Kamber (2012) within the freeware IOLITE package of Paton et al. (2011).

User-defined time intervals were established for the baseline correction procedure to calculate session-wide baseline-corrected values for each isotope. The time-resolved fractionation response of individual standard analyses was then characterised using a user-specified down-hole correction model (such as an exponential curve, a linear fit or a smoothed cubic spline). The data reduction scheme fits this appropriate session-wide "model" U-Th-Pb fractionation curve to the time-resolved standard data and the unknowns. Sample-standard bracketing is applied after the correction of down-hole fractionation to account for long-term drift in isotopic or elemental ratios by normalizing all ratios to those of the U-Pb reference standards. Common Pb in the apatite standards was corrected using the ^{207}Pb-based correction method using a modified version of the VizualAge DRS that accounts for the presence of variable common Pb in the primary standard materials (Chew et al. 2014). Concordia plots were constructed using the Excel macro Isoplot 4.15 (Ludwig, 2003).

Secondary standards were applied to both U-Pb apatite and zircon runs. Madagascar apatite (Thomson et al., 2012) was used as the primary reference standard for U-Pb apatite analysis. For U-Pb apatite, the Durango apatite reference material (32.716 ± 0.072 Ma; Paul et al., 2021) yields a Tera-Wasserburg U-Pb lower intercept age of 32.13 ± 0.44 Ma with a MSWD of 1.6 (n = 78) when anchored at a common Pb ratio of 0.838. McClure Mountain (523.98 ± 0.12 Ma; Schoene and Bowring, 2006) yields a Tera-Wasserburg U-Pb lower intercept age of 521.6 ± 1.7 Ma with a MSWD of 2.7 (n =149) when anchored at a common Pb value of 0.88198.

91500 zircon (1065 Ma; Wiedenbeck et al, 1995; Wiedenbeck et al., 2004) was used as the primary reference standard for U-Pb zircon analysis and Plesovice (337.13 ± 0.37 Ma; Sláma et al., 2008), Temora 2 (416.75 ± 0.24 Ma; Black et al., 2003), and WRS-1348 (526.26 ± 0.70 Ma; Pointon et al., 2012) were employed as secondary standards. Weighted mean ^{206}Pb/^{238}U ages (n = 104) of the standard Plesovice yield an age of 338.54 ± 0.77 and MSWD of 1.19. Weighted mean ^{206}Pb/^{238}U ages (n = 69) of the standard Temora yield an age of 416.9 ± 1.4 and MSWD of 1.06. Weighted mean ^{206}Pb/^{238}U ages (n = 41) of the standard WRS-1348 yield an age of 526.7 ± 3.1 and MSWD of 2.3.

3.2.2 Pb in K-feldspar LA-MC-ICP-MS analyses

Pb isotopic analyses were carried at the National Centre for Isotope Geochemistry, UCD School of Earth Sciences, University College Dublin, Ireland. Prior to analysis, K-feldspar grains and crystals were imaged using backscatter scanning electron microscopy (BSEM) in order to identify any intra-grain variations such that these can be avoided or characterised during subsequent ablation. Target K-feldspar grains were analyzed using the New Wave 193 nm Excimer laser coupled with a Thermo Scientific Neptune multiple collector inductively coupled plasma mass spectrometer, and followed closely the procedures of Tyrrell et al. (2012).

Ablations were performed with the laser at a spot size of 75 µm, a 20 Hz pulse rate and laser energy were adjusted to produce a fluence of between 5 and 6 J/cm^3. This resulted in ^{204}Pb signal intensity of ~0.02 V on the NIST 612 (Pb 38.57µg/g, Tl 15.7 µg/g) standard. Selected raster lines were ablated at rates between 1 and 2 µ/ms, such that track lengths were typically ~200 µm. 250 ratios were collected with a 0.262 second integration time. Standard-sample bracketing was used to monitor Tl based fractionation, with NIST 612 used as the standard. The analytical sequence comprised the standard followed by three unknowns, followed by the standard. NIST 612 and Shap Granite K-feldspar (Souders and Sylvester 2010; Tyrrell et al., 2012; Barham et al., 2021) were run as unknowns as part of the sequence (comprising ~1 in 6 unknowns) in order to verify the data reduction procedure. Data reduction was carried out offline using Microsoft Excel software. Isobaric interference corrections on ^{204}Pb were made using a ^{202}Hg/^{204}Hg ratio of 4.35 based on the natural occurrence of these Hg isotopes (Rosman and Taylor, 1998). External mass bias fractionation corrections were carried out based on ^{203}Tl/^{205}Tl (true value =0.418922; Baker et al 2004) measured in each standard in the sequence and assuming a linear stepped fractionation between each standard. The fractionation correction for each unknown was calculated using exponential fractionation laws. Known unknowns (i.e. NIST 612 and Shap Granite K feldspar) yielded analysis consistent with published ICP-MS and TIMS values (Tyrrell et al., 2006; Souders and Sylvester 2010).

4. Results

All geochronology data are summarized in Table 1.

4.1 2006 MeBo seabed drilling

The MeBo3 orthogneiss core (termed here the North Porcupine High orthogneiss or NPHO) yields a U-Pb zircon crystallization age of 1314 ± 6 Ma (Daly et al., 2008a) and a U-Pb apatite age of 875 ± 8 Ma (Fig. 4) with a $^{207}Pb/^{206}Pb$ initial ratio derived from the unanchored Tera-Wasserburg Concordia intercept of 0.880 ± 0.025.

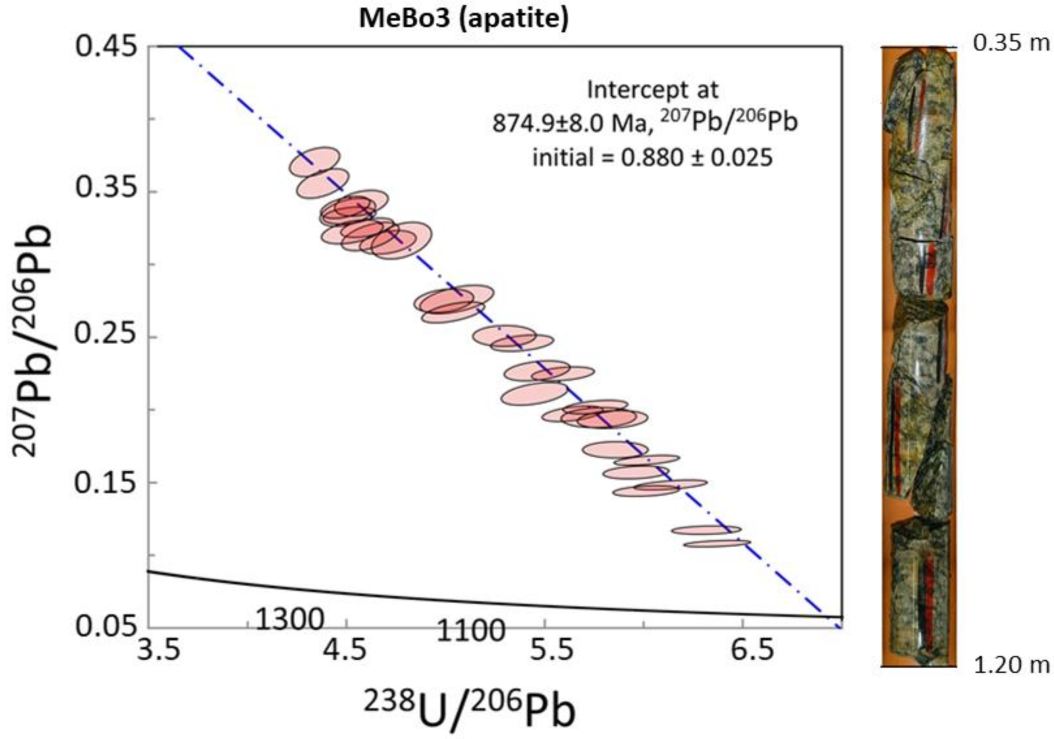

Figure 4. U-Pb apatite concordia plot from the MeBo3 sample (displayed to the right), with a Tera-Wasserburg Concordia intercept of 0.880 ± 0.025.

Clasts in the MeBo2 core include amphibolite, metagabbro and foliated gneiss. U-Pb zircon dating of four clasts from MeBo2 yield dates that span from c. 480 to 500 Ma. All samples yield analytical ellipses that are slightly dispersed along concordia, and so weighted mean $^{206}Pb/^{238}U$ ages are employed. Clast 7.02 (foliated gneiss, Fig. 5A) yields a weighted mean $^{206}Pb/^{238}U$ magmatic crystallization protolith age of 482.3 ± 2.6 (Fig. 5B). Clast 7.13 (amphibolite, Fig. 5C) yields a weighted mean $^{206}Pb/^{238}U$ crystallization age of 484.9 ± 2.3 Ma (Fig. 5D). Clast 7.58 (foliated gneiss, Fig. 5E-F) yields a population of inherited grains from c. 1640 Ma to 1750 Ma (Fig. 5E), and a weighted mean $^{206}Pb/^{238}U$ age of 478.3 ± 3.1 Ma interpreted as the age of magmatic crystallization (Fig. 5G). Clast sample 8.08 (foliated gneiss, Fig. 5H-I) also yields inherited zircons spanning from c. 1300-1750 Ma (Fig. 5I) in age, and a weighted mean $^{206}Pb/^{238}U$ age of 500.8 ± 3.6 Ma interpreted as the age of crystallization (Fig. 5J). Apatite U-Pb dating of the same clast yields an intercept of 384.6 ± 7 Ma (Fig. 5K) with a $^{207}Pb/^{206}Pb$ initial ratio derived from the unanchored Tera-Wasserburg Concordia intercept of 0.847 ± 0.021.

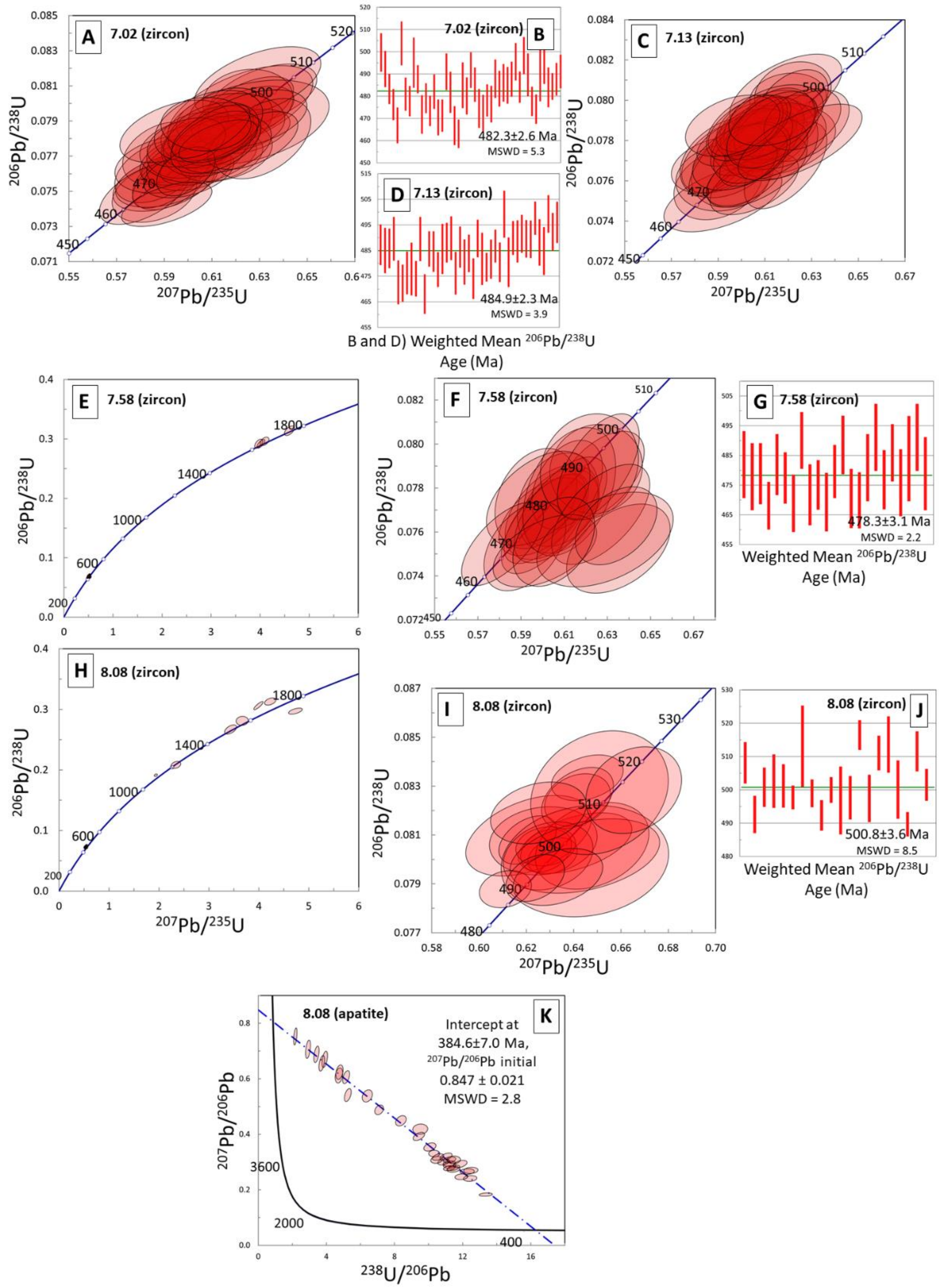

Figure 5. Concordia diagrams and weighted mean $^{206}Pb/^{238}U$ ages of clasts from the MeBo2 core. A) Concordia and B) weighted mean $^{206}Pb/^{238}U$ age of clast 7.02 (foliated gneiss); C) Concordia and D) weighted mean $^{206}Pb/^{238}U$ ages of clast 7.13 (amphibolite); E) Concordia (all crystals), F) Concordia (crystals constraining the igneous crystallization age) and G) weighted mean $^{206}Pb/^{238}U$ age of clast 7.58 (foliated gneiss); H) Concordia (all crystals), I) Concordia (crystals constraining the igneous crystallization age) and J) weighted mean $^{206}Pb/^{238}U$ age of clast 8.08 (foliated gneiss); K) U-Pb apatite Tera-Wasserburg concordia plot of clast 8.08 (foliated gneiss).

4.2 2011 Dredge samples

Samples collected during the 2011 expedition are classified as quartzo-feldspathic psammites and termed the Porcupine High Metasedimentary Sequence (PHMS). For comparison to potential sources, Pb isotopic analysis was undertaken on detrital psammite dredge samples PH4, PH5, PH12, and PH14. Detrital K-feldspars exhibit a Pb isotope composition with a closer affinity to the Annagh Gneiss Complex, with some correspondence to the Rockall Bank (Fig. 6).

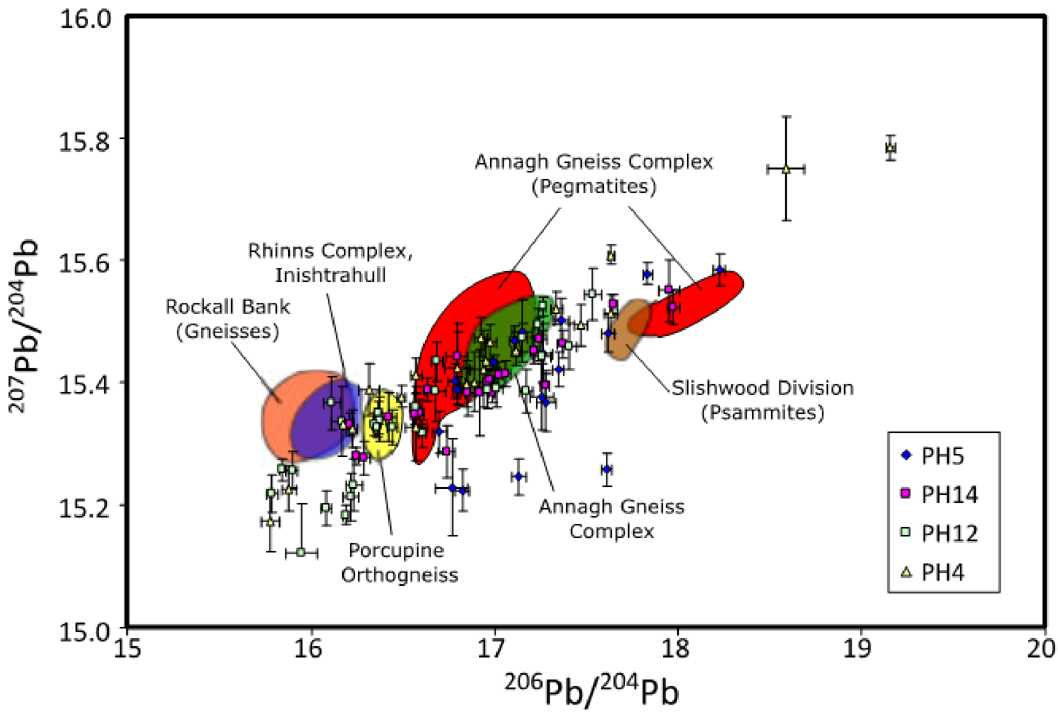

Figure 6. Plot of the Pb isotopic composition of detrital K-feldspar of the PHMS. Data are compared with the Pb isotopic composition of gneisses of the Rockall Bank and pegmatites of the AGC.

All PH samples (PH-1, 4, 5, 9, 10, 11, 12, 15) yield similar U-Pb detrital zircon spectra, and so the data (n = 540) are plotted on a composite probability density diagram which spans an age range of 950-2700 Ma (Fig. 7a). There are significant peaks at c. 950 – 1200 Ma, 1500 and 1750 Ma and a very small cluster of grains between c. 2500-2800 Ma. The U-Pb zircon ages of these peaks are discussed in section 5.2.1. A composite probability density diagram of U-Pb apatite ages (n = 110) of samples 1, 4, 5, 10, and 12 yields a main peak of 800-1000 Ma with a subsidiary peak at 1300-1800 Ma and a solitary grain at 2700 Ma (Fig. 7b).

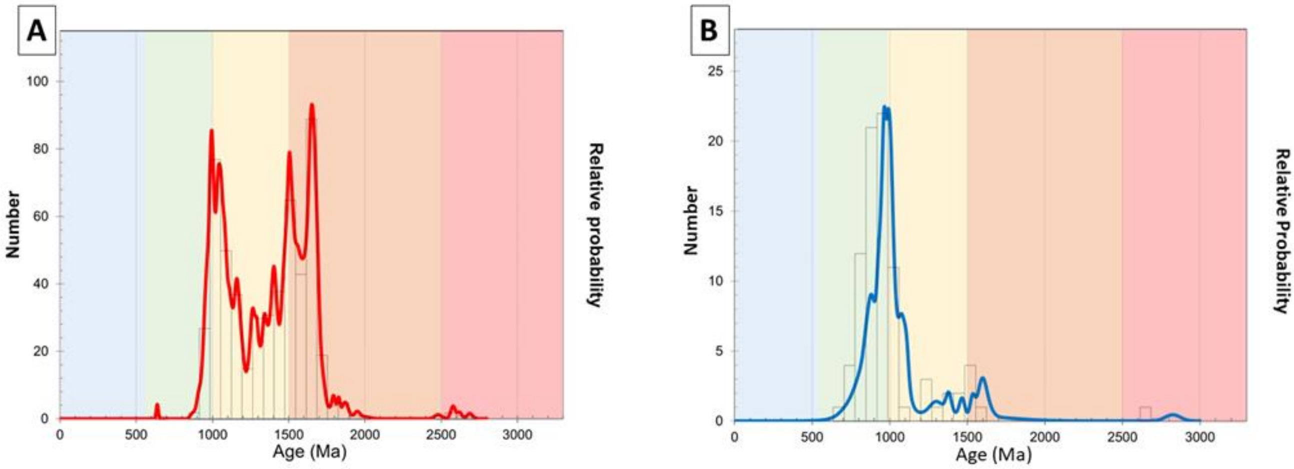

Figure 7. U-Pb age probability density diagrams of (A) zircon from all PHMS dredge samples and (B) apatite (samples PH 1,4,5,10, 12) collected during the 2011 sampling expedition. The coloured bands represent the Phanerozoic (blue), Neoproterozoic (green), Mesoproterozoic (yellow), Palaeoproterozoic (orange) and Archean (red).

4.3 2014 Dredge samples

Dredge samples from the 2014 sampling expedition can be divided into four groups (i-iv) based on their U-Pb zircon and apatite crystallization ages and Pb isotope-in-K-feldspar terrane affinity (hereafter referred to as 'Pb-in-Kfsp'; Fig. 8). Many of the Neoarchean and Paleoproterozoic U-Pb zircon age data are affected by minor reverse discordance, which is attributed to minor metamictization and greater downhole U-Pb fractionation compared to the U-Pb zircon age reference materials. Hence weighted mean $^{207}Pb/^{206}Pb$ ages (which are unaffected by variable downhole fraction behaviour) are presented for all zircons with ± 5% discordance ($^{206}Pb/^{238}U$ *vs* $^{207}Pb/^{235}U$).

(i) Samples 402-1, 402-2, 402-8, and 402-11 yield U-Pb zircon dates of c. 2750 Ma and U-Pb apatite ages of c. 1750 Ma (Fig. 9). Sample 402-1 (banded gneiss) yields a highly dispersed U-Pb zircon upper intercept age of 2831 ± 21 Ma (Fig. 9A),a weighted mean $^{207}Pb/^{206}Pb$ age of 2838 ± 19 Ma (Fig. 9B), and a U-Pb apatite Tera-Wasserburg lower intercept age of 1762 ± 24 (Fig. 9C). Sample 402-2 (lineated granite) yields a U-Pb zircon upper intercept age of 2789 ± 11 Ma (Fig. 9D) and a weighted mean $^{207}Pb/^{206}Pb$ age of 2809.5 ± 7.2 Ma (Fig. 9E). Sample 402-8 (banded grey gneiss) yields a U-Pb zircon upper intercept age of 2945.1 ± 22 Ma (Fig. 9F), a weighted mean ^{207}Pb/^{206}Pb age of 2879 ± 17 Ma (Fig. 9G) and a U-Pb apatite Tera-Wasserburg lower intercept age of 1819 ± 58 Ma (Fig. 9H). Sample 402-11 (gneiss) yields a U-Pb zircon upper intercept age of 2804.2 ± 6.7 Ma (Fig. 9I), a weighted mean ^{207}Pb/^{206}Pb age of 2801.4 ± 3.8 Ma (Fig. 9J) and a U-Pb apatite Tera-Wasserburg lower intercept age of 1772 ± 45 Ma (Fig. 9K).

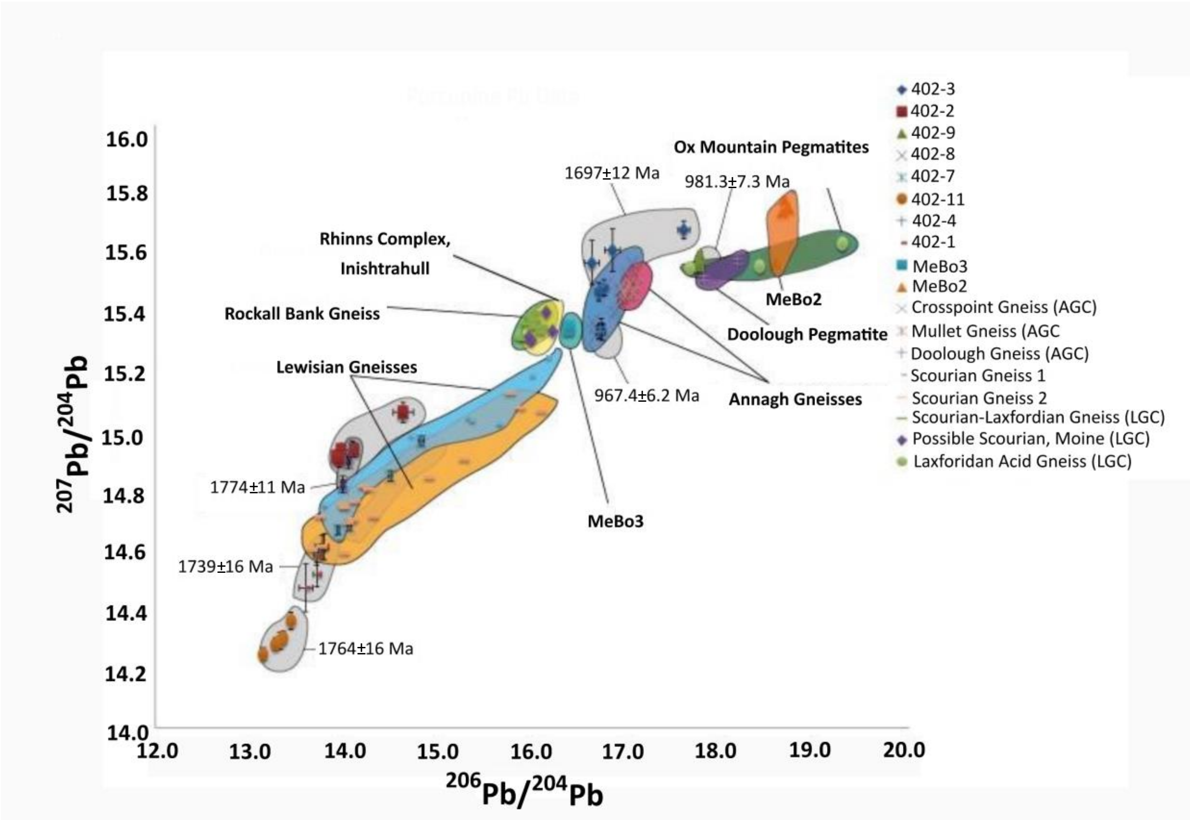

Figure 8. Plot of the Pb isotope-in-K-feldspar for the 2014 dredge samples and a comparison with data from related terranes.

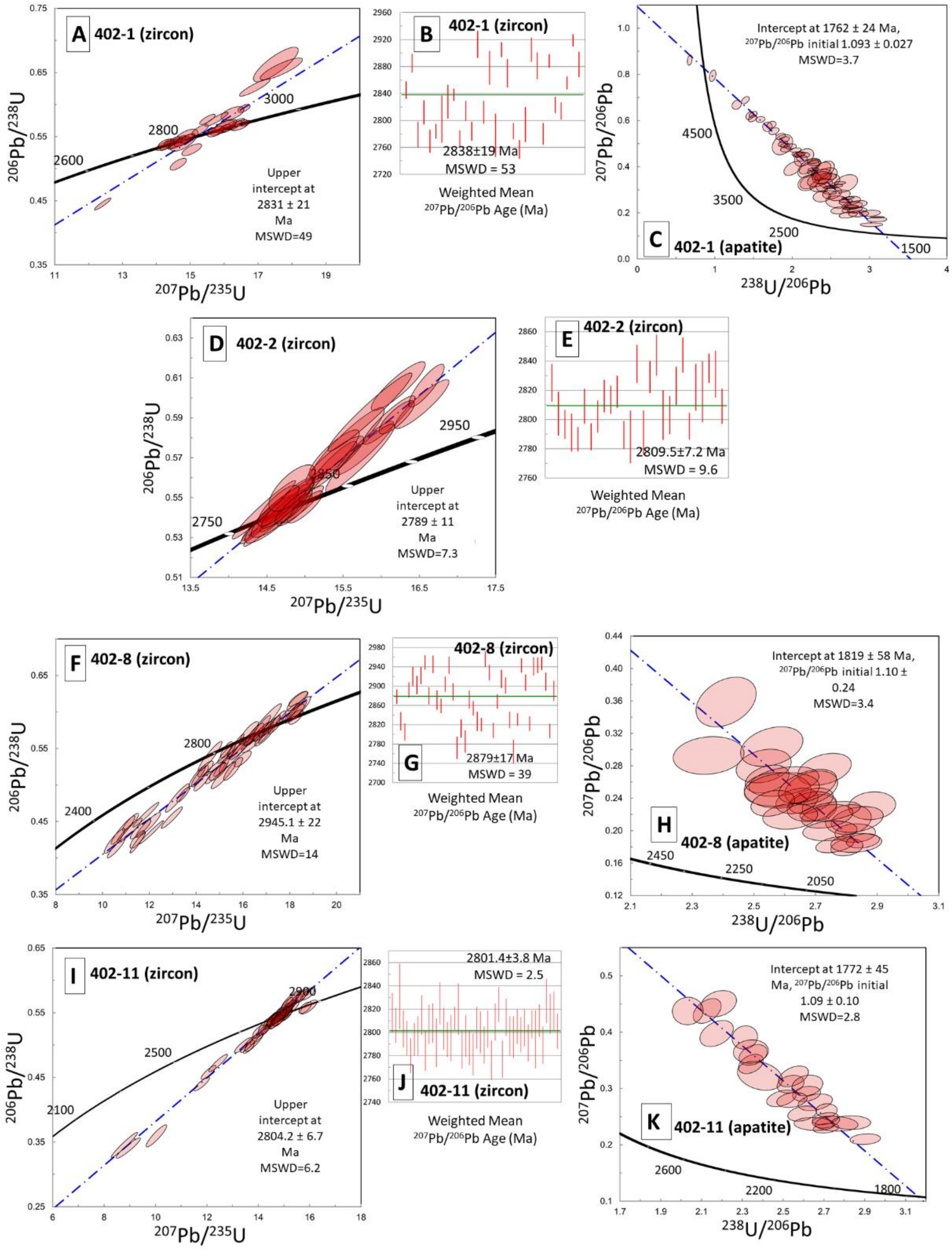
A 402-1 (zircon)
Upper intercept at 2831 ± 21 Ma MSWD=49
B 402-1 (zircon)
2838±19 Ma MSWD = 53
Weighted Mean $^{207}Pb/^{206}Pb$ Age (Ma)
C 402-1 (apatite)
Intercept at 1762 ± 24 Ma, $^{207}Pb/^{206}Pb$ initial 1.093 ± 0.027 MSWD=3.7
D 402-2 (zircon)
Upper intercept at 2789 ± 11 Ma MSWD=7.3
E 402-2 (zircon)
2809.5±7.2 Ma MSWD = 9.6
Weighted Mean $^{207}Pb/^{206}Pb$ Age (Ma)
F 402-8 (zircon)
Upper intercept at 2945.1 ± 22 Ma MSWD=14
G 402-8 (zircon)
2879±17 Ma MSWD = 39
Weighted Mean $^{207}Pb/^{206}Pb$ Age (Ma)
H 402-8 (apatite)
Intercept at 1819 ± 58 Ma, $^{207}Pb/^{206}Pb$ initial 1.10 ± 0.24 MSWD=3.4
I 402-11 (zircon)
Upper intercept at 2804.2 ± 6.7 Ma MSWD=6.2
J 402-11 (zircon)
2801.4±3.8 Ma MSWD = 2.5
Weighted Mean $^{207}Pb/^{206}Pb$ Age (Ma)
K 402-11 (apatite)
Intercept at 1772 ± 45 Ma, $^{207}Pb/^{206}Pb$ initial 1.09 ± 0.10 MSWD=2.8
$^{206}Pb/^{238}U$
$^{207}Pb/^{235}U$
$^{207}Pb/^{206}Pb$
$^{238}U/^{206}Pb$

Figure 9. 2014 dredge samples with a Lewisian Pb-in-Kfsp affinity and yielding U-Pb zircon dates of c. 2750 Ma and U-Pb apatite ages of c. 1750 Ma. A) 402-1 (banded gneiss) with U-Pb zircon age, B) weighted mean $^{207}Pb/^{206}Pb$ age and C) U-Pb apatite age; D) 402-2 (lineated granite) with U-Pb zircon age and E) weighted mean $^{207}Pb/^{206}Pb$ age; F) 402-8 (banded gneiss) with U-Pb zircon age, G) weighted mean $^{207}Pb/^{206}Pb$ age and H) U-Pb apatite age; I) 402-11 (gneiss) with U-Pb zircon age, J) weighted mean $^{207}Pb/^{206}Pb$ age and K) U-Pb apatite age.

ii) Samples 303-1 and 402-3 possess an AGC Pb-in-Kfsp affinity and yield U-Pb zircon ages of c. 1940-1890 Ma and U-Pb apatite ages of c. 1750 Ma (Fig. 10). Sample 303-1 (amphibolite) yields a U-Pb zircon upper intercept age of age of 1831.5 ± 6.0 (Fig. 10A), a weighted mean $^{207}Pb/^{206}Pb$ age of 1831.6 ± 5.5 Ma (Fig. 10B) and a U-Pb apatite Tera-Wasserburg lower intercept age of 1759 ± 20 Ma (Fig. 10C). Sample 402-3 (foliated, banded gneiss) yields a U-Pb zircon upper intercept age of age of 1939 ± 12 Ma (Fig. 10D), a weighted mean $^{207}Pb/^{206}Pb$ age of 1938 ± 10 Ma (Fig. 10E) and a U-Pb apatite Tera-Wasserburg lower intercept age of age of 1681 ± 21 (Fig. 10F).

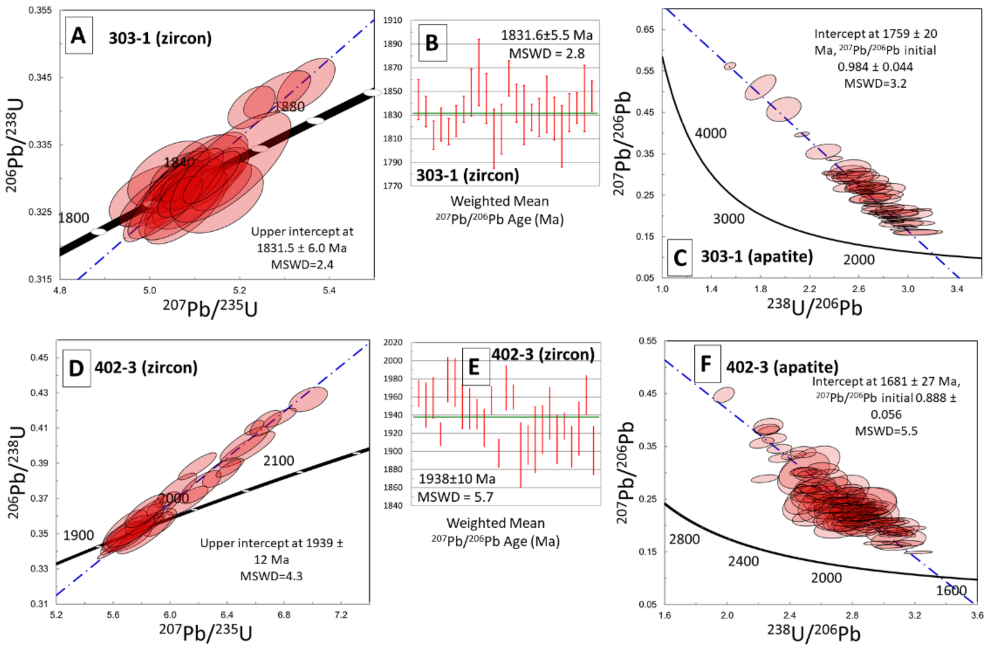

Figure 10. 2014 dredge samples with an AGC Pb-in-Kfsp affinity and yielding U-Pb zircon ages of c. 1940-1890 Ma and U-Pb apatite ages of c. 1750 Ma A) 303-1 (amphibolite) with U-Pb zircon intercept age with B) weighted mean $^{207}Pb/^{206}Pb$ age and C) U-Pb apatite age; D) 402-3 (foliated, banded gneiss) with U-Pb zircon intercept age, E) weighted mean $^{207}Pb/^{206}Pb$ age and F) U-Pb apatite age.

iii) Samples 402-4 (banded pink gneiss) and 402-9 (banded pink-grey gneiss) yield U-Pb zircon ages of c. 1650-1550 Ma and U-Pb apatite ages recording post-Grenville cooling (Fig. 11). Sample 402-4 (banded pink gneiss) yields a U-Pb zircon upper intercept age of 1635 ± 11 Ma (Fig. 11A), a weighted mean $^{207}Pb/^{206}Pb$ age of 1621.8 ± 9.0 (Fig. 11B) and a U-Pb apatite Tera-Wasserburg lower intercept age of 967 ± 10 Ma (Fig. 11C). Sample 402-9 (banded pink-grey gneiss) yields a U-Pb zircon upper intercept age of 1550 ± 14 Ma (Fig. 11D), a weighted mean $^{207}Pb/^{206}Pb$ age of 1512.1 ± 8.8 Ma (Fig. 11E) and a U-Pb apatite Tera-Wasserburg lower intercept age of 974 ± 11 Ma (Fig. 11F).

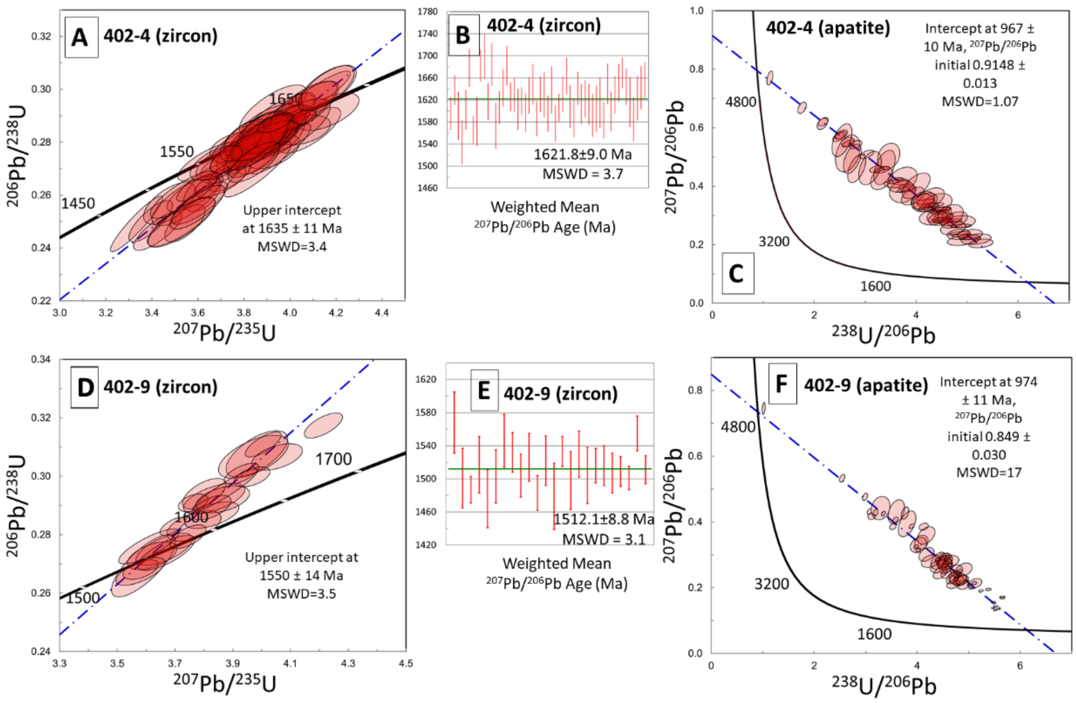

Figure 11. 2014 dredge samples with an AGC Pb-in-Kfsp affinity and yieldg U-Pb zircon ages of c. 1650-1550 Ma and U-Pb apatite ages and U-Pb apatite ages recording post-Grenville cooling. A) 402-4 (banded pink gneiss) with U-Pb zircon age, B) weighted mean $^{207}Pb/^{206}Pb$ age and C) U-Pb apatite age; D) 402-9 (banded pink-grey gneiss) with U-Pb zircon age, E) weighted mean $^{207}Pb/^{206}Pb$ age and F) U-Pb apatite age.

iv) Two samples do not conveniently fit into any of the above three groupings. Sample 402-13 (lineated amphibolite) yields a weighted mean $^{207}Pb/^{206}Pb$ age of 2015.3 ± 8.7 Ma (Fig. 12B) and a U-Pb apatite Tera-Wasserburg lower intercept age of 1120 ± 100 (Fig. 12C). Sample 204-1 is a mica schist which yields U-Pb detrital zircon ages ranging from c. 950-2800 Ma, with peaks clustering at c. 1000 Ma and c. 1400-1700 Ma (Fig. 12D). Sample 302-1 is a psammite which yields U-Pb detrital zircon ages ranging from c. 450-3000 Ma, with major peaks clustering between c. 800-1800 Ma and between c. 2600-3100 Ma (Fig. 12E).

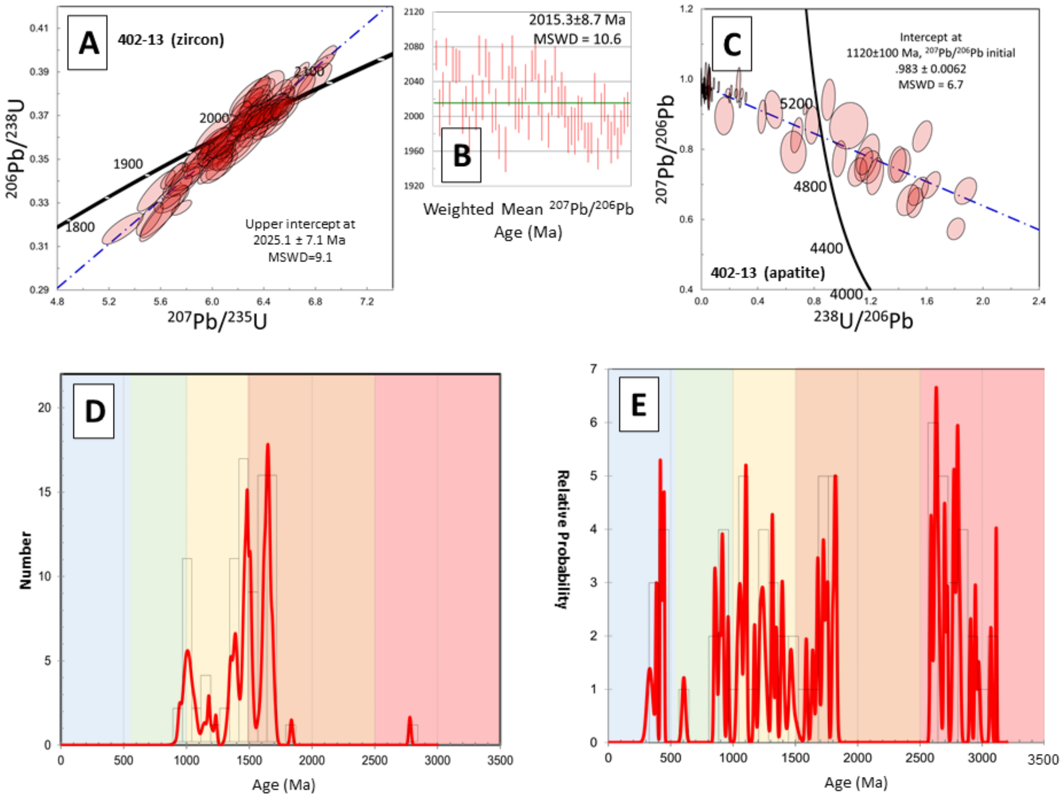

Figure 12. Concordia plots of 402-13 (lineated amphibolite) with A) U-Pb zircon age, B) weighted mean $^{207}Pb/^{206}Pb$ age and C) U-Pb apatite age. U-Pb zircon age probability density diagrams of D) sample 204-1 (mica schist) and E) 302-1 (psammite).

Table 1: Characteristics of samples collected in the 2006, 2011, and 2014 Porcupine High expeditions.						
Suite	**Sample**	**Lithology**	**U-Pb zircon age (Ma)**	**U-Pb apatite age (Ma)**	**Pb-in-Kfsp Affinity**	**Conference Abstract/Report**
2006 25/27-sb(MeBo) Cores	7.02	Foliated gneiss	482.3±2.6 Ma			
	7.13	Amphibolite	484.9±2.3 Ma			
	7.58	Foliated gneiss	478.3±3.1 Ma			
	8.08	Foliated gneiss	500.8±3.6 Ma	384.6±7 Ma		
	MeBo3	Orthogneiss	1314±6 Ma	874.9±8 Ma		Daly et al., 2008; Chew et al., 2019
2011 Dredge Samples	PH1	Psammite	c. 800-1800 Ma	c. 900-1800 Ma		Tyrrell, 2013
	PH4	Psammite	c. 800-1800 Ma	c. 900-1800 Ma	AGC	Tyrrell, 2013
	PH5	Psammite	c. 800-1800 Ma	c. 900-1800 Ma	AGC	Tyrrell, 2013
	PH 9	Psammite	c.1000-1800 Ma, c.2500-2600 Ma			Tyrrell, 2013
	PH10	Psammite	c. 800-1800 Ma	c.900-1800 Ma		Tyrrell, 2013
	PH 11	Psammite	c. 900-1900, c. 2650			Tyrrell, 2013
	PH12	Psammite	c. 800-1800 Ma	c. 900-1800 Ma	AGC	Tyrrell, 2013
	PH 14	Psammite			AGC	Tyrrell, 2013
	PH 15	Psammite	c. 900-1900			Tyrrell, 2013
i) Kfsp Affinity with Lewisian and U-Pb zircon ages of c. 2750 Ma and U-Pb apatite ages of c. 1750 Ma						
2014 Dredge Samples	402-1	Banded gneiss	2831±21 Ma	1762±24 Ma	Lewisian	Barry et al., 2017
	402-2	Lineated granite	2789±11 Ma			Barry et al., 2017
	402-8	Banded grey gneiss	2945.1±22 Ma	1819±58 Ma	Lewisian	Barry et al., 2017
	402-11	Crystalline metamorphic rock, likely gneiss	2804.2±6.7 Ma	1772±45 Ma	Lewisian	Barry et al., 2017
ii) Kfsp Affinity with AGC and U-Pb zircon ages of c. 1940-1890 Ma and U-Pb apatite ages of c. 1750 Ma						
2014 Dredge Samples	303-1	Amphibolite	1831.5±6.0 Ma	1759±20 Ma		Barry et al., 2017
	402-3	Foliated, banded gneisss	1939 ±12 Ma	1681±27 Ma	AGC	Barry et al., 2017
iii) Kfsp affinity with AGC and U-Pb zircon ages of c. 1650-1550 Ma and post-Grenville U-Pb apatite ages						
2014 Dredge Samples	402-4	Banded pink gneiss	1635±11 Ma	967 ± 10 Ma	AGC	Barry et al., 2017; Chew et al., 2019
	402-9	Banded pink-grey gneiss	1550±14 Ma	974±11 Ma	AGC	Barry et al., 2017; Chew et al., 2019
iv) Other samples						
2014 Dredge Samples	204-1	Mica schist replete with K-fsp	950-2800 Ma	1922±57 Ma		Barry et al., 2017
	302-1	Psammite	450-3000 Ma			
	402-13	Lineated amphibolite	2025.1±7.1 Ma	1120±100 Ma		Barry et al., 2017

Table 1. Summary of key features (lithology, Pb-in-fsp affinity and U-Pb zircon and apatite age systematics) of samples from the 2006, 2011 and 2014 Porcupine High sampling campaigns.

5. Discussion

5.1 25/27-sb(MeBo) Cores

The U-Pb zircon dates of samples from the MeBo2 core indicate crystallization at c. 500-478 Ma (Fig. 5, Table 1). Inherited zircons in sample 7.58 (foliated gneiss) also yield dates of c. 1700 - 1800 Ma. The crystallization ages of c. 500-478 Ma likely correlate with the c. 510-490 Ma ophiolitic rocks in the Clew Bay Complex (Chew et al., 2010, see section 2.5.2) in Western Ireland. In western Ireland, these supra-subduction ophiolite rocks are separated by the Fair Head – Clew Bay line (the Irish continuation of the Highland Boundary Fault) from Laurentian margin rocks (the Dalradian Supergroup) to the north (Chew et al., 2010). This occurrence is consistent with deformed Laurentian margin cover sequences (e.g. the Dalradian Supergroup) that can be found to the north of the MeBo2 drill site. The U-Pb apatite age of 384.6 ± 7 Ma from sample 8.08 (U-Pb zircon crystallization age of 500.8 ± 3.6 Ma) at the MeBo2 drill site is considerably younger than the U-Pb apatite ages of all other samples in this study, and likely reflects prolonged residence (c. 100 Ma) above the apatite U-Pb closure temperature (c. 400 – 550 °C) until the termination of the Caledonian orogeny at c. 390 Ma. Although the MeBo2 clasts in this putative rocky shoreline deposit are not *in situ*, their similar U-Pb zircon ages (c. 500-478 Ma) strongly support a proximal source.

The second of the MeBo cores, Borehole 25/7-sb(MeBo)3, is comprised of 0.85 m of a weakly foliated orthogneiss, known as the North Porcupine High Orthogneiss (NPHO) (Daly et al., 2008). This orthogneiss yields a U-Pb zircon age of 1314 ± 6 Ma, an age of magmatism not previously recognized in the region, and was followed by granulite-facies metamorphism (12 kbar, 740°C) of likely Grenville age (Daly et al., 2008a; section 3.1.1). The U-Pb apatite age of 874.9 ± 8 Ma reported in this study from the MeBo3 core (Fig. 4, Table 1) likely reflects post-metamorphic cooling following the Grenville orogeny.

5.2 Dredge samples

5.2.1 2011 Suite

The lower greenschist-facies psammite cobbles of the PHMS sampled during the 2011 dredging expedition yield detrital U-Pb zircon ages consistent with derivation from the Laurentian margin (*cf* Cawood and Nemchin, 2001). In particular, the U-Pb detrital zircon spectra on the composite probability density diagram in (Figure 7a), with peaks at c. 950 – 1200 Ma, 1500 and 1750 Ma and a very minor peak at c. 2500-2800 Ma, strongly resemble those of the Grampian Group (basal Dalradian Supergroup) or the Moine Supergroup (*cf* Cawood et al., 2003). The U-Pb apatite ages of samples PH 1, PH, 4, PH 5, PH 10, and PH 12 yield a main peak from 800-1000 Ma with a subsidiary peak at 1300-1800 Ma.In comparison, the U-Pb zircon spectra exhibit an approximately equal abundance of Grenvillian *vs* Paleoproterozoic detritus. It is probable that regional Grenvillian metamorphism in the source terrane(s) of the PHMS recrystallized or reset primary Archean or Paleoproterozoic apatite. In contrast, detrital apatite ages in the PHMS were not age reset during the Caledonian orogeny, which is consistent with the lower greenschist-facies metamorphic assemblages seen in the PHMS samples. Pb isotope analysis of detrital K-feldspars from the psammite cobbles (section 4.2) indicates that the source of the cobbles shares an affinity with the Annagh Gneiss Complex (AGC; section 2.2.1 and 2.3).

5.2.2. 2014 Suite

The samples from the 2014 suite are derived from multiple sources in the North Atlantic region, including samples from a single site (e.g. site 402). The samples are considered in three groups developed in section 4.3 and listed in Table 1 (Pb-in-Kfsp affinity, and zircon and apatite U-Pb ages).

The first group (Fig. 9; group (i) in Table 1), consists of samples 402-1 (banded gneiss), 402-2 (lineated granite), 402-8 (K-feldspar banded gneiss), and 402-11 (gneiss), and exhibits a Lewisian Pb-in-Kfsp affinity, U-Pb zircon ages of c. 2750 Ma and U-Pb apatite ages of c. 1750 Ma. The Lewisian Pb isotopic affinity and the U-Pb zircon crystallization ages of c. 2750 Ma strongly indicate the Lewisian Complex is a likely source; the U-Pb apatite ages of c. 1750 Ma in these samples likely reflect derivation from Lewisian rocks that had undergone Laxfordian metamorphism.

The second group of clasts (Fig. 10; group (ii) in Table 1), comprises samples 303-1 (amphibolite) and 402-3 (foliated, banded gneiss). They yield U-Pb zircon (c. 1940-1890 Ma) and apatite (c. 1750 Ma) ages that correlate with a Paleoproterozoic source. Although these samples exhibit a Pb-in-Kfsp affinity with the AGC, the lack of any major Grenvillian tectonothermal pulse as evidenced by the Late Paleoproterozoic U-Pb apatite ages is incompatible with sourcing from the present-day AGC outcrop which has experienced ubiquitous Grenvillian metamorphism.

The third group, consisting of samples 402-4 (pink banded gneiss) and 402-9 (banded gneiss) (Fig. 11; group (iii) in Table 1) yields U-Pb zircon ages of c. 1650-1550 Ma with U-Pb apatite dates of c. 970 Ma suggestive of post-Grenvillian cooling, and a Pb-in-Kfsp affinity with the AGC, although the pre-Caledonian U-Pb apatite ages rule out derivation from the present-day outcrop of the AGC which yields Grampian U-Pb ages (Henrichs et al., 2018).

The remaining samples (group (iv) in Table 1) are discussed in turn. Sample 402-13 (lineated amphibolite) (Fig. 12A-C) yields a U-Pb zircon age (2015.3 ± 8.7 Ma). A U-Pb zircon age of c. 2015 Ma is pene-contemporaneous with the emplacement of the c. 2030-2050 Ma Kangâmiut dykes in western Greenland and equivalent dykes in the eastern Nain Province in Canada (e.g. Buchan and Ernst, 2004; Mayborn and Lesher, 2006; Nilsson et al., 2013), and with the 1992 ± 3 Ma Strathan dyke in the Lewisian Complex (Heaman and Tarney, 1989; section 2.1.1).

Detrital sample 204-1 (mica schist) (Fig. 12D), which was sampled northeast of the 402 site, exhibits a range of ages (c. 950-2800 Ma) comparable to the Grampian Group of the Dalradian Supergroup or the Moine Supergroup, and also to the PHMS samples. The U-Pb detrital zircon spectrum of sample 302-1 (psammite) on the probability density diagram presented in Fig. 12E resembles that of the Upper Dalradian (Cawood et al., 2007), but also contain a Caledonian age peak of c. 415-460 Ma. This unit likely represents a metasedimentary sequence derived from a composite terrane of Upper Dalradian metasedimentary rocks (or equivalents) intruded by Caledonian granites. The age of metamorphism in sample 302-1 is constrained by the presence of the youngest detrital zircon (415 ± 7 Ma). The majority of dredge samples in the 2014 suite was collected at site 402. The large variation in lithology, U-Pb zircon and apatite ages and Pb-in-feldspar isotope systematics exhibited by these samples suggests their present-day juxtaposition is due to Quaternary glacial transport. This is supported by the large distance (c. 500 km in the present-day) between the Porcupine High and the nearest sources of rocks (Lewisian Complex, northern Rockall High) with Archean U-Pb zircon crystallization ages (Fig.14a).

5.3 Correlation with Magnetic Data

The Grampian Terrane of Ireland and Scotland is broadly associated with a magnetic anomaly low (Riddihough and Max, 1976). In Co. Mayo, Ireland, a sharp boundary between a low magnetic anomaly in the north and a high magnetic anomaly in the south, which follows the inferred location of the Fair Head – Clew Bay Line (FHCBL) and separates weakly magnetic Neoproterozoic metasediments north of the Laurentian margin (the Dalradian Supergroup) from highly magnetic volcanic arc and accretionary sediments of the Northwestern Terrane to the south (Fig. 13).

A similar sharp E-W trending magnetic boundary occurs on the Porcupine High south of the summit (Fig. 13). The highly magnetic basement south of the lineament has a magnetic expression indistinguishable from the basement south of the FHCBL and likely represents similar peri-Laurentia arc-related metamorphosed volcanic and sedimentary rocks (Fig. 13). The poorly magnetic basement north of the lineament has previously been interpreted as Paleozoic (meta)sedimentary rocks characterised by low magnetisation but higher densities than Cenozoic or Mesozoic sedimentary rocks (Young and Bailey, 1974; Riddihough and Max, 1976; Kimbell et al., 2010).

The dredged PHMS psammites at localities PH10 and PH14 are found within or very close to this low magnetic anomaly. Samples PH1, 4 and 5 are located above a positive magnetic anomaly interpreted as an igneous centre (Tate and Dobson, 1988). The presence of these psammites suggests that the igneous centre is still buried. The NPHO drilled by 25/7-sb(MeBo)3 is also located within the magnetic low, which suggests that it is small as older basement would probably result in a regional magnetic high (Fig 14b). These characteristics are similar to the Annagh Gneiss Complex in NW Co. Mayo, which has an aerial extent of c. 60 km^2 but is not associated with a magnetic high (Fig. 13).

Based on the newly acquired ages, the magnetic anomaly pattern is interpreted to represent the footprint of a Neoproterozoic Dalradian basin with one (or more) inlier(s) of Paleoproterozoic gneiss (Fig. 14b) and a buried Paleogene igneous centre (Fig. 13). The sharp magnetic boundary on Porcupine High is interpreted to represent a terrane boundary and Caledonian lineament, the along-strike continuation of the FHCBL (Fig. 13, Fig. 14b). Although Kimbell et al. (2010) suggested that this magnetic boundary could be the offshore continuation of the Skerd Rocks-Southern Upland Fault, it is possible that these faults have merged to the east of the Porcupine High (Fig. 13, Fig. 14b).

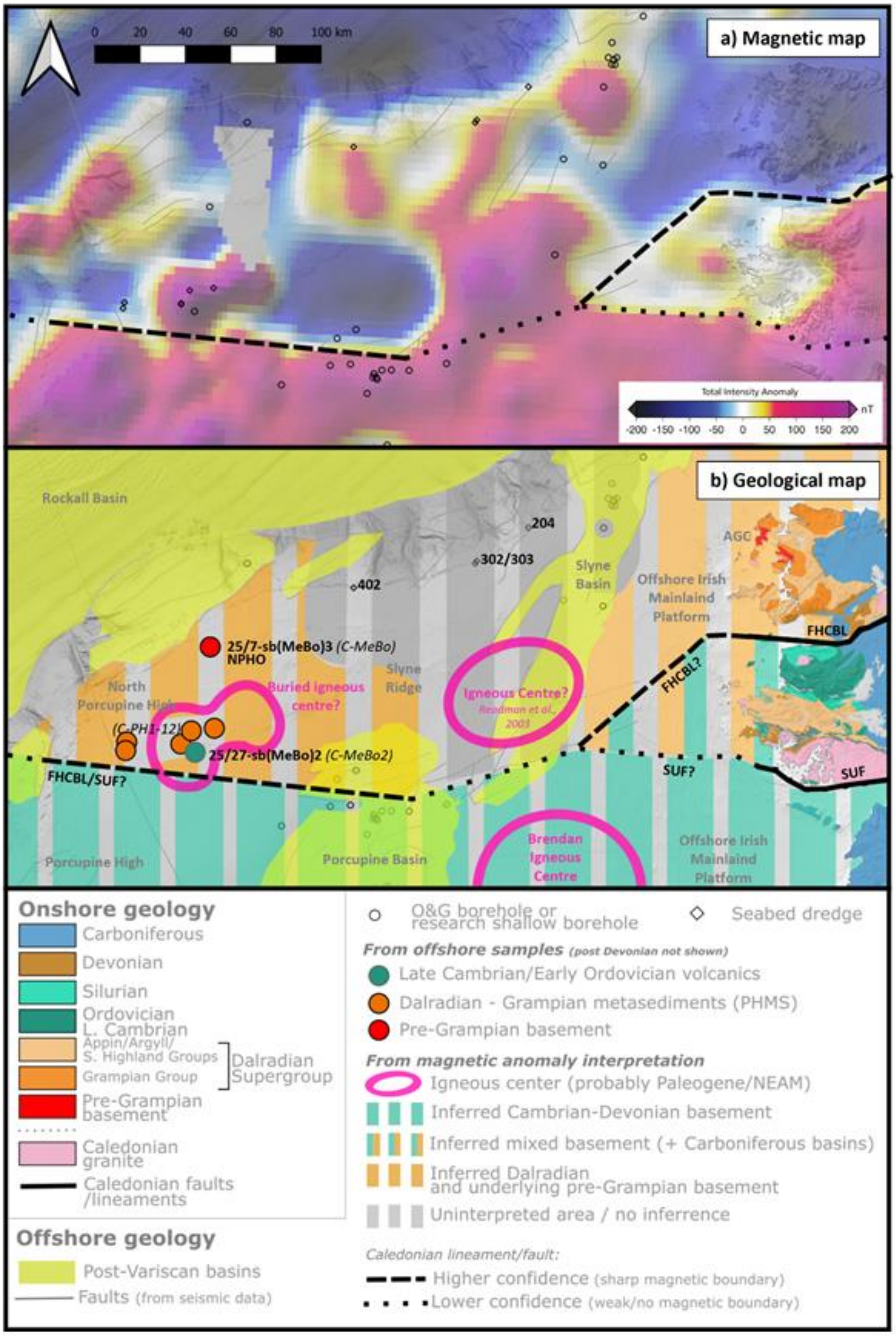

Figure 13. Magnetic and geological map of the basement of the North Porcupine High and surrounding areas. AGC=Annagh Gneiss Complex, FHCBL=Fair Head-Clew Bay line, NPHO=North Porcupine High Orthogneiss, SUF=Southern Uplands Fault.

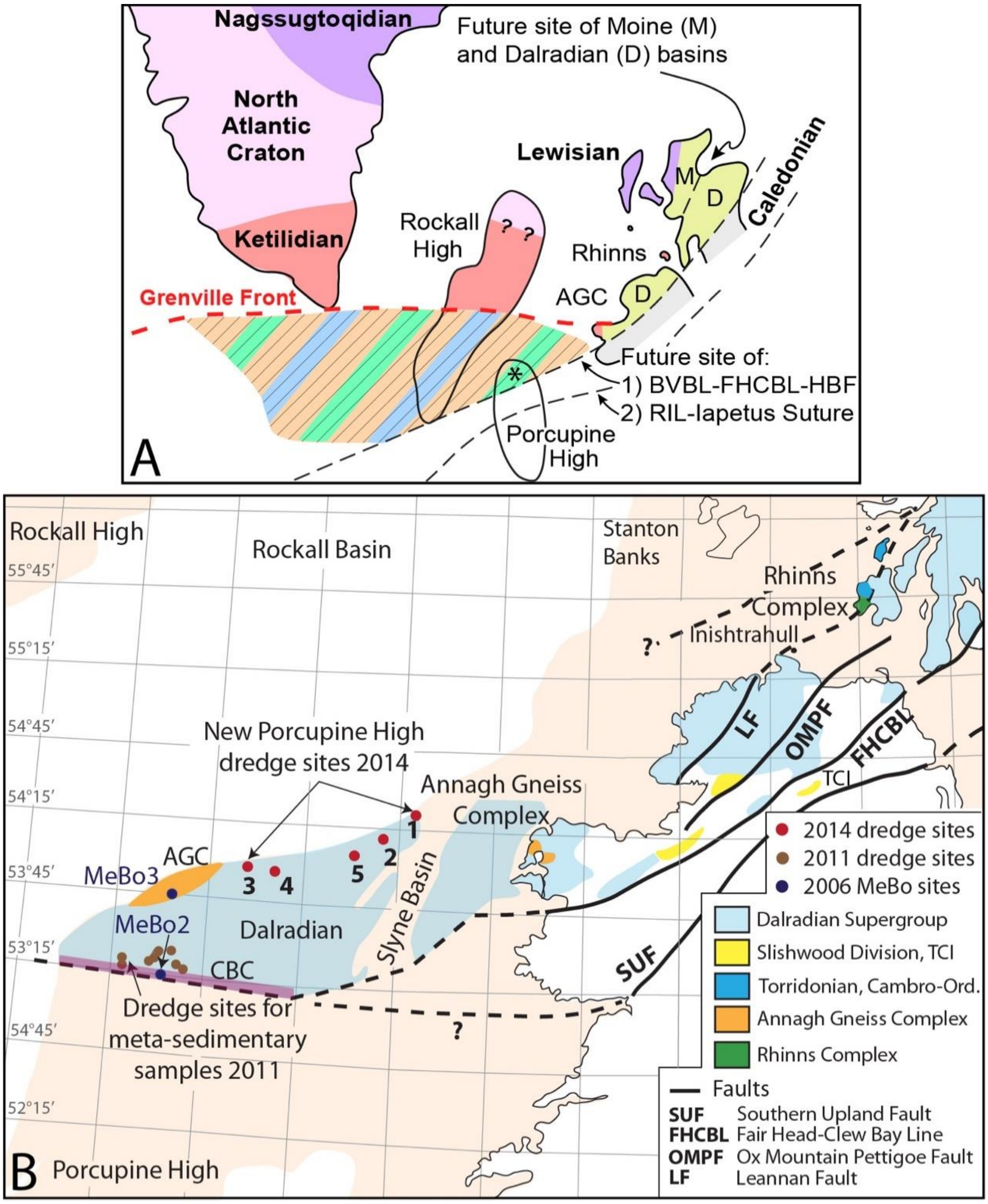

Figure 14. (a) The schematic palaeogeographic reconstruction of the North Atlantic region at ca. 900 Ma from Fig. 1, focussing on the geology adjacent to the northern Porcupine High. The significant distance between the Porcupine High and the nearest sources of rocks (Lewisian Complex, northern Rockall High) with Archean U-Pb zircon crystallization ages means that Quaternary glacial transport must be invoked for some of the 2014 dredge samples. (b) Regional geological map of the northern Porcupine High region. Purple band (CBC) denotes the likely continuation of the Clew Bay Complex; the MeBo3 core represents a Paleoproterozoic inlier of presumed AGC affinity (orange,) but similar to the 2011 dredge samples lacks a pronounced Caledonian thermal overprint. Other such Paleoproterozoic inliers may be present in the northern Porcupine High and in between the Slyne Basin and the NW Irish mainland but cannot be detected based on their magnetic anomalies.

6. Conclusions

Geochronological data from three offshores sampling expeditions yield valuable new constraints on the basement geology of the Porcupine High north of the Iapetus Suture (Fig. 14). The southernmost samples (the MeBo2 core) yield U-Pb zircon ages of c. 500-478 Ma and are correlated with the ophiolitic rocks of the Clew Bay Complex. A 385 Ma apatite U-Pb age records post-Caledonian exhumation; Pb-in-Kfsp data imply a Caledonian affinity. These rocks were sampled adjacent to an E-W trending magnetic boundary extending across the Porcupine High that we interpret as the along-strike continuation of the Fair Head - Clew Bay line (Fig. 14b). To the north on a magnetic anomaly low, dredged lower greenschist-facies psammite cobbles likely represent clasts of local Grampian Group Dalradian, termed the Porcupine High Metasedimentary Sequence (PHMS). Based on the detrital apatite U-Pb age dataset (no ages younger than 800 Ma), the PHMS lacks a strong Caledonian thermal overprint, as does the c. 875 Ma U-Pb apatite age from the North Porcupine High Orthogneiss (NPHO) in the MeBo3 core to the north (Fig. 14b). This orthogneiss yields a U-Pb zircon age of 1314 ± 6 Ma indicative of a period of magmatism not previously known in this sector of the North Atlantic, and which was followed by granulite-facies metamorphism of presumed Grenville age (Daly et al., 2008a).

The dredged metamorphic basement clasts from the 2014 sampling campaign are divided into three groups. The first group yields c. 2750 Ma U-Pb zircon ages and a Pb-in-Kfsp affinity consistent with the Lewisian, and apatite U-Pb ages of 1750 Ma suggestive of Laxfordian metamorphism. The second group of clasts yields 1830-1940 Ma U-Pb zircon ages, 1750 Ma apatite U-Pb ages and an AGC Pb-in-Kfsp affinity. A third group of clasts with 1550-1650 Ma U-Pb zircon ages that are typical of the AGC and has U-Pb apatite ages that record post-Grenville cooling. All three groups were found at one dredge site and a component of Quaternary glacial transport is invoked for these dredged clasts.

Credit authorship contribution statement

Shannon Dennehy: Conceptualization, Data curation, Analysis, Investigation, Writing (original and final draft) and Editing, Funding, Review. **David Chew**: Conceptualization, Analysis, Investigation, Editing, Funding, Review. **Shane Tyrrell**: Investigation, Data curation, Analysis, Editing. **Rémi Rateau**: Investigation, Data curation, Analysis, Editing.

References for Chapter 4 (journal paper)

Atherton, M.P., Ghani, A.A., 2002. Slab breakoff: a model for Caledonian, Late Granite syn-collisional magmatism in the orthotectonic (metamorphic) zone of Scotland and Donegal, Ireland. Lithos 62, 65–85.

Baker, J., Peate, D., Waight, T., and Meyzen, C., 2004, Pb isotopic analysis of standards and samples using a 207 Pb–204 Pb double spike and thallium to correct for mass bias with a double-focusing MC-ICP-MS: Chemical Geology, v. 211, no. 3, p. 275-303

Barham, M., Kirkland, C.L., Hovikoski, J., Alsen, P., Hollis, J. and Tyrrell, S. (2021), Reduce or recycle? Revealing source to sink links through integrated zircon–feldspar provenance fingerprinting. Sedimentology, 68: 531-556

Barry, A., Sun, K., Tyrrell, S., 2017. IS13/10: Sourcelands, sand provenance and supply to North Atlantic margin basins: An integrated, multi-proxy approach (ISPSG Project IS13/10 Final Project Report). PIP.

Beamish, D., Smythe, D.K., 1986. Geophysical images of the deep crust: the Iapetus suture. British Geological Survey 143, 489–497.

Black, L.P., Kamo, S.L., Allen, C.M., Aleinikoff, J.N., Davis, D.W., Korsch, R.J., Foudoulis, C., 2003. TEMORA 1: a new zircon standard for Phanerozoic U–Pb geochronology. Chemical Geology 200, 155–170.

Buchan, K.L., Ernst, R.E., 2004. Diabase dyke swarms and related units in Canada and adjacent regions. Geological Survey of Canada, Map 2022A (scale 1:5,000,000) and Accompanying Notes.

Buchan, K.L., Mertanen, S., Park, R.G., Pesonen, L.J., Elming, S.-Å., Abrahamsen, N., Bylund, G., 2000. Comparing the drift of Laurentia and Baltica in the Proterozoic: the importance of key palaeomagnetic poles. Tectonophysics 319, 167–198.

Cartwright, I., Barnicoat, A.C., 1987. Petrology of Scourian supracrustal rocks and orthogneisses from Stoer, NW Scotland: implications for the geological evolution of the Lewisian complex. Geological Society, London, Special Publications 27, 93–107.

Cawood, P., Strachan, R.A., Cutts, K., Kinny, P., Hand, M., Pisarevsky, S., 2010. Neoproterozoic orogeny along the margin of Rodinia: Valhalla Orogen, North Atlantic. Geology 38, 99–102.

Cawood, P.A., Hawkesworth, C.J., Dhuime, B., 2012. Detrital zircon record and tectonic setting. Geology 40, 875–878.

Cawood, P.A., McCausland, P.J.A., Dunning, G.R., 2001. Opening Iapetus: Constraints from the Laurentian margin in Newfoundland. Geological Society of America Bulletin 113, 443–453.

Cawood, P.A., Nemchin, A.A., 2001. Paleogeographic development of the east Laurentian margin: Constraints from U-Pb dating of detrital zircons in the Newfoundland Appalachians. Geological Society of America Bulletin 113, 1234–1246.

Cawood, P.A., Nemchin, A.A., Smith, M., Loewy, S., 2003. Source of the Dalradian Supergroup constrained by U–Pb dating of detrital zircon and implications for the East Laurentian margin. Journal of the Geological Society 160, 231–246.

Cawood, P.A., Nemchin, A.A., Strachan, R.A., Prave, T., Krabbendam, M., 2007. Sedimentary basin and detrital zircon record along East Laurentia and Baltica during assembly and breakup of Rodinia. Journal of the Geological Society 164, 257–275.

Chew, D., O'Sullivan, G., Caracciolo, L., Mark, C., Tyrrell, S., 2020. Sourcing the sand: Accessory mineral fertility, analytical and other biases in detrital U-Pb provenance analysis. Earth-Science Reviews 202, 103093.
Chew, D., Tyrrell, S., Daly, J.S., Cogne, N., Sun, K., Badenszki, E., 2019. The Basement Geology of the Porcupine High – A Key Transatlantic Link Betewen the Caledonides and Appalachians.
Chew, D.M., Daly, J.S., Magna, T., Page, L.M., Kirkland, C.L., Whitehouse, M.J., Lam, R., 2010. Timing of ophiolite obduction in the Grampian orogen. Geological Society of America Bulletin 122, 1787–1799.
Chew, D.M., Flowerdew, M.J., Page, L.M., Crowley, Q.G., Daly, J.S., Cooper, M., Whitehouse, M.J., 2008. The tectonothermal evolution and provenance of the Tyrone Central Inlier, Ireland: Grampian imbrication of an outboard Laurentian microcontinent? Journal of the Geological Society 165, 675–685.
Chew, D.M., Strachan, R.A., 2014. The Laurentian Caledonides of Scotland and Ireland. Geological Society, London, Special Publications 390, 45–91.
Cliff, R.A., Yardley, B.W.D., Bussy, F.R., 1996. U–Pb and Rb–Sr geochronology of magmatism and metamorphism in the Dalradian of Connemara, western Ireland. Journal of the Geological Society 153, 109–120.
Corfu, F., Crane, A., Moser, D., Rogers, G., 1998. U-Pb zircon systematics at Gruinard Bay, northwest Scotland: implications for the early orogenic evolution of the Lewisian complex. Contributions to Mineralogy and Petrology 133, 329–345.
Corfu, F., Heaman, L.M., Rogers, G., 1994. Polymetamorphic evolution of the Lewisian complex, NW Scotland, as recorded by U-Pb isotopic compositions of zircon, titanite and rutile. Contributions to Mineralogy and Petrology 117, 215–228.
Cutts, K., Hand, M., Kelsey, D., Strachan, R.A., 2009. Orogenic versus extensional settings for regional metamorphism: Knoydartian events in the Moine Supergroup revisited. Journal of The Geological Society – Journal of the Geological Society 166, 201–204.
Daly, J.S., 1996. Pre-Caledonian History of the Annagh Gneiss Complex North-Western Ireland, and Correlation with Laurentia-Baltica. Irish Journal of Earth Sciences 15, 5–18.
Daly, J.S., Muir, R.J., Cliff, R.A., 1991. A precise U-Pb zircon age for the Inishtrahull syenitic gneiss, County Donegal, Ireland. Journal of the Geological Society 148, 639–642.
Daly, S.J., Flowerdew, M.J., 2005. Grampian and late Grenville events recorded by mineral geochronology near a basement–cover contact in north Mayo, Ireland | Journal of the Geological Society.
Daly, J.S., Tyrrell, S., Haughton, P.D.W., and Shannon, P.M., 2007. IS06/10: Petrographic, petrophysical and geochemical characterisation of the northern Porcupine High using recently recovered MeBo shallow cores. Interim Report, June 2007.
Daly, J.S., Tyrrell, S., Badenszki, E., Haughton, P.D.W. and Shannon, P.M. 2008. ISO6/10: Petrographic and geochemical characterisation of the Porcupine High using recently recovered MeBo shallow cores. Interim Report, February 2008.
Davies, J.H.F.L., Heaman, L.M., 2014. New U–Pb baddeleyite and zircon ages for the Scourie dyke swarm: A long-lived large igneous province with implications for the Paleoproterozoic evolution of NW Scotland. Precambrian Research 249, 180–198.
Dewey, J.F., Shackleton, R.M., 1984. A model for the evolution of the Grampian tract in the early Caledonides and Appalachians. Nature 312, 115–121.

Dewey, J.F., Strachan, R.A., 2003. Changing Silurian–Devonian relative plate motion in the Caledonides: sinistral transpression to sinistral transtension. Journal of the Geological Society 160, 219–229.
Dickin, A.P., 1992. Evidence for an Early Proterozoic crustal province in the North Atlantic region. Journal of the Geological Society 149, 483–486.
Dickin, A.P., Bowes, D.R., 1991. Isotopic evidence for the extent of early Proterozoic basement in Scotland and northwest Ireland. Geological Magazine 128, 385–388.
Evans, C.R., 1965. Geochronology of the Lewisian Basement Near Lochinver, Sutherland. Nature 207, 54–56.
Fitches, W.R., Maltman, A.J., 1984. Tectonic development and stratigraphy at the western margin of the Caledonides: Islay and Colonsay, Scotland. Earth and Environmental Science Transactions of The Royal Society of Edinburgh 75, 365–382.
Flowerdew, M.J., Daly, J.S., Whitehouse, M.J., 2005. 470 Ma granitoid magmatism associated with the Grampian Orogeny in the Slishwood Division, NW Ireland. Journal of the Geological Society 162, 563–575.
Flowerdew, M.J., Chew, D.M., Daly, J.S., Millar, I.L., 2009a. Hidden Archaean and Palaeoproterozoic crust in NW Ireland? Evidence from zircon Hf isotopic data from granitoid intrusions. Geological Magazine 146, 903–916.
Friedrich, A.M., Bowring, S.A., Martin, M.W., Hodges, K.V., 1999. Short-lived continental magmatic arc at Connemara, western Irish Caledonides: Implications for the age of the Grampian orogeny. Geology 27, 27.
Friend, C., Kinny, P., 2001. A reappraisal of the Lewisian Gneiss Complex: Geochronological evidence for its tectonic assembly from disparate terranes in the Proterozoic. Contributions to Mineralogy and Petrology 142, 198–218.
Friend, C.R.L., Strachan, R.A., Kinny, P.D., Watt, G.R., 2003. Provenance of the Moine Supergroup of NW Scotland: evidence from geochronology of detrital and inherited zircons from (meta)sedimentary rocks, granites and migmatites. Journal of the Geological Society 160, 247–257.
Halliday, A.N., 1984. Coupled Sm–Nd and U–Pb systematics in late Caledonian granites and the basement under northern Britain. Nature 307, 229–233.
Harris, A.L., Haselock, P.J., Kennedy, M.J., Mendum, J.R., Long, C.B., Winchester, J.A., Tanner, P.W.G., 1994. The Dalradian Supergroup in Scotland, Shetland and Ireland, in: Gibbons, W., Harris, A.L. (Eds.), A Revised Correlation of Pre-Cambrian Rocks in the British Isles. Geological Society of London, p. 0.
Hollis, S.P., Roberts, S., Cooper, M.R., Earls, G., Herrington, R., Condon, D.J., Cooper, M.J., Archibald, S.M., Piercey, S.J., 2012. Episodic arc-ophiolite emplacement and the growth of continental margins: Late accretion in the Northern Irish sector of the Grampian-Taconic orogeny. GSA Bulletin 124, 1702–1723.
Heaman, L.M., Tarney, J., 1989. U–Pb baddeleyite ages for the Scourie dyke swarm, Scotland: evidence for two distinct intrusion events. Nature 340, 705–708.
Hitchen, K., Morton, A.C., Mearns, E.W., Whitehouse, M., Stoker, M.S., 1997. Geological implications from geochemical and isotopic studies of Upper Cretaceous and Lower Tertiary igneous rocks around the northern Rockall Trough. Journal of the Geological Society 154, 517–521.
Johnson, T.E., Fischer, S., White, R.W., Brown, M., Rollinson, H.R., 2012. Archaean Intracrustal Differentiation from Partial Melting of Metagabbro—Field and Geochemical

Evidence from the Central Region of the Lewisian Complex, NW Scotland. Journal of Petrology 53, 2115–2138.
Kimbell, G.S., Ritchie, J.D., Hendersen, A.F., 2010. Three-dimensional gravity and magnetic modelling of the Irish sector of the NE Atlantic margin. Tectonophysics 486, 36–54.
Kinny, P.D., Friend, C.R.L., Love, G.J., 2005. Proposal for a terrane-based nomenclature for the Lewisian Gneiss Complex of NW Scotland. Journal of the Geological Society 162, 175–186.
Love, G.J., Kinny, P.D., Friend, C.R.L., 2004. Timing of magmatism and metamorphism in the Gruinard Bay area of the Lewisian Gneiss Complex: comparisons with the Assynt Terrane and implications for terrane accretion. Contributions to Mineralogy and Petrology 146, 620–636.
Ludwig, K.R. 2012. User's Manuel for Isoplot 3.75: A Geochronological Toolkit for Microsoft Excel. Berkley Geochronological Center Special Publication No. 5.
Mayborn, K.R., Lesher, C.E., 2006. Origin and evolution of the Kangâmiut mafic dyke swarm, West Greenland. GEUS Bulletin 11, 61–86.
McAteer, C.A., Daly, J.S., Flowerdew, M.J., Whitehouse, M.J., Kirkland, C.L., 2010a. A Laurentian provenance for the Dalradian rocks of north Mayo, Ireland, and evidence for an original basement–cover contact with the underlying Annagh Gneiss Complex. Journal of the Geological Society 167, 1033–1048.
McAteer, C.A., Daly, J.S., Flowerdew, M.J., Connelly, J.N., Housh, T.B., Whitehouse, M.J., 2010b. Detrital zircon, detrital titanite and igneous clast U–Pb geochronology and basement–cover relationships of the Colonsay Group, SW Scotland: Laurentian provenance and correlation with the Neoproterozoic Dalradian Supergroup. Precambrian Research 181, 21–42.
McKerrow, W.S., Mac Niocaill, C., Dewey, J.F., 2000. The Caledonian Orogeny redefined. Journal of the Geological Society 157, 1149–1154.
Muir, R.J., Fitches, W.R., Maltman, A.J., 1994. The Rhinns Complex: Proterozoic basement on Islay and Colonsay, Inner Hebrides, Scotland, and on Inishtrahull, NW Ireland. Earth and Environmental Science Transactions of The Royal Society of Edinburgh 85, 77–90.
Muir, R.J., Fitches, W.R., Maltman, A.J., 1992. Rhinns complex: A missing link in the Proterozoic basement of the North Atlantic region. Geology 20, 1043–1046.
Nilsson, M.K.M., Klausen, M.B., Söderlund, U., Ernst, R.E., 2013. Precise U–Pb ages and geochemistry of Palaeoproterozoic mafic dykes from southern West Greenland: Linking the North Atlantic and the Dharwar cratons. Lithos, Large Igneous Provinces (LIPs) and Supercontinents 174, 255–270.
Oliver, G.J.H., Wilde, S.A., Wan, Y., 2008. Geochronology and geodynamics of Scottish granitoids from the late Neoproterozoic break-up of Rodinia to Palaeozoic collision. Journal of the Geological Society 165, 661–674.
Paton, C., Hellstrom, J., Paul, B., Woodhead, J., Hergt, J., 2011. Iolite: Freeware for the visualisation and processing of mass spectrometric data. Journal of Analytical Atomic Spectrometry. 26, 2508–2518.
Paul, A.N., Spikings, R.A., Gaynor, S.P., 2021. U-Pb ID-TIMS reference ages and initial Pb isotope compositions for Durango and Wilberforce apatites. Chemical Geology 586, 120604.
Peach, B.N., Horne, J., Gunn, W., Clough, C.T., Hinxman, L.W., Teall, J.J.H. 1907. The Geological Structure of the North-west Highlands of Scotland. H.M. Stationery Office, Glasgow.

Petrus, J.A., Kamber, B.S., 2012. VizualAge: A Novel Approach to Laser Ablation ICP-MS U-Pb Geochronology Data Reduction. Geostandards and Geoanalytical Research 36, 247–270.

Pointon, M.A., Cliff, R.A., Chew, D.M., 2012. The provenance of Western Irish Namurian Basin sedimentary strata inferred using detrital zircon U–Pb LA-ICP-MS geochronology. Geological Journal 47, 77–98.

Readman, P.W., O'Reilly, B.M., Shannon, P.M., Naylor, D., 2005. The deep structure of the Porcupine Basin, offshore Ireland, from gravity and magnetic studies, in: Doré, A.G., Vining, B.A. (Eds.), Petroleum Geology: North-West Europe and Global Perspectives—Proceedings of the 6th Petroleum Geology Conference. Geological Society of London, 1047–1056.

Riddihough, R.P., Max, M.D., 1976. A geological framework for the continental margin to the west of Ireland. Geological Journal 11(2), 109–120.

Rogers, G., Hyslop, E.K., Strachan, R.A., Paterson, B.A., Holdsworth, R.E., 1998. The structural setting and U–Pb geochronology of Knoydartian pegmatites in W Inverness-shire: evidence for Neoproterozoic tectonothermal events in the Moineof NW Scotland. Journal of the Geological Society 155, 685–696.

Rollinson, H., 2012. Geochemical constraints on the composition of Archaean lower continental crust: Partial melting in the Lewisian granulites. Earth and Planetary Science Letters 351–352, 1–12.

Rosman, K. J. R., andTaylor, P. D. P. (1998). Isotopic compositions of the elements 1997 (Technical Report). Pure and Applied Chemistry, 70(1), 217-235.

Scanlon, R., Daly, J.S., Whitehouse, M., 2003. The c. 1.8 Ga Stanton Banks Terrane, offshore western Scotland, a large juvenile Palaeoproterozoic crustal block within the accretionary Lewisian complex. EGS-AGI-EUG Joint Assembly, Abstracts from the meeting held in Nice, France, 06-11 April 2003 (European Geophysical Society).

Schoene, B., Bowring, S.A., 2006. U–Pb systematics of the McClure Mountain syenite: thermochronological constraints on the age of the 40Ar/39Ar standard MMhb. Contributions to Mineralogy and Petrology 151, 615.

Sláma, J., Košler, J., Condon, D.J., Crowley, J.L., Gerdes, A., Hanchar, J.M., Horstwood, M.S.A., Morris, G.A., Nasdala, L., Norberg, N., Schaltegger, U., Schoene, B., Tubrett, M.N., Whitehouse, M.J., 2008. Plešovice zircon — A new natural reference material for U–Pb and Hf isotopic microanalysis. Chemical Geology 249, 1–35.

Soper, N.J., England, R.W., 1995. Vendian and Riphean rifting in NW Scotland. Journal of the Geological Society 152, 11–14.

Soper, N.J., England, R.W., Snyder, D.B., Ryan, P.D., 1992. The Iapetus suture zone in England, Scotland and eastern Ireland: a reconciliation of geological and deep seismic data. Journal of the Geological Society 149, 697–700.

Souders, A. K., & Sylvester, P. J. (2010). Accuracy and precision of non-matrix-matched calibration for lead isotope ratio measurements of lead-poor minerals by LA-MC-ICPMS. *Journal of Analytical Atomic Spectrometry*, 25(7), 975-988.

Tanner, P.W.G., Evans, J.A., 2003. Late Precambrian U–Pb titanite age for peak regional metamorphism and deformation (Knoydartian orogeny) in the western Moine, Scotland. Journal of the Geological Society 160, 555–564.

Tate, M.P., Dobson, M.R., 1988. Syn- and post-rift igneous activity in the Porcupine Seabight Basin and adjacent continental margin W of Ireland. Geological Society, London, Special Publications 39, 309–334.

Thébaudeau, B., Monteys, X., McCarron, S., O'Toole, R., Caloca, S., 2016. Seabed geomorphology of the Porcupine Bank, West of Ireland. Journal of Maps 12, 947–958.
Tyrrell, S., P.D.W. Haughton, J.S. Daly, T.F. Kokfelt, and D. Gagnevin (2006), The use of the common Pb isotope composition of detrital K-feldspar grains as a provenance tool and its application to upper Carboniferous paleodrainage, northern England. *Journal of Sedimentary Research*, *76*(2), 324-345.
Tyrrell, S., P.D.W. Haughton, J.S. Daly, and P.M. Shannon (2012), The Pb isotopic composition of detrital K-feldspar: a tool for constraining provenance, sedimentary processes and paleodrainage: In: Quantitative Mineralogy and Microanalysis of Sediments and Sedimentary Rocks (P. Sylvester, ed), *Mineralogical Association of Canada, 42*, 203-217.
Tyrrell, S., 2013. Geochemical constraints on the age, affinity and history of the Porcupine High (INFOMAR Research Project). University College Dublin.
Vance, D., Strachan, R.A., Jones, K.A., 1998. Extensional versus compressional settings for metamorphism: Garnet chronometry and pressure-temperature-time histories in the Moine Supergroup, northwest Scotland. Geology 26, 927–930.
Viete, D.R., Oliver, G.J.H., Fraser, G.L., Forster, M.A., Lister, G.S., 2013. Timing and heat sources for the Barrovian metamorphism, Scotland. Lithos 177, 148–163.
Whitehouse, M.J., Bridgwater, D., 2001. Geochronological constraints on Paleoproterozoic crustal evolution and regional correlations of the northern Outer Hebridean Lewisian complex, Scotland. Precambrian Research 105, 227–245.
Wiedenbeck, M., Allé, P., Corfu, F., Griffin, W. l., Meier, M., Oberli, F., Quadt, A.V., Roddick, J. c., Spiegel, W., 1995. Three Natural Zircon Standards for U-Th-Pb, Lu-Hf, Trace Element and Ree Analyses. Geostandards Newsletter 19, 1–23.
Wiedenbeck, M., Hanchar, J.M., Peck, W.H., Sylvester, P., Valley, J., Whitehouse, M., Kronz, A., Morishita, Y., Nasdala, L., Fiebig, J., Franchi, I., Girard, J.-P., Greenwood, R. c., Hinton, R., Kita, N., Mason, P. r. d., Norman, M., Ogasawara, M., Piccoli, P. m., Rhede, D., Satoh, H., Schulz-Dobrick, B., Skår, O., Spicuzza, Mj., Terada, K., Tindle, A., Togashi, S., Vennemann, T., Xie, Q., Zheng, Y.-F., 2004. Further Characterisation of the 91500 Zircon Crystal. Geostandards and Geoanalytical Research 28, 9–39.
Young, D.G.G., Bailey, R.J., 1974. An interpretation of some magnetic date off the west coast of Ireland. Geological Journal 9(2), 137–146.

Chapter 5: Conclusions

The primary objective of this study was to constrain the geologic evolution of the Porcupine High which is key to reconstructing the basement geology of the western Irish offshore and the North Atlantic. Despite serving as the site of extensive petroleum exploration since the 1970s, the geologic evolution of Porcupine High has remained largely unknown and poorly constrained. The results in this study provide clarity into the history of a region linking the circum-Iapetus basement geology of NW Europe and Atlantic Canada, and illustrate the complex and varied geology of the terranes of Laurentia affinity proximal to the Iapetus suture.

5.1 Analytical results

This thesis is the result of several years of sample collection and analysis. I incorporated previously unpublished data in addition to my own results, which focused on the MeBo2 core and the 2014 dredge samples. The main findings are summarized here but are also discussed in section 5 of Chapter 4 and in section 5.2.

Samples from borehole 25/27-sbMeBo2, which was recovered adjacent to a E-W trending magnetic boundary we correlated with the Fair Head – Clew Bay line, yield U-Pb zircon ages of c. 500 – 478 Ma, with a 385 Ma U-Pb apatite age indicating post-Caledonian exhumation. These rocks are assigned to the ophiolitic rocks in the Clay Bay Complex.

Borehole 25/27-sbMebo3, a granitic orthogneiss, yields a previously published 1314 Ma U-Pb zircon crystallization age with Grenville granulite-facies metamorphism, supported by a 875 Ma apatite U-Pb cooling age.

In a region with a magnetic anomaly low, situated between the two MeBo drill sites, dredging recovered over 90% lower greenschist-facies psammite cobbles. Detrital U-

Pb zircon dating of the youngest population at c. 950 Ma implies an affinity with the Moine Supergroup or Grampian Group Dalradian.

The northernmost site recovered dredge samples with over 98% metamorphic clasts. U-Pb detrital zircon ages of two low-grade metasedimentary rocks indicate a Moine/Grampian Group and an Upper Dalradian affinity respectively. Caledonian apatite U-Pb ages are also represented.

The high-grade orthogneisses and amphibolites are divided into three groups: Clasts with 2750 Ma U-Pb zircon crystallization ages, 1750 Ma apatite U-Pb ages, and a Lewisian Pb-in-Kfsp signature, Clasts with 1830-1940 Ma U-Pb zircon ages, 1750 Ma apatite U-Pb ages, and an AGC Pb-in-Kfsp affinity, and AGC Clasts with 1550-1650 Ma U-Pb zircon ages and U-Pb apatite ages recording post-Grenville cooling. These different high-grade rock types were recovered at one dredge site and their deposition is likely the result Quaternary glacial transport, particularly when considering distance to the closest basement outcrops yielding c. 2750 Ma U-Pb zircon crystallization ages.

5.2 Discussion of analytical results

5.2.1 25/27-sb(MeBo) Cores

The samples of the MeBo2 core yield U-Pb zircon ages that are very similar, falling between c. 500-478 Ma, indicating a likely proximal source for the MeBo2 drill site deposit. These crystallization ages correlate with the c. 510-490 Ma ophiolitic rocks of the Clew Bay Complex in Western Ireland (Chew et al., 2010). Based on the separation of the ophiolite rocks from the Dalradian Supergroup by the Fair Head – Clew Bay line, Laurentian margin cover sequences like the Dalradian Supergroup should be found north of the MeBo2 drill site. A U-Pb apatite age of 384.6 ± 7 Ma likely represents prolonged (c. 100 Myr) residence above the apatite U-Pb closure temperature until the cessation of the Caledonian orogeny at c. 390 Ma.

U-Pb zircon dating of the North Porcupine High Orthogneiss (NPHO) in the MeBo3 core provides evidence of magmatism at 1314 ± 6 Ma followed by Grenville granulite-facies metamorphism. U-Pb apatite dating at 874.9 ± 8 Ma likely represents post-Grenville cooling. A previously unknown phase of anorogenic magmatism associated with rifting may have thus have occurred. was of inherited zircons in the NPHO.

5.2.2 2011 Suite Dredge Samples

The Porcupine High Metasedimentary Sequence is represented by the quartzo-feldspathic psammites recovered during the 2011 dredging expedition. U-Pb zircon ages are consistent with derivation from the Laurentian margin, with a U-Pb detrital zircon spectra resembling that of the Grampian Group or the Moine Supergroup.

Although Grenvillian metamorphism in the source terranes of the PHMS may have recrystallized or reset Archean or Paleoproterozoic apatite, there is no evidence of U-Pb resetting during low-grade Caledonian metamorphism. The dominance (> 90%) of metamorphic clasts with Grampian Group or Moine Supergroup affinity strongly implies the clasts are locally derived from nearby Neoproterozoic metasedimentary basement, which in turn was likely sourced from the Annagh Gneiss Complex or correlatives.

5.2.3 2014 Suite Dredge Samples

Dredge samples from this suite point to several potential sources in the North Atlantic. The three groups of the high-grade orthogneisses and amphibolites have a long and varied history. The first group, indicative of the Lewisian Complex based on the Pb-in-Kfsp affinity and U-Pb zircon ages of c. 2750 Ma and with U-Pb apatite ages of c. 1750, are suggestive of Laxfordian metamorphism.

The second group yields U-Pb zircon ages that correlate with a Paleoproterozoic source. Though the samples in this group share a Pb-in-Kfsp affinity with the AGC, their 1750 Ma apatite U-Pb ages are incompatible with the high-grade Grenvillian metamorphism seen in the mainland exposures of the AGC.

The third group, with a Pb-in-Kfsp affinity of the AGC and U-Pb zircon ages of c. 1650-1550 Ma, also yields U-Pb apatite ages of c. 970 Ma, suggestive of post-Grenville cooling. Similarly, the AGC is ruled out as a source due to the lack of Caledonian overprinting of the apatite U-Pb systematics.

Some samples do not fit the characteristics of the aforementioned groups, and do not share similarities with each other. Sample 402-13 (lineated amphibolite) yields a U-Pb zircon age of c. 2015. 3 ± 8.7 Ma, which is pene-contemporaneous with the emplacement of the Kangâmiut dykes in western Greenland and equivalent dykes in the eastern Nain Province in Canada (e.g., Ernst and Buchan, 2004; Mayborn and Lesher, 2006; Nilsson et al., 2013), as well as the Strathan dyke in the Lewisian Complex (Heaman and Tarney, 1989). One dyke from the NAC southern east Greenland also yields a similar U-Pb zircon age of 2015 ± 15 Ma (Nutman et al., 2008). The emplacement of the Kangâmiut dykes at

c. 2030-2050 Ma was part of a series of major events in the Paleoproterozoic of West Greenland and was followed by the Nagssugtoqidian orogeny that initiated at c. 1820 Ma. Geochemical (Ba/La and Nb/La ratio comparisons) analyses indicate that the dykes are related to passive rifting, (e.g., Mayborn and Lesher, 2006).

Two samples, 204-1 (mica schist) and 302-1 (psammite) are detrital samples from metasedimentary rocks. 204-1 (mica schist) is comparable to the Grampian Group of the Dalradian Supergroup or the Moine Supergroup, and the samples of the PHMS described in this study. The U-Pb detrital zircon spectra of 302-1 (psammite) is similar to the detrital zircon spectra of the Upper Dalradian but also contains a Caledonian age peak at c. 460-415 Ma that is likely derived from Caledonian granitoids. Hence the source may be a low-grade equivalent of the Old Red Sandstone, which is associated with the erosion from the Caledonides, including Dalradian rocks and Caledonian granites.

Ice-rafted debris by Quaternary glacial systems is a proposed method of transport for 2014 suite of dredge samples. Reconstructions have shown that the British-Irish Ice Sheet (BIIS) covered ~840,000 km^2 at its maximum extent at c. 27 ka (Clark et al., 2012). The glacial deposits of the Donegal Bay Moraine (Cofaigh et al., 2012; Cofaigh et al., 2019), located at the mouth of Donegal Bay , and the Connemara Fan (McCarron et al., 2018), a shelf of ~ 9000 km^2, which extends from the Irish mainland westward towards the Porcupine High, may be the sediment source.

5.3 Future directions

Although this study brings forth new insights into the geologic evolution of the Porcupine High, further research is needed to shed clearer light on the basement geology of the region, and the extent of Caledonian metamorphism and deformation. The geochronological data paired with the magnetic data presented in section 5.3 of Chapter 4 and the accompanying map (Fig. 14b) provide a framework in which to plan supplemental and complementary research.

The Porcupine and Slyne basins have been the site of exploration wells in search of hydrocarbons (e.g. Moore and Shannon, 1995; Stoker et al., 2017; O'Sullivan and Childs, 2021). Additional geochronological studies of these sites, particularly if the wells reached basement, would shed light on the extent of the Caledonian orogeny. More focused study into the area north of the E-W trending magnetic boundary adjacent to the MeBo2 drill site we correlated with the Fair Head – Clew Bay Fault line should reveal Laurentian margin cover sequences, as discussed in section 5.1 of Chapter 4.

Additional data from the 2014 dredge sites would be useful in determining the source and evolution of Quaternary glacial transport in the region, particularly if potentially source diagnostic clasts (e.g. the 2015 Ma lineated amphibolite which has few potential source areas) can be found.

Further studies narrowing first-order constraints on the location of the Iapetus suture in the western Irish offshore would also supplement the findings of this study. Although the data presented here positions the Iapetus suture south of the 2011 dredging site, a more exact location is needed to construct a thorough understanding of the geological history of Ireland and its western offshore. This will also ensure that future planning for Irish offshore infrastructure, such as for renewable energy or carbon capture and storage, is approached with a robust geologic foundation.

References (Chapters 1-3 and 5)

Albarède, F., Telouk, P., Blichert-Toft, J., Boyet, M., Agranier, A., Nelson, B., 2004. Precise and accurate isotopic measurements using multiple-collector ICPMS1 1Associate editor: Y. Amelin. Geochimica et Cosmochimica Acta 68, 2725–2744.

Allen, C.M., Campbell, I.H., 2012. Identification and elimination of a matrix-induced systematic error in LA–ICP–MS 206Pb/238U dating of zircon. Chemical Geology 332–333, 157–165.

Amelin, Y., Kaltenbach, A., Iizuka, T., Stirling, C.H., Ireland, T.R., Petaev, M., Jacobsen, S.B., 2010. U–Pb chronology of the Solar System's oldest solids with variable 238U/235U. Earth and Planetary Science Letters 300, 343–350.

Andersen, T., 2002. Correction of common lead in U–Pb analyses that do not report 204Pb. Chemical Geology 192, 59–79.

Andersen, T., Elburg, M.A., Magwaza, B.N., 2019. Sources of bias in detrital zircon geochronology: Discordance, concealed lead loss and common lead correction. Earth-Science Reviews 197, 102899.

Andrén, H., Rodushkin, I., Stenberg, A., Malinovsky, D., Baxter, D.C., 2004. Sources of mass bias and isotope ratio variation in multi-collector ICP-MS: optimization of instrumental parameters based on experimental observations. Journal of Analytical Atomic Spectrometry 19, 1217–1224.

Bea, F., 1996. Controls on the trace element composition of crustal melts. Earth and Environmental Science Transactions of The Royal Society of Edinburgh 87, 33–41.

Buchan, K.L., Mertanen, S., Park, R.G., Pesonen, L.J., Elming, S.-Å., Abrahamsen, N., Bylund, G., 2000. Comparing the drift of Laurentia and Baltica in the Proterozoic: the importance of key palaeomagnetic poles. Tectonophysics 319, 167–198.

Carswell, D.A., Wilson, R.N., Zhai, M., 1996. Ultra-high pressure aluminous titanites in carbonate-bearing eclogites at Shuanghe in Dabieshan, central China. Mineralogical Magazine 60, 461–471.

Cawood, P.A., Nemchin, A.A., 2001. Paleogeographic development of the east Laurentian margin: Constraints from U-Pb dating of detrital zircons in the Newfoundland Appalachians. Geological Society of America Bulletin 113, 1234–1246.

Chakoumakos, B.C., Murakami, T., Lumpkin, G.R., Ewing, R.C., 1987. Alpha-Decay—Induced Fracturing in Zircon: The Transition from the Crystalline to the Metamict State. Science 236, 1556–1559.

Chang, Z., Vervoort, J.D., McClelland, W.C., Knaack, C., 2006. U-Pb dating of zircon by LA-ICP-MS. Geochemistry, Geophysics, Geosystems 7.

Cherniak, D.J., 2000. Pb diffusion in rutile. Contributions to Mineralogy and Petrology 139, 198–207.

Cherniak, D.J., Hanchar, J.M., Watson, E.B., 1997. Diffusion of tetravalent cations in zircon. Contributions to Mineralogy and Petrology 127, 383–390.

Cherniak, D.J., Watson, E.B., 2003. Diffusion in Zircon. Reviews in Mineralogy and Geochemistry 53, 113–143.

Cherniak, D.J., Watson, E.B., 2001. Pb diffusion in zircon. Chemical Geology, What are we dating? Understanding the Crystallogernesis of U-Pb 172, 5–24.
Chew, D., Daly, J.S., Magna, T., Page, L.M., Kirkland, C.L., Whitehouse, M.J., Lam, R., 2010. Timing of ophiolite obduction in the Grampian orogen. Geological Society of America Bulletin 122, 1787–1799.
Chew, D., O'Sullivan, G., Caracciolo, L., Mark, C., Tyrrell, S., 2020. Sourcing the sand: Accessory mineral fertility, analytical and other biases in detrital U-Pb provenance analysis. Earth-Science Reviews 202, 103093.
Chew, D., Tyrrell, S., Daly, J.S., Cogne, N., Sun, K., Badenszki, E., 2019. The Basement Geology of the Porucpine High – A Key Transatlantic Link Betewen the Caledonides and Appalachians. Presented at the Geologic Society of America.
Chew, D.M., Spikings, R.A., 2015. Geochronology and Thermochronology Using Apatite: Time and Temperature, Lower Crust to Surface. Elements 11, 189–194.
Chew, D., Sylvester, P.J., Tubrett, M.N., 2011. U–Pb and Th–Pb dating of apatite by LA-ICPMS. Chemical Geology 280, 200–216.
Chu, N.-C., Taylor, R.N., Chavagnac, V., Nesbitt, R.W., Boella, R.M., Milton, J.A., German, C.R., Bayon, G., Burton, K., 2002. Hf isotope ratio analysis using multi-collector inductively coupled plasma mass spectrometry: an evaluation of isobaric interference corrections. Journal of Analytical Atomic Spectrometry 17, 1567–1574.
Clark, C.D., Hughes, A.L.C., Greenwood, S.L., Jordan, C., Sejrup, H.P., 2012. Pattern and timing of retreat of the last British-Irish Ice Sheet. Quaternary Science Reviews, Quaternary Glaciation History of Northern Europe 44, 112–146.
Cochrane, R., Spikings, R.A., Chew, D., Wotzlaw, J.-F., Chiaradia, M., Tyrrell, S., Schaltegger, U., Van der Lelij, R., 2014. High temperature (>350°C) thermochronology and mechanisms of Pb loss in apatite. Geochimica et Cosmochimica Acta 127, 39–56.
Cofaigh, C.Ó., Dunlop, P., Benetti, S., 2012. Marine geophysical evidence for Late Pleistocene ice sheet extent and recession off northwest Ireland. Quaternary Science Reviews, Quaternary Glaciation History of Northern Europe 44, 147–159.
Cofaigh, C., Weilbach, K., Lloyd, J., Benetti, S., Callard, S.L., Purcell, C., Chiverrell, R., Dunlop, P., Livingstone, S., Saher, M., Van Landeghem, K.J.J., Moreton, S., Clark, C., Fabel, D., 2018. Early deglaciation of the British-Irish Ice Sheet on the Atlantic shelf northwest of Ireland driven by glacioisostatic depression and high relative sea level. Quaternary Science Reviews 208.
Crowley, Q., Heron, K., Riggs, N., Kamber, B., Chew, D., McConnell, B., Benn, K., 2014. Chemical Abrasion Applied to LA-ICP-MS U–Pb Zircon Geochronology. Minerals 4, 503–518.
Dröllner, M., Barham, M., Kirkland, C.L., Ware, B., 2021. Every zircon deserves a date: selection bias in detrital geochronology. Geol. Mag. 158, 1135–1142.
Eggins, S.M., Grün, R., McCulloch, M.T., Pike, A.W.G., Chappell, J., Kinsley, L., Mortimer, G., Shelley, M., Murray-Wallace, C.V., Spötl, C., Taylor, L., 2005. In situ U-series dating by laser-ablation multi-collector ICPMS: new prospects for Quaternary geochronology. Quaternary Science Reviews 24, 2523–2538.
Eggins, S.M., Kinsley, L.P.J., Shelley, J.M.G., 1998. Deposition and element fractionation processes during atmospheric pressure laser sampling for analysis by ICP-MS. Applied Surface Science 127–129, 278–286.
Ernst, R.E., Buchan, K.L., 2004. Igneous Rock Associations in Canada 3. Large Igneous Provinces (LIPs) in Canada and Adjacent Regions: 3 Ga to Present. Geoscience Canada 31, 103–126.

Ewing, R.C., Meldrum, A., Wang, L., Weber, W.J., Corrales, L.R., 2003. Radiation Effects in Zircon. Reviews in Mineralogy and Geochemistry 53, 387–425.
Finch, R.J., Hanchar, J.M., 2003. Structure and Chemistry of Zircon and Zircon-Group Minerals. Reviews in Mineralogy and Geochemistry 53, 1–25.
Fletcher, I.R., Rasmussen, B., McNaughton, N.J., 2000. SHRIMP U–Pb geochronology of authigenic xenotime and its potential for dating sedimentary basins. Australian Journal of Earth Sciences 47, 845–859.
Franz, L., Romer, R.L., Reiner, K., Schmid, R., Oberhansli, R., Wagner, T., Shuwen, D., 2001. Eclogite-facies quartz veins within metabasites of the Dabie Shan (eastern China): pressure–temperature–time–deformation path, composition of the fluid phase and fluid flow during exhumation of high-pressure rocks. Contributions to Mineralogy and Petrology 141, 322–346.
Fraser, G., Ellis, D., Eggins, S., 1997. Zirconium abundance in granulite-facies minerals, with implications for zircon geochronology in high-grade rocks. Geology 25, 607–610.
Frondel, C., 1957. Mineralogy of Uranium. American Mineralogist 42, 125–132.
Frost, B.R., Chamberlain, K.R., Schumacher, J.C., 2001. Sphene (titanite): phase relations and role as a geochronometer. Chemical Geology, What are we dating? Understanding the Crystallogernesis of U-Pb 172, 131–148.
Goodenough, K.M., Crowley, Q.G., Krabbendam, M., Parry, S.F., 2013. New U-Pb age constraints for the Laxford Shear Zone, NW Scotland: Evidence for tectono-magmatic processes associated with the formation of a Paleoproterozoic supercontinent. Precambrian Research 233, 1–19.
Gray, A.L., 1985. Solid sample introduction by laser ablation for inductively coupled plasma source mass spectrometry. Analyst 110, 551–556.
Greegor, R.B., Lytle, F.W., Arnold, G.W., Ewing, R.C., 1990. Pb-implanted SrTiO3 analyzed using Rutherford backscattering and surface sensitive EXAFS/XANES spectroscopy. Journal of Non-Crystalline Solids 122, 121–132.
Hanchar, J.M., Rudnick, R.L., 1995. Revealing hidden structures: The application of cathodoluminescence and back-scattered electron imaging to dating zircons from lower crustal xenoliths. Lithos 36, 289–303.
Hawkins, D.P., Bowring, S.A., 1997. U-Pb systematics of monazite and xenotime: case studies from the Paleoproterozoic of the Grand Canyon, Arizona. Contributions to Mineralogy and Petrology 127, 87–103.
Hay, D.C., Dempster, T.J., 2009. Zircon Behaviour during Low-temperature Metamorphism | Journal of Petrology | Oxford Academic. Journal of Petrology 50, 571–589.
Headley, T.J., Arnold, G.W., Northrup, C.J.M., 1981a. Dose-Dependence of Pb-Ion Implantation Damage in Zirconolite, Hollandite, and Zircon. MRS Online Proceedings Library (OPL) 11, 379.
Headley, T.J., Ewing, R.C., Haaker, R.F., 1981b. Amorphous structure of metamict minerals observed by TEM. Nature 293, 449–450.
Heaman, L.M., Tarney, J., 1989. U–Pb baddeleyite ages for the Scourie dyke swarm, Scotland: evidence for two distinct intrusion events. Nature 340, 705–708.
Hemming, S.R., Broecker, W.S., Sharp, W.D., Bond, G.C., Gwiazda, R.H., McManus, J.F., Klas, M., Hajdas, I., 1998. Provenance of Heinrich layers in core V28-82, northeastern Atlantic: 40Ar/39Ar ages of ice-rafted hornblende, Pb isotopes in feldspar grains, and Nd–Sr–Pb isotopes in the fine sediment fraction. Earth and Planetary Science Letters 164, 317–333.

Henrichs, I.A., O'Sullivan, G., Chew, D.M., Mark, C., Babechuk, M.G., McKenna, C., Emo, R., 2018. The trace element and U-Pb systematics of metamorphic apatite. Chemical Geology 483, 218–238.
Hetherington, C.J., Jercinovic, M.J., Williams, M.L., Mahan, K., 2008. Understanding geologic processes with xenotime: Composition, chronology, and a protocol for electron probe microanalysis. Chemical Geology, The role of accessory minerals in metamorphic and igneous processes 254, 133–147.
Heumann, K.G., Gallus, S.M., Rädlinger, G., Vogl, J., 1998. Precision and accuracy in isotope ratio measurements by plasma source mass spectrometry. Journal of Analytical Atomic Spectrometry 13, 1001–1008.
Hietpas, J., Samson, S., Moecher, D., Chakraborty, S., 2011. Enhancing tectonic and provenance information from detrital zircon studies: assessing terrane-scale sampling and grain-scale characterization. Journal of the Geological Society 168, 309–318.
Hiess, J., Condon, D.J., McLean, N., Noble, S.R., 2012. 238U/235U Systematics in Terrestrial Uranium-Bearing Minerals. Science 335, 1610–1614.
Higgins, J.B., Ribbe, P.H., 1977. The structure of malayaite, CaSnOSiO4, a tin analog of titanite. American Mineralogist 62, 801–806.
Hirata, T., Nesbitt, R., 1995. UPb isotope geochronology of zircon: evaluation of the laser probe-inductively coupled plasma mass spectrometry technique. Geochimica et Cosmochimica Acta 59, 2491–2500.
Hoskin, P.W.O., Schaltegger, U., 2003. The Composition of Zircon and Igneous and Metamorphic Petrogenesis. Reviews in Mineralogy and Geochemistry 53, 27–62.
Hurley, P.M., Fairbairn, H.W., 1952. Alpha-Radiation Damage in Zircon. Journal of Applied Physics 23, 1408–1408.
Ibañez-Mejia, M., Pullen, A., Pepper, M., Urbani, F., Ghoshal, G., Ibañez-Mejia, J.C., 2018. Use and abuse of detrital zircon U-Pb geochronology—A case from the Río Orinoco delta, eastern Venezuela. Geology 46, 1019–1022.
Ireland, T.R., Williams, I.S., 2003. Considerations in zircon geochronology by SIMS. Reviews in Mineralogy and Geochemistry 53, 215–241.
Jackson, S.E., Pearson, N.J., Griffin, W.L., Belousova, E.A., 2004. The application of laser ablation-inductively coupled plasma-mass spectrometry to in situ U–Pb zircon geochronology. Chemical Geology 211, 47–69.
Knudsen, T.-L., Andersen, T., Whitehouse, M.J., Vestin, J., 1997. Detrital zircon ages from southern Norway – implications for the Proterozoic evolution of the southwestern Baltic Shield. Contributions to Mineralogy and Petrology 130, 47–58.
Kryza, R., Crowley, Q.G., Larionov, A., Pin, C., Oberc-Dziedzic, T., Mochnacka, K., 2012. Chemical abrasion applied to SHRIMP zircon geochronology: An example from the Variscan Karkonosze Granite (Sudetes, SW Poland). Gondwana Research, Advances in High-Resolution Ion-Microprobe Geochronology 21, 757–767.
Layer, P.W., Kröner, A., McWilliams, M., York, D., 1989. Elements of the Archean thermal history and apparent polar wander of the eastern Kaapvaal Craton, Swaziland, from single grain dating and paleomagnetism. Earth and Planetary Science Letters 93, 23–34.
Lee, J.K.W., Williams, I.S., Ellis, D.J., 1997. Pb, U and Th diffusion in natural zircon. Nature 390, 159–162.
Li, J.-W., Deng, X.-D., Zhou, M.-F., Liu, Y.-S., Zhao, X.-F., Guo, J.-L., 2010. Laser ablation ICP-MS titanite U–Th–Pb dating of hydrothermal ore deposits: A case study of the Tonglushan Cu–Fe–Au skarn deposit, SE Hubei Province, China. Chemical Geology 270, 56–67.
Ludwig, K.R. 2012. User's Manuel for Isoplot 3.75: A Geochronological Toolkit for Microsoft Excel. Berkley Geochronological Center Special Publication No. 5.

Magee, C., Jackson, C.A.-L., Schofield, N., 2014. Diachronous sub-volcanic intrusion along deep-water margins: insights from the Irish Rockall Basin. Basin Research 26, 85–105.
Makris, J., Ginzburg, A., Shannon, P.M., Jacob, A.W.B., Bean, C.J., Vogt, U., 1991. A new look at the Rockall region, offshore Ireland. Marine and Petroleum Geology 8, 410–416.
Malczewski, D., Dziurowicz, M., Krzykawski, T., Stryjewski, A., 2018. 222Rn and 220Rn Emanations from Zircon Crystals As a Function of Absorbed α-Doses. The Canadian Mineralogist 56, 451–462.
Malinovsky, D., Stenberg, A., Rodushkin, I., Andren, H., Ingri, J., Öhlander, B., Baxter, D.C., 2003. Performance of high resolution MC-ICP-MS for Fe isotope ratio measurements in sedimentary geological materials. Journal of Analytical Atomic Spectrometry 18, 687–695.
Maréchal, C.N., Télouk, P., Albarède, F., 1999. Precise analysis of copper and zinc isotopic compositions by plasma-source mass spectrometry. Chemical Geology 156, 251–273.
Mattinson, J.M., 2005. Zircon U–Pb chemical abrasion ("CA-TIMS") method: Combined annealing and multi-step partial dissolution analysis for improved precision and accuracy of zircon ages. Chemical Geology 220, 47–66.
Mayborn, K.R., Lesher, C.E., 2006. Origin and evolution of the Kangâmiut mafic dyke swarm, West Greenland. GEUS Bulletin 11, 61–86.
McCarron, S., Praeg, D., Ó Cofaigh, C., Monteys, X., Thébaudeau, B., Craven, K., Saqab, M.M., Cova, A., 2018. A Plio-Pleistocene sediment wedge on the continental shelf west of central Ireland: The Connemara Fan. Marine Geology 399, 97–114.
Meis, C., Gale, J.D., 1998. Computational study of tetravalent uranium and plutonium lattice diffusion in zircon. Materials Science and Engineering: B 57, 52–61.
Mezger, K., Krogstad, E.J., 1997. Interpretation of discordant U-Pb zircon ages: An evaluation. Journal of Metamorphic Geology 15, 127–140.
Moore, J.G., Shannon, P.M., 1995. The Cretaceous succession in the Porcupine Basin, offshore Ireland: facies distribution and hydrocarbon potential. Geological Society, London, Special Publications 93, 345–370.
Nasdala, L., Lengauer, C.L., Hanchar, J.M., Kronz, A., Wirth, R., Blanc, P., Kennedy, A.K., Seydoux-Guillaume, A.-M., 2002. Annealing radiation damage and the recovery of cathodoluminescence. Chemical Geology, Chemistry and Physics of Accessory Minerals: Crystallisation, Transformation and Geochronoligical Applications 191, 121–140.
Nasdala, L., Zhang, M., Kempe, U., Panczer, G., Gaft, M., Andrut, M., Plötze, M., 2003. Spectroscopic methods applied to zircon. Reviews in Mineralogy and Geochemistry 53, 427–467.
Nesbitt, R.W., Hirata, T., Butler, I.B., Milton, J.A., 1997. UV Laser Ablation ICP-MS: Some Applications in the Earth Sciences. Geostandards Newsletter 21, 231–243.
Nilsson, M.K.M., Klausen, M.B., Söderlund, U., Ernst, R.E., 2013. Precise U–Pb ages and geochemistry of Palaeoproterozoic mafic dykes from southern West Greenland: Linking the North Atlantic and the Dharwar cratons. Lithos, Large Igneous Provinces (LIPs) and Supercontinents 174, 255–270.
Nutman, A.P., Kalsbeek, F., Friend, C.R.L., 2008. The Nagssugtoqidian orogen in South-East Greenland: Evidence for Paleoproterozoic collision and plate assembly. American Journal of Science 308, 529–572.
O'Hara, M.J., Fry, N., Prichard, H.M., 2001. Minor Phases as Carriers of Trace Elements in Non-Modal Crystal–Liquid Separation Processes II: Illustrations and Bearing on Behaviour of REE, U, Th and the PGE in Igneous Processes. Journal of Petrology 42, 1887–1910.

Olierook, H.K.H., Taylor, R.J.M., Erickson, T.M., Clark, C., Reddy, S.M., Kirkland, C.L., Jahn, I., Barham, M., 2019. Unravelling complex geologic histories using U–Pb and trace element systematics of titanite. Chemical Geology 504, 105–122.
O'Sullivan, C., Childs, C., 2021. Kinematic interaction between stratigraphically discrete salt layers; the structural evolution of the Corrib gas field, offshore NW Ireland. Marine and Petroleum Geology 133.
Orejana, D., Merino Martínez, E., Villaseca, C., Andersen, T., 2015. Ediacaran–Cambrian paleogeography and geodynamic setting of the Central Iberian Zone: Constraints from coupled U–Pb–Hf isotopes of detrital zircons. Precambrian Research 261, 234–251.
Pabst, A., 1952. The metamict state. American Mineralogist 37, 137–157.
Parrish, R.R., Noble, S.R., 2003. Zircon U-Th-Pb Geochronology by Isotope Dilution — Thermal Ionization Mass Spectrometry (ID-TIMS). Reviews in Mineralogy and Geochemistry 53, 183–213.
Paton, C., Hellstrom, J., Paul, B., Woodhead, J., Hergt, J., 2011. Iolite: Freeware for the visualisation and processing of mass spectrometric data. Journal of Analytical Atomic Spectrometry. 26, 2508–2518.
Petrus, J.A., Kamber, B.S., 2012. VizualAge: A Novel Approach to Laser Ablation ICP-MS U-Pb Geochronology Data Reduction. Geostandards and Geoanalytical Research 36, 247–270.
Pidgeon, R.T., Chapman, P.G., Danišík, M., Nemchin, A.A., 2017. Dry annealing of metamict zircon: A differential scanning calorimetry study. American Mineralogist 102, 1066–1072.
Poller, U., Huth, J., Hoppe, P., Williams, I.S., 2001. Ree, U, Th, and Hf Distribution in Zircon from Western Carpathian Variscan Granitoids: A Combined Cathodoluminescence and Ion Microprobe Study. American Journal of Science 301, 858–867.
Prowatke, S., Klemme, S., 2006. Trace element partitioning between apatite and silicate melts. Geochimica et Cosmochimica Acta 70, 4513–4527.
Pyle, J.M., Spear, F.S., Rudnick, R.L., McDonough, W.F., 2001. Monazite–Xenotime–Garnet Equilibrium in Metapelites and a New Monazite–Garnet Thermometer. Journal of Petrology 42, 2083–2107.
Rakovan, J., McDaniel, D.K., Reeder, R.J., 1997. Use of surface-controlled REE sectoral zoning in apatite from Llallagua, Bolivia, to determine a single-crystal SmNd age. Earth and Planetary Science Letters 146, 329–336.
Rakovan, J., Reeder, R.J., 1996. Intracrystalline rare earth element distributions in apatite: Surface structural influences on incorporation during growth. Geochimica et Cosmochimica Acta 60, 4435–4445.
Rasmussen, B., 2005. Radiometric dating of sedimentary rocks: the application of diagenetic xenotime geochronology. Earth-Science Reviews 68, 197–243.
Resentini, A., Malusà, M.G., Garzanti, E., 2013. MinSORTING: An Excel® worksheet for modelling mineral grain-size distribution in sediments, with application to detrital geochronology and provenance studies. Computers & Geosciences 59, 90–97.
Rosenblum, S., 1958. Magnetic susceptibilities of minerals in the Frantz Isodynamic magnetic separator1. American Mineralogist 43, 170–173.
Rubatto, D., 2017. Zircon: The Metamorphic Mineral. Reviews in Mineralogy and Geochemistry 83, 261–295.
Rubatto, D., Hermann, J., 2007. Experimental zircon/melt and zircon/garnet trace element partitioning and implications for the geochronology of crustal rocks. Chemical Geology, Crustal Dynamics; links between geochronology and petrology 241, 38–61.
Schaltegger, U., Fanning, C.M., Günther, D., Maurin, J.C., Schulmann, K., Gebauer, D., 1999. Growth, annealing and recrystallization of zircon and preservation of monazite in high-

grade metamorphism: conventional and in-situ U-Pb isotope, cathodoluminescence and microchemical evidence. Contributions to Mineralogy and Petrology 134, 186–201.
Spear, F.S., Pyle, J.M., 2002. Apatite, Monazite, and Xenotime in Metamorphic Rocks. Reviews in Mineralogy and Geochemistry 48.
Stacey, J.S., Kramers, J.D., 1975. Approximation of terrestrial lead isotope evolution by a two-stage model. Earth and Planetary Science Letters 26, 207–221.
Steiger, R.H., Jäger, E., 1977. Subcommission on geochronology: convention on the use of decay constants in geo- and cosmochronology. Earth and Planetary Science Letters 359–362.
Stirling, C.H., Andersen, M.B., Potter, E.-K., Halliday, A.N., 2007. Low-temperature isotopic fractionation of uranium. Earth and Planetary Science Letters 264, 208–225.
Stoker, M.S., Stewart, M.A., Shannon, P.M., Bjerager, M., Nielsen, T., Blischke, A., Hjelstuen, B.O., Gaina, C., McDermott, K., Ólavsdóttir, J., 2017. An overview of the Upper Palaeozoic–Mesozoic stratigraphy of the NE Atlantic region. Geological Society, London, Special Publications 447, 11–68.
Sylvester, P., Jackson, S., 2016. A Brief History of Laser Ablation Inductively Coupled Plasma Mass Spectrometry (LA–ICP–MS) | Elements | GeoScienceWorld. Elements 12, 307–310.
Tanner, S.D., 1992. Space charge in ICP-MS: calculation and implications. Spectrochimica Acta Part B: Atomic Spectroscopy 47, 809–823.
Tanner, S.D., Bandura, D.R., Baranov, V.I., Beres, S.A., 2004. Controlling the temporal response of mass spectrometers for mass spectrometry. US6713757B2.
Tanner, S.D., Cousins, L.M., Douglas, D.J., 1994. Reduction of Space Charge Effects Using a Three-Aperture Gas Dynamic Vacuum Interface for Inductively Coupled Plasma-Mass Spectrometry. Applied Spectroscopy 48, 1367–1372.
Tate, M.P., Dodd, C.D., Grant, N.T., 1999. The Northeast Rockall Basin and its significance in the evolution of the Rockall-Faeroes/East Greenland rift system. Geological Society, London, Petroleum Geology Conference Series 5, 391–406.
Terra, F., Wasserburg, J.A., 1972. U-Pb method of the isotopic dating of the minerals. Earth and Planetary Science Letters 17, 36–51.
Thomas, J.B., Bodnar, R.J., Shimizu, N., Chesner, C.A., 2003. Melt Inclusions in Zircon. Reviews in Mineralogy and Geochemistry 53, 63–87.
Thomson, S.N., Gehrels, G.E., Ruiz, J., 2012. Routine low-damage apatite U-Pb dating using laserablation–multicollector–ICPMS. Geochemistry Geophysics Geosystems American Geophysical Union 13.
Tyrrell, S., Haughton, P.D.W., Daly, J.S., Kokfelt, T.F., Gagnevin, D., 2006. The Use of the Common Pb Isotope Composition of Detrital K-Feldspar Grains as a Provenance Tool and Its Application to Upper Carboniferous Paleodrainage, Northern England. Journal of Sedimentary Research 76, 324–345.
Trachenko, K., Dove, M.T., Salje, E.K.H., 2002. Structural changes in zircon under alpha-decay irradiation. Physical Review B 65, 180102.
Vanhaecke, F., Dams, R., Vandecasteele, C., 1993. ‘Zone model’ as an explanation for signal behaviour and non-spectral interferences in inductively coupled plasma mass spectrometry. Journal of Analytical Atomic Spectrometry 8, 433–438.
Ver Hoeve, T.J., Scoates, J.S., Wall, C.J., Weis, D., Amini, M., 2018. Evaluating downhole fractionation corrections in LA-ICP-MS U-Pb zircon geochronology. Chemical Geology 483, 201–217.
Walker, S., Bird, A., Strachan, R., Thirwall, M., 2019. Garnet dating of Caledonian metamorphism in the Grampian Highlands and Shetland Islands, Scotland. Geophysical Research Abstracts 21, 1.

Watson, E.B., 1996. Dissolution, growth and survival of zircons during crustal fusion: kinetic principals, geological models and implications for isotopic inheritance. Earth and Environmental Science Transactions of The Royal Society of Edinburgh 87, 43–56.
Watson, E.B., Wark, D.A., Thomas, J.B., 2006. Crystallization thermometers for zircon and rutile. Contributions to Mineralogy and Petrology 151, 413.
Watts, K.E., Coble, M.A., Vazquez, J.A., Henry, C.D., Colgan, J.P., John, D.A., 2016. Chemical abrasion-SIMS (CA-SIMS) U-Pb dating of zircon from the late Eocene Caetano caldera, Nevada. Chemical Geology 439, 139–151.
Wenk, H.-R., Bulakh, A., 2016. Minerals: Their Constitution and Origin. Cambridge University Press.
Wetherill, G.W., 1956. Discordant uranium-lead ages, I. Eos, Transactions American Geophysical Union 37, 320–326.
Woodhead, J.D., Hellstrom, J., Hergt, J.M., Greig, A., Maas, R., 2007. Isotopic and Elemental Imaging of Geological Materials by Laser Ablation Inductively Coupled Plasma-Mass Spectrometry. Geostandards and Geoanalytical Research 31, 331–343.
Woodhead, J.D., Horstwood, M.S.A., Cottle, J.M., 2016. Advances in Isotope Ratio Determination by LA–ICP–MS. Elements 12, 317–322.
Yang, B., Luff, B.J., Townsend, P.D., 1992. Cathodoluminescence of natural zircons. Journal of Physics: Condensed Matter 4, 5617–5624.
Yang, L., 2009. Accurate and precise determination of isotopic ratios by MC-ICP-MS: A review. Mass Spectrometry Reviews 28, 990–1011.
Zack, T., Stockli, D.F., Luvizotto, G.L., Barth, M.G., Belousova, E., Wolfe, M.R., Hinton, R.W., 2011. In situ U–Pb rutile dating by LA-ICP-MS: 208Pb correction and prospects for geological applications. Contributions to Mineralogy and Petrology 162, 515–530.

Appendix

Appendix A: U-Pb apatite and U-Pb zircon data used to construct concordia plots.

Table 2: Apatite Sample Data (2006 Boreholes Sample Analytical Run)

Identification		Location		Geochronological Data													
Sample	Sample Reference	Latitude	Longitude	$^{207}Pb/^{235}U$	2σ	$^{206}Pb/^{238}U$	2σ	Error Correlation	$^{238}U/^{206}Pb$	2σ	$^{207}Pb/^{206}Pb$	2σ	Error Correlation	$^{206}Pb/^{238}U$ Age (Ma)	2σ	$^{207}Pb/^{235}U$ Age (Ma)	2σ
8.08	Mebo_2_1	53.2	-13.45	3.82	0.14	0.0919	0.0024	0.19	10.88	0.28	0.304	0.009	0.33	566	14	1599	24
	Mebo_2_2			5.82	0.26	0.1052	0.004	0.61	9.51	0.36	0.421	0.015	0.07	644	23	1921	30
	Mebo_2_4			3.86	0.14	0.0891	0.0024	0.24	11.22	0.30	0.311	0.009	0.29	549.9	14	1596	23
	Mebo_2_5			18.06	0.83	0.2119	0.0082	0.53	4.72	0.18	0.6130	0.0220	0.26	1239	43	2990	40
	Mebo_2_6			2.64	0.098	0.0804	0.0021	0.47	12.44	0.32	0.244	0.009	0.13	498	13	1305	23
	Mebo_2_7			18.33	0.83	0.2106	0.0079	0.75	4.75	0.18	0.625	0.021	0.33	1229	42	2985	37
	Mebo_2_8			4.01	0.15	0.0955	0.0026	0.46	10.47	0.29	0.3110	0.0100	0.18	588	15	1632	25
	Mebo_2_9			3.011	0.12	0.0815	0.0023	0.47	12.27	0.35	0.269	0.008	0.09	506	14	1403	23
	Mebo_2_10			7.44	0.28	0.1195	0.0037	0.36	8.37	0.26	0.451	0.015	0.34	728	21	2153	29
	Mebo_2_11			4.76	0.18	0.0993	0.0029	0.28	10.07	0.29	0.3570	0.0120	0.35	610	17	1772	25
	Mebo_2_12			2.984	0.11	0.0801	0.0022	0.52	12.48	0.34	0.273	0.009	0.14	496.5	13	1393	24
	Mebo_2_13			23.68	0.98	0.2574	0.0089	0.54	3.89	0.13	0.671	0.024	0.48	1476	45	3256	35
	Mebo_2_14			3.65	0.13	0.0892	0.0024	0.34	11.21	0.30	0.2977	0.0083	0.24	551	14	1559	22
	Mebo_2_15			3.5	0.13	0.089	0.0024	0.41	11.24	0.30	0.292	0.009	0.16	550	14	1523	24
	Mebo_2_16			3.4	0.13	0.0843	0.0023	0.11	11.86	0.32	0.296	0.011	0.41	521	14	1506	27
	Mebo_2_17			4.05	0.14	0.0907	0.0024	0.02	11.03	0.29	0.322	0.011	0.49	560	14	1643	23
	Mebo_2_18			14.13	0.54	0.1909	0.006	0.31	5.24	0.16	0.5430	0.0190	0.48	1127	33	2767	29
	Mebo_2_19			3.363	0.11	0.0872	0.0023	0.19	11.47	0.30	0.282	0.008	0.45	538.9	14	1494	20
	Mebo_2_20			5.72	0.19	0.1061	0.0031	0.11	9.43	0.28	0.395	0.012	0.51	652	18	1936	23
	Mebo_2_21			3.69	0.16	0.0872	0.0025	0.58	11.47	0.33	0.3110	0.0110	0.04	540	15	1562	28
	Mebo_2_22			3.32	0.12	0.0873	0.0024	0.39	11.45	0.31	0.277	0.008	0.19	539.2	14	1478	24
	Mebo_2_23			16.23	0.58	0.1944	0.0064	0.37	5.14	0.17	0.607	0.019	0.49	1146	35	2886	28
	Mebo_2_24			4.44	0.16	0.0968	0.0025	0.49	10.33	0.27	0.333	0.010	0.02	595.5	15	1714	25
	Mebo_2_25			9.33	0.34	0.1412	0.0042	0.54	7.08	0.21	0.490	0.014	0.31	850	24	2373	26
	Mebo_2_26			11.74	0.53	0.1566	0.006	0.67	6.39	0.24	0.540	0.018	0.27	936	33	2563	37
	Mebo_2_27			27.93	1.1	0.2947	0.011	0.59	3.39	0.13	0.689	0.024	0.47	1660	53	3409	33
	Mebo_2_28			33.5	1.5	0.345	0.014	0.65	2.90	0.12	0.707	0.027	0.44	1910	69	3591	37
	Mebo_2_29			48.3	2	0.465	0.018	0.65	2.15	0.08	0.7530	0.0250	0.48	2456	81	3957	34
	Mebo_2_30			1.962	0.067	0.07482	0.0018	0.21	13.37	0.32	0.1867	0.0049	0.21	465	11	1098	18
	Mebo_2_31			3.449	0.11	0.089	0.002	0.21	11.21	0.28	0.281	0.007	0.35	551	13	1514	20
	Mebo_2_32			24.7	0.96	0.2696	0.01	0.61	3.71	0.14	0.657	0.023	0.48	1534	50	3296	31
	Mebo_2_33			4.16	0.14	0.0948	0.0025	0.14	10.55	0.28	0.321	0.0096	0.43	584	15	1659	22
	Mebo_2_34			2.894	0.11	0.0838	0.0022	0.38	11.93	0.31	0.2505	0.0084	0.15074	520	13	1372	24
MeBo3	Mebo1_1			4.998	0.13	0.1764	0.0038	0.04	5.67	0.12	0.203	0.0042	0.47	1047	21	1817	22
	Mebo1_2			2.73	0.076	0.158	0.0035	0.47	6.33	0.14	0.1257	0.0023	0.18	945	20	1336	21
	Mebo1_3			9.21	0.25	0.2103	0.005	0.29	4.76	0.11	0.3169	0.0064	0.36	1230	27	2357	25
	Mebo1_4			5.43	0.16	0.1824	0.0045	0.12	5.48	0.14	0.2162	0.0062	0.44	1080	24	1888	26
	Mebo1_5			3.517	0.089	0.1626	0.0039	0.51	6.15	0.15	0.1557	0.0026	0.52	971	21	1533	20
	Mebo1_6			4.83	0.16	0.1725	0.0045	0.43	5.80	0.15	0.2004	0.0055	0.11	1026	25	1787	29
	Mebo1_7			6.36	0.17	0.1845	0.0043	0.44	5.42	0.13	0.2499	0.0045	0.37	1091	24	2027	23
	Mebo1_8			5.609	0.14	0.1779	0.004	0.39	5.62	0.13	0.2294	0.0038	0.36	1055	22	1918	21
	Mebo1_9			11.62	0.32	0.2275	0.0052	0.20	4.40	0.10	0.3701	0.0079	0.42	1321	27	2572	25
	Mebo1_10			9.11	0.31	0.2074	0.0052	0.04	4.82	0.12	0.318	0.01	0.37	1215	28	2344	31
	Mebo1_11			4.21	0.14	0.1701	0.0038	0.41	5.88	0.13	0.179	0.0044	0.00	1012	21	1674	27
	Mebo1_13			4.962	0.12	0.173	0.0039	0.26	5.78	0.13	0.2074	0.0037	0.41	1030	22	1812	21

Table 2: Apatite Sample Data (2006 Boreholes Sample Analytical Run)

Identification		Location		Geochronological Data													
Sample	Sample Reference	Latitude	Longitude	$^{207}Pb/^{235}U$	2σ	$^{206}Pb/^{238}U$	2σ	Error Correlation	$^{238}U/^{206}Pb$	2σ	$^{207}Pb/^{206}Pb$	2σ	Error Correlation	$^{206}Pb/^{238}U$ Age (Ma)	2σ	$^{207}Pb/^{235}U$ Age (Ma)	2σ
	Mebo1_16			9.43	0.26	0.2142	0.0053	0.00	4.67	0.12	0.3207	0.0077	0.54	1251	28	2378	25
	Mebo1_18			3.78	0.11	0.1672	0.0037	-0.09	5.98	0.13	0.164	0.0035	0.23	997	20	1589	23
	Mebo1_19			9.64	0.22	0.2149	0.0049	0.29	4.65	0.11	0.3266	0.0053	0.49	1255	26	2400	21
	Mebo1_20			11.03	0.29	0.2255	0.0053	0.00	4.43	0.10	0.3559	0.008	0.50	1311	28	2524	24
	Mebo1_21			7.48	0.24	0.1963	0.0057	0.09	5.09	0.15	0.2789	0.0078	0.49	1155	31	2170	27
	Mebo1_22			7.58	0.21	0.1988	0.0047	0.13	5.03	0.12	0.2779	0.0064	0.28	1169	25	2183	24
	Mebo1_23			10.06	0.3	0.2194	0.0054	0.34	4.56	0.11	0.3368	0.0076	0.43	1278	28	2440	26
	Mebo1_24			6.61	0.21	0.1875	0.0045	0.55	5.33	0.13	0.2546	0.0057	0.04	1107	24	2052	26
	Mebo1_25			10.17	0.26	0.219	0.0051	0.59	4.57	0.11	0.3346	0.0047	0.32	1276	27	2450	23
	Mebo1_27			4.72	0.14	0.1705	0.0041	0.27	5.87	0.14	0.1992	0.0049	0.20	1015	23	1767	26
	Mebo1_28			7.36	0.2	0.197	0.0049	0.17	5.08	0.13	0.2703	0.0056	0.56	1161	27	2153	24
	Mebo1_29			9.76	0.29	0.2183	0.0059	0.49	4.58	0.12	0.3237	0.0065	0.44	1272	31	2422	26
	Mebo1_30			2.506	0.061	0.1567	0.0033	0.15	6.38	0.13	0.1167	0.0018	0.43	938.5	18	1273	18
	Mebo1_31			5.83	0.17	0.182	0.0044	0.03	5.49	0.13	0.2315	0.0054	0.34	1078	24	1949	26
	Mebo1_32			10.17	0.26	0.2162	0.005	0.15	4.63	0.11	0.3429	0.007	0.36	1261	26	2451	23
	Mebo1_33			3.484	0.095	0.1658	0.0037	0.10	6.03	0.13	0.1516	0.0029	0.32	989	20	1525	21
	Mebo1_34			3.944	0.089	0.1657	0.0036	0.17	6.04	0.13	0.1721	0.0026	0.51	990	21	1622	18
	Mebo1_35			10.36	0.25	0.22	0.0048	0.28	4.55	0.10	0.34	0.006	0.46	1281	25	2467	22

Table 3: Zircon Sample Data (2006 Boreholes Sample Analytical Run)

Identification		Location		Geochronological Data												
Sample	Sample Reference	Latitude	Longitude	$^{207}Pb/^{235}U$	2σ	$^{206}Pb/^{238}U$	2σ	Error Correlation	$^{207}Pb/^{206}Pb$	2σ	$^{207}Pb/^{235}U$ Age (Ma)	2σ	$^{206}Pb/^{238}U$ Age (Ma)	2σ	$^{207}Pb/^{206}Pb$ Age (Ma)	2σ
7.02	X7_02a_1	53.2	-13.45	0.632	0.018	0.0805	0.0014	0.50	0.0565	0.0014	497	11	499.5	8.4	458	53
	X7_02a_2			0.619	0.014	0.0793	0.0013	0.15	0.0581	0.0015	489.2	8.8	492.2	7.9	519	55
	X7_02a_3			0.615	0.013	0.0778	0.0011	0.56	0.0569	0.001	486.8	8	483.4	6.6	484	41
	X7_02a_4			0.602	0.014	0.0766	0.0011	0.22	0.0571	0.0014	478.7	8.9	476.5	6.8	491	54
	X7_02a_5			0.588	0.014	0.0751	0.0013	0.32	0.057	0.0014	469.7	9.2	467.3	7.8	492	52
	X7_02a_6			0.630	0.021	0.0812	0.0016	0.53	0.0564	0.0016	495	13	503.5	9.6	472	65
	X7_02a_7			0.602	0.014	0.0774	0.0012	0.23	0.0566	0.0014	478.3	8.8	481.1	7.2	490	52
	X7_02a_9			0.610	0.016	0.0769	0.0011	0.50	0.0571	0.0013	484.8	9.7	478	6.6	503	53
	X7_02a_10			0.623	0.024	0.0798	0.0019	0.58	0.0573	0.0018	491	15	495	11	488	72
	X7_02a_11			0.626	0.014	0.0785	0.0010	0.40	0.0577	0.0012	493.8	8.8	487.7	6.1	515	43
	X7_02a_12			0.595	0.013	0.0759	0.0014	0.48	0.0578	0.0012	474.4	8.3	472.1	8.4	517	45
	X7_02a_14			0.615	0.014	0.0771	0.0011	0.34	0.0582	0.0013	486.7	8.7	479.3	6.5	538	49
	X7_02a_15			0.602	0.015	0.0762	0.0011	0.42	0.0569	0.0013	480	9.5	473.7	6.6	479	50
	X7_02a_16			0.608	0.014	0.0776	0.0013	0.15	0.057	0.0015	484.7	8.8	482.2	7.5	475	58
	X7_02a_17			0.592	0.017	0.0757	0.0013	0.44	0.0573	0.0015	472	11	470.8	7.8	490	57
	X7_02a_18			0.593	0.017	0.0758	0.0012	0.41	0.0566	0.0015	472	11	471.6	7	460	58
	X7_02a_19			0.619	0.018	0.0790	0.0013	0.13	0.0572	0.0018	489	11	491	8	519	63
	X7_02a_20			0.609	0.022	0.0775	0.0015	0.15	0.0574	0.0022	484	14	481.9	9	492	88
	X7_02a_21			0.584	0.015	0.0751	0.0014	0.58	0.0564	0.0012	467.2	9.7	467.2	8.5	475	52
	X7_02a_22			0.593	0.015	0.0745	0.0010	0.58	0.058	0.0012	472.8	9.6	463.6	6.2	528	46
	X7_02a_23			0.632	0.016	0.0781	0.0018	0.44	0.0584	0.0015	497.3	9.7	485	10	536	53
	X7_02a_24			0.591	0.013	0.0773	0.0014	0.34	0.0559	0.0013	471.3	8.4	480.3	8.1	444	50
	X7_02a_25			0.628	0.018	0.0792	0.0013	0.44	0.0577	0.0015	497	11	491.7	7.8	506	59
	X7_02a_26			0.609	0.015	0.0781	0.0012	0.07	0.0569	0.0016	483	9.6	485.3	7.5	474	66
	X7_02a_27			0.589	0.014	0.0763	0.0014	0.41	0.0558	0.0013	470.2	9.1	474.8	8.5	435	53
	X7_02a_28			0.595	0.013	0.0760	0.0014	0.63	0.0571	0.001	473.9	8.3	472.5	8.2	485	41
	X7_02a_29			0.600	0.014	0.0769	0.0012	0.46	0.0563	0.0012	477	8.6	478.3	7	467	47
	X7_02a_30			0.594	0.018	0.0767	0.0013	0.30	0.0567	0.0017	473	12	476.7	8	476	65
	X7_02a_31			0.596	0.018	0.0785	0.0014	0.46	0.0553	0.0015	472	11	487.9	8.4	414	62
	X7_02a_32			0.616	0.016	0.0778	0.0013	0.31	0.0573	0.0015	487.4	9.8	483.5	7.8	508	60
	X7_02a_34			0.610	0.015	0.0782	0.0014	0.45	0.0567	0.0013	483.7	9.7	486.1	8.2	474	51
	X7_02a_35			0.628	0.015	0.0780	0.0013	0.54	0.0586	0.0012	495.1	9.1	485	8	559	46
	X7_02a_36			0.612	0.015	0.0785	0.0013	0.32	0.0567	0.0014	484.6	9.2	487.7	7.6	471	54
	X7_02a_37			0.625	0.016	0.0798	0.0014	0.58	0.0572	0.0012	494	10	495.4	8.2	493	49
	X7_02a_38			0.643	0.018	0.0824	0.0015	0.41	0.057	0.0015	505	11	510.6	9.2	515	56
	X7_02a_39			0.601	0.013	0.0779	0.0011	0.35	0.0563	0.0012	479.3	7.9	484.2	6.8	471	49
	X7_02a_40			0.626	0.015	0.0802	0.0014	0.10	0.0567	0.0016	494.7	9.1	498.1	8.1	472	60
	X7_02a_41			0.610	0.018	0.0788	0.0016	0.37	0.0555	0.0016	483	11	489.6	9.4	422	65
	X7_02a_42			0.598	0.013	0.0769	0.0011	0.37	0.0567	0.0012	477.2	8.8	477.9	6.4	487	46
	X7_02a_43			0.601	0.010	0.0763	0.0011	0.44	0.05721	0.00093	478.1	6.1	474.5	6.4	498	35
	X7_02a_44			0.626	0.027	0.0790	0.0019	0.38	0.0567	0.0023	492	17	490	12	450	89
	X7_02a_45			0.624	0.017	0.0794	0.0013	0.55	0.057	0.0013	492	11	493.2	7.5	476	52

Table 3: Zircon Sample Data (2006 Boreholes Sample Analytical Run)

Identification		Location		Geochronological Data													
Sample	Sample Reference	Latitude	Longitude	$^{207}Pb/^{235}U$	2σ	$^{206}Pb/^{238}U$	2σ	Error Correlation	$^{207}Pb/^{206}Pb$	2σ	$^{207}Pb/^{235}U$ Age (Ma)	2σ	$^{206}Pb/^{238}U$ Age (Ma)	2σ	$^{207}Pb/^{206}Pb$ Age (Ma)	2σ
	X7_02a_46			0.613	0.015	0.0779	0.0014	0.45	0.0569	0.0013	486.5	9.3	484.1	8.7	481	50
	X7_02a_47			0.614	0.013	0.0780	0.0010	0.56	0.0571	0.001	486.4	8.1	484.5	5.8	488	39
	X7_02a_48			0.611	0.013	0.0785	0.0012	0.67	0.05711	0.0009	484	8	487.7	7.1	489	35
	X7_02a_49			0.609	0.015	0.0789	0.0012	0.02	0.0558	0.0016	485.3	9.2	491.1	7.3	443	63
7.58	X7_02d_1	53.2	-13.45	0.692	0.021	0.0806	0.0019	0.52	0.0627	0.0017	533	13	500	11	688	60
	X7_02d_2			0.599	0.015	0.0776	0.0018	0.29	0.0558	0.0016	476.7	9.2	482	11	436	62
	X7_02d_3			0.594	0.019	0.0721	0.0015	0.45	0.0582	0.0017	474	12	449.5	9	523	66
	X7_02d_4			0.574	0.016	0.0698	0.0018	0.50	0.0594	0.0016	461	10	435	11	577	59
	X7_02d_5			0.628	0.018	0.0769	0.0018	0.59	0.0586	0.0014	497	11	478	11	546	52
	X7_02d_6			0.606	0.017	0.0770	0.0017	0.47	0.0569	0.0015	481	10	479	10	493	58
	X7_02d_7			0.675	0.020	0.0832	0.0019	0.69	0.06	0.0013	525	12	516	12	601	45
	X7_02d_8			4.047	0.066	0.2925	0.0058	0.72	0.1003	0.0014	1643	13	1654	29	1630	27
	X7_02d_9			4.006	0.066	0.2926	0.0060	0.55	0.1003	0.0018	1635	13	1655	30	1636	34
	X7_02d_10			2.855	0.077	0.2347	0.0044	0.32	0.0875	0.0024	1371	20	1359	23	1377	49
	X7_02d_11			0.603	0.019	0.0753	0.0013	0.50	0.0586	0.0016	479	12	468.4	7.8	541	59
	X7_02d_12			0.600	0.019	0.0776	0.0017	0.48	0.0563	0.0016	478	13	482	10	452	61
	X7_02d_13			0.619	0.020	0.0723	0.0021	0.27	0.0622	0.0023	490	12	450	13	703	74
	X7_02d_14			0.602	0.016	0.0768	0.0014	0.53	0.0567	0.0013	479	10	477.6	8.4	468	50
	X7_02d_15			0.636	0.019	0.0754	0.0016	0.44	0.0608	0.0017	501	12	469.2	9.4	624	58
	X7_02d_16			0.626	0.017	0.0789	0.0016	0.07	0.0572	0.002	493	11	490	9.3	489	76
	X7_02d_17			0.630	0.025	0.0758	0.0017	0.43	0.0608	0.0022	497	16	472	10	611	79
	X7_02d_18			4.121	0.072	0.2964	0.0057	0.47	0.0999	0.0019	1658	14	1678	27	1629	36
	X7_02d_19			0.488	0.016	0.0652	0.0015	0.29	0.0556	0.0019	405	11	407.8	9.1	440	73
	X7_02d_20			0.527	0.025	0.0616	0.0019	0.48	0.0613	0.0026	428	17	386	11	624	85
	X7_02d_21			0.635	0.015	0.0764	0.0014	0.41	0.0605	0.0014	499.2	9.5	475.3	8.1	629	48
	X7_02d_22			0.626	0.017	0.0732	0.0015	0.20	0.0623	0.0019	493	11	455.9	9.2	674	65
	X7_02d_23			0.594	0.015	0.0755	0.0016	0.43	0.0561	0.0014	473.5	9.5	469.6	9.6	475	57
	X7_02d_24			0.610	0.014	0.0772	0.0014	0.33	0.0581	0.0014	483.5	8.7	479.7	8.7	520	53
	X7_02d_25			0.628	0.016	0.0786	0.0016	0.53	0.0575	0.0013	494.5	9.8	488.5	9.6	530	51
	X7_02d_26			0.607	0.015	0.0757	0.0016	0.38	0.0583	0.0015	483.2	9	470.8	9.7	526	55
	X7_02d_27			0.584	0.015	0.0756	0.0015	0.66	0.0565	0.0011	468.5	9.9	470.2	9.2	473	44
	X7_02d_28			0.609	0.015	0.0774	0.0018	0.24	0.0575	0.0017	482.6	9.2	481	11	496	65
	X7_02d_29			0.627	0.015	0.0790	0.0019	0.57	0.0587	0.0013	495.7	9.2	491	11	551	45
	X7_02d_30			0.603	0.015	0.0767	0.0016	0.65	0.0569	0.0011	478.9	9.4	477	9.7	481	42
	X7_02d_31			0.613	0.013	0.0782	0.0016	0.39	0.0565	0.0013	485.2	8.5	485.9	9.4	478	55
	X7_02d_32			0.639	0.022	0.0802	0.0019	0.54	0.0577	0.0017	500	14	498	11	514	64
	X7_02d_33			0.653	0.017	0.0814	0.0019	0.52	0.0577	0.0014	512	10	505	11	523	56
	X7_02d_34			0.603	0.016	0.0765	0.0018	0.66	0.0575	0.0012	479	10	476	11	507	45
	X7_02d_35			0.614	0.017	0.0779	0.0023	0.39	0.057	0.0018	488	11	484	14	472	69
	X7_02d_36			0.623	0.018	0.0790	0.0019	0.15	0.0578	0.002	495	12	491	11	524	73
	X7_02d_37			0.599	0.016	0.0699	0.0019	0.53	0.0615	0.0016	476	10	436	11	674	57
	X7_02d_38			0.610	0.017	0.0771	0.0019	0.63	0.0574	0.0013	485	11	479	12	516	48
	X7_02d_39			0.606	0.016	0.0741	0.0018	0.43	0.059	0.0016	481	10	463	11	566	56

Table 3: Zircon Sample Data (2006 Boreholes Sample Analytical Run)

Identification		Location		Geochronological Data													
Sample	Sample Reference	Latitude	Longitude	$^{207}Pb/^{235}U$	2σ	$^{206}Pb/^{238}U$	2σ	Error Correlation	$^{207}Pb/^{206}Pb$	2σ	$^{207}Pb/^{235}U$ Age (Ma)	2σ	$^{206}Pb/^{238}U$ Age (Ma)	2σ	$^{207}Pb/^{206}Pb$ Age (Ma)	2σ
	X7_02d_40			4.618	0.083	0.3136	0.0064	0.58	0.1071	0.0019	1752	15	1759	31	1748	31
7.13	X7_13_2	53.2	-13.45	0.611	0.015	0.0784	0.0013	0.11	0.0572	0.0016	484.6	9.2	487.3	7.7	494	59
	X7_13_3			0.641	0.022	0.0813	0.0016	0.40	0.0564	0.0018	502	14	504.4	9.7	451	73
	X7_13_4			0.615	0.021	0.0781	0.0014	0.27	0.056	0.0019	486	13	485.1	8.6	437	78
	X7_13_5			0.609	0.013	0.0782	0.0013	0.18	0.0569	0.0014	482.7	8.3	485.9	7.5	484	56
	X7_13_7			0.614	0.016	0.0788	0.0014	0.31	0.0566	0.0015	486.2	9.8	489.6	8.3	465	56
	X7_13_9			0.606	0.014	0.0752	0.0019	0.52	0.0589	0.0014	483.9	9.1	468	12	558	52
	X7_13_10			0.592	0.015	0.0760	0.0014	0.29	0.0562	0.0015	472.3	9.7	472.9	8.3	491	59
	X7_13_11			0.607	0.015	0.0760	0.0012	0.54	0.0572	0.0012	483.9	9.6	472.6	7	502	43
	X7_13_12			0.598	0.014	0.0766	0.0014	0.20	0.0564	0.0015	477.6	9.4	476.5	8.1	458	58
	X7_13_13			0.620	0.014	0.0769	0.0017	0.58	0.0588	0.0012	490	8.5	478	10	557	42
	X7_13_14			0.603	0.013	0.0763	0.0011	0.50	0.0577	0.0011	479.4	8.4	474.3	6.7	517	42
	X7_13_15			0.628	0.015	0.0788	0.0014	0.45	0.0579	0.0013	494.6	9.4	489.5	8.4	516	48
	X7_13_16			0.594	0.020	0.0753	0.0013	0.54	0.0565	0.0016	473	13	468.4	7.5	484	67
	X7_13_17			0.604	0.017	0.0782	0.0011	0.57	0.0562	0.0013	481	10	485.7	6.7	453	49
	X7_13_18			0.606	0.014	0.0780	0.0013	0.56	0.0565	0.0011	480.9	8.9	484.7	7.7	472	45
	X7_13_19			0.591	0.015	0.0769	0.0011	0.31	0.0562	0.0014	473	10	477.8	6.6	464	54
	X7_13_20			0.615	0.015	0.0782	0.0016	0.11	0.0566	0.0017	486.8	9.3	485.7	9.5	471	62
	X7_13_21			0.613	0.012	0.0786	0.0013	0.32	0.0566	0.0012	485.7	7.6	488.1	7.5	465	48
	X7_13_23			0.616	0.013	0.0789	0.0014	0.32	0.057	0.0013	487.2	8.4	489.8	8.3	481	49
	X7_13_24			0.646	0.017	0.0787	0.0015	0.23	0.0594	0.0017	506	10	488.7	8.8	574	64
	X7_13_25			0.608	0.017	0.0766	0.0014	0.59	0.0576	0.0013	483	11	476.4	8.1	504	49
	X7_13_26			0.616	0.017	0.0783	0.0013	0.25	0.0564	0.0016	487	11	486.4	7.8	471	62
	X7_13_27			0.653	0.018	0.0825	0.0012	0.67	0.0577	0.0012	510	11	511.7	6.9	509	45
	X7_13_28			0.594	0.014	0.0773	0.0014	0.48	0.055	0.0012	473.1	8.8	480.7	8.6	405	50
	X7_13_29			0.612	0.014	0.0777	0.0012	0.32	0.0562	0.0013	484.9	8.7	484	7.1	453	53
	X7_13_30			0.594	0.016	0.0763	0.0013	0.12	0.0567	0.0017	475	11	474.3	7.7	467	70
	X7_13_31			0.616	0.014	0.0788	0.0012	0.55	0.0574	0.0011	489.9	9.4	489.7	7.1	498	44
	X7_13_32			0.597	0.014	0.0775	0.0017	0.78	0.0559	0.00084	475.3	8.7	481.9	9.9	448	35
	X7_13_33			0.605	0.010	0.0770	0.0009	0.46	0.05669	0.00085	480.5	6.2	478.7	5.4	479	34
	X7_13_34			0.606	0.013	0.0775	0.0012	0.37	0.0564	0.0012	481.3	8.3	481.8	7.4	475	44
	X7_13_35			0.607	0.013	0.0784	0.0010	0.29	0.0557	0.0012	481.5	8.2	486.8	6.2	426	49
	X7_13_36			0.601	0.016	0.0773	0.0013	0.42	0.0565	0.0014	479	10	480.6	7.5	467	52
	X7_13_38			0.620	0.019	0.0804	0.0015	0.56	0.0551	0.0014	489	12	499	8.9	410	58
	X7_13_39			0.597	0.017	0.0773	0.0016	0.37	0.0567	0.0016	475	11	480.6	9.4	479	60
	X7_13_40			0.606	0.012	0.0789	0.0011	0.48	0.0557	0.001	481.1	7.4	489.9	6.4	431	40
	X7_13_41			0.603	0.013	0.0787	0.0013	0.48	0.0555	0.0011	480.5	8.2	488.6	8	448	44
	X7_13_42			0.627	0.013	0.0791	0.0012	0.35	0.0575	0.0012	494.5	8	491.5	7.2	504	46
	X7_13_43			0.605	0.014	0.0788	0.0012	0.55	0.0563	0.0011	480.1	9	489.6	7.1	459	43
	X7_13_44			0.598	0.016	0.0788	0.0012	0.38	0.0555	0.0014	475.6	9.9	489.4	7.1	418	55
	X7_13_45			0.621	0.013	0.0801	0.0010	0.11	0.0562	0.0013	491.6	7.8	497.5	6.3	446	51
	X7_13_46			0.614	0.015	0.0786	0.0015	0.48	0.0574	0.0013	486	9.5	488.2	8.8	494	53
	X7_13_47			0.626	0.021	0.0780	0.0015	0.65	0.0588	0.0015	493	13	484.9	9.1	550	56

Table 3: Zircon Sample Data (2006 Boreholes Sample Analytical Run)

Identification		Location		Geochronological Data													
Sample	Sample Reference	Latitude	Longitude	$^{207}Pb/^{235}U$	2σ	$^{206}Pb/^{238}U$	2σ	Error Correlation	$^{207}Pb/^{206}Pb$	2σ	$^{207}Pb/^{235}U$ Age (Ma)	2σ	$^{206}Pb/^{238}U$ Age (Ma)	2σ	$^{207}Pb/^{206}Pb$ Age (Ma)	2σ
	X7_13_48			0.623	0.013	0.0804	0.0012	0.20	0.0564	0.0013	491.8	8	499.1	7.1	455	51
	X7_13_49			0.616	0.016	0.0793	0.0012	0.36	0.0563	0.0014	488	10	492.2	7.2	457	56
	X7_13_50			0.623	0.012	0.0799	0.0013	0.41	0.0565	0.0011	492.1	7.2	495.9	7.8	470	43
8.08	MeBo2-1	53.2	-13.45	0.627	0.016	0.082	0.001	0.26	0.0555	0.0014	493	9.9	508.1	6.1	414	56
	MeBo2-2			0.635	0.015	0.07947	0.00092	0.34	0.0579	0.0013	498.1	9	492.9	5.5	505	50
	MeBo2-3			0.642	0.019	0.08081	0.00098	0.47	0.0572	0.0015	502	11	500.9	5.8	488	60
	MeBo2-4			2.405	0.079	0.2118	0.0045	0.31	0.0814	0.0027	1240	24	1238	24	1211	66
	MeBo2-5			4.750	0.110	0.2975	0.0039	0.57	0.116	0.0022	1771	19	1678	20	1886	33
	MeBo2-6			0.623	0.021	0.0811	0.0013	0.43	0.0557	0.0017	491	13	502.7	7.9	423	69
	MeBo2-7			0.629	0.018	0.0809	0.0011	0.13	0.0565	0.0017	494	11	501.3	6.4	445	66
	MeBo2-8			0.633	0.008	0.0803	0.00059	0.30	0.05706	0.00074	497.1	5.2	497.9	3.5	480	29
	MeBo2-9			3.477	0.096	0.2683	0.006	0.54	0.0938	0.0023	1521	21	1532	30	1500	46
	MeBo2-10			0.652	0.023	0.0828	0.002	0.19	0.0568	0.0022	509	14	513	12	464	88
	MeBo2-11			0.6301	0.0085	0.08051	0.00069	0.29	0.05673	0.00078	496	5.4	499.1	4.1	467	31
	MeBo2-12			0.626	0.010	0.07943	0.00076	0.35	0.05706	0.00087	492.7	6.1	492.6	4.5	480	34
	MeBo2-13			0.630	0.010	0.08068	0.00063	0.15	0.05658	0.00094	495.2	6.4	500.1	3.8	462	37
	MeBo2-14			0.646	0.028	0.0801	0.0018	0.13	0.0585	0.0027	505	17	497	10	520	100
	MeBo2-15			3.706	0.097	0.2821	0.0059	0.06	0.0953	0.0031	1571	21	1601	29	1525	62
	MeBo2-16			0.631	0.015	0.0803	0.0011	0.23	0.0569	0.0014	495.4	9.5	497.8	6.4	469	55
	MeBo2-18			0.647	0.012	0.08339	0.00074	0.32	0.0562	0.001	505	7.1	516.3	4.4	440	39
	MeBo2-19			4.256	0.092	0.313	0.0047	0.43	0.0987	0.002	1681	18	1754	23	1586	39
	MeBo2-20			0.646	0.025	0.0803	0.0012	0.36	0.0582	0.0021	504	16	497.6	7	506	80
	MeBo2-21			0.643	0.011	0.08251	0.00085	0.25	0.0566	0.001	503.8	6.9	511	5.1	456	40
	MeBo2-22			4.025	0.075	0.3064	0.0054	0.86	0.09511	0.00091	1632	15	1719	27	1525	18
	MeBo2-24			0.666	0.016	0.0829	0.0014	0.24	0.0579	0.0015	517	10	513.5	8.3	504	56
	MeBo2-25			0.639	0.015	0.0799	0.0013	0.50	0.0578	0.0012	500.6	9.3	495.3	7.6	514	47
	MeBo2-26			0.634	0.010	0.07962	0.00068	0.17	0.0577	0.00096	498.1	6.5	493.8	4.1	501	37
	MeBo2-27			0.649	0.019	0.0807	0.0014	0.29	0.0578	0.0017	507	11	500.2	8.6	515	68
	MeBo2-28			0.6135	0.0087	0.07899	0.0006	0.20	0.05643	0.00083	485.5	5.6	490	3.6	452	33
	MeBo2-29			0.643	0.012	0.08259	0.00099	0.40	0.0564	0.001	503.5	7.2	511.5	5.9	457	40
	MeBo2-30			0.623	0.010	0.08093	0.00078	0.44	0.05575	0.00079	491.2	6.1	501.6	4.7	427	31

Table 4: Apatite Standard Data (2011 Dredge Sample Analytical Run)

Identification		Location		Geochronological Data									
Sample	Sample Reference	Latitude	Longitude	$^{207}Pb/^{235}U$	2σ	$^{206}Pb/^{238}U$	2σ	Error Correlation	$^{238}U/^{206}Pb$	2σ	$^{207}Pb/^{206}Pb$	2σ	Error Correlation
PH4	Ph4_1	53.3572	-13.6678	6.73	0.34	0.2066	0.0067	0.38	4.84	0.16	0.24	0.011	0.27
	Ph4_2			15.1	1.3	0.276	0.014	0.36	3.62	0.18	0.404	0.031	0.04
	Ph4_3			358	64	3.44	0.56	0.94	0.291	0.047	0.775	0.052	0.09
	Ph4_4			114	20	1.06	0.16	0.92	0.94	0.14	0.733	0.045	0.00
	Ph4_5			11.64	0.94	0.26	0.012	0.21	3.85	0.18	0.341	0.029	0.31
	Ph4_6			308	25	2.61	0.20	0.80	0.383	0.029	0.851	0.04	0.32
	Ph4_7			16.9	1.1	0.278	0.013	0.14	3.60	0.17	0.439	0.031	0.42
	Ph4_8			59	8.8	0.565	0.051	0.17	1.77	0.16	0.701	0.08	0.06
	Ph4_9			20.12	0.99	0.308	0.011	0.52	3.25	0.12	0.479	0.023	0.24
	Ph4_10			41	5	0.478	0.034	0.08	2.09	0.15	0.605	0.052	0.13
	Ph4_1			12.4	0.51	0.243	0.0053	0.02	4.115	0.090	0.368	0.017	0.45
	Ph4_2			9.11	0.61	0.2358	0.0059	0.31	4.24	0.11	0.283	0.019	0.07
	Ph4_3			45	1.9	0.504	0.015	0.43	1.984	0.059	0.662	0.026	0.26
	Ph4_4			13.82	0.65	0.2577	0.0061	0.18	3.880	0.092	0.391	0.019	0.30
	Ph4_5			19.3	1.6	0.321	0.014	0.83	3.12	0.14	0.437	0.024	-0.31
	Ph4_6			59.6	3.1	0.616	0.026	0.58	1.623	0.069	0.708	0.032	0.23
	Ph4_7			8.19	0.46	0.2137	0.0044	0.52	4.68	0.10	0.277	0.014	-0.09
	Ph4_8			22.4	1.1	0.3351	0.0088	0.39	2.984	0.078	0.488	0.022	0.23
	Ph4_9			94.8	2.1	0.944	0.016	0.37	1.059	0.018	0.729	0.018	0.36
	Ph4_10			240	140	2.1	1.1	1.00	0.48	0.25	0.587	0.038	-0.79
	Ph4_11			11.13	0.49	0.2249	0.0048	0.23	4.446	0.095	0.359	0.017	0.33
	Ph4_12			11.65	0.86	0.2472	0.009	0.04	4.05	0.15	0.363	0.028	0.21
	Ph4_13			25.3	1.1	0.3719	0.0081	0.29	2.689	0.059	0.494	0.019	0.18
	Ph4_14			42.2	2.1	0.483	0.018	0.20	2.070	0.077	0.656	0.036	0.47
	Ph4_15			18.4	1	0.398	0.011	0.05	2.513	0.069	0.341	0.021	0.46
PH1	Ph1_1	53.3415	-13.8242	12.81	0.84	0.2513	0.0075	0.22	3.98	0.12	0.384	0.023	0.25
	Ph1_2			9.53	0.35	0.217	0.0038	0.02	4.608	0.081	0.311	0.013	0.39
	Ph1_3			34.6	2.3	0.508	0.022	0.04	1.969	0.085	0.499	0.04	0.43
	Ph1_4			5.18	0.2	0.1992	0.0032	0.26	5.020	0.081	0.1882	0.0073	0.17
	Ph1_5			12.46	0.45	0.2433	0.0034	0.05	4.110	0.057	0.366	0.014	0.32
	Ph1_6			19.11	0.85	0.292	0.0075	0.32	3.425	0.088	0.472	0.02	0.26
	Ph1_7			24.4	1.8	0.338	0.018	0.21	2.96	0.16	0.526	0.037	0.26
	Ph1_8			7.95	0.3	0.218	0.0036	-0.07	4.587	0.076	0.265	0.011	0.45

Table 4: Apatite Standard Data (2011 Dredge Sample Analytical Run)

Identification		Location		Geochronological Data									
Sample	Sample Reference	Latitude	Longitude	$^{207}Pb/^{235}U$	2σ	$^{206}Pb/^{238}U$	2σ	Error Correlation	$^{238}U/^{206}Pb$	2σ	$^{207}Pb/^{206}Pb$	2σ	Error Correlation
	Ph1_9			8.42	0.67	0.2579	0.0067	0.13	3.88	0.10	0.236	0.02	0.38
	Ph1_10			9.64	0.29	0.2153	0.003	0.32	4.645	0.065	0.3218	0.0094	0.11
	Ph1_11			12.74	0.36	0.2489	0.0037	0.13	4.018	0.060	0.372	0.011	0.37
	Ph1_12			37.5	1.7	0.4095	0.0092	0.05	2.442	0.055	0.663	0.032	0.45
	Ph1_13			8.88	0.65	0.2994	0.0077	0.05	3.340	0.086	0.217	0.016	0.29
	Ph1_14			29.1	1.3	0.37	0.01	0.52	2.703	0.073	0.573	0.022	0.06
	Ph1_15			13.04	0.57	0.252	0.005	0.00	3.968	0.079	0.364	0.018	0.44
	Ph1_16			18.16	0.98	0.2817	0.0071	0.13	3.550	0.089	0.47	0.028	0.38
	Ph1_17			6.04	0.24	0.2061	0.003	0.21	4.852	0.071	0.2094	0.0082	0.17
	Ph1_18			12.63	0.67	0.2423	0.0059	0.02	4.13	0.10	0.368	0.02	0.45
	Ph1_19			4.37	0.32	0.197	0.0045	-0.02	5.08	0.12	0.161	0.012	0.25
	Ph1_20			4.21	0.15	0.1761	0.0028	0.22	5.679	0.090	0.1729	0.0068	0.17
	Ph1_21			6.21	0.21	0.2074	0.0029	0.15	4.822	0.067	0.2143	0.0073	0.29
	Ph1_22			8.5	0.46	0.2103	0.0046	0.23	4.76	0.10	0.296	0.016	0.14
	Ph1_23			4.64	0.18	0.1776	0.0034	0.08	5.63	0.11	0.1875	0.0083	0.37
PH5	Ph5_1	53.2755	-14.2498	12.93	0.75	0.3463	0.0077	0.15	2.888	0.064	0.269	0.015	0.29
	Ph5_2			42.5	2.6	0.465	0.015	0.15	2.151	0.069	0.665	0.042	0.45
	Ph5_3			20.43	0.85	0.3312	0.0073	0.09	3.019	0.067	0.456	0.02	0.36
	Ph5_4			12.75	0.64	0.2337	0.0066	0.55	4.28	0.12	0.396	0.017	0.12
	Ph5_5			5.6	0.31	0.2839	0.0052	0.18	3.522	0.065	0.1417	0.0075	0.10
	Ph5_6			11.07	0.58	0.3373	0.0079	0.31	2.965	0.069	0.242	0.012	0.15
	Ph5_7			148.2	7.7	1.301	0.055	0.60	0.769	0.032	0.829	0.036	0.12
	Ph5_8			10.33	0.52	0.238	0.0064	0.24	4.20	0.11	0.317	0.017	0.21
	Ph5_9			5.67	0.25	0.2002	0.0033	0.08	4.995	0.082	0.2023	0.0083	0.31
	Ph5_10			26.5	1	0.3474	0.0073	0.17	2.879	0.060	0.554	0.026	0.36
	Ph5_11			12.4	0.89	0.2534	0.009	-0.01	3.95	0.14	0.355	0.028	0.49
	Ph5_12			13.96	0.6	0.2594	0.0056	0.30	3.855	0.083	0.392	0.016	0.25
	Ph5_13			31.21	0.94	0.3893	0.0081	0.57	2.569	0.053	0.587	0.017	0.09
	Ph5_14			25.64	0.98	0.3606	0.0084	0.42	2.773	0.065	0.517	0.017	0.19
	Ph5_15			12.29	0.35	0.2514	0.0039	0.31	3.978	0.062	0.356	0.01	0.32
	Ph5_16			52.8	3.9	0.591	0.026	0.42	1.692	0.074	0.666	0.047	0.28
	Ph5_17			27.2	1.2	0.351	0.0086	0.13	2.849	0.070	0.545	0.025	0.42
	Ph5_18			85.9	6.5	0.827	0.05	0.63	1.209	0.073	0.769	0.045	0.09
	Ph5_19			25.5	1.5	0.34	0.011	-0.09	2.94	0.10	0.546	0.037	0.51

Table 4: Apatite Standard Data (2011 Dredge Sample Analytical Run)

Identification		Location		Geochronological Data									
Sample	Sample Reference	Latitude	Longitude	$^{207}Pb/^{235}U$	2σ	$^{206}Pb/^{238}U$	2σ	Error Correlation	$^{238}U/^{206}Pb$	2σ	$^{207}Pb/^{206}Pb$	2σ	Error Correlation
	Ph5_20			26.9	1.1	0.353	0.01	0.18	2.833	0.080	0.557	0.026	0.45
	Ph5_21			21.26	0.71	0.3192	0.0065	0.19	3.133	0.064	0.479	0.017	0.44
	Ph5_22			68.2	3.1	0.695	0.023	0.15	1.439	0.048	0.721	0.038	0.49
	Ph5_23			8.73	0.42	0.2217	0.0054	0.19	4.51	0.11	0.283	0.014	0.29
	Ph5_24			10.22	0.47	0.2954	0.0054	0.22	3.385	0.062	0.252	0.012	0.16
PH10	Ph10_1	53.2755	-14.2498	44.8	2.1	0.479	0.015	0.20	2.088	0.065	0.674	0.033	0.42
	Ph10_2			23.4	1.2	0.335	0.0086	0.33	2.985	0.077	0.502	0.024	0.23
	Ph10_3			11.67	0.64	0.3429	0.0099	0.15	2.916	0.084	0.248	0.013	0.31
	Ph10_4			10.3	1.1	0.283	0.011	-0.09	3.53	0.14	0.267	0.03	0.58
	Ph10_5			43.1	1.3	0.477	0.011	0.38	2.096	0.048	0.661	0.019	0.41
	Ph10_6			27.73	0.97	0.3583	0.0074	0.20	2.791	0.058	0.554	0.02	0.31
	Ph10_7			55.3	3.3	0.64	0.024	0.29	1.563	0.059	0.633	0.039	0.35
	Ph10_8			19.2	0.85	0.3095	0.0065	0.41	3.231	0.068	0.453	0.019	0.13
	Ph10_9			3.69	0.18	0.1783	0.0025	0.10	5.609	0.079	0.1504	0.0075	0.18
	Ph10_10			53.3	1.8	0.574	0.013	0.27	1.742	0.039	0.676	0.025	0.42
	Ph10_11			18.3	1.3	0.2857	0.0089	-0.03	3.50	0.11	0.465	0.038	0.31
	Ph10_12			10.73	0.62	0.2407	0.0056	0.03	4.15	0.10	0.323	0.02	0.38
	Ph10_13			38.7	2.2	0.446	0.015	0.35	2.242	0.075	0.613	0.032	0.23
	Ph10_14			7.29	0.4	0.215	0.0043	0.19	4.651	0.093	0.241	0.013	0.18
	Ph10_15			32.7	1.3	0.673	0.013	0.37	1.486	0.029	0.363	0.016	-0.05
	Ph10_16			15.1	0.63	0.2729	0.0057	0.26	3.664	0.077	0.399	0.017	0.23
	Ph10_17			222.2	3.9	1.901	0.027	0.49	0.526	0.007	0.851	0.013	0.38
	Ph10_18			78.2	2.3	0.757	0.018	0.24	1.321	0.031	0.752	0.024	0.52
	Ph10_19			4800	1200	39.6	9.8	0.99	0.025	0.006	0.892	0.029	0.20
	Ph10_20			9.78	0.37	0.225	0.004	0.20	4.444	0.079	0.31	0.013	0.32
	Ph10_21			8.91	0.33	0.2147	0.0032	0.07	4.658	0.069	0.303	0.011	0.36
	Ph10_22			88.2	4.3	0.864	0.032	0.33	1.157	0.043	0.737	0.036	0.34
	Ph10_23			7.95	0.31	0.2163	0.0042	0.15	4.623	0.090	0.268	0.011	0.34
	Ph10_24			17.63	0.41	0.3088	0.0042	0.13	3.238	0.044	0.413	0.01	0.44
PH12	Ph12_1	53.2881	-13.8748	680	810	5.4	6.1	1.00	0.19	0.21	0.75	0.27	0.04
	Ph12_2			90.9	4.8	0.9	0.034	0.31	1.111	0.042	0.733	0.042	0.45
	Ph12_3			10.01	0.46	0.3059	0.0061	0.49	3.269	0.065	0.2338	0.0095	-0.02
	Ph12_4			26	13	0.39	0.1	1.00	2.56	0.66	0.308	0.033	-0.90
	Ph12_5			48.8	1.6	0.518	0.013	0.28	1.931	0.048	0.676	0.023	0.40

Table 4: Apatite Standard Data (2011 Dredge Sample Analytical Run)

Identification		Location		Geochronological Data									
Sample	Sample Reference	Latitude	Longitude	$^{207}Pb/^{235}U$	2σ	$^{206}Pb/^{238}U$	2σ	Error Correlation	$^{238}U/^{206}Pb$	2σ	$^{207}Pb/^{206}Pb$	2σ	Error Correlation
	Ph12_6			36.9	2.1	0.446	0.012	0.15	2.242	0.060	0.602	0.035	0.40
	Ph12_7			5.6	0.27	0.2158	0.0037	-0.09	4.634	0.079	0.185	0.011	0.42
	Ph12_8			28.3	1.2	0.3883	0.009	0.15	2.575	0.060	0.535	0.024	0.25
	Ph12_9			26.4	2.7	0.372	0.023	0.97	2.69	0.17	0.508	0.026	-0.63
	Ph12_10			81.8	4.7	0.78	0.03	0.39	1.282	0.049	0.759	0.041	0.32
	Ph12_11			12.15	0.71	0.2479	0.0056	0.22	4.034	0.091	0.359	0.022	0.24
	Ph12_12			3.83	0.17	0.1785	0.0043	0.45	5.60	0.13	0.1583	0.0065	0.01
	Ph12_13			17.27	0.88	0.2898	0.0068	0.25	3.451	0.081	0.429	0.021	0.21
	Ph12_14			29.4	1.5	0.379	0.013	0.60	2.639	0.091	0.554	0.025	0.17
	Ph12_15			12.77	0.55	0.2539	0.0047	-0.01	3.939	0.073	0.363	0.018	0.46
	Ph12_16			33.7	1.8	0.429	0.014	0.22	2.331	0.076	0.563	0.031	0.46
	Ph12_17			9.87	0.51	0.2229	0.0047	0.19	4.486	0.095	0.312	0.016	0.25
	Ph12_18			62	33	0.44	0.2	0.39	2.27	1.03	0.73	0.35	-0.56
	Ph12_19			73	11	0.698	0.081	0.93	1.43	0.17	0.717	0.035	-0.22
	Ph12_20			43	19	0.51	0.15	1.00	1.96	0.58	0.512	0.038	-0.54
	Ph12_21			28.3	1.3	0.3811	0.0086	0.27	2.624	0.059	0.533	0.024	0.28
	Ph12_22			7.82	0.45	0.2196	0.0048	0.52	4.55	0.10	0.262	0.014	-0.11
	Ph12_23			8.83	0.38	0.2354	0.0041	0.19	4.248	0.074	0.268	0.012	0.24

Table 5: Zircon Sample Data (2011 Dredge Sample Analytical Run)

Identification		Location		Geochronological Data													
Sample	Sample Reference	Latitude	Longitude	$^{207}Pb/^{235}U$	2σ	$^{206}Pb/^{238}U$	2σ	Error Correlation	$^{238}U/^{206}Pb$	2σ	$^{207}Pb/^{206}Pb$	2σ	$^{207}Pb/^{235}U$ Age (Ma)	2σ	$^{206}Pb/^{238}U$ Age (Ma)	2σ
PH1	Porc_1_1	53.3415	-13.8242	2.57	0.11	0.2274	0.009	0.55	4.40	0.17	0.0816	0.003	1283	32	1317	47
	Porc_1_2			3.08	0.1	0.2507	0.0089	0.67	3.99	0.14	0.0917	0.0023	1426	26	1434	46
	Porc_1_3			4.07	0.12	0.2976	0.0096	0.70	3.36	0.11	0.0993	0.0021	1646	23	1674	48
	Porc_1_4			4.01	0.12	0.293	0.0096	0.66	3.41	0.11	0.0981	0.0023	1630	26	1652	48
	Porc_1_5			3.038	0.077	0.2448	0.0065	0.65	4.08	0.11	0.0937	0.0021	1412	20	1408	34
	Porc_1_6			2.104	0.043	0.1952	0.004	0.59	5.12	0.10	0.0798	0.0011	1148	14	1149	22
	Porc_1_7			4.025	0.075	0.2925	0.0061	0.61	3.42	0.07	0.1006	0.0015	1635	15	1651	31
	Porc_1_8			3.96	0.11	0.2879	0.008	0.61	3.47	0.10	0.0999	0.0022	1620	23	1624	40
	Porc_1_9			1.724	0.045	0.1719	0.0029	0.24	5.82	0.10	0.074	0.0019	1014	17	1023	16
	Porc_1_11			3.476	0.082	0.2697	0.0077	0.72	3.71	0.11	0.0956	0.0018	1523	19	1536	39
	Porc_1_12			2.723	0.069	0.2331	0.0074	0.78	4.29	0.14	0.0847	0.0016	1336	19	1348	39
	Porc_1_13			3.798	0.091	0.2816	0.0079	0.78	3.55	0.10	0.0991	0.0015	1591	19	1598	39
	Porc_1_14			4.07	0.1	0.2951	0.0077	0.71	3.389	0.088	0.1001	0.0016	1651	21	1662	38
	Porc_1_15			4.183	0.089	0.2961	0.008	0.66	3.377	0.091	0.1006	0.0018	1669	18	1673	40
	Porc_1_16			3.312	0.05	0.258	0.0047	0.56	3.876	0.071	0.0942	0.0013	1482	12	1481	24
	Porc_1_18			1.372	0.036	0.1451	0.0033	0.53	6.89	0.16	0.0713	0.0015	878	15	872	18
	Porc_1_19			4.02	0.1	0.2907	0.0087	0.71	3.44	0.10	0.101	0.0019	1635	21	1644	44
	Porc_1_20			3.42	0.12	0.264	0.0098	0.53	3.79	0.14	0.0945	0.0032	1498	29	1503	50
	Porc_1_21			2.097	0.064	0.1958	0.0074	0.72	5.11	0.19	0.0764	0.0018	1142	21	1147	40
	Porc_1_22			1.6	0.047	0.1648	0.0056	0.72	6.07	0.21	0.0702	0.0016	969	19	982	31
	Porc_1_23			3.9	0.11	0.2887	0.009	0.71	3.46	0.11	0.1002	0.0019	1606	22	1627	45
	Porc_1_24			4.5	0.11	0.311	0.0091	0.77	3.215	0.094	0.1053	0.0018	1725	20	1741	45
	Porc_1_25			1.604	0.052	0.1648	0.0056	0.66	6.07	0.21	0.0719	0.0018	965	20	980	31
	Porc_1_26			3.317	0.095	0.2632	0.0091	0.72	3.80	0.13	0.0911	0.0019	1479	23	1502	47
	Porc_1_27			3.53	0.12	0.2671	0.0095	0.74	3.74	0.13	0.0976	0.0021	1536	27	1518	48
	Porc_1_28			3.9	0.11	0.2842	0.0085	0.57	3.52	0.11	0.1005	0.0025	1616	21	1609	43
	Porc_1_29			4.04	0.11	0.294	0.01	0.70	3.40	0.12	0.1017	0.0023	1646	23	1651	52
	Porc_1_30			4.42	0.12	0.305	0.011	0.80	3.28	0.12	0.103	0.002	1718	23	1707	52
	Porc_1_31			3.365	0.098	0.2645	0.0092	0.76	3.78	0.13	0.0926	0.002	1489	23	1505	47
	Porc_1_32			3.51	0.11	0.272	0.0099	0.64	3.68	0.13	0.0934	0.0025	1524	25	1541	50
	Porc_1_33			3.85	0.1	0.2792	0.0088	0.64	3.58	0.11	0.1023	0.0024	1598	22	1580	44
	Porc_1_35			3.379	0.095	0.2646	0.0091	0.75	3.78	0.13	0.0921	0.0018	1491	22	1505	47
	Porc_1_36			3.99	0.11	0.2876	0.0094	0.78	3.48	0.11	0.1014	0.0018	1624	22	1620	47
	Porc_1_37			3.268	0.088	0.2572	0.0085	0.81	3.89	0.13	0.0921	0.0017	1473	21	1480	45
	Porc_1_38			4.02	0.12	0.292	0.01	0.60	3.42	0.12	0.1021	0.0022	1633	24	1639	50
	Porc_1_39			3.81	0.11	0.2837	0.0099	0.71	3.52	0.12	0.0981	0.0022	1595	23	1601	50
	Porc_1_40			2.627	0.071	0.2267	0.0079	0.80	4.41	0.15	0.0832	0.0016	1303	21	1311	42
	Porc_1_41			2.544	0.077	0.2214	0.0067	0.61	4.52	0.14	0.0834	0.0019	1282	21	1284	35
	Porc_1_42			1.834	0.055	0.1766	0.0057	0.72	5.66	0.18	0.0761	0.0016	1055	20	1044	31
	Porc_1_43			4.06	0.11	0.2892	0.0088	0.75	3.46	0.11	0.1012	0.0018	1641	22	1629	44

Table 5: Zircon Sample Data (2011 Dredge Sample Analytical Run)

Identification		Location		Geochronological Data												
Sample	Sample Reference	Latitude	Longitude	$^{207}Pb/^{235}U$	2σ	$^{206}Pb/^{238}U$	2σ	Error Correlation	$^{238}U/^{206}Pb$	2σ	$^{207}Pb/^{206}Pb$	2σ	$^{207}Pb/^{235}U$ Age (Ma)	2σ	$^{206}Pb/^{238}U$ Age (Ma)	2σ
	Porc_1_44			1.576	0.05	0.1615	0.0049	0.53	6.19	0.19	0.071	0.002	955	20	962	27
	Porc_1_45			3.337	0.087	0.2601	0.0077	0.68	3.84	0.11	0.094	0.0018	1487	20	1484	40
	Porc_1_46			3.31	0.1	0.2566	0.0088	0.64	3.90	0.13	0.0949	0.0024	1482	25	1464	45
	Porc_1_47			2.623	0.083	0.2217	0.0072	0.70	4.51	0.15	0.0851	0.0019	1301	23	1287	38
	Porc_1_48			1.777	0.048	0.1743	0.0053	0.68	5.74	0.17	0.074	0.0016	1033	18	1034	29
	Porc_1_49			3.9	0.13	0.284	0.01	0.56	3.52	0.12	0.1002	0.0028	1607	28	1603	51
	Porc_1_50			3.059	0.084	0.2453	0.0082	0.73	4.08	0.14	0.0909	0.0018	1418	21	1406	43
	Porc_1_52			3.9	0.11	0.286	0.0098	0.78	3.50	0.12	0.0994	0.0019	1605	22	1611	49
	Porc_1_53			2.832	0.072	0.2308	0.008	0.71	4.33	0.15	0.0904	0.002	1367	19	1333	42
	Porc_1_54			4.18	0.11	0.2955	0.0091	0.73	3.38	0.10	0.1025	0.0019	1666	21	1660	45
	Porc_1_55			4.15	0.12	0.2912	0.0095	0.73	3.43	0.11	0.1026	0.002	1659	24	1638	48
	Porc_1_56			3.534	0.094	0.2663	0.0086	0.77	3.76	0.12	0.0968	0.0019	1534	21	1514	44
	Porc_1_57			1.55	0.03	0.1579	0.0037	0.55	6.33	0.15	0.0714	0.0012	949	12	943	21
	Porc_1_58			3.165	0.089	0.2497	0.0082	0.79	4.00	0.13	0.0922	0.0016	1447	22	1429	43
	Porc_1_59			3.32	0.1	0.2561	0.0082	0.64	3.90	0.13	0.0937	0.0023	1484	23	1468	42
	Porc_1_61			6.13	0.18	0.36	0.013	0.77	2.78	0.10	0.1259	0.0026	1990	26	1968	60
	Porc_1_62			4.022	0.081	0.2899	0.0067	0.71	3.449	0.080	0.0997	0.0013	1636	17	1636	33
	Porc_1_63			3.798	0.079	0.2753	0.0066	0.71	3.632	0.087	0.1011	0.0013	1591	17	1563	33
	Porc_1_64			4.029	0.091	0.2873	0.0074	0.68	3.481	0.090	0.1013	0.0017	1638	19	1623	37
	Porc_1_66			3.275	0.077	0.2549	0.0065	0.68	3.92	0.10	0.0923	0.0015	1472	19	1462	34
	Porc_1_67			1.636	0.097	0.1648	0.0068	0.18	6.07	0.25	0.0798	0.0053	988	41	982	38
	Porc_1_68			3.229	0.087	0.2528	0.0082	0.74	3.96	0.13	0.0926	0.0019	1466	21	1445	42
	Porc_1_69			4.16	0.12	0.294	0.01	0.78	3.40	0.12	0.1016	0.002	1664	23	1653	50
	Porc_1_70			1.744	0.06	0.1722	0.006	0.67	5.81	0.20	0.0731	0.0019	1018	22	1020	33
	Porc_1_71			1.528	0.047	0.1548	0.0051	0.68	6.46	0.21	0.0708	0.0017	944	19	924	29
	Porc_1_72			4.1	0.12	0.2911	0.0079	0.64	3.435	0.093	0.0993	0.002	1651	24	1641	40
	Porc_1_73			3.981	0.093	0.285	0.0076	0.75	3.509	0.094	0.0994	0.0015	1627	19	1610	39
	Porc_1_74			1.594	0.047	0.1619	0.0043	0.55	6.18	0.16	0.0706	0.0016	965	18	966	24
	Porc_1_75			3.12	0.1	0.2479	0.0092	0.75	4.03	0.15	0.0888	0.002	1436	25	1425	48
	Porc_1_76			3.97	0.11	0.287	0.01	0.77	3.48	0.12	0.0981	0.002	1622	24	1618	52
	Porc_1_77			1.794	0.056	0.1765	0.0064	0.75	5.67	0.21	0.0724	0.0017	1041	20	1044	35
	Porc_1_78			3.002	0.086	0.2423	0.0078	0.72	4.13	0.13	0.0887	0.0018	1406	22	1392	41
	Porc_1_79			1.893	0.056	0.1819	0.0063	0.75	5.50	0.19	0.0743	0.0015	1076	20	1075	35
PH9	porc_9_1	53.2522	-14.2556	3.38	0.18	0.2608	0.0089	0.43	3.83	0.13	0.0948	0.002	1499	42	1497	47
	porc_9_2			2.42	0.21	0.2199	0.0088	0.03	4.55	0.18	0.0827	0.0065	1249	64	1281	47
	porc_9_3			1.648	0.098	0.1682	0.0069	0.71	5.95	0.24	0.0709	0.0016	987	38	1007	36
	porc_9_4			2.71	0.16	0.2171	0.0083	0.23	4.61	0.18	0.0921	0.0031	1334	42	1271	41
	porc_9_5			2.22	0.11	0.2068	0.0075	0.29	4.84	0.18	0.0783	0.0016	1187	36	1212	40
	porc_9_6			2.74	0.16	0.2303	0.0092	0.91	4.34	0.17	0.0866	0.0012	1340	41	1344	48
	porc_9_7			11.42	0.58	0.482	0.019	0.53	2.075	0.082	0.1725	0.0034	2558	48	2536	81
	porc_9_8			1.75	0.11	0.178	0.0065	0.00	5.62	0.21	0.0725	0.0037	1029	41	1056	36

Table 5: Zircon Sample Data (2011 Dredge Sample Analytical Run)

Identification		Location		Geochronological Data													
Sample	Sample Reference	Latitude	Longitude	$^{207}Pb/^{235}U$	2σ	$^{206}Pb/^{238}U$	2σ	Error Correlation	$^{238}U/^{206}Pb$	2σ	$^{207}Pb/^{206}Pb$	2σ	$^{207}Pb/^{235}U$ Age (Ma)	2σ	$^{206}Pb/^{238}U$ Age (Ma)	2σ
	porc_9_9			3.05	0.17	0.2488	0.0096	0.84	4.02	0.16	0.089	0.0018	1417	42	1431	50
	porc_9_10			3.51	0.22	0.271	0.014	0.89	3.69	0.19	0.0957	0.002	1536	49	1542	69
	porc_9_11			3.94	0.21	0.291	0.012	0.77	3.44	0.14	0.1004	0.002	1622	44	1648	60
	porc_9_13			4.19	0.24	0.295	0.011	0.48	3.39	0.13	0.1021	0.0029	1674	44	1668	53
	porc_9_14			3.94	0.22	0.291	0.011	0.59	3.44	0.13	0.1	0.0023	1620	44	1647	57
	porc_9_15			2.49	0.13	0.2158	0.0079	0.38	4.63	0.17	0.0849	0.002	1272	41	1259	42
	porc_9_16			3.68	0.2	0.282	0.011	0.27	3.55	0.14	0.0942	0.0027	1566	43	1601	56
	porc_9_17			1.74	0.1	0.1741	0.0074	0.08	5.74	0.24	0.0728	0.003	1029	35	1034	41
PH9	porc_9B_1	53.2522	-14.2556	2.02	0.23	0.1979	0.0075	0.00	5.05	0.19	0.0771	0.009	1150	80	1163	40
	porc_9B_2			2.12	0.11	0.1981	0.0057	0.12	5.05	0.15	0.0782	0.0034	1156	36	1165	31
	porc_9B_3			2.19	0.12	0.1962	0.0068	0.50	5.10	0.18	0.0826	0.0035	1184	37	1154	36
	porc_9B_4			4.17	0.23	0.2978	0.009	0.38	3.36	0.10	0.1005	0.0043	1672	44	1680	45
	porc_9B_5			3.03	0.17	0.242	0.0081	0.77	4.13	0.14	0.0937	0.0038	1417	40	1396	42
	porc_9B_6			3.95	0.23	0.287	0.0099	0.26	3.48	0.12	0.1003	0.005	1622	46	1626	49
	porc_9B_7			2.14	0.11	0.1959	0.0057	0.57	5.10	0.15	0.0798	0.0032	1159	36	1153	31
	porc_9B_8			3.34	0.18	0.2597	0.0072	0.31	3.85	0.11	0.0945	0.004	1490	41	1488	37
	porc_9B_9			2.98	0.16	0.2468	0.0074	0.50	4.05	0.12	0.0893	0.0038	1400	42	1421	38
	porc_9B_10			3.09	0.17	0.2435	0.0085	0.78	4.11	0.14	0.093	0.0038	1429	42	1404	44
	porc_9B_11			4.06	0.22	0.2939	0.0093	0.49	3.40	0.11	0.1014	0.0044	1645	45	1665	45
	porc_9B_12			3.25	0.17	0.2582	0.0074	0.27	3.87	0.11	0.0923	0.0039	1470	42	1480	38
	porc_9B_13			3.77	0.21	0.2923	0.0093	0.62	3.42	0.11	0.0933	0.0039	1585	46	1652	47
	porc_9B_14			2.01	0.15	0.1785	0.0077	0.92	5.60	0.24	0.0813	0.0036	1118	50	1058	42
	porc_9B_15			10.61	0.54	0.463	0.013	0.52	2.160	0.061	0.1676	0.0066	2489	48	2452	59
	porc_9B_16			2.84	0.15	0.2359	0.0066	0.60	4.24	0.12	0.0877	0.0035	1366	38	1365	34
	porc_9B_17			4.21	0.22	0.299	0.0084	0.52	3.344	0.094	0.1027	0.0041	1675	43	1686	42
	porc_9B_18			3.03	0.17	0.2485	0.0077	0.66	4.02	0.12	0.0891	0.0038	1414	44	1430	40
	porc_9B_19			2.73	0.14	0.2272	0.0066	0.64	4.40	0.13	0.0862	0.0034	1336	39	1320	35
	porc_9B_20			3.94	0.26	0.288	0.013	0.86	3.47	0.16	0.101	0.0043	1618	54	1642	62
	porc_9B_21			2.5	0.16	0.2157	0.0063	0.04	4.64	0.14	0.0853	0.0049	1267	49	1259	34
	porc_9B_22			1.94	0.1	0.186	0.0058	0.70	5.38	0.17	0.0749	0.0029	1093	35	1100	31
	porc_9B_24			2.08	0.12	0.191	0.0053	0.36	5.24	0.15	0.0787	0.0034	1140	38	1127	29
	porc_9B_25			1.92	0.1	0.1859	0.0055	0.68	5.38	0.16	0.0757	0.003	1088	35	1101	29
	porc_9B_26			2.82	0.15	0.2377	0.007	0.44	4.21	0.12	0.0863	0.0035	1362	39	1374	36
	porc_9B_27			3.54	0.21	0.2671	0.0085	0.70	3.74	0.12	0.096	0.0043	1538	47	1526	43
	porc_9B_28			1.81	0.1	0.1763	0.0052	0.43	5.67	0.17	0.075	0.0034	1050	39	1047	28
	porc_9B_29			3.27	0.17	0.2536	0.0075	0.79	3.94	0.12	0.0937	0.0036	1474	41	1456	38
	porc_9B_30			2.11	0.14	0.1969	0.0063	0.24	5.08	0.16	0.0779	0.0043	1151	46	1159	34
	porc_9B_31			1.84	0.23	0.1868	0.0086	0.25	5.35	0.25	0.0724	0.0085	1057	87	1103	47
	porc_9B_32			1.92	0.12	0.1832	0.0057	0.48	5.46	0.17	0.0765	0.0037	1089	40	1084	31
	porc_9B_33			2.87	0.16	0.2357	0.0071	0.65	4.24	0.13	0.0886	0.0038	1379	40	1364	37
	porc_9B_34			3.14	0.17	0.2526	0.0074	0.61	3.96	0.12	0.091	0.0038	1443	41	1452	38

Table 5: Zircon Sample Data (2011 Dredge Sample Analytical Run)

Identification		Location		Geochronological Data													
Sample	Sample Reference	Latitude	Longitude	$^{207}Pb/^{235}U$	2σ	$^{206}Pb/^{238}U$	2σ	Error Correlation	$^{238}U/^{206}Pb$	2σ	$^{207}Pb/^{206}Pb$	2σ	$^{207}Pb/^{235}U$ Age (Ma)	2σ	$^{206}Pb/^{238}U$ Age (Ma)	2σ
	porc_9B_35			1.88	0.11	0.184	0.0064	0.37	5.43	0.19	0.0734	0.0035	1071	37	1093	33
	porc_9B_36			4.46	0.24	0.3107	0.0099	0.62	3.22	0.10	0.104	0.0044	1721	46	1743	49
	porc_9B_37			1.92	0.1	0.1863	0.0061	0.39	5.37	0.18	0.0752	0.0032	1086	35	1101	33
	porc_9B_38			2.22	0.13	0.198	0.0061	0.34	5.05	0.16	0.081	0.0037	1183	40	1164	33
	porc_9B_39			2.99	0.16	0.2374	0.0082	0.70	4.21	0.15	0.0918	0.0038	1405	41	1373	43
	porc_9B_40			2.14	0.11	0.1979	0.0057	0.66	5.05	0.15	0.0799	0.0032	1164	38	1164	31
	porc_9B_41			1.74	0.11	0.1743	0.0051	0.40	5.74	0.17	0.0724	0.0036	1019	40	1035	28
	porc_9B_42			3.77	0.24	0.28	0.011	0.89	3.57	0.14	0.0971	0.004	1581	52	1590	53
	porc_9B_43			2.28	0.16	0.1969	0.0088	0.37	5.08	0.23	0.0879	0.0058	1201	49	1158	47
	porc_9B_44			4.17	0.22	0.2959	0.0093	0.67	3.38	0.11	0.1043	0.0042	1668	44	1671	46
	porc_9B_45			2.7	0.15	0.2301	0.0066	0.56	4.35	0.12	0.0859	0.0036	1328	41	1335	35
	porc_9B_46			1.88	0.11	0.1798	0.0051	0.47	5.56	0.16	0.0753	0.0033	1070	38	1066	28
	porc_9B_47			2.03	0.11	0.1921	0.0061	0.35	5.21	0.17	0.0763	0.0033	1125	37	1133	33
	porc_9B_48			2.6	0.24	0.2144	0.0078	0.06	4.66	0.17	0.0908	0.0084	1306	69	1256	41
	porc_9B_49			2.56	0.16	0.2165	0.0068	0.28	4.62	0.15	0.0858	0.0042	1286	45	1263	36
	porc_9B_50			1.75	0.1	0.1766	0.0053	0.48	5.66	0.17	0.073	0.0033	1027	36	1050	28
	porc_9B_51			1.86	0.13	0.1772	0.0057	0.18	5.64	0.18	0.0763	0.0047	1065	47	1052	31
	porc_9B_54			2.55	0.13	0.2192	0.0066	0.56	4.56	0.14	0.0872	0.0035	1286	38	1277	35
PH10	porc_10_1	53.2755	-14.2498	3.45	0.19	0.2632	0.0091	0.50	3.80	0.13	0.0939	0.0024	1516	42	1506	46
	porc_10_2			3.82	0.21	0.281	0.01	0.71	3.56	0.13	0.0989	0.0017	1596	44	1595	52
	porc_10_3			2.38	0.14	0.2137	0.0096	0.81	4.68	0.21	0.081	0.0017	1236	42	1248	51
	porc_10_4			3.24	0.18	0.2583	0.0099	0.75	3.87	0.15	0.0926	0.002	1467	43	1481	51
	porc_10_5			3.61	0.21	0.2691	0.0095	0.60	3.72	0.13	0.0985	0.0025	1561	47	1536	48
	porc_10_6			1.65	0.1	0.1677	0.0063	0.47	5.96	0.22	0.0722	0.0023	992	41	999	35
	porc_10_7			3.19	0.19	0.256	0.01	0.82	3.91	0.15	0.0904	0.0017	1453	45	1471	53
	porc_10_8			1.79	0.11	0.1757	0.0062	0.25	5.69	0.20	0.0745	0.0023	1042	38	1044	34
	porc_10_9			3.14	0.2	0.263	0.011	0.19	3.80	0.16	0.0861	0.0036	1447	50	1507	53
	porc_10_10			2.12	0.11	0.1956	0.0067	0.45	5.11	0.18	0.0791	0.0017	1160	34	1152	36
	porc_10_11			4.01	0.23	0.294	0.01	0.38	3.40	0.12	0.0988	0.0024	1635	45	1663	51
	porc_10_13			2.11	0.11	0.1958	0.0066	0.75	5.11	0.17	0.0783	0.0011	1152	36	1153	35
	porc_10_14			1.9	0.098	0.1832	0.0062	0.71	5.46	0.18	0.0754	0.001	1080	34	1086	35
	porc_10_15			3.27	0.18	0.2541	0.0087	0.44	3.94	0.13	0.0935	0.0019	1476	40	1459	45
	porc_10_16			1.61	0.11	0.1672	0.0084	0.42	5.98	0.30	0.0692	0.0031	974	46	996	46
	porc_10_17			3.4	0.2	0.2641	0.0095	0.34	3.79	0.14	0.0908	0.0031	1507	47	1511	48
	porc_10_18			1.618	0.084	0.1631	0.0055	0.62	6.13	0.21	0.0718	0.0012	977	32	974	31
	porc_10_19			3.06	0.16	0.2335	0.008	0.42	4.28	0.15	0.0947	0.0022	1421	41	1353	42
	porc_10_20			3.74	0.19	0.2693	0.0089	0.37	3.71	0.12	0.1006	0.0017	1580	41	1537	45
	porc_10_21			3.28	0.18	0.2566	0.0093	0.60	3.90	0.14	0.0922	0.0018	1474	42	1472	48
	porc_10_22			3.23	0.19	0.25	0.0088	0.74	4.00	0.14	0.0946	0.0017	1470	40	1438	46
	porc_10_23			4.09	0.22	0.291	0.011	0.53	3.44	0.13	0.1011	0.0025	1650	45	1644	53
	porc_10_24			3.92	0.22	0.2817	0.0097	0.53	3.55	0.12	0.0997	0.0022	1615	45	1599	49

Table 5: Zircon Sample Data (2011 Dredge Sample Analytical Run)

Identification		Location		Geochronological Data													
Sample	Sample Reference	Latitude	Longitude	$^{207}Pb/^{235}U$	2σ	$^{206}Pb/^{238}U$	2σ	Error Correlation	$^{238}U/^{206}Pb$	2σ	$^{207}Pb/^{206}Pb$	2σ	$^{207}Pb/^{235}U$ Age (Ma)	2σ	$^{206}Pb/^{238}U$ Age (Ma)	2σ
	porc_10_25			2.83	0.16	0.232	0.0091	0.44	4.31	0.17	0.0884	0.0025	1362	42	1345	48
	porc_10_26			1.64	0.1	0.167	0.0059	0.17	5.99	0.21	0.0714	0.0026	980	39	995	33
	porc_10_27			3.34	0.17	0.2611	0.0091	0.58	3.83	0.13	0.0924	0.0013	1489	40	1495	46
	porc_10_28			3.66	0.2	0.277	0.0095	0.22	3.61	0.12	0.0961	0.0023	1562	44	1576	48
	porc_10_30			3.3	0.19	0.257	0.01	0.49	3.89	0.15	0.0925	0.0023	1483	44	1478	49
	porc_10_31			3.49	0.19	0.2646	0.0098	0.40	3.78	0.14	0.0947	0.0027	1523	43	1513	50
	porc_10_33			2.52	0.16	0.22	0.012	0.90	4.55	0.25	0.083	0.0016	1274	45	1279	63
	porc_10_34			3.11	0.16	0.2486	0.0093	0.59	4.02	0.15	0.0907	0.0018	1438	43	1431	48
	porc_10_38			4.36	0.23	0.304	0.014	0.78	3.29	0.15	0.1019	0.0023	1704	45	1708	70
	porc_10_39			1.624	0.092	0.1652	0.0064	0.86	6.05	0.23	0.0714	0.0013	978	35	985	35
	porc_10_40			4.09	0.23	0.298	0.012	0.84	3.36	0.14	0.1003	0.0017	1649	46	1678	61
	porc_10_42			4.17	0.22	0.295	0.01	0.09	3.39	0.11	0.1021	0.0025	1668	43	1667	51
	porc_10_43			2.42	0.13	0.2116	0.0075	0.11	4.73	0.17	0.0823	0.0023	1248	38	1237	40
	porc_10_44			1.87	0.13	0.1753	0.0065	0.44	5.70	0.21	0.0762	0.0031	1067	45	1041	35
	porc_10_45			3.39	0.18	0.2634	0.0088	0.18	3.80	0.13	0.0935	0.002	1500	41	1507	45
	porc_10_47			4.21	0.27	0.306	0.017	0.46	3.27	0.18	0.0989	0.0047	1674	53	1720	83
	porc_10_48			3.78	0.25	0.274	0.01	0.22	3.65	0.13	0.099	0.0043	1589	55	1566	55
	porc_10_49			4.89	0.26	0.326	0.012	0.83	3.07	0.11	0.1063	0.0017	1800	45	1825	63
	porc_10_50			1.6	0.083	0.1638	0.0055	0.33	6.11	0.20	0.07	0.0014	970	33	978	31
	porc_10_51			3.44	0.19	0.2666	0.0093	0.36	3.75	0.13	0.0932	0.0024	1511	42	1523	47
	porc_10_53			3.38	0.18	0.2639	0.0096	0.76	3.79	0.14	0.0933	0.0014	1498	41	1510	49
	porc_10_54			4.06	0.21	0.29	0.01	0.36	3.45	0.12	0.1011	0.0022	1645	42	1640	50
PH10	porc_10B_1	53.2755	-14.2498	3.52	0.2	0.2736	0.0091	0.60	3.65	0.12	0.0943	0.0041	1530	44	1558	46
	porc_10B_2			1.72	0.14	0.1691	0.0059	0.25	5.91	0.21	0.0748	0.0053	1019	51	1010	31
	porc_10B_3			4.03	0.23	0.2897	0.0095	0.57	3.45	0.11	0.1012	0.0044	1638	46	1639	48
	porc_10B_4			2.6	0.16	0.2157	0.007	0.64	4.64	0.15	0.0889	0.0041	1300	46	1258	37
	porc_10B_5			1.57	0.11	0.1563	0.0048	0.47	6.40	0.20	0.074	0.004	957	43	936	27
	porc_10B_6			2.03	0.11	0.1917	0.0056	0.59	5.22	0.15	0.0773	0.0031	1124	36	1130	30
	porc_10B_7			4.29	0.26	0.31	0.01	0.70	3.23	0.10	0.0997	0.0044	1689	49	1741	49
	porc_10B_8			3.92	0.21	0.2828	0.0088	0.51	3.54	0.11	0.1015	0.0041	1617	43	1605	44
	porc_10B_9			3.61	0.2	0.2747	0.0093	0.72	3.64	0.12	0.0959	0.0042	1550	45	1564	47
	porc_10B_10			5.4	0.31	0.345	0.014	0.75	2.90	0.12	0.1147	0.0052	1887	52	1909	68
	porc_10B_11			1.82	0.13	0.1736	0.0058	0.09	5.76	0.19	0.0762	0.0049	1050	47	1032	32
	porc_10B_12			1.712	0.099	0.1732	0.0054	0.29	5.77	0.18	0.0717	0.0034	1012	37	1030	30
	porc_10B_13			5.06	0.3	0.334	0.01	0.27	2.99	0.09	0.1089	0.0054	1827	50	1856	49
	porc_10B_14			4.11	0.25	0.2927	0.0095	0.50	3.42	0.11	0.1027	0.0048	1656	49	1659	46
	porc_10B_15			3.67	0.2	0.2792	0.0083	0.43	3.58	0.11	0.0943	0.0041	1563	45	1587	42
	porc_10B_16			3.48	0.19	0.2694	0.009	0.71	3.71	0.12	0.0944	0.0039	1521	42	1537	46
	porc_10B_17			1.51	0.18	0.1659	0.0074	0.05	6.03	0.27	0.0653	0.0076	940	68	988	41
	porc_10B_18			1.73	0.13	0.1714	0.0054	0.47	5.83	0.18	0.0732	0.0044	1014	45	1020	30
	porc_10B_19			1.68	0.1	0.1638	0.0047	0.28	6.11	0.18	0.0742	0.0038	1000	39	978	26

Table 5: Zircon Sample Data (2011 Dredge Sample Analytical Run)

Identification		Location		Geochronological Data													
Sample	Sample Reference	Latitude	Longitude	$^{207}Pb/^{235}U$	2σ	$^{206}Pb/^{238}U$	2σ	Error Correlation	$^{238}U/^{206}Pb$	2σ	$^{207}Pb/^{206}Pb$	2σ	$^{207}Pb/^{235}U$ Age (Ma)	2σ	$^{206}Pb/^{238}U$ Age (Ma)	2σ
	porc_10B_20			2.4	0.13	0.2129	0.006	0.45	4.70	0.13	0.0817	0.0035	1245	38	1244	32
PH11	Porc11_14_1	53.2755	-14.2498	1.916	0.089	0.1842	0.004	0.42	5.43	0.12	0.0759	0.0027	1083	31	1090	22
	Porc11_14_2			1.826	0.071	0.179	0.0041	0.61	5.59	0.13	0.0747	0.0017	1054	25	1061	22
	Porc11_14_3			2.18	0.084	0.2022	0.0049	0.50	4.95	0.12	0.0789	0.0021	1174	27	1187	26
	Porc11_14_4			1.87	0.11	0.183	0.0046	0.00	5.46	0.14	0.0747	0.0046	1079	41	1083	25
	Porc11_14_5			1.788	0.072	0.1826	0.0037	0.48	5.48	0.11	0.0726	0.0021	1045	28	1081	20
	Porc11_14_6			1.799	0.064	0.1789	0.0036	0.46	5.59	0.11	0.0737	0.0017	1045	23	1061	20
	Porc11_14_7			2.08	0.11	0.1997	0.0047	0.20	5.01	0.12	0.0767	0.0036	1138	36	1173	25
	Porc11_14_8			2.135	0.075	0.1981	0.0037	0.65	5.05	0.09	0.0789	0.0016	1160	24	1167	21
	Porc11_14_9			1.583	0.066	0.1603	0.0034	0.14	6.24	0.13	0.0732	0.0026	963	26	958	19
	Porc11_14_10			1.842	0.076	0.1789	0.0036	0.49	5.59	0.11	0.0745	0.002	1059	27	1061	19
	Porc11_14_11			1.867	0.096	0.1838	0.0068	0.56	5.44	0.20	0.0753	0.0033	1069	34	1087	37
	Porc11_14_12			1.86	0.11	0.177	0.0046	0.20	5.65	0.15	0.0749	0.0039	1069	36	1050	25
	Porc11_14_13			1.87	0.089	0.1786	0.004	0.28	5.60	0.13	0.0771	0.003	1075	32	1059	22
	Porc11_14_14			2.92	0.11	0.2407	0.0047	0.56	4.15	0.08	0.0885	0.0021	1385	29	1390	24
	Porc11_14_15			3.02	0.1	0.2435	0.0042	0.67	4.11	0.07	0.0903	0.0018	1413	25	1405	22
	Porc11_14_16			1.612	0.068	0.1618	0.0028	0.14	6.18	0.11	0.0725	0.0024	973	27	967	15
	Porc11_14_17			1.715	0.071	0.1722	0.0035	0.09	5.81	0.12	0.0731	0.0027	1013	26	1024	20
	Porc11_14_18			2.6	0.14	0.2152	0.0049	0.45	4.65	0.11	0.0886	0.0041	1296	40	1256	26
	Porc11_14_19			1.831	0.099	0.1775	0.0047	0.24	5.63	0.15	0.0744	0.0032	1054	35	1053	25
	Porc11_14_20			2.134	0.079	0.1971	0.004	0.20	5.07	0.10	0.0784	0.0022	1161	25	1159	22
	Porc11_14_21			3.7	0.16	0.2774	0.0075	0.67	3.60	0.10	0.0984	0.0025	1575	37	1577	38
	Porc11_14_22			1.575	0.067	0.1607	0.0039	0.00	6.22	0.15	0.072	0.0031	962	28	961	22
	Porc11_14_23			4.05	0.14	0.2894	0.0059	0.56	3.46	0.07	0.1016	0.0021	1643	29	1638	29
	Porc11_14_24			2.15	0.13	0.1979	0.0081	0.90	5.05	0.21	0.0784	0.002	1158	42	1162	43
	Porc11_14_25			3.7	0.17	0.281	0.0073	0.36	3.56	0.09	0.0977	0.0037	1573	35	1596	37
	Porc11_14_26			2.09	0.1	0.1949	0.0045	0.53	5.13	0.12	0.079	0.0027	1146	34	1147	24
	Porc11_14_27			4.48	0.17	0.3084	0.0058	0.31	3.24	0.06	0.1058	0.0026	1727	31	1732	28
	Porc11_14_28			1.751	0.074	0.1738	0.0035	0.19	5.75	0.12	0.0731	0.0023	1026	27	1033	19
	Porc11_14_29			2.13	0.12	0.1934	0.0054	0.39	5.17	0.14	0.079	0.0035	1154	39	1144	28
	Porc11_14_30			3.33	0.13	0.2614	0.0064	0.37	3.83	0.09	0.0931	0.0028	1491	29	1501	32
	Porc11_14_31			2.241	0.093	0.2056	0.0055	0.71	4.86	0.13	0.0792	0.002	1192	29	1205	30
	Porc11_14_32			2.012	0.071	0.1888	0.0031	0.53	5.30	0.09	0.077	0.0016	1119	24	1115	17
	Porc11_14_33			1.891	0.064	0.1801	0.0028	0.52	5.55	0.09	0.0766	0.0014	1078	22	1067	15
	Porc11_14_34			2.78	0.096	0.2275	0.0045	0.69	4.40	0.09	0.0889	0.0018	1350	26	1321	23
	Porc11_14_35			2.425	0.091	0.2146	0.0051	0.75	4.66	0.11	0.0828	0.0018	1252	26	1253	27
	Porc11_14_36			4.18	0.15	0.2977	0.0058	0.50	3.36	0.07	0.1038	0.0023	1670	29	1679	29
	Porc11_14_37			1.792	0.09	0.1796	0.0035	0.49	5.57	0.11	0.0719	0.0025	1039	32	1064	19
	Porc11_14_38			2.43	0.12	0.21	0.0042	0.31	4.76	0.10	0.0829	0.0034	1248	35	1228	22
	Porc11_14_39			1.694	0.082	0.1672	0.0035	0.10	5.98	0.13	0.0737	0.003	1004	31	997	19
	Porc11_14_40			1.746	0.082	0.1678	0.0037	0.25	5.96	0.13	0.0757	0.0029	1027	29	1000	20

Table 5: Zircon Sample Data (2011 Dredge Sample Analytical Run)

Identification		Location		Geochronological Data												
Sample	Sample Reference	Latitude	Longitude	$^{207}Pb/^{235}U$	2σ	$^{206}Pb/^{238}U$	2σ	Error Correlation	$^{238}U/^{206}Pb$	2σ	$^{207}Pb/^{206}Pb$	2σ	$^{207}Pb/^{235}U$ Age (Ma)	2σ	$^{206}Pb/^{238}U$ Age (Ma)	2σ
	Porc11_14_42			2.66	0.11	0.2246	0.0045	0.21	4.45	0.09	0.086	0.0028	1322	30	1306	24
	Porc11_14_43			1.766	0.065	0.1751	0.0036	0.41	5.71	0.12	0.0734	0.002	1037	26	1040	20
	Porc11_14_44			2.75	0.11	0.2308	0.0044	0.32	4.33	0.08	0.0866	0.0025	1344	32	1339	23
	Porc11_14_45			1.842	0.069	0.1784	0.0041	0.66	5.61	0.13	0.0747	0.0017	1060	25	1058	22
	Porc11_14_47			1.775	0.078	0.1714	0.0045	0.51	5.83	0.15	0.0748	0.0023	1035	28	1019	25
	Porc11_14_48			1.954	0.09	0.186	0.0054	0.74	5.38	0.16	0.0769	0.0022	1098	31	1105	28
	Porc11_14_49			2.79	0.1	0.2328	0.0048	0.47	4.30	0.09	0.0865	0.0021	1353	27	1349	25
	Porc11_14_50			4.19	0.15	0.2932	0.0059	0.55	3.41	0.07	0.1039	0.0023	1674	31	1657	29
	Porc11_14_51			2.74	0.11	0.2295	0.004	0.00	4.36	0.08	0.0873	0.0031	1342	32	1331	21
	Porc11_14_52			1.595	0.082	0.1637	0.0032	0.34	6.11	0.12	0.0706	0.003	965	32	977	18
	Porc11_14_53			3.76	0.14	0.2739	0.0055	0.14	3.65	0.07	0.0986	0.0026	1586	28	1560	28
	Porc11_14_54			2.266	0.082	0.203	0.0036	0.55	4.93	0.09	0.0812	0.0017	1201	26	1191	19
	Porc11_14_55			1.799	0.074	0.1661	0.0033	0.22	6.02	0.12	0.0784	0.0025	1044	27	990	18
	Porc11_14_56			1.969	0.076	0.1856	0.0035	0.37	5.39	0.10	0.0775	0.0022	1104	26	1097	19
	Porc11_14_57			1.777	0.066	0.1738	0.0035	0.53	5.75	0.12	0.0749	0.0017	1036	24	1033	19
	Porc11_14_58			5.86	0.24	0.3513	0.0079	0.23	2.85	0.06	0.1196	0.0037	1959	35	1940	38
	Porc11_14_59			1.994	0.074	0.1895	0.0036	0.64	5.28	0.10	0.0767	0.0017	1113	25	1118	19
	Porc11_14_60			1.823	0.084	0.1763	0.0034	0.00	5.67	0.11	0.0764	0.0032	1055	32	1046	19
	Porc11_14_61			1.884	0.067	0.1834	0.0036	0.67	5.45	0.11	0.0743	0.0015	1075	24	1085	19
	Porc11_14_62			1.75	0.11	0.1793	0.0036	0.13	5.58	0.11	0.0715	0.0044	1030	42	1063	20
	Porc11_14_63			1.855	0.076	0.1785	0.0034	0.33	5.60	0.11	0.076	0.0021	1064	27	1058	19
	Porc11_14_64			3.34	0.11	0.2551	0.005	0.41	3.92	0.08	0.0936	0.0021	1489	27	1468	25
	Porc11_14_65			2.89	0.12	0.2369	0.0055	0.13	4.22	0.10	0.0879	0.0031	1377	32	1370	29
	Porc11_14_66			1.66	0.1	0.1683	0.0038	0.19	5.94	0.13	0.0701	0.0039	991	38	1005	20
	Porc11_14_67			1.714	0.064	0.1689	0.0033	0.62	5.92	0.12	0.073	0.0017	1015	23	1009	19
	Porc11_14_68			3.73	0.19	0.2806	0.0067	0.22	3.56	0.09	0.0979	0.0041	1572	41	1594	34
	Porc11_14_69			3.29	0.13	0.2584	0.0051	0.28	3.87	0.08	0.0929	0.0026	1483	31	1481	26
	Porc11_14_70			1.962	0.076	0.1863	0.0041	0.37	5.37	0.12	0.0772	0.0022	1101	26	1104	21
	Porc11_14_71			2.84	0.12	0.2345	0.006	0.63	4.26	0.11	0.0874	0.0024	1370	31	1358	32
	Porc11_14_72			1.676	0.094	0.1685	0.0044	0.25	5.93	0.15	0.0735	0.0037	1003	35	1003	24
	Porc11_14_73			1.674	0.058	0.1676	0.0032	0.50	5.97	0.11	0.0728	0.0016	998	22	999	18
	Porc11_14_74			2.384	0.084	0.2104	0.0043	0.58	4.75	0.10	0.0821	0.0019	1237	25	1235	24
	Porc11_14_75			2.66	0.11	0.2251	0.0047	0.54	4.442	0.093	0.0856	0.0021	1315	30	1309	25
	Porc11_14_76			1.615	0.069	0.1631	0.0037	0.13	6.13	0.14	0.0716	0.0026	977	28	974	20
	Porc11_14_77			1.571	0.057	0.1596	0.0032	0.42	6.27	0.13	0.0705	0.0017	960	23	954	18
	Porc11_14_78			2.29	0.1	0.2064	0.005	0.52	4.84	0.12	0.0822	0.0028	1208	30	1209	27
	Porc11_14_79			1.942	0.097	0.1821	0.0038	0.19	5.49	0.11	0.0763	0.0032	1097	32	1078	21
	Porc11_14_80			4.15	0.15	0.2935	0.0053	0.63	3.407	0.062	0.1027	0.0022	1665	30	1659	27
	Porc11_14_81			13.07	0.5	0.514	0.011	0.50	1.946	0.042	0.1833	0.0042	2683	36	2681	43
	Porc11_14_82			1.86	0.09	0.1746	0.004	0.00	5.73	0.13	0.0773	0.0033	1068	33	1037	22
PH 15	porc15_1	53.2845	-13.8748	4.07	0.15	0.2976	0.0074	0.87	3.360	0.084	0.0998	0.0023	1645	29	1678	37

Table 5: Zircon Sample Data (2011 Dredge Sample Analytical Run)

Identification		Location		Geochronological Data													
Sample	Sample Reference	Latitude	Longitude	$^{207}Pb/^{235}U$	2σ	$^{206}Pb/^{238}U$	2σ	Error Correlation	$^{238}U/^{206}Pb$	2σ	$^{207}Pb/^{206}Pb$	2σ	$^{207}Pb/^{235}U$ Age (Ma)	2σ	$^{206}Pb/^{238}U$ Age (Ma)	2σ
	porc15_2			2.86	0.11	0.2417	0.0056	0.45	4.14	0.10	0.0846	0.0033	1369	28	1395	29
	porc15_3			4.15	0.14	0.2991	0.0081	0.86	3.343	0.091	0.1034	0.0026	1663	28	1686	40
	porc15_4			3.97	0.12	0.2874	0.0055	0.46	3.479	0.067	0.1018	0.0029	1627	24	1628	28
	porc15_5			4.27	0.16	0.2999	0.0054	0.33	3.334	0.060	0.1032	0.0035	1682	32	1690	27
	porc15_6			4.13	0.15	0.2955	0.0078	0.82	3.384	0.089	0.1011	0.0029	1657	30	1677	42
	porc15_7			5.27	0.13	0.333	0.012	0.63	3.00	0.11	0.1115	0.0035	1864	21	1851	59
	porc15_8			4.26	0.17	0.3036	0.0083	0.23	3.294	0.090	0.1015	0.004	1685	32	1709	41
	porc15_9			1.949	0.064	0.1884	0.0029	0.34	5.308	0.082	0.0752	0.0025	1100	21	1113	15
	porc15_10			3.527	0.091	0.2736	0.0051	0.76	3.655	0.068	0.0947	0.0022	1533	21	1559	26
	porc15_11			2.68	0.12	0.2307	0.0042	0.00	4.335	0.079	0.0839	0.0042	1321	33	1338	22
	porc15_12			4.32	0.11	0.3084	0.0079	0.36	3.243	0.083	0.1004	0.0034	1697	20	1733	39
	porc15_13			4.71	0.16	0.3192	0.0072	0.30	3.133	0.071	0.1082	0.0044	1767	28	1785	35
	porc15_14			3.29	0.16	0.2583	0.0077	0.64	3.87	0.12	0.0921	0.0036	1479	36	1486	38
	porc15_15			3.325	0.081	0.2605	0.0037	0.65	3.839	0.055	0.0925	0.0021	1486	19	1492	19
	porc15_16			3.96	0.13	0.2883	0.006	0.65	3.469	0.072	0.0989	0.0031	1624	26	1632	30
	porc15_17			3.78	0.12	0.2843	0.0053	0.36	3.517	0.066	0.0972	0.0031	1591	25	1613	27
	porc15_18			1.726	0.08	0.1713	0.0028	0.50	5.84	0.10	0.0732	0.0029	1014	29	1019	16
	porc15_19			3.311	0.076	0.267	0.011	0.15	3.75	0.15	0.0924	0.0044	1483	18	1527	54
	porc15_21			3.96	0.14	0.2914	0.0091	0.88	3.43	0.11	0.0992	0.0025	1624	28	1648	45
	porc15_22			2.183	0.076	0.2015	0.0047	0.78	4.96	0.12	0.0791	0.0021	1173	25	1187	24
	porc15_23			1.488	0.054	0.1558	0.0034	0.43	6.42	0.14	0.0694	0.0024	923	22	933	19
	porc15_24			3.86	0.12	0.2835	0.0053	0.14	3.527	0.066	0.1012	0.0036	1602	26	1608	26
	porc15_25			3.2	0.12	0.26	0.0069	0.22	3.85	0.10	0.091	0.0042	1455	29	1489	35
	porc15_26			1.578	0.086	0.1634	0.0034	0.21	6.12	0.13	0.0716	0.0044	962	36	979	20
	porc15_27			2.24	0.076	0.2052	0.0041	0.76	4.87	0.10	0.0802	0.0021	1191	24	1207	21
	porc15_28			1.697	0.058	0.171	0.0037	0.60	5.85	0.13	0.072	0.0024	1006	22	1018	20
	porc15_29			1.85	0.051	0.1706	0.0032	0.73	5.86	0.11	0.0784	0.002	1065	19	1015	18
	porc15_30			1.624	0.076	0.1599	0.004	0.42	6.25	0.16	0.0743	0.0036	978	29	956	22
	porc15_31			2.15	0.12	0.2023	0.0044	0.13	4.94	0.11	0.0768	0.0039	1163	40	1187	23
	porc15_32			1.908	0.049	0.185	0.0043	0.50	5.41	0.13	0.0757	0.0022	1086	18	1094	23
	porc15_33			3.86	0.17	0.286	0.0056	0.48	3.497	0.068	0.0979	0.004	1604	36	1621	28
	porc15_34			4.1	0.14	0.2957	0.0062	0.45	3.382	0.071	0.0994	0.0032	1654	27	1670	31
	porc15_35			2.073	0.095	0.1908	0.0045	0.13	5.24	0.12	0.0767	0.0038	1137	32	1125	25
	porc15_36			1.795	0.053	0.1747	0.0039	0.32	5.72	0.13	0.0742	0.0023	1043	19	1041	20
	porc15_37			4.05	0.1	0.2892	0.005	0.63	3.458	0.060	0.1016	0.0028	1643	21	1637	25
	porc15_38			3.32	0.11	0.2601	0.006	0.60	3.845	0.089	0.0928	0.0029	1484	25	1490	31
	porc15_39			2.544	0.07	0.2223	0.0029	0.38	4.498	0.059	0.0843	0.0022	1284	20	1294	15
	porc15_40			2.199	0.082	0.2031	0.0031	0.50	4.924	0.075	0.0792	0.0026	1178	26	1192	17
	porc15_41			4.3	0.17	0.303	0.011	0.82	3.30	0.12	0.1027	0.0029	1690	33	1706	53
	porc15_42			4.11	0.18	0.3015	0.0067	0.30	3.317	0.074	0.1002	0.0044	1655	35	1699	33
	porc15_43			4.04	0.11	0.293	0.0047	0.59	3.413	0.055	0.1008	0.0026	1642	21	1656	23

Table 5: Zircon Sample Data (2011 Dredge Sample Analytical Run)

Identification		Location		Geochronological Data													
Sample	Sample Reference	Latitude	Longitude	$^{207}Pb/^{235}U$	2σ	$^{206}Pb/^{238}U$	2σ	Error Correlation	$^{238}U/^{206}Pb$	2σ	$^{207}Pb/^{206}Pb$	2σ	$^{207}Pb/^{235}U$ Age (Ma)	2σ	$^{206}Pb/^{238}U$ Age (Ma)	2σ
	porc15_44			1.732	0.068	0.1707	0.0026	0.28	5.858	0.089	0.0744	0.0028	1018	25	1016	14
	porc15_45			2.75	0.1	0.2316	0.0054	0.11	4.32	0.10	0.0869	0.0035	1339	28	1343	28
	porc15_46			4.19	0.13	0.2987	0.0088	0.66	3.35	0.10	0.1023	0.003	1671	25	1684	43
	porc15_47			1.69	0.083	0.166	0.0037	0.40	6.02	0.13	0.0738	0.0031	1000	32	990	20
	porc15_48			2.203	0.061	0.1994	0.0036	0.48	5.015	0.091	0.0804	0.0024	1181	19	1172	19
	porc15_49			3.61	0.11	0.2718	0.0046	0.49	3.679	0.062	0.0961	0.0027	1550	25	1550	24
	porc15_50			1.616	0.099	0.1672	0.0042	0.17	5.98	0.15	0.0709	0.004	983	36	996	23
	porc15_51			1.644	0.049	0.1646	0.0029	0.57	6.08	0.11	0.0729	0.002	986	19	982	16
	porc15_52			4.04	0.12	0.2941	0.0063	0.88	3.400	0.073	0.0996	0.0023	1641	25	1661	31
	porc15_53			2.258	0.089	0.2066	0.0056	0.78	4.84	0.13	0.0804	0.0023	1201	27	1210	30
	porc15_54			4.11	0.14	0.2946	0.0078	0.75	3.394	0.090	0.1011	0.003	1653	27	1663	39
	porc15_55			1.939	0.071	0.1873	0.005	0.63	5.34	0.14	0.0744	0.0025	1093	25	1106	27
	porc15_56			4.36	0.15	0.3038	0.0056	0.60	3.292	0.061	0.1058	0.0031	1703	27	1709	28
	porc15_58			3.408	0.093	0.2642	0.0046	0.57	3.785	0.066	0.0944	0.0026	1505	22	1511	23
	porc15_59			5.07	0.12	0.3272	0.0048	0.52	3.056	0.045	0.113	0.0028	1830	20	1824	24
	porc15_60			2.084	0.058	0.197	0.0056	0.76	5.08	0.14	0.0779	0.0022	1143	19	1159	30
	porc15_61			4.17	0.14	0.2991	0.0064	0.69	3.343	0.072	0.1021	0.0028	1665	27	1686	32
	porc15_62			1.76	0.1	0.1747	0.0036	0.24	5.72	0.12	0.0724	0.004	1029	39	1038	20
	porc15_63			2.85	0.13	0.2396	0.0087	0.86	4.17	0.15	0.0886	0.0025	1372	33	1384	46
	porc15_64			1.622	0.051	0.168	0.0031	0.21	5.95	0.11	0.0727	0.0025	978	20	1001	17
	porc15_65			3.92	0.14	0.289	0.011	0.89	3.46	0.13	0.0988	0.0026	1616	29	1636	53
	porc15_66			4.24	0.11	0.3015	0.0039	0.40	3.317	0.043	0.1012	0.0028	1682	21	1699	19
	porc15_67			3.96	0.13	0.2893	0.0086	0.77	3.46	0.10	0.1021	0.0033	1625	27	1650	48
	porc15_69			4.82	0.11	0.328	0.0079	0.31	3.049	0.073	0.1079	0.0032	1791	21	1828	38
	porc15_70			3.84	0.13	0.2817	0.0052	0.32	3.550	0.066	0.101	0.0036	1602	28	1600	26
	porc15_71			4.05	0.14	0.292	0.007	0.42	3.425	0.082	0.1024	0.0035	1643	27	1657	34
	porc15_72			2.95	0.12	0.2455	0.0063	0.42	4.07	0.10	0.0872	0.0036	1398	30	1420	31
	porc15_74			1.758	0.053	0.172	0.0034	0.78	5.81	0.11	0.0748	0.0018	1031	20	1023	19
	porc15_75			3.5	0.12	0.2683	0.0046	0.53	3.727	0.064	0.0944	0.0026	1524	27	1532	23
	porc15_76			3.375	0.084	0.2632	0.003	0.49	3.799	0.043	0.0929	0.0024	1498	20	1506	15
	porc15_77			3.77	0.12	0.2844	0.008	0.38	3.52	0.10	0.0976	0.0037	1586	27	1613	40
	porc15_78			3.275	0.095	0.254	0.0052	0.76	3.94	0.08	0.0961	0.0024	1475	22	1459	27
	porc15_79			1.872	0.085	0.1767	0.0034	0.20	5.66	0.11	0.0788	0.0036	1067	30	1048	19
PH4	Porc_4_1	53.3572	-13.6678	3.74	0.15	0.2753	0.0076	0.54	3.63	0.10	0.0991	0.0022	1583	29	1567	39
	Porc_4_2			1.776	0.068	0.1762	0.0052	0.17	5.68	0.17	0.0736	0.0021	1036	25	1046	28
	Porc_4_3			4.02	0.17	0.2901	0.0082	0.32	3.45	0.10	0.0993	0.0029	1636	34	1642	41
	Porc_4_4			1.869	0.069	0.1825	0.005	0.41	5.48	0.15	0.0745	0.0017	1070	24	1081	27
	Porc_4_5			1.84	0.1	0.1833	0.0057	0.38	5.46	0.17	0.0722	0.0032	1056	36	1085	31
	Porc_4_6			4.45	0.19	0.3053	0.0085	0.45	3.28	0.09	0.1055	0.0032	1720	36	1717	42
	Porc_4_8			4.18	0.16	0.3009	0.009	0.64	3.32	0.10	0.1004	0.0021	1670	30	1699	46
	Porc_4_9			1.674	0.086	0.1657	0.0047	0.35	6.04	0.17	0.0722	0.0029	995	33	988	26

Table 5: Zircon Sample Data (2011 Dredge Sample Analytical Run)

Identification		Location		Geochronological Data													
Sample	Sample Reference	Latitude	Longitude	$^{207}Pb/^{235}U$	2σ	$^{206}Pb/^{238}U$	2σ	Error Correlation	$^{238}U/^{206}Pb$	2σ	$^{207}Pb/^{206}Pb$	2σ	$^{207}Pb/^{235}U$ Age (Ma)	2σ	$^{206}Pb/^{238}U$ Age (Ma)	2σ
	Porc_4_10			4.28	0.16	0.3026	0.0088	0.73	3.30	0.10	0.1025	0.0022	1688	31	1704	43
	Porc_4_11			3.56	0.13	0.27	0.0074	0.43	3.70	0.10	0.0948	0.0021	1539	29	1541	37
	Porc_4_12			3.61	0.14	0.2769	0.0087	0.77	3.61	0.11	0.0948	0.002	1550	32	1575	44
	Porc_4_14			2.12	0.15	0.1958	0.0068	0.39	5.11	0.18	0.0796	0.005	1151	47	1152	37
	Porc_4_15			3.85	0.14	0.2828	0.0078	0.58	3.54	0.10	0.0982	0.002	1602	29	1605	39
	Porc_4_16			1.76	0.07	0.1726	0.0052	0.69	5.79	0.17	0.0741	0.0018	1030	26	1026	28
	Porc_4_17			3.63	0.15	0.273	0.0091	0.86	3.66	0.12	0.0959	0.002	1555	33	1555	46
	Porc_4_18			3.76	0.14	0.2801	0.0092	0.47	3.57	0.12	0.098	0.003	1583	31	1592	46
	Porc_4_19			2.08	0.11	0.1844	0.0062	0.15	5.42	0.18	0.0814	0.0041	1150	34	1091	34
	Porc_4_21			5.3	0.21	0.336	0.01	0.10	2.98	0.09	0.113	0.0031	1867	33	1868	49
	Porc_4_22			3.43	0.12	0.2632	0.0074	0.57	3.80	0.11	0.0939	0.0019	1512	28	1506	38
	Porc_4_23			1.644	0.063	0.1648	0.0044	0.32	6.07	0.16	0.0712	0.0018	987	25	983	24
	Porc_4_24			4.17	0.16	0.2952	0.0086	0.48	3.39	0.10	0.103	0.0026	1667	32	1667	43
	Porc_4_25			2.06	0.08	0.1906	0.005	0.19	5.25	0.14	0.0783	0.0021	1134	27	1125	27
	Porc_4_26			4.08	0.15	0.2919	0.0082	0.52	3.43	0.10	0.1012	0.0023	1651	31	1651	41
	Porc_4_27			4	0.15	0.2871	0.0083	0.37	3.48	0.10	0.1005	0.0026	1633	31	1626	42
	Porc_4_29			3.48	0.13	0.2664	0.0078	0.06	3.75	0.11	0.0946	0.0028	1522	30	1522	40
	Porc_4_30			3.44	0.13	0.2645	0.0075	0.55	3.78	0.11	0.0938	0.0019	1514	30	1516	37
	Porc_4_33			1.837	0.07	0.179	0.005	0.61	5.59	0.16	0.0737	0.0016	1058	25	1061	27
	Porc_4_34			4.06	0.15	0.2906	0.0083	0.47	3.44	0.10	0.1011	0.0024	1646	30	1644	42
	Porc_4_35			5.03	0.18	0.33	0.01	0.58	3.03	0.09	0.1114	0.0023	1823	31	1839	49
	Porc_4_36			1.756	0.071	0.1643	0.0053	0.41	6.09	0.20	0.078	0.0024	1028	26	980	29
	Porc_4_37			1.58	0.11	0.1607	0.0067	0.42	6.22	0.26	0.0714	0.0044	958	43	960	37
	Porc_4_38			1.548	0.085	0.1606	0.0048	0.00	6.23	0.19	0.07	0.0036	952	35	960	27
	Porc_4_39			4.02	0.17	0.2905	0.0096	0.38	3.44	0.11	0.1005	0.003	1638	34	1644	48
	Porc_4_41			4.26	0.16	0.2964	0.0084	0.43	3.37	0.10	0.1041	0.0024	1688	33	1673	42
	Porc_4_42			4.03	0.15	0.2897	0.0084	0.52	3.45	0.10	0.1004	0.0026	1643	32	1639	42
	Porc_4_43			2.131	0.076	0.1959	0.0053	0.53	5.10	0.14	0.0786	0.0017	1158	25	1155	28
	Porc_4_44			4.25	0.16	0.2983	0.0082	0.69	3.35	0.09	0.1028	0.0021	1682	30	1683	41
	Porc_4_45			2.013	0.078	0.1903	0.0054	0.42	5.25	0.15	0.0762	0.002	1119	27	1123	29
	Porc_4_46			2.126	0.078	0.1981	0.0056	0.69	5.05	0.14	0.0779	0.0016	1157	25	1165	30
	Porc_4_49			3.42	0.15	0.2675	0.0091	0.43	3.74	0.13	0.0917	0.0027	1513	32	1527	46
	Porc_4_50			3.44	0.13	0.264	0.0074	0.59	3.79	0.11	0.0944	0.0022	1514	31	1513	39
	Porc_4_51			1.636	0.072	0.1655	0.0044	0.19	6.04	0.16	0.0716	0.0025	986	29	987	24
	Porc_4_52			3.06	0.12	0.2463	0.0071	0.19	4.06	0.12	0.0896	0.0022	1421	29	1419	37
	Porc_4_53			5.33	0.21	0.3373	0.0094	0.67	2.965	0.083	0.1131	0.0027	1873	33	1873	45
	Porc_4_54			1.717	0.075	0.164	0.0054	0.28	6.10	0.20	0.0767	0.0024	1016	27	978	30
	Porc_4_55			3.52	0.13	0.2692	0.008	0.59	3.71	0.11	0.0947	0.0021	1533	31	1536	40
	Porc_4_56			4.18	0.16	0.282	0.009	0.83	3.55	0.11	0.1077	0.0021	1668	32	1601	45
	Porc_4_57			3.47	0.13	0.2693	0.0071	0.16	3.71	0.10	0.0927	0.0023	1520	29	1539	37
	Porc_4_58			3.41	0.12	0.2643	0.007	0.27	3.78	0.10	0.0926	0.0019	1506	27	1512	36

Table 5: Zircon Sample Data (2011 Dredge Sample Analytical Run)																
Identification		Location		Geochronological Data												
Sample	Sample Reference	Latitude	Longitude	$^{207}Pb/^{235}U$	2σ	$^{206}Pb/^{238}U$	2σ	Error Correlation	$^{238}U/^{206}Pb$	2σ	$^{207}Pb/^{206}Pb$	2σ	$^{207}Pb/^{235}U$ Age (Ma)	2σ	$^{206}Pb/^{238}U$ Age (Ma)	2σ
	Porc_4_59			3.7	0.14	0.2783	0.0084	0.57	3.59	0.11	0.0939	0.0022	1569	30	1586	44
	Porc_4_61			4.41	0.19	0.3125	0.0091	0.26	3.200	0.093	0.1008	0.0035	1713	36	1753	45
	Porc_4_62			1.651	0.071	0.1665	0.0046	0.24	6.01	0.17	0.0734	0.0024	988	27	993	26
	Porc_4_64			4.21	0.16	0.3015	0.0093	0.47	3.32	0.10	0.1011	0.0027	1674	32	1703	48
	Porc_4_65			3.59	0.17	0.263	0.011	0.92	3.80	0.16	0.0965	0.002	1544	38	1504	54
	Porc_4_67			3.4	0.14	0.2614	0.0073	0.28	3.83	0.11	0.0927	0.0029	1505	34	1500	39
	Porc_4_68			1.591	0.057	0.1627	0.0045	0.51	6.15	0.17	0.0704	0.0015	966	22	972	25
	Porc_4_69			4.17	0.15	0.2922	0.008	0.30	3.422	0.094	0.1042	0.0026	1669	31	1656	42
	Porc_4_70			1.688	0.071	0.1667	0.0051	0.51	6.00	0.18	0.0737	0.002	1003	27	994	28
	Porc_4_71			1.652	0.09	0.1661	0.0049	0.27	6.02	0.18	0.074	0.0032	995	32	990	27
PH5	porc_5_1	53.2755	-14.2498	2.75	0.1	0.2297	0.0064	0.66	4.35	0.12	0.0864	0.0019	1343	29	1332	34
	porc_5_2			4.14	0.19	0.2921	0.0093	0.73	3.42	0.11	0.1009	0.0025	1661	38	1652	46
	porc_5_5			3.38	0.13	0.2627	0.0083	0.74	3.81	0.12	0.0937	0.002	1499	29	1503	42
	porc_5_6			3.43	0.14	0.2662	0.0093	0.74	3.76	0.13	0.0943	0.0022	1509	32	1521	47
	porc_5_7			1.668	0.097	0.1654	0.0053	0.00	6.05	0.19	0.0742	0.004	990	37	986	29
	porc_5_8			3.52	0.14	0.2701	0.008	0.70	3.70	0.11	0.0941	0.0021	1530	31	1545	40
	porc_5_9			2.35	0.14	0.198	0.01	0.93	5.05	0.26	0.0841	0.002	1221	41	1165	54
	porc_5_11			1.691	0.073	0.1698	0.0052	0.64	5.89	0.18	0.0724	0.0021	1007	29	1011	29
	porc_5_12			3.4	0.13	0.2653	0.0076	0.63	3.77	0.11	0.0921	0.0021	1502	30	1517	39
	porc_5_13			4.12	0.15	0.2931	0.0085	0.56	3.41	0.10	0.1019	0.0023	1657	31	1657	43
	porc_5_14			1.63	0.1	0.1654	0.005	0.40	6.05	0.18	0.0703	0.0037	977	39	986	28
	porc_5_15			1.672	0.078	0.1675	0.0047	0.36	5.97	0.17	0.0731	0.0026	1002	32	998	26
	porc_5_16			3.68	0.15	0.2762	0.0087	0.64	3.62	0.11	0.0968	0.0021	1565	32	1572	44
	porc_5_17			4.3	0.16	0.3055	0.0091	0.45	3.27	0.10	0.1015	0.0023	1692	30	1718	45
	porc_5_18			1.513	0.088	0.1491	0.0046	0.65	6.71	0.21	0.0729	0.0036	933	35	896	26
	porc_5_19			3.44	0.15	0.2689	0.008	0.79	3.72	0.11	0.0926	0.002	1515	36	1535	41
	porc_5_20			2.78	0.12	0.22	0.0073	0.70	4.55	0.15	0.0906	0.0023	1348	31	1281	39
	porc_5_21			3.44	0.16	0.2589	0.0084	0.41	3.86	0.13	0.0977	0.0034	1517	34	1484	43
	porc_5_22			4.18	0.23	0.2975	0.0093	0.62	3.36	0.11	0.1021	0.0049	1664	45	1678	46
	porc_5_23			3.54	0.14	0.2696	0.0076	0.67	3.71	0.10	0.0959	0.0024	1535	32	1539	38
	porc_5_24			1.662	0.073	0.1673	0.0051	0.22	5.98	0.18	0.0717	0.0025	993	28	997	28
	porc_5_25			4.15	0.17	0.3036	0.0096	0.68	3.29	0.10	0.0995	0.0022	1665	34	1708	48
	porc_5_29			4.18	0.16	0.2979	0.0083	0.55	3.36	0.09	0.1027	0.0022	1671	31	1681	41
	porc_5_30			3.52	0.13	0.2708	0.0079	0.63	3.69	0.11	0.0947	0.002	1531	29	1545	40
	porc_5_31			1.656	0.084	0.165	0.0052	0.21	6.06	0.19	0.0742	0.0032	988	33	984	29
	porc_5_32			1.775	0.066	0.1737	0.0052	0.44	5.76	0.17	0.075	0.0017	1036	24	1032	29
	porc_5_33			3.48	0.12	0.2661	0.0074	0.51	3.76	0.10	0.0953	0.0019	1522	28	1521	37
	porc_5_34			1.702	0.07	0.167	0.0049	0.30	5.99	0.18	0.0746	0.0022	1008	26	998	26
	porc_5_35			3.44	0.13	0.2683	0.0089	0.76	3.73	0.12	0.0949	0.002	1514	30	1538	43
	porc_5_36			2.579	0.095	0.222	0.006	0.65	4.50	0.12	0.0848	0.0018	1296	28	1292	32
	porc_5_37			3.64	0.14	0.2747	0.0085	0.43	3.64	0.11	0.0957	0.0026	1561	29	1564	43

Table 5: Zircon Sample Data (2011 Dredge Sample Analytical Run)

Identification		Location		Geochronological Data													
Sample	Sample Reference	Latitude	Longitude	$^{207}Pb/^{235}U$	2σ	$^{206}Pb/^{238}U$	2σ	Error Correlation	$^{238}U/^{206}Pb$	2σ	$^{207}Pb/^{206}Pb$	2σ	$^{207}Pb/^{235}U$ Age (Ma)	2σ	$^{206}Pb/^{238}U$ Age (Ma)	2σ
	porc_5_39			3.43	0.14	0.2652	0.0078	0.49	3.77	0.11	0.0948	0.0025	1513	30	1516	40
	porc_5_40			3.47	0.13	0.2699	0.0078	0.40	3.71	0.11	0.0941	0.0024	1518	30	1543	38
PH5	porc5_1	53.2755	-14.2498	1.549	0.054	0.1589	0.0054	0.57	6.29	0.21	0.0706	0.0027	952	22	950	30
	porc5_2			4.12	0.15	0.292	0.01	0.48	3.42	0.12	0.1031	0.0042	1659	29	1650	51
	porc5_3			3.19	0.11	0.249	0.0086	0.93	4.02	0.14	0.0942	0.0037	1454	26	1433	44
	porc5_4			3.007	0.099	0.2406	0.0084	0.29	4.16	0.15	0.0927	0.0038	1411	26	1389	43
	porc5_5			3.81	0.2	0.283	0.012	0.54	3.53	0.15	0.0992	0.0048	1602	39	1606	59
	porc5_6			3.35	0.1	0.2579	0.0089	0.51	3.88	0.13	0.0946	0.0035	1492	24	1479	45
	porc5_7			4.25	0.13	0.296	0.01	0.45	3.38	0.11	0.1054	0.0039	1683	25	1669	50
	porc5_8			3.93	0.13	0.2866	0.0099	0.70	3.49	0.12	0.1012	0.0037	1623	28	1624	50
	porc5_9			4.12	0.19	0.292	0.01	0.00	3.42	0.12	0.1018	0.0055	1658	36	1652	52
	porc5_10			2.032	0.06	0.1901	0.0064	0.51	5.26	0.18	0.0777	0.0028	1126	20	1122	35
	porc5_11			3.09	0.1	0.2437	0.0084	0.61	4.10	0.14	0.0925	0.0035	1430	26	1406	43
	porc5_12			3.38	0.11	0.262	0.0093	0.50	3.82	0.14	0.0945	0.0037	1502	27	1500	48
	porc5_13			4.16	0.13	0.2924	0.0099	0.37	3.42	0.12	0.1047	0.004	1666	26	1653	49
	porc5_14			1.983	0.059	0.1884	0.0064	0.16	5.31	0.18	0.077	0.0029	1113	20	1113	35
	porc5_15			1.538	0.074	0.1544	0.0055	0.05	6.48	0.23	0.0719	0.0042	951	30	926	31
	porc5_16			3.63	0.12	0.2696	0.0093	0.25	3.71	0.13	0.0983	0.0039	1555	26	1538	47
	porc5_17			3.25	0.12	0.2535	0.0095	0.81	3.94	0.15	0.0941	0.0034	1468	29	1456	49
	porc5_18			3.37	0.12	0.261	0.009	0.28	3.83	0.13	0.0956	0.004	1497	27	1495	46
	porc5_19			1.556	0.058	0.1582	0.0055	0.34	6.32	0.22	0.0708	0.003	954	22	946	31
	porc5_20			3.89	0.11	0.2825	0.0095	0.64	3.54	0.12	0.1001	0.0036	1614	23	1604	48
	porc5_21			1.526	0.071	0.1555	0.0057	0.00	6.43	0.24	0.073	0.0039	946	28	932	32
	porc5_22			1.881	0.062	0.1829	0.0062	0.41	5.47	0.19	0.0744	0.0028	1074	22	1083	34
	porc5_23			2.443	0.077	0.2156	0.0073	0.31	4.64	0.16	0.0825	0.0032	1255	23	1258	39
	porc5_24			3.94	0.12	0.29	0.01	0.34	3.45	0.12	0.1	0.004	1624	27	1642	50
	porc5_25			2.57	0.11	0.2192	0.0073	0.21	4.56	0.15	0.0862	0.0039	1296	29	1278	39
	porc5_26			3.31	0.11	0.2566	0.0087	0.48	3.90	0.13	0.0931	0.0036	1483	26	1472	45
	porc5_27			3.23	0.11	0.2538	0.0088	0.18	3.94	0.14	0.0939	0.0038	1464	27	1461	44
	porc5_28			3.29	0.11	0.2523	0.0086	0.70	3.96	0.14	0.0943	0.0035	1479	26	1450	44
	porc5_29			1.614	0.098	0.1638	0.0058	0.06	6.11	0.22	0.07	0.0046	972	39	977	32
	porc5_30			3.35	0.1	0.2585	0.0085	0.47	3.87	0.13	0.0941	0.0035	1492	23	1482	44
	porc5_31			4.17	0.13	0.296	0.01	0.45	3.38	0.11	0.1015	0.0038	1668	25	1677	52
	porc5_32			3.15	0.11	0.2515	0.0085	0.30	3.98	0.13	0.091	0.0038	1443	27	1446	44
	porc5_33			1.613	0.066	0.1626	0.0056	0.00	6.15	0.21	0.0715	0.0034	973	25	971	31
	porc5_34			4.22	0.16	0.298	0.011	0.40	3.36	0.12	0.1032	0.0045	1675	30	1680	54
	porc5_35			4.29	0.13	0.302	0.011	0.01	3.31	0.12	0.103	0.0042	1690	26	1701	52
	porc5_36			3.41	0.12	0.2583	0.0085	0.20	3.87	0.13	0.0956	0.0038	1505	27	1481	43
	porc5_37			1.817	0.085	0.1789	0.0062	0.20	5.59	0.19	0.0736	0.0038	1056	31	1061	34
	porc5_38			3.52	0.11	0.2701	0.009	0.49	3.70	0.12	0.0945	0.0035	1530	26	1541	46
	porc5_39			4.03	0.13	0.281	0.0098	0.52	3.56	0.12	0.1036	0.004	1640	27	1596	49

Table 5: Zircon Sample Data (2011 Dredge Sample Analytical Run)

Identification		Location		Geochronological Data													
Sample	Sample Reference	Latitude	Longitude	$^{207}Pb/^{235}U$	2σ	$^{206}Pb/^{238}U$	2σ	Error Correlation	$^{238}U/^{206}Pb$	2σ	$^{207}Pb/^{206}Pb$	2σ	$^{207}Pb/^{235}U$ Age (Ma)	2σ	$^{206}Pb/^{238}U$ Age (Ma)	2σ
PH12	porc12_1	53.2881	-13.8748	3.49	0.1	0.2565	0.0085	0.21	3.90	0.13	0.0987	0.0037	1524	23	1472	43
	porc12_2			1.989	0.074	0.1884	0.0063	0.29	5.31	0.18	0.0767	0.0031	1114	24	1113	34
	porc12_3			2.92	0.11	0.2461	0.0083	0.13	4.06	0.14	0.0867	0.0039	1392	30	1418	43
	porc12_4			4.19	0.15	0.291	0.01	0.32	3.44	0.12	0.1055	0.0044	1671	29	1644	50
	porc12_5			1.927	0.083	0.1819	0.0064	0.19	5.50	0.19	0.0766	0.0036	1094	29	1077	35
	porc12_6			3.71	0.14	0.277	0.011	0.58	3.61	0.14	0.0963	0.0039	1571	30	1580	55
	porc12_7			3.27	0.14	0.2559	0.0088	0.44	3.91	0.13	0.0933	0.0041	1481	34	1468	45
	porc12_8			4.08	0.14	0.291	0.011	0.72	3.44	0.13	0.1006	0.0039	1649	28	1646	57
	porc12_9			1.665	0.077	0.1678	0.006	0.00	5.96	0.21	0.0722	0.0038	997	28	1000	33
	porc12_10			4.86	0.17	0.322	0.011	0.21	3.11	0.11	0.109	0.0044	1793	29	1801	54
	porc12_11			2.253	0.074	0.2034	0.0067	0.37	4.92	0.16	0.0803	0.0031	1197	23	1194	36
	porc12_12			3.05	0.1	0.2463	0.0084	0.46	4.06	0.14	0.09	0.0034	1425	26	1419	43
	porc12_13			1.855	0.068	0.1753	0.0059	0.16	5.70	0.19	0.0766	0.0033	1067	23	1041	32
	porc12_14			2.01	0.12	0.1859	0.0076	0.41	5.38	0.22	0.0796	0.0051	1116	43	1098	41
	porc12_15			1.93	0.062	0.1846	0.0061	0.37	5.42	0.18	0.0755	0.0029	1091	21	1092	33
	porc12_16			4.07	0.14	0.293	0.01	0.27	3.41	0.12	0.1013	0.004	1647	28	1657	51
	porc12_17			1.9	0.11	0.178	0.0068	0.18	5.62	0.21	0.0778	0.0049	1076	40	1059	36
	porc12_18			2.92	0.1	0.238	0.008	0.20	4.20	0.14	0.0883	0.0036	1386	27	1376	41
	porc12_19			2.49	0.11	0.2144	0.0078	0.37	4.66	0.17	0.0853	0.0045	1267	34	1252	41
	porc12_20			1.96	0.16	0.1768	0.0073	0.34	5.66	0.23	0.08	0.0065	1097	57	1049	40
	porc12_21			2.743	0.09	0.2284	0.0082	0.73	4.38	0.16	0.0872	0.0032	1339	25	1326	43
	porc12_22			2.95	0.13	0.2434	0.0086	0.29	4.11	0.15	0.0876	0.0043	1392	34	1404	45
	porc12_23			3.8	0.13	0.2776	0.0095	0.20	3.60	0.12	0.0987	0.0041	1592	28	1579	48
	porc12_24			4.05	0.21	0.291	0.011	0.28	3.44	0.13	0.1017	0.0055	1650	42	1645	55
	porc12_25			2.77	0.1	0.233	0.0084	0.58	4.29	0.15	0.0856	0.0035	1347	28	1350	44
	porc12_26			2.258	0.081	0.205	0.0071	0.19	4.88	0.17	0.0785	0.0034	1198	25	1202	38
	porc12_27			3.41	0.11	0.2608	0.0088	0.44	3.83	0.13	0.0949	0.0035	1506	25	1494	45
	porc12_28			3.06	0.13	0.2415	0.0088	0.16	4.14	0.15	0.0908	0.0047	1420	33	1398	48
	porc12_29			4.11	0.16	0.295	0.011	0.28	3.39	0.13	0.1016	0.0047	1654	32	1668	53
	porc12_30			4.75	0.18	0.32	0.013	0.52	3.13	0.13	0.1074	0.0044	1775	33	1789	61
	porc12_31			2.97	0.15	0.2389	0.0083	0.46	4.19	0.15	0.0908	0.0047	1396	37	1381	43
	porc12_32			1.966	0.099	0.1812	0.0068	0.11	5.52	0.21	0.0786	0.0043	1099	34	1073	37
	porc12_33			2.57	0.19	0.2187	0.0083	0.00	4.57	0.17	0.0844	0.0068	1286	52	1274	44
	porc12_34			2.039	0.067	0.1855	0.0063	0.17	5.39	0.18	0.0788	0.0032	1130	23	1099	33
	porc12_35			1.83	0.11	0.1738	0.0069	0.03	5.75	0.23	0.0753	0.0049	1053	40	1032	38
	porc12_36			1.786	0.092	0.1736	0.0063	0.00	5.76	0.21	0.0757	0.0044	1046	34	1032	35
	porc12_37			3.11	0.18	0.2397	0.0084	0.65	4.17	0.15	0.0924	0.0049	1430	42	1385	44
	porc12_38			1.61	0.1	0.1606	0.0063	0.23	6.23	0.24	0.0742	0.0051	974	42	960	35
	porc12_39			3.64	0.11	0.2646	0.0089	0.46	3.78	0.13	0.0991	0.0036	1558	24	1513	45
	porc12_40			3.78	0.14	0.2708	0.0098	0.51	3.69	0.13	0.1003	0.0042	1586	31	1544	50
	porc12_41			4.01	0.13	0.287	0.0099	0.48	3.48	0.12	0.0999	0.0038	1635	27	1626	50

Table 5: Zircon Sample Data (2011 Dredge Sample Analytical Run)

Identification		Location		Geochronological Data												
Sample	Sample Reference	Latitude	Longitude	$^{207}Pb/^{235}U$	2σ	$^{206}Pb/^{238}U$	2σ	Error Correlation	$^{238}U/^{206}Pb$	2σ	$^{207}Pb/^{206}Pb$	2σ	$^{207}Pb/^{235}U$ Age (Ma)	2σ	$^{206}Pb/^{238}U$ Age (Ma)	2σ
	porc12_42			4.13	0.15	0.295	0.01	0.43	3.39	0.11	0.1018	0.0041	1658	29	1667	52
	porc12_43			2.78	0.13	0.2343	0.0082	0.33	4.27	0.15	0.0854	0.0044	1355	35	1360	41
	porc12_44			4.03	0.16	0.287	0.01	0.34	3.48	0.12	0.101	0.0044	1637	32	1625	50
	porc12_45			1.703	0.066	0.1657	0.0061	0.17	6.04	0.22	0.0746	0.0034	1008	25	988	34
	porc12_46			3.9	0.12	0.2828	0.0098	0.38	3.54	0.12	0.1004	0.0038	1614	26	1605	49
	porc12_47			3.23	0.095	0.2481	0.0083	0.25	4.03	0.13	0.0948	0.0035	1466	22	1429	43
	porc12_48			2.57	0.12	0.216	0.0076	0.05	4.63	0.16	0.0871	0.0043	1293	32	1264	39
	porc12_49			2.5	0.12	0.2139	0.0074	0.25	4.68	0.16	0.0817	0.0041	1273	33	1249	40
	porc12_50			1.784	0.057	0.1755	0.0058	0.15	5.70	0.19	0.0735	0.0029	1039	21	1042	32
	porc12_51			12.2	0.38	0.491	0.018	0.60	2.037	0.075	0.1807	0.0067	2619	29	2576	77
	porc12_52			11.7	0.35	0.48	0.016	0.57	2.083	0.069	0.1778	0.0064	2582	27	2526	70
	porc12_53			3.41	0.11	0.2598	0.0087	0.18	3.85	0.13	0.0949	0.0039	1505	26	1488	45
	porc12_54			2.155	0.087	0.2001	0.0069	0.12	5.00	0.17	0.0782	0.0037	1164	28	1175	37
	porc12_55			1.879	0.075	0.1849	0.0066	0.22	5.41	0.19	0.0729	0.0035	1072	26	1093	36
	porc12_56			1.883	0.065	0.1815	0.0061	0.07	5.51	0.19	0.0764	0.0034	1074	23	1075	34
	porc12_57			2.11	0.11	0.1953	0.0068	0.30	5.12	0.18	0.0768	0.0039	1146	36	1150	37
	porc12_58			2.925	0.096	0.2401	0.0079	0.21	4.16	0.14	0.089	0.0035	1388	25	1387	41
	porc12_59			2.992	0.097	0.246	0.0084	0.30	4.07	0.14	0.0888	0.0034	1404	25	1421	41
	porc12_60			1.761	0.054	0.1745	0.0059	0.52	5.73	0.19	0.0727	0.0026	1031	20	1037	32
	porc12_61			1.6	0.068	0.1612	0.0055	0.10	6.20	0.21	0.0722	0.0033	971	26	963	30
	porc12_62			3.98	0.12	0.2883	0.0095	0.41	3.47	0.11	0.1006	0.0037	1629	24	1633	48
	porc12_63			1.896	0.082	0.181	0.006	0.27	5.52	0.18	0.076	0.0036	1077	29	1072	33
	porc12_64			1.547	0.053	0.1574	0.0056	0.27	6.35	0.23	0.0717	0.0029	949	21	942	31
	porc12_65			3.24	0.11	0.2489	0.0086	0.46	4.02	0.14	0.0929	0.0036	1465	26	1433	44
	porc12_66			2.964	0.088	0.244	0.0089	0.69	4.10	0.15	0.0886	0.0032	1400	24	1407	46
	porc12_67			1.714	0.063	0.168	0.0058	0.28	5.95	0.21	0.0734	0.0031	1012	23	1001	32
	porc12_68			2.661	0.085	0.2243	0.0077	0.48	4.46	0.15	0.086	0.0033	1317	24	1305	41
	porc12_69			1.813	0.072	0.1735	0.0059	0.21	5.76	0.20	0.077	0.0035	1051	25	1031	33
	porc12_70			4.01	0.14	0.2921	0.0097	0.30	3.42	0.11	0.1	0.0038	1636	27	1652	48
	porc12_71			3.91	0.17	0.285	0.01	0.10	3.51	0.12	0.0999	0.0048	1622	34	1618	52
	porc12_72			2.99	0.11	0.2422	0.0083	0.09	4.13	0.14	0.0901	0.0039	1404	27	1398	43
	porc12_73			2.844	0.082	0.236	0.0082	0.47	4.24	0.15	0.0878	0.0032	1367	22	1366	43
	porc12_74			4.05	0.12	0.291	0.01	0.39	3.44	0.12	0.1007	0.0037	1645	24	1645	51
	porc12_75			1.538	0.085	0.1583	0.0054	0.11	6.32	0.22	0.0699	0.0041	941	34	947	30
	porc12_76			2.587	0.097	0.2214	0.0078	0.18	4.52	0.16	0.0851	0.0037	1295	28	1289	41
	porc12_77			3.7	0.2	0.278	0.01	0.00	3.60	0.13	0.0986	0.0058	1574	44	1583	51
	porc12_78			3.24	0.12	0.2571	0.0087	0.17	3.89	0.13	0.0919	0.004	1468	28	1475	45
	porc12_79			3.57	0.13	0.2707	0.0094	0.35	3.69	0.13	0.0948	0.0037	1541	27	1544	48
	porc12_80			2.292	0.086	0.2053	0.0072	0.57	4.87	0.17	0.0816	0.0035	1208	27	1204	38

Table 6: Apatite Sample Data (2014 Dredge Sample Analytical Run)

Identification		Location		Geochronological Data														
Sample	Sample Reference	Latitude	Longitude	$^{207}Pb/^{235}U$	2σ	$^{206}Pb/^{238}U$	2σ	Error Correlation	$^{238}U/^{206}Pb$	2σ	$^{207}Pb/^{206}Pb$	2σ	Error Correlation	$^{206}Pb/^{238}U$ Age (Ma)	2σ	$^{207}Pb/^{235}U$ Age (Ma)	2σ
204-1	X204_2	54.22	-11.63	123.9	5	1.092	0.053	0.72	0.916	0.044	0.816	0.023	0.08	4760	170	4901	41
	X204_3			187	6	1.682	0.07	0.48	0.595	0.025	0.798	0.024	0.33	6340	170	5311	32
	X204_4			2020	120	17.6	1.2	0.91	0.057	0.004	0.844	0.023	0.21	18710	420	7704	59
	X204_5			286.2	7.6	2.463	0.095	0.49	0.406	0.016	0.852	0.019	0.38	8000	180	5750	26
	X204_6			4430	570	34.6	4.4	0.97	0.029	0.004	0.892	0.025	0.17	22280	690	8380	120
	X204_7			29.9	1	0.3602	0.013	0.43	2.776	0.100	0.596	0.018	0.30	1986	60	3486	33
	X204_8			41	1.2	0.4312	0.015	0.31	2.319	0.081	0.687	0.018	0.46	2313	67	3799	28
	X204_9			26.9	0.9	0.3182	0.011	0.15	3.143	0.109	0.619	0.019	0.45	1780	55	3376	33
	X204_10			182.1	6.3	1.573	0.06	0.61	0.636	0.024	0.827	0.022	0.20	6091	150	5279	35
	X204_11			21.56	0.48	0.2737	0.0092	0.48	3.654	0.12	0.577	0.012	0.22	1559	46	3159	21
	X204_12			13.85	0.66	0.2599	0.0092	0.22	3.848	0.14	0.389	0.019	0.21	1488	47	2742	44
	X204_13			9.82	0.32	0.2008	0.0069	0.20	4.980	0.17	0.355	0.012	0.22	1179	37	2416	30
	X204_14			94.8	2.5	0.836	0.031	0.30	1.196	0.044	0.815	0.022	0.33	3919	110	4625	27
	X204_15			40.6	1.3	0.4389	0.016	0.22	2.278	0.083	0.669	0.022	0.45	2343	71	3796	30
	X204_16			72.1	1.8	0.695	0.024	0.35	1.439	0.050	0.761	0.021	0.29	3397	91	4365	24
	X204_17			25.21	0.82	0.3338	0.012	0.21	3.00	0.11	0.544	0.018	0.35	1855	58	3319	30
	X204_18			107.2	3.3	0.987	0.038	0.32	1.013	0.039	0.777	0.024	0.43	4416	120	4757	33
	X204_19			12.97	0.57	0.2693	0.0094	0.51	3.71	0.13	0.346	0.011	0.09	1537	48	2676	41
	X204_20			100.1	3.1	0.897	0.034	0.39	1.115	0.042	0.805	0.023	0.38	4119	120	4681	31
	X204_21			75.2	2.2	0.689	0.026	0.50	1.451	0.055	0.785	0.02	0.29	3374	99	4402	30
	X204_22			15.5	0.59	0.255	0.009	0.21	3.92	0.14	0.438	0.016	0.30	1466	46	2833	37
	X204_23			83.4	2.7	0.793	0.029	0.29	1.261	0.046	0.758	0.025	0.42	3758	100	4498	32
	X204_24			33.01	0.96	0.39	0.015	0.41	2.564	0.099	0.618	0.019	0.30	2120	69	3580	30
	X204_25			64.6	1.8	0.621	0.023	0.14	1.610	0.060	0.75	0.022	0.50	3121	87	4241	27
	X204_26			101.1	3	0.908	0.032	0.53	1.101	0.039	0.801	0.019	0.11	4174	110	4691	30
	X204_27			1574	73	13.02	0.75	0.88	0.077	0.004	0.882	0.019	0.33	16940	330	7461	47
	X204_28			72	2	0.706	0.028	0.64	1.416	0.056	0.734	0.02	0.15	3446	110	4363	27
	X204_29			504	20	4.21	0.21	0.79	0.238	0.012	0.858	0.023	0.24	10670	260	6314	41
	X204_30			106	3.5	0.962	0.036	0.54	1.040	0.039	0.785	0.022	0.34	4338	120	4734	34
302-1	X302_1_1	54.08	-11.97	11.79	0.78	0.1648	0.0077	0.38	6.07	0.28	0.539	0.036	0.22	982	43	2580	63
	X302_1_2			21.13	0.86	0.2469	0.012	0.36	4.05	0.20	0.614	0.029	0.49	1418	64	3135	38
	X302_1_3			5.67	0.24	0.1158	0.0052	0.35	8.64	0.39	0.36	0.016	0.45	705	30	1935	36
	X302_1_4			6.3	0.21	0.3242	0.011	0.23	3.08	0.10	0.1397	0.0046	0.14	1810	52	2014	29
	X302_1_5			11.8	1.3	0.163	0.015	0.93	6.13	0.56	0.536	0.033	-0.05	952	75	2515	89
	X302_1_6			17.6	2.9	0.227	0.027	0.97	4.41	0.52	0.576	0.04	-0.12	1290	130	2800	100
	X302_1_7			7.5	1.1	0.135	0.014	0.96	7.41	0.77	0.395	0.036	-0.32	792	72	2020	120
	X302_1_8			19.5	1.6	0.233	0.016	0.94	4.29	0.29	0.604	0.027	-0.13	1341	81	3023	73
	X302_1_9			14.65	0.46	0.1896	0.007	0.00	5.27	0.19	0.548	0.021	0.55	1118	38	2784	30
	X302_1_10			5.4	0.5	0.297	0.015	0.30	3.37	0.17	0.132	0.012	0.17	1669	77	1868	83
	X302_1_11			16.4	1.8	0.201	0.018	0.94	4.98	0.45	0.58	0.033	-0.07	1167	91	2829	86
	X302_1_12			13.5	1.9	0.355	0.02	0.93	2.82	0.16	0.267	0.027	-0.50	1932	82	2610	110
	X302_1_13			14.57	0.7	0.1845	0.0086	0.33	5.42	0.25	0.558	0.032	0.33	1090	47	2785	46
	X302_1_14			4.32	0.16	0.2023	0.0071	0.21	4.94	0.17	0.1525	0.0059	0.21	1187	38	1691	30
	X302_1_15			22.8	1	0.2484	0.011	0.79	4.03	0.18	0.649	0.026	0.15	1427	59	3207	42

Table 6: Apatite Sample Data (2014 Dredge Sample Analytical Run)																	
Identification		Location		Geochronological Data													
Sample	Sample Reference	Latitude	Longitude	$^{207}Pb/^{235}U$	2σ	$^{206}Pb/^{238}U$	2σ	Error Correlation	$^{238}U/^{206}Pb$	2σ	$^{207}Pb/^{206}Pb$	2σ	Error Correlation	$^{206}Pb/^{238}U$ Age (Ma)	2σ	$^{207}Pb/^{235}U$ Age (Ma)	2σ
204-1	X204_2	54.22	-11.63	123.9	5	1.092	0.053	0.72	0.916	0.044	0.816	0.023	0.08	4760	170	4901	41
	X302_1_16			8.64	0.41	0.3474	0.013	-0.01	2.88	0.11	0.176	0.0096	0.41	1925	64	2288	44
	X302_1_17			11.36	0.49	0.2556	0.0095	0.28	3.91	0.15	0.316	0.012	0.19	1466	49	2538	40
	X302_1_18			26.7	2.4	0.47	0.026	0.60	2.13	0.12	0.408	0.034	0.22	2486	120	3330	82
	X302_1_19			11.82	0.52	0.1629	0.0063	0.33	6.14	0.24	0.522	0.023	0.22	972	35	2601	41
	X302_1_20			4.58	0.21	0.0996	0.0042	0.42	10.04	0.42	0.335	0.015	0.29	611	25	1745	42
	X302_1_21			14.3	1	0.18	0.013	0.48	5.56	0.40	0.558	0.035	0.36	1061	68	2741	67
	X302_1_22			14.02	0.6	0.1854	0.0077	0.19	5.39	0.22	0.55	0.024	0.45	1095	42	2747	40
	X302_1_23			16.4	0.59	0.1979	0.0078	0.41	5.05	0.20	0.595	0.021	0.23	1163	42	2902	35
	X302_1_24			35.1	1.5	0.357	0.016	0.53	2.80	0.13	0.709	0.027	0.43	1961	78	3634	44
	X302_1_25			10.94	0.72	0.1579	0.0074	-0.04	6.33	0.30	0.49	0.038	0.57	943	41	2515	64
	X302_1_26			16.95	0.67	0.2014	0.0075	0.08	4.97	0.18	0.611	0.026	0.41	1182	40	2957	41
	X302_1_27			3.83	0.19	0.095	0.0035	0.05	10.53	0.39	0.288	0.014	0.41	586	20	1591	38
	X302_1_28			8.97	0.46	0.1372	0.0058	0.25	7.29	0.31	0.48	0.025	0.35	828	33	2349	47
	X302_1_29			13.62	0.44	0.1813	0.0071	0.11	5.52	0.22	0.538	0.02	0.56	1076	37	2721	32
	X302_1_30			11.07	0.64	0.1554	0.0075	0.29	6.44	0.31	0.503	0.026	0.39	930	42	2525	51
302-1 (2)	X302_1_1			7.1	0.18	0.1205	0.0029	0.59	8.30	0.20	0.428	0.0061	0.19	733.5	17	2121	13
	X302_1_2			16.62	0.49	0.2044	0.0056	0.72	4.89	0.13	0.594	0.012	0.26	1198	30	2910	19
	X302_1_3			12.15	0.42	0.2653	0.0075	0.48	3.77	0.11	0.3319	0.0082	0.24	1517	38	2611	26
	X302_1_4			10.53	0.4	0.1495	0.0043	0.84	6.69	0.19	0.5083	0.0091	-0.30	897	24	2470	29
	X302_1_5			6.54	0.25	0.2136	0.0054	0.39	4.68	0.12	0.2226	0.0072	0.06	1247	29	2044	29
	X302_1_6			10.98	0.36	0.245	0.0065	0.50	4.08	0.11	0.324	0.007	0.18	1411	34	2518	23
	X302_1_7			32.32	1.1	0.983	0.03	0.33	1.017	0.031	0.2388	0.0067	0.43	4408	95	3557	26
	X302_1_8			22.37	0.53	0.4357	0.01	0.38	2.295	0.053	0.3727	0.0047	0.36	2332	45	3199	11
	X302_1_9			8.16	0.21	0.3163	0.0073	0.51	3.162	0.073	0.1882	0.0026	0.04	1772	35	2247	13
	X302_1_10			9.33	0.23	0.3454	0.0078	0.24	2.895	0.065	0.197	0.003	0.27	1912	38	2370	13
	X302_1_11			8.76	0.22	0.3325	0.0074	0.19	3.008	0.067	0.1909	0.0026	0.29	1851	36	2312	13
	X302_1_12			7.707	0.19	0.326	0.0073	0.34	3.067	0.069	0.1721	0.0022	0.23	1822	36	2198	11
	X302_1_13			14.5	1.3	0.377	0.014	0.97	2.65	0.10	0.267	0.014	-0.87	2055	62	2705	71
	X302_1_14			10.13	0.41	0.3196	0.0074	0.56	3.129	0.072	0.2283	0.0067	-0.27	1788	36	2434	31
	X302_1_15			291	14	2.34	0.12	0.92	0.427	0.022	0.914	0.024	0.26	7620	200	5743	41
	X302_1_16			309	16	2.49	0.13	0.90	0.402	0.021	0.886	0.023	0.31	7940	220	5794	46
	X302_1_17			13.87	0.52	0.3224	0.0084	0.65	3.102	0.081	0.3139	0.0087	-0.16	1800	41	2731	30
	X302_1_18			29.87	0.99	0.3762	0.012	0.58	2.658	0.085	0.578	0.013	0.34	2057	55	3477	26
	X302_1_19			76.1	3.1	0.783	0.029	0.86	1.277	0.047	0.696	0.016	0.25	3718	100	4398	33
	X302_1_20			46.4	1.6	0.59	0.018	0.82	1.695	0.052	0.571	0.013	0.12	2981	72	3907	27
	X302_1_21			5.61	0.53	0.2021	0.0063	0.96	4.95	0.15	0.189	0.01	-0.77	1181	31	1809	41
	X302_1_22			47.1	2.6	0.575	0.025	0.90	1.74	0.08	0.604	0.014	-0.34	2905	100	3904	51
	X302_1_23			16.17	0.5	0.1991	0.0054	0.83	5.02	0.14	0.5901	0.0091	0.01	1169	29	2881	21
	X302_1_24			16.6	0.96	0.3346	0.012	0.94	2.99	0.11	0.358	0.011	-0.50	1854	57	2864	38
	X302_1_25			25.34	0.62	0.2773	0.0067	0.18	3.606	0.087	0.664	0.011	0.61	1577	34	3320	13
	X302_1_26			7.04	0.23	0.1234	0.0033	0.76	8.10	0.22	0.4194	0.0085	-0.11	750	19	2108	22
	X302_1_27			21.92	0.88	0.4094	0.012	0.91	2.443	0.072	0.389	0.009	-0.45	2208	54	3162	31
	X302_1_28			22.27	1	0.4037	0.013	0.92	2.477	0.080	0.3932	0.009	-0.58	2181	57	3168	38
	X302_1_29			13.03	0.45	0.2429	0.0063	0.67	4.12	0.11	0.3871	0.0079	-0.09	1403	32	2677	26
	X302_1_30			14.26	0.34	0.1846	0.0043	0.54	5.42	0.13	0.5594	0.0066	0.28	1092	24	2767	12

Table 6: Apatite Sample Data (2014 Dredge Sample Analytical Run)																		
Identification		Location		Geochronological Data														
Sample	Sample Reference	Latitude	Longitude	$^{207}Pb/^{235}U$	2σ	$^{206}Pb/^{238}U$	2σ	Error Correlation	$^{238}U/^{206}Pb$	2σ	$^{207}Pb/^{206}Pb$	2σ	Error Correlation	$^{206}Pb/^{238}U$ Age (Ma)	2σ	$^{207}Pb/^{235}U$ Age (Ma)	2σ
204-1	X204_2	54.22	-11.63	123.9	5	1.092	0.053	0.72	0.916	0.044	0.816	0.023	0.08	4760	170	4901	41
	X302_1_31			72.8	5.1	0.815	0.051	0.94	1.227	0.077	0.662	0.025	0.07	3730	150	4307	57
	X302_1_32			71.1	3.5	0.803	0.037	0.82	1.245	0.057	0.65	0.024	0.34	3770	130	4325	47
	X302_1_33			18.01	0.85	0.3417	0.01	0.84	2.927	0.086	0.383	0.012	-0.35	1892	48	2970	39
	X302_1_34			14.09	0.37	0.185	0.0047	0.84	5.41	0.14	0.5559	0.0058	0.17	1094	26	2751	16
	X302_1_35			181.6	7.8	1.514	0.064	0.73	0.661	0.028	0.87	0.026	0.43	5950	160	5265	37
402-1	X402_1_1	53.95	-12.79	10.53	0.6	0.3522	0.013	0.27	2.84	0.10	0.212	0.01	0.13	1951	61	2473	53
	X402_1_2			10.76	0.61	0.3602	0.014	0.13	2.78	0.11	0.215	0.012	0.33	1985	68	2493	54
	X402_1_3			28.2	2	0.464	0.022	0.11	2.16	0.10	0.441	0.031	0.36	2458	95	3400	67
	X402_1_4			20.8	1.7	0.41	0.02	0.24	2.44	0.12	0.361	0.029	0.38	2231	92	3085	89
	X402_1_5			6.84	0.34	0.3304	0.013	0.39	3.03	0.12	0.1497	0.0068	0.05	1838	61	2075	44
	X402_1_6			21.3	1.5	0.448	0.021	0.11	2.23	0.10	0.336	0.026	0.40	2378	94	3158	64
	X402_1_7			9.32	0.54	0.3325	0.012	0.20	3.01	0.11	0.199	0.011	0.23	1853	59	2375	53
	X402_1_8			24.6	2	0.452	0.023	0.21	2.21	0.11	0.395	0.034	0.47	2392	100	3272	82
	X402_1_9			11.8	0.68	0.3531	0.014	0.11	2.83	0.11	0.237	0.014	0.41	1952	64	2596	54
	X402_1_10			25.1	1.4	0.448	0.023	0.22	2.23	0.11	0.401	0.025	0.62	2377	100	3316	56
	X402_1_11			15.9	1.2	0.397	0.016	0.23	2.52	0.10	0.287	0.021	0.25	2150	76	2858	71
	X402_1_12			9.85	0.64	0.3497	0.013	0.30	2.86	0.11	0.197	0.011	0.10	1931	64	2407	64
	X402_1_13			7.72	0.39	0.323	0.011	0.30	3.10	0.11	0.1722	0.0082	0.09	1803	55	2197	43
	X402_1_14			22.4	1.7	0.421	0.018	0.07	2.38	0.10	0.382	0.032	0.48	2262	83	3196	77
	X402_1_15			19.1	1.4	0.403	0.018	0.25	2.48	0.11	0.34	0.025	0.22	2202	84	3028	75
	X402_1_16			19	1.3	0.421	0.021	0.26	2.38	0.12	0.321	0.023	0.39	2265	98	3051	68
	X402_1_17			13.27	0.82	0.3642	0.015	0.05	2.75	0.11	0.253	0.016	0.35	2011	72	2702	61
	X402_1_18			14.16	0.92	0.383	0.017	0.16	2.61	0.12	0.277	0.019	0.34	2091	79	2768	62
	X402_1_19			11.79	0.72	0.3601	0.014	0.13	2.78	0.11	0.232	0.014	0.33	1985	67	2569	59
	X402_1_20			26.6	1.6	0.498	0.023	0.17	2.01	0.09	0.394	0.025	0.49	2607	100	3367	58
	X402_1_21			17.3	1.6	0.371	0.017	0.12	2.70	0.12	0.329	0.031	0.35	2037	77	2908	94
	X402_1_22			13.7	1.5	0.386	0.019	0.46	2.59	0.13	0.248	0.022	-0.15	2096	89	2700	100
	X402_1_23			9.89	0.54	0.367	0.013	0.17	2.72	0.10	0.192	0.011	0.36	2019	63	2427	51
	X402_1_24			36.3	2.7	0.533	0.031	0.37	1.88	0.11	0.497	0.036	0.29	2730	130	3673	70
	X402_1_25			21	1.5	0.419	0.018	0.23	2.39	0.10	0.359	0.026	0.24	2253	82	3118	72
	X402_1_26			15.9	1.1	0.4193	0.016	0.20	2.385	0.091	0.271	0.019	0.13	2254	72	2845	69
	X402_1_27			11.36	0.71	0.3808	0.015	0.15	2.626	0.103	0.213	0.013	0.29	2077	68	2564	59
	X402_1_28			22.4	1.8	0.415	0.019	0.09	2.410	0.110	0.384	0.034	0.45	2232	86	3163	85
	X402_1_29			21	1.8	0.453	0.022	0.20	2.208	0.107	0.331	0.028	0.27	2399	96	3091	85
	X402_1_30			20.4	1.5	0.426	0.022	0.20	2.347	0.121	0.347	0.027	0.41	2288	99	3100	71
	PH402_1_1			20.47	0.97	0.405	0.014	0.54	2.469	0.085	0.359	0.012	0.00	2188	65	3089	46
	PH402_1_2			39.88	1.2	0.5401	0.015	0.55	1.852	0.051	0.532	0.011	0.38	2783	62	3764	30
	PH402_1_3			58.2	1.9	0.688	0.02	0.49	1.453	0.042	0.622	0.014	0.35	3367	75	4146	31
	PH402_1_4			17.27	0.48	0.3824	0.0096	0.56	2.615	0.066	0.3305	0.0049	0.17	2086	45	2950	27
	PH402_1_5			13.34	0.35	0.3673	0.0089	0.31	2.723	0.066	0.2655	0.0038	0.42	2016	42	2702	24
	PH402_1_6			16.96	0.52	0.3985	0.01	0.58	2.509	0.063	0.3125	0.0058	0.07	2163	48	2933	29
	PH402_1_7			35.5	1	0.5241	0.014	0.53	1.908	0.051	0.4932	0.008	0.26	2717	58	3652	27
	PH402_1_8			31.94	0.97	0.4888	0.014	0.65	2.046	0.059	0.4729	0.0081	0.26	2561	59	3545	29
	PH402_1_9			58.1	1.7	0.668	0.019	0.64	1.497	0.043	0.627	0.011	0.40	3292	74	4135	29
	PH402_1_10			56.3	1.7	0.671	0.02	0.66	1.490	0.044	0.61	0.012	0.43	3304	76	4105	30

Table 6: Apatite Sample Data (2014 Dredge Sample Analytical Run)

Identification		Location		Geochronological Data													
Sample	Sample Reference	Latitude	Longitude	$^{207}Pb/^{235}U$	2σ	$^{206}Pb/^{238}U$	2σ	Error Correlation	$^{238}U/^{206}Pb$	2σ	$^{207}Pb/^{206}Pb$	2σ	Error Correlation	$^{206}Pb/^{238}U$ Age (Ma)	2σ	$^{207}Pb/^{235}U$ Age (Ma)	2σ
204-1	X204_2	54.22	-11.63	123.9	5	1.092	0.053	0.72	0.916	0.044	0.816	0.023	0.08	4760	170	4901	41
	PH402_1_11			17.7	1.1	0.4195	0.011	0.62	2.384	0.063	0.31	0.016	-0.25	2259	49	2938	60
	PH402_1_12			23.04	0.62	0.4418	0.011	0.58	2.263	0.056	0.3784	0.0064	0.30	2357	49	3222	25
	PH402_1_13			23.48	0.63	0.4393	0.011	0.33	2.276	0.057	0.3891	0.006	0.24	2346	50	3246	25
	PH402_1_14			30.37	0.96	0.484	0.013	0.64	2.066	0.055	0.4564	0.0077	0.14	2541	58	3503	31
	PH402_1_15			28.32	0.95	0.4699	0.013	0.44	2.128	0.059	0.4369	0.0097	0.09	2486	55	3421	32
	PH402_1_16			17.26	0.45	0.4037	0.01	0.50	2.477	0.061	0.3116	0.0049	0.40	2184	47	2950	25
	PH402_1_17			30.4	2.5	0.555	0.017	0.68	1.802	0.055	0.387	0.025	-0.41	2841	69	3421	74
	PH402_1_18			16.8	0.45	0.3885	0.01	0.52	2.574	0.066	0.3176	0.005	0.37	2114	47	2924	25
	PH402_1_19			67.9	2	0.716	0.021	0.52	1.397	0.041	0.689	0.013	0.49	3478	79	4305	31
	PH402_1_20			10.88	0.3	0.3641	0.0093	0.51	2.746	0.070	0.2193	0.0032	0.31	2004	45	2511	26
	PH402_1_21			36.14	1.1	0.5309	0.014	0.42	1.884	0.050	0.501	0.01	0.36	2742	59	3664	31
	PH402_1_22			70.9	3	0.779	0.03	0.74	1.284	0.049	0.669	0.016	0.21	3698	110	4330	43
	PH402_1_23			52.2	1.7	0.628	0.018	0.81	1.592	0.046	0.606	0.011	0.16	3140	71	4026	33
	PH402_1_24			51	5.6	0.702	0.038	0.89	1.425	0.077	0.473	0.033	-0.64	3420	150	3800	120
	PH402_1_25			12.71	0.39	0.371	0.0097	0.42	2.695	0.070	0.2526	0.0053	0.23	2032	45	2655	29
	PH402_1_26			37.42	1.2	0.5262	0.015	0.37	1.900	0.054	0.518	0.011	0.36	2732	60	3708	32
	PH402_1_27			176.8	7.2	1.478	0.058	0.81	0.677	0.027	0.863	0.018	0.25	5860	150	5248	41
	PH402_1_28			47.6	2	0.595	0.018	0.13	1.681	0.051	0.574	0.017	0.01	3001	74	3919	36
	PH402_1_29			8.07	0.22	0.3227	0.0078	0.47	3.099	0.075	0.1817	0.0026	0.18	1802	38	2235	24
	PH402_1_30			15.94	0.6	0.4017	0.011	0.65	2.489	0.068	0.2892	0.0065	-0.11	2180	51	2871	35
	PH402_1_31			11.21	0.38	0.362	0.01	0.52	2.762	0.076	0.228	0.0049	0.18	1989	48	2536	32
	PH402_1_32			23.76	0.89	0.496	0.015	0.36	2.016	0.061	0.349	0.01	0.29	2595	64	3248	37
	PH402_1_33			24.67	0.83	0.4361	0.013	0.57	2.293	0.068	0.4158	0.009	0.17	2340	56	3286	33
	PH402_1_34			33.55	1.2	0.505	0.016	0.71	1.980	0.063	0.489	0.0097	0.10	2634	67	3603	36
	PH402_1_35			33.74	1.1	0.521	0.015	0.60	1.919	0.055	0.476	0.01	0.14	2696	64	3591	33
	PH402_1_36			28.86	0.92	0.4638	0.013	0.63	2.156	0.060	0.4514	0.0088	0.08	2456	55	3457	31
	PH402_1_37			110.7	4.4	1.027	0.038	0.71	0.974	0.036	0.795	0.02	0.34	4538	120	4774	40
	PH402_1_38			26.11	0.83	0.5085	0.014	0.41	1.967	0.054	0.3711	0.0075	0.28	2650	59	3343	31
	PH402_1_39			25.76	0.88	0.4395	0.013	0.57	2.275	0.067	0.4253	0.0092	0.27	2348	59	3332	34
	PH402_1_40			29.51	0.9	0.48	0.013	0.38	2.083	0.056	0.4529	0.0092	0.38	2528	57	3465	30
	PH402_1_41			42.3	1.4	0.566	0.017	0.55	1.767	0.053	0.555	0.012	0.38	2886	70	3827	33
	PH402_1_42			45.9	1.5	0.576	0.016	0.65	1.736	0.048	0.583	0.012	0.22	2933	65	3906	32
	PH402_1_43			29.61	0.93	0.4763	0.013	0.51	2.100	0.057	0.4543	0.0089	0.31	2510	59	3465	31
402-3	X402_3_1	53.95	-12.79	10	1.1	0.346	0.016	0.03	2.89	0.13	0.208	0.023	0.22	1910	78	2410	120
	X402_3_2			9.92	0.89	0.354	0.016	0.09	2.82	0.13	0.206	0.018	0.21	1956	76	2420	86
	X402_3_5			13.5	1.3	0.367	0.02	0.07	2.72	0.15	0.262	0.028	0.38	2018	93	2650	110
	X402_3_6			11.73	0.87	0.388	0.02	0.24	2.58	0.13	0.219	0.016	0.45	2103	93	2596	69
	X402_3_7			10.75	0.99	0.36	0.015	0.12	2.78	0.12	0.214	0.021	0.26	1978	71	2499	86
	X402_3_8			10.1	1.1	0.34	0.015	0.07	2.94	0.13	0.217	0.025	0.19	1883	74	2400	120
	X402_3_9			13.1	1.2	0.403	0.017	0.13	2.48	0.10	0.236	0.023	0.21	2178	80	2685	96
	X402_3_10			9.82	0.77	0.368	0.018	0.14	2.72	0.13	0.196	0.016	0.32	2012	83	2422	77
	X402_3_11			7.58	0.65	0.323	0.015	0.20	3.10	0.14	0.173	0.016	0.21	1807	70	2176	78
	X402_3_12			14.2	1.3	0.385	0.021	0.04	2.60	0.14	0.275	0.026	0.39	2090	97	2738	94
	X402_3_13			12.3	1.2	0.368	0.018	0.03	2.72	0.13	0.243	0.025	0.51	2020	86	2615	92
	X402_3_14			8.9	0.86	0.327	0.015	0.09	3.06	0.14	0.192	0.019	0.30	1820	73	2291	90

Table 6: Apatite Sample Data (2014 Dredge Sample Analytical Run)

Identification		Location		Geochronological Data													
Sample	Sample Reference	Latitude	Longitude	$^{207}Pb/^{235}U$	2σ	$^{206}Pb/^{238}U$	2σ	Error Correlation	$^{238}U/^{206}Pb$	2σ	$^{207}Pb/^{206}Pb$	2σ	Error Correlation	$^{206}Pb/^{238}U$ Age (Ma)	2σ	$^{207}Pb/^{235}U$ Age (Ma)	2σ
204-1	X204_2	54.22	-11.63	123.9	5	1.092	0.053	0.72	0.916	0.044	0.816	0.023	0.08	4760	170	4901	41
	X402_3_15			17.7	1.9	0.402	0.022	0.16	2.49	0.14	0.299	0.033	0.40	2168	100	2960	100
	X402_3_16			11.4	1.3	0.346	0.019	0.31	2.89	0.16	0.241	0.026	0.10	1905	92	2540	120
	X402_3_17			12.3	1.2	0.383	0.019	-0.05	2.61	0.13	0.241	0.028	0.35	2083	89	2683	96
	X402_3_18			11.03	0.9	0.362	0.016	0.11	2.76	0.12	0.212	0.019	0.35	1987	78	2509	83
	X402_3_19			11.45	0.95	0.357	0.015	0.07	2.80	0.12	0.229	0.019	0.26	1968	71	2539	77
	X402_3_20			11.8	1.2	0.363	0.016	0.17	2.75	0.12	0.24	0.024	0.22	1994	78	2556	98
	X402_3_21			12.1	1	0.374	0.018	0.08	2.67	0.13	0.237	0.02	0.36	2042	83	2584	82
	X402_3_22			11.8	1.1	0.353	0.016	0.14	2.83	0.13	0.233	0.023	0.28	1944	77	2571	90
	X402_3_23			13.7	1.3	0.379	0.018	0.03	2.64	0.13	0.26	0.026	0.47	2064	82	2696	94
	X402_3_24			18.1	1.6	0.396	0.025	0.13	2.53	0.16	0.311	0.033	0.50	2140	110	2951	92
	X402_3_25			11.12	0.95	0.367	0.017	0.05	2.72	0.13	0.217	0.02	0.27	2010	80	2498	91
	X402_3_26			14.2	1.4	0.395	0.021	-0.07	2.53	0.13	0.257	0.029	0.51	2139	96	2742	99
	X402_3_27			10.87	0.92	0.37	0.017	0.42	2.70	0.12	0.208	0.015	0.03	2023	80	2474	86
	X402_3_28			13.9	1.4	0.391	0.019	0.27	2.56	0.12	0.259	0.025	0.16	2119	90	2720	100
	X402_3_29			11.7	1.1	0.344	0.017	0.09	2.91	0.14	0.243	0.024	0.22	1897	83	2547	91
	X402_3_30			9.89	0.88	0.352	0.016	0.23	2.84	0.13	0.2	0.016	0.22	1945	73	2425	82
	PH402_3_1			11.45	0.32	0.3544	0.0085	0.17	2.822	0.068	0.2349	0.0046	0.38	1955	40	2557	26
	PH402_3_2			8.97	0.68	0.3286	0.01	0.81	3.043	0.093	0.193	0.01	-0.60	1828	50	2286	66
	PH402_3_3			10.88	0.31	0.3614	0.0094	0.44	2.767	0.072	0.2214	0.004	0.35	1987	44	2513	26
	PH402_3_4			10.71	0.39	0.3529	0.01	0.47	2.834	0.080	0.2205	0.0051	0.08	1946	48	2488	33
	PH402_3_5			19.01	0.56	0.4126	0.011	0.40	2.424	0.065	0.3337	0.0067	0.39	2227	50	3043	28
	PH402_3_6			9.23	0.28	0.3256	0.0081	0.42	3.071	0.076	0.2061	0.0042	0.19	1816	39	2361	29
	PH402_3_7			16.1	0.49	0.3955	0.01	0.42	2.528	0.064	0.2984	0.0061	0.25	2149	48	2880	29
	PH402_3_8			9.78	0.27	0.3394	0.0081	0.21	2.946	0.070	0.2083	0.0038	0.41	1883	39	2411	25
	PH402_3_9			12.46	0.35	0.3565	0.0086	0.27	2.805	0.068	0.252	0.0048	0.34	1965	41	2641	27
402-3 (2)	PH402_3_10			7.49	0.26	0.3243	0.0081	0.82	3.084	0.077	0.1662	0.0029	-0.52	1810	39	2162	29
	PH402_3_11			6.375	0.17	0.3103	0.0072	0.05	3.223	0.075	0.1494	0.0022	0.39	1742	35	2026	23
	PH402_3_12			23.02	0.67	0.4415	0.011	0.33	2.265	0.056	0.3803	0.0075	0.39	2355	51	3231	28
	PH402_3_13			9.4	0.28	0.3287	0.0081	0.20	3.042	0.075	0.2098	0.004	0.22	1831	40	2376	27
	PH402_3_14			10.24	0.27	0.3475	0.0086	0.11	2.878	0.071	0.2149	0.0039	0.57	1922	41	2455	25
	PH402_3_15			10.64	0.32	0.3406	0.0087	0.43	2.936	0.075	0.2266	0.0045	0.22	1888	42	2493	28
	PH402_3_16			18.61	0.67	0.4023	0.011	0.55	2.486	0.068	0.3396	0.0087	0.07	2179	52	3023	33
	PH402_3_17			13.35	0.42	0.3602	0.0091	0.32	2.776	0.070	0.2711	0.0061	0.23	1984	44	2701	30
	PH402_3_18			8.37	0.24	0.3268	0.0078	0.26	3.060	0.073	0.1869	0.0034	0.29	1822	38	2269	26
	PH402_3_19			8.79	0.7	0.3238	0.01	0.90	3.088	0.095	0.192	0.011	-0.80	1811	50	2260	71
	PH402_3_20			8.61	0.27	0.3227	0.0083	0.42	3.099	0.080	0.1926	0.0042	0.21	1802	40	2294	29
	PH402_3_21			10.4	0.35	0.3069	0.009	0.46	3.258	0.096	0.2453	0.006	0.33	1725	44	2472	31
	PH402_3_22			11.79	0.38	0.3501	0.0096	0.47	2.856	0.078	0.2454	0.0048	0.28	1938	45	2585	29
	PH402_3_23			12.28	0.37	0.3591	0.0098	0.37	2.785	0.076	0.248	0.0053	0.37	1975	46	2621	28
	PH402_3_24			23.27	0.77	0.4443	0.013	0.58	2.251	0.066	0.383	0.0082	0.26	2369	60	3235	33
	PH402_3_25			9.59	0.29	0.3328	0.0087	0.27	3.005	0.079	0.2098	0.0043	0.22	1850	42	2394	27
	PH402_3_26			13.31	0.37	0.3717	0.0091	0.35	2.690	0.066	0.259	0.0049	0.30	2036	43	2701	26
	PH402_3_27			13.25	0.43	0.3591	0.0097	0.57	2.785	0.075	0.266	0.0054	0.21	1981	45	2695	30
	PH402_3_28			11.19	0.32	0.3397	0.0082	0.38	2.944	0.071	0.2384	0.0046	0.19	1886	39	2534	27
	PH402_3_29			12.5	0.37	0.3625	0.0092	0.36	2.759	0.070	0.2482	0.0043	0.21	1993	44	2639	28

Table 6: Apatite Sample Data (2014 Dredge Sample Analytical Run)

Identification		Location		Geochronological Data													
Sample	Sample Reference	Latitude	Longitude	$^{207}Pb/^{235}U$	2σ	$^{206}Pb/^{238}U$	2σ	Error Correlation	$^{238}U/^{206}Pb$	2σ	$^{207}Pb/^{206}Pb$	2σ	Error Correlation	$^{206}Pb/^{238}U$ Age (Ma)	2σ	$^{207}Pb/^{235}U$ Age (Ma)	2σ
204-1	X204_2	54.22	-11.63	123.9	5	1.092	0.053	0.72	0.916	0.044	0.816	0.023	0.08	4760	170	4901	41
	PH402_3_30			7.28	0.28	0.3174	0.0087	0.14	3.151	0.086	0.1665	0.0044	0.04	1778	43	2133	34
	PH402_3_31			11.15	0.38	0.3425	0.0094	0.56	2.920	0.080	0.2336	0.0049	0.11	1896	45	2529	32
	PH402_3_32			9.9	0.32	0.3527	0.01	0.52	2.835	0.080	0.204	0.004	0.24	1948	47	2425	30
	PH402_3_33			20.58	0.64	0.4285	0.012	0.50	2.334	0.065	0.3457	0.0068	0.25	2296	53	3118	30
	PH402_3_34			7.25	0.22	0.3287	0.0088	0.49	3.042	0.081	0.1607	0.0028	0.30	1834	43	2141	26
	PH402_3_35			9.21	0.34	0.3294	0.0093	0.62	3.036	0.086	0.2044	0.0045	-0.02	1838	45	2354	34
	PH402_3_36			9.28	0.26	0.3453	0.0087	0.11	2.896	0.073	0.1965	0.0035	0.48	1911	42	2369	26
	PH402_3_37			14.03	0.49	0.4018	0.01	0.69	2.489	0.062	0.251	0.0053	-0.20	2176	47	2742	32
	PH402_3_38			10.9	0.34	0.3481	0.0089	0.36	2.873	0.073	0.2285	0.0051	0.25	1924	42	2515	29
	PH402_3_39			10.28	0.36	0.3622	0.01	0.77	2.761	0.076	0.2041	0.0041	0.08	1990	48	2448	32
	PH402_3_40			19.24	0.57	0.4279	0.011	0.44	2.337	0.060	0.3278	0.0065	0.26	2297	50	3053	28
	PH402_3_41			12.66	0.41	0.371	0.0091	0.28	2.695	0.066	0.2466	0.0054	0.12	2033	43	2650	30
	PH402_3_1			17.53	0.57	0.4469	0.014	0.31	2.238	0.070	0.2892	0.0061	0.40	2376	60	2963	31
	PH402_3_2			21.85	0.71	0.4348	0.012	0.57	2.300	0.063	0.3655	0.008	0.17	2327	55	3172	30
	PH402_3_3			10.73	0.34	0.341	0.0094	0.45	2.933	0.081	0.2257	0.0049	0.30	1889	45	2502	30
	PH402_3_4			16.62	0.54	0.4031	0.011	0.45	2.481	0.068	0.3014	0.0063	0.18	2183	50	2914	32
	PH402_3_5			22.21	0.71	0.4504	0.013	0.42	2.220	0.064	0.3572	0.0085	0.39	2393	57	3190	31
	PH402_3_6			9.39	0.26	0.3379	0.0081	0.44	2.959	0.071	0.2008	0.0034	0.20	1876	39	2380	25
	PH402_3_7			14.82	0.49	0.3985	0.011	0.45	2.509	0.069	0.2688	0.0061	0.25	2159	52	2806	32
	PH402_3_8			10.45	0.37	0.3511	0.01	0.35	2.848	0.081	0.2151	0.0057	0.26	1940	48	2474	31
	PH402_3_9			8.48	0.24	0.3148	0.0078	0.28	3.177	0.079	0.1948	0.0036	0.30	1763	38	2281	27
	PH402_3_10			16.17	1	0.394	0.015	0.73	2.538	0.097	0.296	0.012	-0.27	2138	68	2881	61
	PH402_3_11			12.52	0.37	0.3661	0.0094	0.41	2.731	0.070	0.2468	0.0046	0.27	2009	44	2641	28
	PH402_3_12			10.41	0.35	0.348	0.0097	0.47	2.874	0.080	0.2151	0.0048	0.28	1934	46	2464	31
	PH402_3_13			12.42	0.39	0.3626	0.0098	0.53	2.758	0.075	0.2476	0.0045	0.24	1992	46	2636	30
	PH402_3_14			7.82	0.23	0.3369	0.009	0.54	2.968	0.079	0.1671	0.0031	0.27	1870	43	2206	27
	PH402_3_15			11.98	0.4	0.3786	0.01	0.51	2.641	0.070	0.2294	0.0049	0.14	2067	48	2602	31
	PH402_3_16			16.32	0.6	0.3825	0.012	0.23	2.614	0.082	0.3085	0.009	-0.07	2091	54	2881	35
	PH402_3_17			12.02	0.55	0.3771	0.011	0.57	2.652	0.077	0.2331	0.0072	-0.10	2073	55	2597	42
	PH402_3_18			11.45	0.44	0.3632	0.011	0.53	2.753	0.083	0.2297	0.006	0.12	1994	51	2556	36
	PH402_3_19			23.39	0.99	0.442	0.015	0.59	2.262	0.077	0.389	0.012	0.19	2357	66	3238	41
	PH402_3_20			10.5	0.31	0.3574	0.0089	0.42	2.798	0.070	0.2093	0.0038	0.28	1969	42	2479	27
	PH402_3_21			14.56	0.47	0.3918	0.011	0.39	2.552	0.072	0.2694	0.0064	0.32	2129	51	2786	30
	PH402_3_22			30.93	1	0.5056	0.014	0.35	1.978	0.055	0.448	0.012	0.36	2638	62	3511	33
	PH402_3_23			11.33	0.31	0.351	0.0085	0.38	2.849	0.069	0.237	0.0038	0.26	1938	41	2548	25
	PH402_3_24			10.54	0.3	0.3589	0.0087	0.44	2.786	0.068	0.214	0.0037	0.13	1978	42	2484	27
	PH402_3_25			10.65	0.31	0.3559	0.0089	0.34	2.810	0.070	0.218	0.0039	0.30	1962	42	2494	27
	PH402_3_26			11.04	0.34	0.3629	0.009	0.46	2.756	0.068	0.221	0.0044	0.14	1995	43	2521	29
	PH402_3_27			11.68	0.35	0.3582	0.0091	0.37	2.792	0.071	0.2378	0.0046	0.25	1974	43	2579	28
	PH402_3_28			10.56	0.33	0.342	0.0088	0.42	2.924	0.075	0.2241	0.0046	0.19	1897	42	2498	29
	PH402_3_29			13.09	0.36	0.3789	0.0094	0.23	2.639	0.065	0.2494	0.0042	0.49	2070	44	2684	26
	PH402_3_30			11.52	0.38	0.3499	0.0091	0.42	2.858	0.074	0.2383	0.0057	0.22	1933	43	2567	31
	PH402_3_31			8.67	0.3	0.3287	0.0085	0.71	3.042	0.079	0.1916	0.0038	-0.16	1831	41	2299	31
	PH402_3_32			8.14	0.23	0.3228	0.0079	0.48	3.098	0.076	0.1844	0.0031	0.14	1804	39	2245	25
	PH402_3_33			11.09	0.35	0.3474	0.0086	0.28	2.879	0.071	0.2306	0.005	-0.02	1923	42	2521	28

Table 6: Apatite Sample Data (2014 Dredge Sample Analytical Run)

Identification		Location		Geochronological Data													
Sample	Sample Reference	Latitude	Longitude	$^{207}Pb/^{235}U$	2σ	$^{206}Pb/^{238}U$	2σ	Error Correlation	$^{238}U/^{206}Pb$	2σ	$^{207}Pb/^{206}Pb$	2σ	Error Correlation	$^{206}Pb/^{238}U$ Age (Ma)	2σ	$^{207}Pb/^{235}U$ Age (Ma)	2σ
204-1	X204_2	54.22	-11.63	123.9	5	1.092	0.053	0.72	0.916	0.044	0.816	0.023	0.08	4760	170	4901	41
	PH402_3_34			8.25	0.22	0.3267	0.0077	0.28	3.061	0.072	0.1824	0.003	0.28	1822	38	2258	25
	PH402_3_35			12.56	0.37	0.3703	0.0092	0.53	2.701	0.067	0.245	0.0043	0.08	2030	43	2648	28
	PH402_3_36			9.8	0.31	0.3368	0.0086	0.64	2.969	0.076	0.2111	0.0042	-0.01	1870	41	2410	29
	PH402_3_37			14.18	0.46	0.379	0.01	0.56	2.639	0.070	0.2723	0.0058	0.07	2072	46	2760	30
	PH402_3_38			13.57	0.45	0.3861	0.01	0.71	2.590	0.067	0.2544	0.0046	-0.11	2106	48	2722	31
	PH402_3_39			14.76	0.48	0.3974	0.011	0.56	2.516	0.070	0.2686	0.0056	0.08	2157	48	2799	31
	PH402_3_40			14.7	1.3	0.388	0.016	0.93	2.58	0.11	0.261	0.014	-0.82	2117	77	2703	85
	PH402_3_41			12.36	0.46	0.3641	0.0094	0.63	2.746	0.071	0.2453	0.0061	-0.17	2000	45	2627	35
	PH402_3_42			11.09	0.37	0.3506	0.0092	0.50	2.852	0.075	0.2317	0.0054	0.13	1936	44	2525	31
	PH402_3_43			16.7	0.59	0.401	0.011	0.55	2.494	0.068	0.3026	0.0072	0.09	2174	52	2917	35
	PH402_3_44			9.73	0.27	0.3535	0.0084	0.35	2.829	0.067	0.1998	0.0033	0.25	1950	40	2414	26
402-4	X402_4_1	53.95	-12.79	14.8	1.4	0.268	0.015	0.40	3.73	0.21	0.382	0.031	0.10	1524	76	2777	93
	X402_4_2			8.14	0.52	0.2048	0.0095	0.35	4.88	0.23	0.28	0.017	0.13	1203	50	2243	64
	X402_4_3			27.6	2.8	0.376	0.028	0.26	2.66	0.20	0.513	0.052	0.34	2050	140	3390	110
	X402_4_4			6.13	0.43	0.2025	0.011	0.38	4.94	0.27	0.217	0.015	0.40	1191	60	1964	60
	X402_4_5			6	0.42	0.1931	0.009	0.27	5.18	0.24	0.22	0.015	0.24	1136	48	1960	59
	X402_4_6			16	1.4	0.268	0.017	0.32	3.73	0.24	0.423	0.035	0.34	1532	88	2875	84
	X402_4_7			9.7	0.67	0.2245	0.01	0.13	4.45	0.20	0.303	0.023	0.38	1303	54	2406	68
	X402_4_8			10.53	0.79	0.2263	0.012	0.30	4.42	0.23	0.343	0.027	0.29	1317	60	2494	69
	X402_4_9			11.74	0.86	0.2333	0.012	0.08	4.29	0.22	0.361	0.028	0.42	1354	61	2571	71
	X402_4_10			5.49	0.34	0.1897	0.0071	0.17	5.27	0.20	0.205	0.012	0.27	1119	39	1875	53
	X402_4_11			7.93	0.65	0.2116	0.0091	0.23	4.73	0.20	0.257	0.019	0.26	1244	46	2218	80
	X402_4_12			6.99	0.44	0.2068	0.008	0.32	4.84	0.19	0.236	0.014	0.17	1211	43	2114	55
	X402_4_13			13.14	0.92	0.2539	0.012	0.03	3.94	0.19	0.367	0.025	0.48	1461	63	2670	65
	X402_4_14			9.55	0.76	0.2305	0.012	0.31	4.34	0.23	0.294	0.021	0.18	1339	62	2371	78
	X402_4_15			18.7	1.7	0.296	0.015	-0.05	3.38	0.17	0.465	0.048	0.49	1668	76	3016	91
	X402_4_16			11.92	0.82	0.242	0.011	0.22	4.13	0.19	0.353	0.025	0.32	1394	57	2582	67
	X402_4_17			31.2	2.4	0.393	0.025	0.28	2.54	0.16	0.558	0.046	0.49	2120	110	3531	76
	X402_4_18			18.1	1.4	0.301	0.016	0.21	3.32	0.18	0.428	0.032	0.39	1690	78	2983	72
	X402_4_19			20.5	1.9	0.323	0.019	0.29	3.10	0.18	0.463	0.047	0.40	1806	90	3123	84
	X402_4_20			9.4	0.6	0.2234	0.0096	0.11	4.48	0.19	0.29	0.019	0.31	1298	51	2376	57
	X402_4_21			6.57	0.39	0.1977	0.0078	0.16	5.06	0.20	0.236	0.014	0.20	1165	43	2038	53
	X402_4_22			8.22	0.59	0.2106	0.0094	-0.03	4.75	0.21	0.285	0.023	0.43	1230	50	2254	64
	X402_4_23			11.48	0.87	0.2417	0.011	0.39	4.14	0.19	0.344	0.025	0.11	1393	58	2584	72
	X402_4_25			23.5	1.9	0.353	0.018	0.00	2.83	0.14	0.462	0.04	0.53	1940	87	3249	76
	X402_4_26			14.5	1.2	0.25	0.014	0.08	4.00	0.22	0.402	0.036	0.56	1435	75	2802	73
	X402_4_27			20.2	1.5	0.289	0.015	0.33	3.46	0.18	0.503	0.037	0.24	1639	74	3120	70
	X402_4_28			25.3	1.8	0.364	0.019	0.03	2.75	0.14	0.494	0.041	0.50	1993	90	3289	71
	X402_4_29			9.06	0.89	0.214	0.0094	0.08	4.67	0.21	0.302	0.03	0.27	1265	52	2342	90
	X402_4_30			11.71	0.74	0.2393	0.011	0.21	4.18	0.19	0.349	0.024	0.32	1380	55	2573	59
	X402_4_1			9.17	0.34	0.2201	0.0077	0.15	4.54	0.16	0.3	0.0058	0.37	1283	41	2351	34
	X402_4_2			10.74	0.4	0.2345	0.0083	0.13	4.26	0.15	0.3342	0.0063	0.50	1360	43	2502	35
	X402_4_3			38.85	1.5	0.459	0.017	0.40	2.18	0.08	0.621	0.012	0.44	2434	74	3743	38
	X402_4_4			52.8	2.1	0.568	0.022	0.42	1.76	0.07	0.669	0.016	0.47	2895	89	4047	40
	X402_4_5			19.58	0.77	0.3099	0.011	0.33	3.23	0.11	0.459	0.0099	0.39	1741	55	3065	38

Table 6: Apatite Sample Data (2014 Dredge Sample Analytical Run)																		
Identification		Location		Geochronological Data														
Sample	Sample Reference	Latitude	Longitude	$^{207}Pb/^{235}U$	2σ	$^{206}Pb/^{238}U$	2σ	Error Correlation	$^{238}U/^{206}Pb$	2σ	$^{207}Pb/^{206}Pb$	2σ	Error Correlation	$^{206}Pb/^{238}U$ Age (Ma)	2σ	$^{207}Pb/^{235}U$ Age (Ma)	2σ
204-1	X204_2	54.22	-11.63	123.9	5	1.092	0.053	0.72	0.916	0.044	0.816	0.023	0.08	4760	170	4901	41
	X402_4_6			31.21	1.2	0.3949	0.015	0.27	2.53	0.10	0.578	0.013	0.51	2149	68	3531	39
	X402_4_7			23.17	0.89	0.3303	0.013	0.41	3.03	0.12	0.51	0.012	0.59	1837	62	3236	37
	X402_4_8			8.25	0.3	0.2127	0.0074	0.33	4.70	0.16	0.2832	0.0046	0.26	1243	39	2257	34
	X402_4_9			31.29	1.2	0.3973	0.014	0.27	2.52	0.09	0.575	0.011	0.55	2154	67	3527	38
	X402_4_10			31.61	1.2	0.4041	0.015	0.21	2.47	0.09	0.569	0.013	0.52	2186	68	3541	39
	X402_4_11			13.93	0.52	0.2635	0.0093	0.11	3.80	0.13	0.3891	0.0076	0.56	1507	48	2748	35
	X402_4_12			8.81	0.32	0.2221	0.0077	0.36	4.50	0.16	0.2894	0.0042	0.33	1292	41	2318	34
	X402_4_13			18.55	0.71	0.3	0.011	0.29	3.33	0.12	0.4575	0.0095	0.48	1692	54	3014	38
	X402_4_14			16.05	0.59	0.2784	0.0098	0.09	3.59	0.13	0.4206	0.0086	0.52	1582	49	2876	35
	X402_4_15			8.75	0.32	0.2226	0.0078	0.13	4.49	0.16	0.285	0.0054	0.51	1295	41	2312	33
	X402_4_16			6.83	0.25	0.2058	0.0071	0.08	4.86	0.17	0.2403	0.0045	0.48	1206	38	2090	33
	X402_4_17			28.67	1.3	0.3762	0.015	0.67	2.66	0.11	0.552	0.013	0.20	2054	70	3431	44
	X402_4_18			15.46	0.66	0.2702	0.01	0.68	3.70	0.14	0.4162	0.0088	0.03	1540	52	2838	39
	X402_4_19			6.015	0.22	0.1982	0.0068	0.16	5.05	0.17	0.2218	0.0038	0.43	1166	37	1981	31
	X402_4_20			92.9	3.9	0.885	0.038	0.56	1.13	0.05	0.771	0.02	0.49	4082	130	4609	41
	X402_4_21			15.75	1.4	0.2754	0.016	0.53	3.63	0.21	0.409	0.011	0.12	1567	75	2856	56
	X402_4_22			14.21	0.65	0.2609	0.0097	0.63	3.83	0.14	0.3945	0.0099	-0.09	1493	49	2759	43
	X402_4_23			6.54	0.24	0.204	0.007	0.05	4.90	0.17	0.232	0.004	0.46	1197	37	2050	32
	X402_4_24			39.6	1.7	0.4636	0.018	0.40	2.16	0.08	0.614	0.016	0.42	2455	79	3756	42
	X402_4_25			27.8	1	0.3747	0.014	0.26	2.67	0.10	0.5466	0.0097	0.61	2049	64	3414	36
	X402_4_26			11.37	0.43	0.2391	0.0084	0.18	4.18	0.15	0.3481	0.007	0.48	1384	44	2558	35
	X402_4_27			10.56	0.39	0.2293	0.0079	0.22	4.36	0.15	0.3371	0.0056	0.42	1330	41	2487	34
	X402_4_28			10.67	0.41	0.2374	0.0083	0.20	4.21	0.15	0.3235	0.0066	0.38	1373	43	2495	35
	X402_4_29			8.52	0.31	0.2205	0.0077	0.16	4.54	0.16	0.2815	0.0047	0.46	1284	40	2287	33
	X402_4_30			9.91	0.36	0.2231	0.0078	0.26	4.48	0.16	0.3223	0.005	0.44	1299	41	2428	33
	X402_4_31			7.48	0.29	0.2049	0.0071	0.21	4.88	0.17	0.2644	0.0054	0.30	1201	38	2168	36
	X402_4_32			9.9	0.39	0.2224	0.0079	0.30	4.50	0.16	0.3227	0.007	0.33	1294	42	2428	36
	X402_4_33			26.55	1	0.3555	0.013	0.35	2.81	0.10	0.543	0.012	0.41	1962	61	3365	39
	X402_4_34			9.78	0.36	0.2238	0.0078	0.07	4.47	0.16	0.3135	0.0061	0.49	1301	41	2414	34
303-1	X303_1_1	54.07	-11.98	9.38	0.42	0.3308	0.016	0.05	3.02	0.15	0.2043	0.0097	0.26	1841	79	2381	40
	X303_1_2			14.27	0.49	0.3714	0.019	0.12	2.69	0.14	0.274	0.01	0.31	2038	86	2762	33
	X303_1_3			12.97	0.62	0.3577	0.019	0.02	2.80	0.15	0.262	0.014	0.40	1977	88	2681	44
	X303_1_4			8.41	0.27	0.3292	0.016	0.25	3.04	0.15	0.1825	0.0051	0.15	1834	79	2268	29
	X303_1_5			7.21	0.27	0.3268	0.016	0.16	3.06	0.15	0.1613	0.0057	0.11	1822	77	2131	34
	X303_1_6			9.69	0.46	0.3447	0.018	0.38	2.90	0.15	0.2048	0.0077	0.23	1907	88	2402	45
	X303_1_7			7.1	0.27	0.3241	0.017	0.40	3.09	0.16	0.1602	0.0053	0.28	1807	85	2116	33
	X303_1_8			32.2	1.7	0.503	0.029	0.35	1.99	0.11	0.458	0.024	0.26	2620	120	3545	50
	X303_1_9			9.83	0.36	0.3437	0.017	0.14	2.91	0.14	0.2068	0.0071	0.25	1903	82	2415	35
	X303_1_10			8.71	0.35	0.3396	0.017	0.29	2.94	0.15	0.1817	0.007	0.18	1887	84	2298	37
	X303_1_11			11.79	0.52	0.3606	0.018	0.25	2.77	0.14	0.241	0.01	0.17	1991	86	2602	39
	X303_1_12			14.44	0.54	0.3925	0.02	0.06	2.55	0.13	0.272	0.011	0.50	2137	89	2775	37
	X303_1_13			12.3	0.55	0.3584	0.018	0.36	2.79	0.14	0.252	0.01	0.04	1977	83	2626	44
	X303_1_14			10.52	0.44	0.3585	0.018	0.27	2.79	0.14	0.2145	0.0081	0.20	1973	87	2475	41
	X303_1_15			12.78	0.54	0.3724	0.019	0.15	2.69	0.14	0.242	0.01	0.25	2039	89	2662	41
	X303_1_16			10.15	0.43	0.3439	0.017	0.22	2.91	0.14	0.2167	0.0086	0.16	1904	81	2446	39

Table 6: Apatite Sample Data (2014 Dredge Sample Analytical Run)																	
Identification		Location		Geochronological Data													
Sample	Sample Reference	Latitude	Longitude	$^{207}Pb/^{235}U$	2σ	$^{206}Pb/^{238}U$	2σ	Error Correlation	$^{238}U/^{206}Pb$	2σ	$^{207}Pb/^{206}Pb$	2σ	Error Correlation	$^{206}Pb/^{238}U$ Age (Ma)	2σ	$^{207}Pb/^{235}U$ Age (Ma)	2σ
204-1	X204_2	54.22	-11.63	123.9	5	1.092	0.053	0.72	0.916	0.044	0.816	0.023	0.08	4760	170	4901	41
	X303_1_17			10.81	0.46	0.3575	0.018	0.30	2.80	0.14	0.2209	0.0088	0.09	1969	86	2501	37
	X303_1_18			13.74	0.52	0.3772	0.019	0.37	2.65	0.13	0.2696	0.0094	0.13	2062	89	2738	37
	X303_1_19			14.08	0.59	0.3768	0.02	0.23	2.65	0.14	0.269	0.011	0.26	2059	91	2764	40
	X303_1_20			16.93	0.84	0.4005	0.021	0.09	2.50	0.13	0.303	0.016	0.35	2186	94	2927	49
	X303_1_21			16.27	0.74	0.3877	0.02	0.16	2.58	0.13	0.299	0.014	0.32	2115	96	2873	45
	X303_1_22			13.27	0.49	0.3706	0.02	0.32	2.70	0.15	0.264	0.0096	0.23	2029	93	2695	37
	X303_1_23			21.17	0.85	0.4327	0.022	0.12	2.31	0.12	0.356	0.015	0.34	2316	99	3140	40
	X303_1_24			16.04	0.66	0.3842	0.02	0.31	2.60	0.14	0.296	0.011	0.19	2093	93	2863	40
	X303_1_25			16.68	0.93	0.3946	0.021	0.21	2.53	0.13	0.314	0.018	0.14	2147	93	2920	59
	X303_1_26			16	0.72	0.3915	0.021	0.28	2.55	0.14	0.293	0.013	0.23	2127	95	2865	42
	X303_1_27			39.6	1.5	0.556	0.032	0.07	1.80	0.10	0.511	0.025	0.61	2851	130	3748	39
	X303_1_28			12.25	0.53	0.3708	0.019	0.16	2.70	0.14	0.2439	0.0098	0.32	2031	90	2622	41
	X303_1_29			14.37	0.74	0.3747	0.02	-0.03	2.67	0.14	0.28	0.015	0.45	2049	93	2765	50
303-1 (2)	X303_1_1			17.76	0.51	0.4229	0.0096	0.55	2.365	0.054	0.303	0.0048	-0.13	2273	43	2975	19
	X303_1_2			10.69	0.24	0.3512	0.0077	0.06	2.847	0.062	0.2206	0.0021	0.49	1939.9	37	2496	8.5
	X303_1_3			19.37	0.48	0.417	0.0097	0.50	2.398	0.056	0.3391	0.0043	0.21	2247	44	3060	13
	X303_1_4			9.53	0.23	0.3221	0.0073	0.35	3.105	0.070	0.2155	0.0025	0.28	1800	35	2392	14
	X303_1_5			14.02	0.34	0.377	0.0084	0.35	2.653	0.059	0.2693	0.0034	0.22	2062	39	2750	12
	X303_1_6			12.09	0.27	0.3692	0.0082	0.36	2.709	0.060	0.2377	0.0023	0.45	2026	39	2611.5	8.7
	X303_1_7			10.56	0.24	0.3615	0.0081	0.34	2.766	0.062	0.2123	0.0021	0.42	1989	38	2484.9	9
	X303_1_8			13.64	0.38	0.3783	0.0084	0.48	2.643	0.059	0.259	0.0043	-0.09	2069	39	2721	18
	X303_1_9			9.113	0.21	0.3501	0.0077	0.30	2.856	0.063	0.189	0.0016	0.38	1934.7	37	2349.7	8
	X303_1_10			9.666	0.22	0.3489	0.0077	0.37	2.866	0.063	0.2014	0.0017	0.35	1929	37	2403	8.2
	X303_1_11			8.281	0.19	0.338	0.0075	0.29	2.959	0.066	0.1772	0.0017	0.43	1879	36	2262.1	7.4
	X303_1_12			8.755	0.2	0.3304	0.0074	0.21	3.027	0.068	0.1933	0.0021	0.45	1840	36	2314.8	9.7
	X303_1_13			25.76	0.61	0.4682	0.011	0.38	2.136	0.050	0.3974	0.0044	0.49	2475	48	3339	11
	X303_1_14			8.851	0.2	0.3463	0.0078	0.45	2.888	0.065	0.1844	0.0017	0.38	1917	37	2321.4	8.6
	X303_1_15			11.43	0.26	0.3659	0.0082	0.31	2.733	0.061	0.2274	0.0023	0.46	2010	39	2559.3	9.1
	X303_1_16			8.896	0.2	0.3457	0.0077	0.34	2.893	0.064	0.1871	0.0017	0.48	1914	37	2327	7.5
	X303_1_17			9.515	0.21	0.3528	0.0078	0.35	2.834	0.063	0.1955	0.0017	0.37	1948	37	2387.9	7.6
	X303_1_18			7.886	0.18	0.3412	0.0074	0.32	2.931	0.064	0.168	0.0015	0.32	1892.2	36	2217.6	7.9
	X303_1_19			7.949	0.18	0.3333	0.0075	0.32	3.000	0.068	0.1724	0.0017	0.39	1854	36	2225.4	8.9
	X303_1_20			11.5	0.27	0.3691	0.0083	0.43	2.709	0.061	0.2265	0.0023	0.40	2026	40	2564.8	9.5
	X303_1_21			16.75	0.39	0.4092	0.0094	0.32	2.444	0.056	0.2955	0.0034	0.46	2212	42	2921	10
	X303_1_22			10.4	0.26	0.3646	0.0084	0.63	2.743	0.063	0.206	0.0021	0.04	2003	39	2471	13
	X303_1_23			9.134	0.21	0.3443	0.0076	0.28	2.904	0.064	0.192	0.0019	0.39	1907	37	2351	8.6
	X303_1_25			16.33	0.41	0.3902	0.0088	0.46	2.563	0.058	0.3025	0.004	0.12	2123	41	2894	14
	X303_1_26			10.14	0.23	0.3546	0.008	0.32	2.820	0.064	0.2079	0.0022	0.44	1956	38	2446.8	9.5
	X303_1_27			49.85	1.3	0.645	0.016	0.52	1.550	0.038	0.5627	0.007	0.34	3206	61	3991	14
	X303_1_28			9.491	0.21	0.3492	0.0078	0.45	2.864	0.064	0.1965	0.0015	0.42	1930	37	2385.7	7.5
	X303_1_29			16.85	0.41	0.4013	0.0094	0.39	2.492	0.058	0.3055	0.0039	0.40	2174	43	2926	12
	X303_1_30			17.54	0.4	0.4198	0.0095	0.24	2.382	0.054	0.3044	0.0033	0.44	2260	43	2966.4	9.1
	X303_1_31			14.18	0.32	0.3751	0.0083	0.19	2.666	0.059	0.2745	0.003	0.45	2054	39	2760.4	9.1
	X303_1_32			15.34	0.35	0.3939	0.0088	0.30	2.539	0.057	0.2824	0.0028	0.49	2142	41	2836.2	9
	X303_1_33			13.35	0.31	0.3771	0.0085	0.48	2.652	0.060	0.2576	0.0024	0.31	2062	40	2706	10

Table 6: Apatite Sample Data (2014 Dredge Sample Analytical Run)

Identification		Location		Geochronological Data													
Sample	Sample Reference	Latitude	Longitude	$^{207}Pb/^{235}U$	2σ	$^{206}Pb/^{238}U$	2σ	Error Correlation	$^{238}U/^{206}Pb$	2σ	$^{207}Pb/^{206}Pb$	2σ	Error Correlation	$^{206}Pb/^{238}U$ Age (Ma)	2σ	$^{207}Pb/^{235}U$ Age (Ma)	2σ
204-1	X204_2	54.22	-11.63	123.9	5	1.092	0.053	0.72	0.916	0.044	0.816	0.023	0.08	4760	170	4901	41
	X303_1_34			10.65	0.25	0.3618	0.0082	0.46	2.764	0.063	0.2126	0.0021	0.33	1990	39	2493.4	9.7
402-8	X402_8_1	53.95	-12.79	11.59	0.73	0.3686	0.0065	0.23	2.713	0.046	0.229	0.013	0.13	2022	31	2557	61
	X402_8_2			13.89	0.74	0.3664	0.0093	0.03	2.729	0.071	0.276	0.016	0.33	2009	44	2753	49
	X402_8_3			8.73	0.49	0.3569	0.0054	0.16	2.802	0.043	0.1798	0.0087	0.25	1966	26	2299	52
	X402_8_4			10.92	0.69	0.3468	0.0077	0.24	2.884	0.063	0.231	0.014	0.11	1917	37	2502	61
	X402_8_5			10.6	0.67	0.3563	0.0076	0.08	2.807	0.061	0.214	0.015	0.15	1967	37	2481	60
	X402_8_6			12.06	0.68	0.3724	0.0084	0.04	2.685	0.059	0.237	0.013	0.39	2038	39	2609	51
	X402_8_7			15.1	1	0.395	0.012	0.32	2.532	0.073	0.28	0.017	0.25	2140	53	2804	65
	X402_8_8			8.98	0.44	0.3619	0.0063	0.03	2.763	0.051	0.183	0.0082	0.39	1990	30	2340	46
	X402_8_9			9.65	0.48	0.3535	0.0071	0.35	2.829	0.054	0.1974	0.0093	0.08	1949	34	2392	46
	X402_8_11			9.21	0.45	0.3504	0.0055	0.25	2.854	0.044	0.1876	0.0072	0.23	1935	26	2355	44
	X402_8_12			12.29	0.71	0.3788	0.0081	0.19	2.640	0.056	0.237	0.013	0.28	2073	38	2616	56
	X402_8_13			12.38	0.79	0.3723	0.0099	0.04	2.686	0.070	0.253	0.017	0.32	2048	45	2636	59
	X402_8_14			10.34	0.63	0.3527	0.0084	0.08	2.835	0.069	0.214	0.013	0.31	1945	40	2464	56
	X402_8_15			11.78	0.83	0.372	0.0089	0.21	2.688	0.066	0.23	0.015	0.22	2041	41	2566	66
	X402_8_16			13.89	0.79	0.3932	0.0091	0.09	2.543	0.058	0.264	0.014	0.33	2135	42	2727	57
	X402_8_17			11.1	0.64	0.3652	0.0093	0.24	2.738	0.068	0.218	0.012	0.32	2014	43	2515	53
	X402_8_18			10.2	0.52	0.3641	0.0095	0.34	2.746	0.072	0.2	0.01	0.18	1999	45	2441	48
	X402_8_19			13.85	0.88	0.385	0.014	0.30	2.597	0.093	0.261	0.015	0.35	2092	64	2734	58
	X402_8_20			13.09	0.9	0.388	0.013	0.37	2.577	0.089	0.25	0.018	0.01	2108	60	2660	66
	X402_8_21			13.02	0.97	0.386	0.015	0.34	2.59	0.10	0.251	0.017	0.20	2097	69	2650	72
	X402_8_22			20.2	1.5	0.415	0.013	0.13	2.410	0.080	0.359	0.025	0.34	2241	62	3108	68
	X402_8_23			10.98	0.52	0.364	0.01	0.06	2.747	0.080	0.224	0.01	0.46	1998	49	2523	43
	X402_8_24			16.5	1	0.425	0.016	0.29	2.353	0.094	0.293	0.019	0.13	2274	73	2885	63
	X402_8_25			13.06	0.8	0.374	0.01	0.07	2.674	0.077	0.255	0.017	0.46	2052	49	2679	60
	X402_8_26			11.33	0.76	0.382	0.011	0.19	2.618	0.073	0.218	0.013	0.16	2082	49	2541	66
	X402_8_27			12.67	0.76	0.3904	0.009	0.19	2.561	0.058	0.234	0.013	0.27	2122	42	2660	57
	X402_8_28			16.4	1	0.391	0.012	0.20	2.558	0.083	0.304	0.02	0.31	2121	57	2897	58
	X402_8_29			9.22	0.55	0.3531	0.0089	0.26	2.832	0.068	0.1852	0.0096	0.19	1946	42	2351	55
402-8 (2)	X402_8_1			14.76	0.19	0.3945	0.0038	0.13	2.535	0.025	0.2724	0.0041	0.54	2143	63	2798	13
	X402_8_2			7.668	0.09	0.3351	0.0027	0.35	2.984	0.023	0.1668	0.0018	0.30	1864	55	2195	11
	X402_8_3			11.07	0.15	0.3662	0.0029	0.38	2.731	0.022	0.2182	0.0029	0.24	2011	59	2529	13
	X402_8_4			30.99	0.68	0.4875	0.0079	0.24	2.051	0.034	0.46	0.01	0.48	2557	78	3514	22
	X402_8_5			20.2	0.4	0.4148	0.006	0.38	2.411	0.035	0.3543	0.0068	0.36	2240	68	3110	19
	X402_8_6			6.964	0.066	0.3237	0.002	0.17	3.089	0.019	0.1552	0.0017	0.39	1807.4	53	2105.7	8.4
	X402_8_7			7.453	0.083	0.3321	0.0022	0.33	3.011	0.020	0.1628	0.0018	0.29	1848	54	2166	10
	X402_8_8			10.36	0.14	0.3623	0.003	0.20	2.760	0.022	0.2069	0.0032	0.38	1992	59	2464	13
	X402_8_9			6.303	0.075	0.3217	0.002	0.20	3.108	0.020	0.1418	0.0017	0.21	1797.6	53	2017	10
	X402_8_10			8.1	0.11	0.3341	0.0025	0.17	2.993	0.023	0.1736	0.0024	0.38	1859	55	2239	13
	X402_8_11			23.85	0.79	0.453	0.01	0.88	2.208	0.045	0.3791	0.0084	-0.13	2404	77	3246	30
	X402_8_12			5.66	0.089	0.3038	0.0033	0.05	3.292	0.036	0.1354	0.0027	0.50	1710	50	1930	14
	X402_8_13			7.697	0.07	0.3411	0.002	0.26	2.932	0.016	0.1639	0.0016	0.34	1891.5	55	2195.8	8.3
	X402_8_14			6.574	0.063	0.329	0.0022	0.33	3.040	0.021	0.1444	0.0013	0.40	1833	54	2054.6	8.4
	X402_8_15			14.76	0.25	0.3823	0.0042	0.26	2.616	0.028	0.2801	0.0051	0.39	2088	63	2800	16
	X402_8_16			7.37	0.089	0.3233	0.0023	0.26	3.093	0.023	0.1648	0.0021	0.33	1806	53	2157	11

Table 6: Apatite Sample Data (2014 Dredge Sample Analytical Run)

Identification		Location		Geochronological Data													
Sample	Sample Reference	Latitude	Longitude	$^{207}Pb/^{235}U$	2σ	$^{206}Pb/^{238}U$	2σ	Error Correlation	$^{238}U/^{206}Pb$	2σ	$^{207}Pb/^{206}Pb$	2σ	Error Correlation	$^{206}Pb/^{238}U$ Age (Ma)	2σ	$^{207}Pb/^{235}U$ Age (Ma)	2σ
204-1	X204_2	54.22	-11.63	123.9	5	1.092	0.053	0.72	0.916	0.044	0.816	0.023	0.08	4760	170	4901	41
	X402_8_17			8.34	0.12	0.3371	0.0026	0.28	2.966	0.022	0.1795	0.0025	0.28	1872	55	2267	13
	X402_8_18			8.329	0.096	0.3532	0.0024	0.34	2.831	0.019	0.17	0.0019	0.27	1949	57	2268	10
	X402_8_19			11.48	0.21	0.3669	0.004	0.32	2.726	0.030	0.2261	0.004	0.29	2016	61	2561	17
	X402_8_20			7.69	0.1	0.3321	0.0028	0.19	3.011	0.025	0.1677	0.0021	0.44	1848	55	2196	12
	X402_8_21			8.03	0.11	0.3455	0.0026	0.34	2.894	0.022	0.1694	0.0021	0.21	1913	56	2234	13
	X402_8_22			7.006	0.084	0.3287	0.0022	0.21	3.042	0.021	0.1546	0.0019	0.35	1832	54	2113	10
	X402_8_23			6.974	0.07	0.3309	0.0023	0.18	3.022	0.021	0.1524	0.0016	0.45	1844	54	2108.3	8.9
	X402_8_24			7.733	0.09	0.3371	0.0022	0.43	2.966	0.020	0.1667	0.0018	0.15	1873	55	2200	11
	X402_8_25			32.75	0.68	0.5096	0.0085	0.56	1.962	0.034	0.4675	0.0085	0.34	2665	82	3569	21
	X402_8_26			8.233	0.087	0.3469	0.0025	0.32	2.883	0.020	0.1711	0.0018	0.33	1919	57	2256.2	9.7
	X402_8_27			9.08	0.12	0.3483	0.0026	0.18	2.871	0.021	0.1898	0.0026	0.37	1926	56	2346	12
	X402_8_28			7.518	0.092	0.3286	0.0022	0.34	3.043	0.021	0.1645	0.0019	0.19	1831	54	2174	11
	X402_8_29			7.713	0.086	0.3311	0.0023	0.41	3.020	0.021	0.1684	0.0018	0.24	1843	54	2196	10
	X402_8_30			8.321	0.098	0.3586	0.0026	0.40	2.789	0.021	0.169	0.0019	0.25	1975	57	2268	11
	X402_8_31			6.834	0.067	0.3328	0.0021	0.33	3.005	0.019	0.1491	0.0014	0.35	1852	54	2091.9	8.7
	X402_8_32			8.209	0.083	0.3338	0.002	0.25	2.996	0.018	0.1777	0.002	0.34	1856.5	54	2252.9	9.2
	X402_8_33			15.97	0.27	0.3855	0.005	0.17	2.594	0.033	0.2989	0.0054	0.51	2103	64	2878	16
	X402_8_34			9.72	0.11	0.3563	0.0025	0.20	2.807	0.020	0.1969	0.0024	0.39	1964	57	2408	10
	X402_8_35			9.41	0.15	0.3456	0.0029	0.11	2.894	0.024	0.1975	0.0034	0.42	1913	56	2379	14
402-9	X402_9_1	53.95	-12.79	8.25	0.59	0.2178	0.0084	0.47	4.59	0.18	0.282	0.015	0.19	1267	44	2233	65
	X402_9_2			8.55	0.41	0.2266	0.0066	0.18	4.41	0.13	0.266	0.016	0.30	1320	34	2286	45
	X402_9_3			11.72	0.67	0.2451	0.0068	0.30	4.08	0.11	0.339	0.018	0.20	1420	35	2553	56
	X402_9_4			8.96	0.42	0.2227	0.0056	0.10	4.49	0.11	0.289	0.014	0.38	1295	29	2334	41
	X402_9_5			14.2	1.1	0.2629	0.009	0.11	3.80	0.14	0.395	0.032	0.47	1501	46	2734	74
	X402_9_6			19	1.6	0.304	0.014	0.47	3.29	0.15	0.443	0.029	0.18	1703	68	3014	82
	X402_9_7			11.34	0.62	0.2395	0.0078	0.15	4.18	0.14	0.36	0.022	0.40	1382	41	2558	53
	X402_9_8			11.37	0.7	0.2483	0.0073	0.32	4.03	0.13	0.331	0.019	0.27	1427	38	2546	58
	X402_9_9			5.84	0.29	0.1952	0.0041	-0.01	5.12	0.11	0.214	0.012	0.36	1149	22	1945	43
	X402_9_10			8.03	0.4	0.2192	0.0049	-0.11	4.56	0.1	0.26	0.014	0.43	1283	26	2238	43
	X402_9_11			17.1	1.2	0.278	0.01	0.13	3.60	0.13	0.432	0.03	0.37	1582	54	2916	66
	X402_9_12			7.19	0.44	0.2036	0.0054	0.12	4.91	0.13	0.256	0.016	0.31	1193	29	2144	55
	X402_9_13			7.49	0.34	0.2174	0.0051	0.15	4.60	0.11	0.244	0.012	0.42	1267	27	2161	41
	X402_9_14			8.19	0.52	0.2184	0.0044	0.03	4.58	0.087	0.267	0.017	0.29	1272	23	2225	60
	X402_9_15			7.08	0.45	0.2118	0.0039	-0.03	4.72	0.085	0.234	0.016	0.28	1240	20	2113	57
	X402_9_16			10.01	0.6	0.2391	0.0069	0.15	4.18	0.12	0.302	0.017	0.35	1380	36	2433	55
	X402_9_17			6.42	0.41	0.206	0.0041	0.33	4.85	0.1	0.224	0.013	0.19	1207	22	2032	54
	X402_9_18			6.79	0.42	0.2138	0.004	-0.05	4.68	0.09	0.23	0.014	0.38	1248	21	2087	55
	X402_9_19			7.31	0.48	0.2098	0.0045	0.28	4.77	0.097	0.252	0.015	0.17	1230	23	2144	61
	X402_9_20			6.01	0.36	0.2045	0.0043	0.32	4.89	0.1	0.21	0.011	0.14	1199	23	1968	53
	X402_9_21			8.79	0.53	0.221	0.0054	-0.01	4.52	0.11	0.282	0.02	0.45	1286	29	2321	57
	X402_9_22			8.73	0.51	0.2196	0.0055	0.03	4.55	0.11	0.282	0.015	0.37	1279	29	2295	55
	X402_9_23			6.36	0.4	0.2081	0.0039	0.22	4.81	0.093	0.22	0.012	0.21	1218	21	2032	54
	X402_9_24			6.53	0.39	0.2051	0.0041	0.11	4.88	0.1	0.224	0.012	0.33	1202	22	2039	51
	X402_9_25			9.24	0.59	0.2344	0.008	0.28	4.27	0.15	0.282	0.016	0.32	1355	42	2340	62
	X402_9_26			8.59	0.43	0.2205	0.0062	0.27	4.54	0.11	0.274	0.015	0.15	1287	32	2297	46

Table 6: Apatite Sample Data (2014 Dredge Sample Analytical Run)

Identification		Location		Geochronological Data													
Sample	Sample Reference	Latitude	Longitude	$^{207}Pb/^{235}U$	2σ	$^{206}Pb/^{238}U$	2σ	Error Correlation	$^{238}U/^{206}Pb$	2σ	$^{207}Pb/^{206}Pb$	2σ	Error Correlation	$^{206}Pb/^{238}U$ Age (Ma)	2σ	$^{207}Pb/^{235}U$ Age (Ma)	2σ
204-1	X204_2	54.22	-11.63	123.9	5	1.092	0.053	0.72	0.916	0.044	0.816	0.023	0.08	4760	170	4901	41
	X402_9_27			7.78	0.47	0.2248	0.0053	0.04	4.45	0.11	0.246	0.015	0.46	1306	28	2196	54
	X402_9_28			6.17	0.36	0.2124	0.0051	0.26	4.71	0.11	0.211	0.01	0.35	1244	28	1998	51
	X402_9_29			6.43	0.39	0.2086	0.0056	0.23	4.79	0.13	0.228	0.014	0.21	1220	30	2017	52
	X402_9_30			8.8	0.6	0.2264	0.0061	0.04	4.42	0.12	0.283	0.021	0.42	1314	32	2311	62
402-9 (2)	X402_9_1			15.57	0.26	0.2796	0.0033	0.20	3.577	0.042	0.4062	0.0082	0.46	1590	49	2853	36
	X402_9_2			11.23	0.16	0.2513	0.0023	0.29	3.979	0.037	0.325	0.0049	0.36	1445	44	2543	34
	X402_9_3			19.36	0.32	0.3257	0.0036	0.33	3.070	0.032	0.432	0.0074	0.39	1818	55	3063	37
	X402_9_4			12.81	0.33	0.2422	0.0043	0.40	4.129	0.074	0.3868	0.0089	0.28	1397	43	2667	35
	X402_9_5			6.804	0.085	0.2097	0.0016	0.18	4.769	0.037	0.2357	0.0032	0.42	1226.8	38	2084	31
	X402_9_6			28.72	0.56	0.393	0.0065	0.45	2.545	0.043	0.5339	0.0099	0.45	2134	67	3442	37
	X402_9_7			18.55	0.36	0.3133	0.0039	0.11	3.192	0.039	0.4289	0.0085	0.29	1756	54	3010	36
	X402_9_8			6.63	0.1	0.2108	0.0015	0.24	4.744	0.034	0.227	0.0035	0.28	1233.1	38	2061	32
	X402_9_9			8.4	0.14	0.2195	0.0024	0.41	4.556	0.051	0.2761	0.0041	0.32	1279	40	2274	34
	X402_9_10			3.313	0.034	0.1814	0.00087	0.11	5.513	0.027	0.1324	0.0015	0.34	1074.5	33	1483	27
	X402_9_11			7.26	0.11	0.2071	0.0021	0.23	4.829	0.048	0.2517	0.0039	0.39	1213	38	2147	31
	X402_9_12			3.365	0.039	0.1794	0.0011	0.34	5.574	0.034	0.1359	0.0016	0.17	1063.7	33	1499.2	28
	X402_9_13			4.184	0.098	0.1769	0.0012	0.38	5.653	0.04	0.1708	0.0037	-0.08	1049.9	33	1668	34
	X402_9_14			8.96	0.19	0.222	0.0024	0.28	4.505	0.049	0.2918	0.0058	0.27	1292	41	2330	35
	X402_9_15			15.81	0.49	0.2657	0.0045	0.13	3.764	0.061	0.428	0.015	0.41	1518	47	2861	36
	X402_9_16			13.66	0.17	0.2568	0.0027	0.20	3.894	0.042	0.3881	0.0062	0.58	1473	46	2726	33
	X402_9_17			17.74	0.24	0.2988	0.0029	0.24	3.347	0.032	0.4262	0.0062	0.45	1685	51	2975	35
	X402_9_18			18.75	0.51	0.3211	0.0061	0.72	3.114	0.059	0.4177	0.0075	0.05	1792	59	3023	42
	X402_9_19			10.77	0.17	0.2488	0.0024	0.33	4.019	0.039	0.3158	0.0048	0.29	1432	44	2503	35
	X402_9_20			8.68	0.13	0.2183	0.0023	0.29	4.581	0.048	0.2901	0.0045	0.40	1272	40	2304	33
	X402_9_21			3.931	0.058	0.1823	0.0012	0.03	5.485	0.035	0.156	0.0023	0.11	1079.9	34	1618	29
	X402_9_22			101.9	2.8	0.982	0.023	0.69	1.018	0.024	0.746	0.015	0.30	4417	130	4701	42
	X402_9_23			5.448	0.07	0.1979	0.0015	0.28	5.053	0.039	0.1997	0.0026	0.29	1163.6	36	1891	31
	X402_9_24			6.194	0.086	0.2018	0.0015	0.15	4.955	0.037	0.2201	0.0033	0.37	1184.8	37	2001	31
	X402_9_25			3.597	0.054	0.1809	0.0012	0.30	5.528	0.036	0.1445	0.0021	0.18	1071.5	33	1548	29
	X402_9_26			4.181	0.055	0.1769	0.0013	0.32	5.653	0.043	0.1725	0.0021	0.27	1049.9	33	1671	30
	X402_9_27			5.081	0.072	0.1908	0.0014	0.23	5.241	0.037	0.1917	0.0027	0.31	1125.6	35	1831	31
	X402_9_28			7.02	0.1	0.2084	0.0017	0.30	4.798	0.041	0.2452	0.0036	0.30	1221	38	2112	33
	X402_9_29			15.07	0.33	0.2835	0.0039	0.45	3.527	0.049	0.3864	0.0072	0.21	1609	51	2818	38
	X402_9_30			5.77	0.11	0.1956	0.0016	0.33	5.112	0.042	0.2149	0.0038	0.10	1151.5	36	1942	33
	X402_9_31			9.01	0.12	0.2273	0.0022	0.18	4.399	0.044	0.2872	0.0046	0.46	1321	42	2340	32
	X402_9_32			5.732	0.072	0.1995	0.0016	0.33	5.013	0.04	0.2091	0.0027	0.28	1172.2	37	1937	32
	X402_9_33			21.98	0.43	0.3347	0.0046	0.38	2.988	0.041	0.4772	0.0089	0.41	1864	58	3181	37
	X402_9_34			5.004	0.085	0.1858	0.0015	0.34	5.382	0.045	0.1954	0.0031	0.14	1099.1	35	1819	31
	X402_9_35			3.498	0.045	0.1826	0.0011	0.47	5.476	0.032	0.1388	0.0014	-0.03	1081.8	34	1527	28
402-11	X402_11_1	53.95	-12.79	23.9	1.1	0.4325	0.01	0.34	2.3	0.1	0.391	0.017	0.09	2314	43	3268	43
	X402_11_2			11.83	0.42	0.37	0.01	0.41	2.7	0.1	0.23	0.0069	0.24	2023	32	2584	35
	X402_11_3			11.83	0.72	0.36	0.01	0.74	2.8	0.1	0.238	0.011	-0.16	1992	53	2574	57
	X402_11_4			16.74	0.67	0.39	0.01	0.21	2.5	0.1	0.308	0.013	0.22	2140	37	2915	39
	X402_11_5			14.36	0.67	0.38	0.01	0.36	2.7	0.1	0.276	0.012	0.32	2056	44	2778	45
	X402_11_6			18.1	1.3	0.42	0.02	0.66	2.4	0.1	0.323	0.021	-0.27	2249	70	3008	73

Table 6: Apatite Sample Data (2014 Dredge Sample Analytical Run)

Identification		Location		Geochronological Data														
Sample	Sample Reference	Latitude	Longitude	$^{207}Pb/^{235}U$	2σ	$^{206}Pb/^{238}U$	2σ	Error Correlation	$^{238}U/^{206}Pb$	2σ	$^{207}Pb/^{206}Pb$	2σ	Error Correlation	$^{206}Pb/^{238}U$ Age (Ma)	2σ	$^{207}Pb/^{235}U$ Age (Ma)	2σ
204-1	X204_2	54.22	-11.63	123.9	5	1.092	0.053	0.72	0.916	0.044	0.816	0.023	0.08	4760	170	4901	41
	X402_11_8			13.6	0.67	0.37	0.01	0.40	2.7	0.0	0.2615	0.0097	0.06	2022	28	2722	47
	X402_11_10			13.67	0.7	0.39	0.01	0.33	2.6	0.1	0.256	0.011	0.31	2100	38	2722	47
	X402_11_11			12.36	0.52	0.37	0.01	0.30	2.7	0.0	0.2409	0.009	0.40	2018	36	2616	41
	X402_11_12			12.61	0.39	0.37	0.01	0.16	2.7	0.1	0.2470	0.0087	0.33	2025	33	2658	28
	X402_11_15			15.46	0.67	0.38	0.01	0.30	2.6	0.1	0.291	0.011	0.22	2085	39	2859	41
	X402_11_16			17.62	0.87	0.39	0.01	0.21	2.6	0.1	0.322	0.015	0.42	2135	46	2971	48
	X402_11_17			28.7	1.3	0.470	0.013	0.16	2.1	0.1	0.438	0.018	0.42	2477	56	3439	46
	X402_11_18			15.66	0.77	0.40	0.01	0.25	2.5	0.1	0.283	0.012	0.40	2172	43	2848	47
	X402_11_19			20.67	0.98	0.43	0.01	0.22	2.3	0.1	0.344	0.014	0.37	2289	40	3127	44
	X402_11_20			25.7	1.3	0.46	0.01	0.30	2.2	0.1	0.398	0.019	0.38	2434	61	3315	50
	X402_11_21			11.79	0.75	0.35	0.01	0.58	2.8	0.1	0.24	0.01	0.00	1951	43	2581	59
	X402_11_22			16.18	0.88	0.38	0.01	0.34	2.6	0.1	0.306	0.015	0.19	2082	42	2880	51
	X402_11_23			21.14	0.99	0.43	0.01	0.43	2.4	0.1	0.36	0.015	0.33	2286	46	3139	45
	X402_11_24			13.2	0.67	0.38	0.01	0.61	2.7	0.1	0.2375	0.0093	-0.08	2059	47	2668	53
	X402_11_25			29.5	1.6	0.46	0.02	0.49	2.2	0.1	0.451	0.019	0.26	2424	67	3443	53
	X402_11_26			21.6	1.2	0.43	0.01	0.45	2.3	0.1	0.366	0.017	0.07	2286	54	3166	56
	X402_11_27			9.99	0.44	0.34	0.01	0.31	2.9	0.1	0.2105	0.0078	0.16	1906	35	2432	42
	X402_11_28			15.38	0.75	0.39	0.01	0.28	2.5	0.1	0.280	0.011	0.25	2134	46	2823	46
	X402_11_30			30.4	1.9	0.49	0.02	0.45	2.0	0.1	0.438	0.02	0.03	2570	66	3471	58
402-11 (2)	X402_11_1			16.58	0.18	0.4016	0.0029	0.43	2.490	0.018	0.2976	0.003	0.30	2179	64	2912.1	32
	X402_11_2			21.01	0.38	0.4363	0.0046	0.63	2.292	0.025	0.3447	0.0054	-0.13	2333	68	3135	38
	X402_11_3			15.13	0.22	0.3814	0.0033	0.57	2.622	0.023	0.2884	0.0035	-0.01	2082	61	2822	35
	X402_11_4			12.17	0.19	0.3614	0.0025	0.48	2.767	0.019	0.2441	0.0032	0.02	1988	58	2615	34
	X402_11_5			18.29	0.58	0.3922	0.0057	0.73	2.550	0.04	0.3345	0.0081	-0.36	2134	67	2993	45
	X402_11_6			11.76	0.21	0.3551	0.003	0.67	2.816	0.024	0.2397	0.0037	-0.30	1958	58	2581	36
	X402_11_7			28.56	0.4	0.472	0.0045	0.34	2.119	0.021	0.4364	0.006	0.33	2491	71	3436	36
	X402_11_8			18.33	0.39	0.404	0.0042	0.60	2.475	0.026	0.3267	0.0056	-0.19	2188	64	3010	37
	X402_11_9			12.36	0.21	0.3558	0.0027	0.65	2.811	0.022	0.249	0.0035	-0.29	1962	57	2631	35
	X402_11_10			22.88	0.41	0.4234	0.0043	0.60	2.362	0.024	0.3917	0.0056	-0.09	2275	66	3218	37
	X402_11_11			19.87	0.88	0.4178	0.006	0.76	2.393	0.034	0.339	0.011	-0.53	2251	69	3062	54
	X402_11_12			30.78	0.77	0.4829	0.0081	0.43	2.071	0.036	0.465	0.012	0.33	2545	79	3509	56
	X402_11_13			14.69	0.48	0.3734	0.0055	0.72	2.678	0.04	0.281	0.0065	-0.32	2046	63	2794	44
	X402_11_14			17.35	0.25	0.4159	0.0033	0.21	2.404	0.019	0.3025	0.0042	0.13	2241	64	2952	34
	X402_11_15			41.81	0.93	0.5484	0.0084	0.74	1.823	0.028	0.5468	0.0085	-0.15	2818	83	3807	41
	X402_11_16			15.85	0.21	0.3847	0.0031	0.50	2.599	0.021	0.2972	0.0036	0.09	2098	61	2867	34
	X402_11_17			13.24	0.2	0.3689	0.0029	0.66	2.711	0.022	0.2608	0.0029	-0.11	2024	59	2698	35
	X402_11_18			14.99	0.18	0.3584	0.0024	0.37	2.790	0.019	0.303	0.0035	0.23	1974	57	2813	34
	X402_11_19			16.42	0.31	0.3949	0.0042	0.64	2.532	0.026	0.3001	0.0046	-0.14	2145	64	2898	37
	X402_11_20			31.49	0.34	0.4914	0.0042	0.35	2.035	0.019	0.4592	0.0054	0.43	2580	75	3535	33
	X402_11_21			39.3	1.4	0.537	0.015	0.84	1.862	0.051	0.537	0.01	-0.07	2771	97	3748	50
	X402_11_22			24.59	0.68	0.4457	0.005	0.70	2.244	0.025	0.3953	0.0084	-0.37	2377	69	3283	43
	X402_11_23			13.37	0.3	0.3901	0.0046	0.69	2.563	0.031	0.2454	0.0038	-0.14	2122	63	2700	37
	X402_11_24			20.67	0.31	0.4241	0.0039	0.53	2.358	0.022	0.3514	0.0046	0.09	2278	66	3121	36
	X402_11_25			12.72	0.18	0.3736	0.0033	0.51	2.677	0.024	0.2475	0.0031	0.20	2046	60	2658	34
	X402_11_26			17.27	0.31	0.4087	0.0053	0.70	2.447	0.033	0.307	0.004	-0.04	2207	67	2946	37

Table 6: Apatite Sample Data (2014 Dredge Sample Analytical Run)

Identification		Location		Geochronological Data														
Sample	Sample Reference	Latitude	Longitude	$^{207}Pb/^{235}U$	2σ	$^{206}Pb/^{238}U$	2σ	Error Correlation	$^{238}U/^{206}Pb$	2σ	$^{207}Pb/^{206}Pb$	2σ	Error Correlation	$^{206}Pb/^{238}U$ Age (Ma)	2σ	$^{207}Pb/^{235}U$ Age (Ma)	2σ
204-1	X204_2	54.22	-11.63	123.9	5	1.092	0.053	0.72	0.916	0.044	0.816	0.023	0.08	4760	170	4901	41
	X402_11_27			27.35	0.34	0.4689	0.0045	0.40	2.133	0.021	0.4241	0.0053	0.41	2477	71	3399	34
	X402_11_29			15.79	0.36	0.4048	0.0034	0.56	2.470	0.021	0.2831	0.0053	-0.19	2191	64	2867	39
	X402_11_30			45.1	1.2	0.5878	0.0096	0.82	1.701	0.027	0.5513	0.0087	-0.34	2980	88	3887	42
	X402_11_31			42.12	0.6	0.5854	0.0072	0.45	1.708	0.021	0.5172	0.0071	0.41	2968	84	3822	35
	X402_11_32			14.53	0.22	0.3955	0.0032	0.61	2.528	0.021	0.2664	0.0032	-0.05	2149	62	2782	34
	X402_11_33			11.96	0.13	0.3757	0.0026	0.43	2.662	0.019	0.2311	0.0023	0.30	2057	60	2603	34
	X402_11_34			13.06	0.31	0.3647	0.0036	0.56	2.742	0.028	0.2587	0.0049	-0.16	2004	60	2677	38
	X402_11_35			19.98	0.23	0.415	0.0029	0.24	2.410	0.017	0.3478	0.0043	0.33	2237	64	3091	35
402-13	X402_13_1	53.95	-12.79	2640	470	19.5	3.7	0.89	0.051	0.0076	0.976	0.048	0.17	17470	620	7680	100
	X402_13_2			298	65	1.95	0.28	0.94	0.513	0.051	0.914	0.044	-0.22	6600	470	5500	140
	X402_13_3			154.8	8.3	1.109	0.046	0.65	0.902	0.039	0.942	0.048	0.20	4780	140	5114	54
	X402_13_4			299	23	2.32	0.13	0.68	0.431	0.025	0.894	0.039	0.24	7670	260	5776	77
	X402_13_5			520	29	3.81	0.2	0.55	0.262	0.013	0.984	0.041	0.43	10070	270	6324	56
	X402_13_6			2710	400	19	2.7	1.0	0.053	0.0058	0.978	0.054	0.09	18260	590	7880	110
	X402_13_7			4570	740	32.4	4.8	0.94	0.031	0.0058	0.995	0.044	0.13	21320	880	8340	150
	X402_13_8			111.6	6.6	1.021	0.042	0.40	0.979	0.04	0.774	0.042	0.29	4510	130	4783	62
	X402_13_9			59.2	3.2	0.659	0.02	0.33	1.517	0.047	0.649	0.035	0.32	3265	77	4167	54
	X402_13_10			63.3	3.1	0.649	0.024	0.34	1.541	0.059	0.681	0.033	0.48	3259	97	4206	49
	X402_13_11			62.2	3.2	0.681	0.029	0.43	1.468	0.065	0.656	0.036	0.36	3340	110	4190	53
	X402_13_12			43.4	2.2	0.553	0.017	0.27	1.808	0.051	0.574	0.025	0.27	2845	69	3847	51
	X402_13_14			74.4	5.1	0.707	0.031	0.47	1.414	0.058	0.755	0.039	0.27	3440	120	4382	72
	X402_13_15			179.6	9.8	1.477	0.074	0.46	0.677	0.035	0.841	0.041	0.42	5820	190	5270	54
	X402_13_16			100.7	6.9	0.85	0.051	0.38	1.176	0.072	0.777	0.055	0.48	3940	180	4713	66
	X402_13_17			75.3	3.4	0.637	0.023	0.31	1.570	0.056	0.838	0.036	0.47	3167	90	4405	45
	X402_13_18			60.6	2.5	0.613	0.021	0.11	1.631	0.055	0.699	0.031	0.53	3072	81	4184	41
	X402_13_19			121	13	0.956	0.099	0.86	1.05	0.11	0.868	0.054	0.09	4180	300	4778	99
	X402_13_20			164	13	1.274	0.067	0.69	0.785	0.04	0.87	0.044	0.10	5280	190	5206	77
	X402_13_21			173	30	1.53	0.24	0.98	0.654	0.074	0.793	0.049	-0.02	5530	440	5030	100
	X402_13_22			78.4	4.5	0.719	0.026	0.35	1.391	0.051	0.757	0.042	0.30	3478	96	4450	55
	X402_13_23			51	2.5	0.533	0.017	0.26	1.876	0.064	0.682	0.031	0.34	2746	73	3994	48
	X402_13_24			97.2	6	0.902	0.044	0.72	1.109	0.055	0.736	0.033	0.28	4110	140	4632	62
	X402_13_25			91.1	4.7	0.834	0.042	0.60	1.199	0.061	0.75	0.038	0.26	3880	150	4591	53
	X402_13_26			870	320	6.2	2.1	1.0	0.161	0.054	0.896	0.044	0.05	9180	840	6030	210
	X402_13_27			2710	540	18.6	3.4	1.0	0.0538	0.0076	0.975	0.05	0.23	17520	690	7720	120
	X402_13_28			2410	270	17.2	1.9	0.91	0.0581	0.0065	0.986	0.04	0.15	18280	660	7810	110
	X402_13_29			95.3	4.8	0.863	0.034	0.53	1.159	0.048	0.767	0.032	0.32	3990	120	4626	49
	X402_13_30			87.1	5	0.81	0.034	0.24	1.235	0.049	0.724	0.043	0.38	3800	120	4547	59
402-13 (2)	X402_13_1			459.2	8.4	3.624	0.068	0.76	0.2759	0.0052	0.933	0.012	0.46	9845	190	6232	19
	X402_13_2			7890	730	58.6	5.4	1.0	0.0171	0.0014	0.976	0.014	0.11	25350	470	8927	70
	X402_13_3			1529	61	11.25	0.43	0.95	0.0889	0.0034	0.988	0.014	0.17	16070	290	7424	40
	X402_13_4			6450	340	48.9	2.7	0.98	0.0204	0.0011	0.96	0.012	0.19	24880	390	8858	51
	X402_13_5			18000	2200	135	17	1.0	0.0074	0.0013	0.974	0.012	0.15	30090	820	9700	120
	X402_13_6			6420	660	47.5	4.8	0.99	0.0211	0.0026	0.985	0.013	-0.03	23960	670	8730	110
	X402_13_7			7350	660	55.5	5	1.0	0.0180	0.0014	0.959	0.017	0.00	25180	460	8915	71
	X402_13_8			5480	290	40.1	2	0.98	0.0249	0.0013	0.968	0.012	0.17	23840	370	8702	51

Table 6: Apatite Sample Data (2014 Dredge Sample Analytical Run)

Identification		Location		Geochronological Data														
Sample	Sample Reference	Latitude	Longitude	$^{207}Pb/^{235}U$	2σ	$^{206}Pb/^{238}U$	2σ	Error Correlation	$^{238}U/^{206}Pb$	2σ	$^{207}Pb/^{206}Pb$	2σ	Error Correlation	$^{206}Pb/^{238}U$ Age (Ma)	2σ	$^{207}Pb/^{235}U$ Age (Ma)	2σ
204-1	X204_2	54.22	-11.63	123.9	5	1.092	0.053	0.72	0.916	0.044	0.816	0.023	0.08	4760	170	4901	41
	X402_13_9			6990	420	51.6	3.1	0.98	0.0194	0.0013	0.979	0.012	0.19	25150	430	8932	61
	X402_13_10			3060	150	22.5	1.1	0.97	0.0444	0.0023	0.974	0.013	0.04	20210	370	8107	52
	X402_13_11			458	13	3.484	0.096	0.88	0.2870	0.0081	0.959	0.013	0.22	9640	220	6223	27
	X402_13_12			4830	320	36.6	2.3	0.98	0.0273	0.002	0.962	0.016	-0.02	23240	400	8571	61
	X402_13_13			6150	520	45.2	3.7	0.98	0.0221	0.0018	0.954	0.014	0.12	24090	520	8741	79
	X402_13_14			1770	81	13.49	0.62	0.93	0.0741	0.0034	0.957	0.017	0.20	17150	330	7578	46
	X402_13_15			2415	90	18.02	0.65	0.94	0.0555	0.0021	0.968	0.012	0.08	18910	300	7895	37
	X402_13_16			5500	1200	40.4	8.6	0.99	0.0248	0.005	0.987	0.015	0.06	20180	680	8110	110
	X402_13_17			9800	1300	72.3	9	1.0	0.0138	0.0012	0.98	0.012	-0.11	26230	470	9077	74
	X402_13_18			3300	600	24.4	4.2	1.0	0.0410	0.0083	0.962	0.015	-0.09	18200	770	7760	130
	X402_13_19			1087	29	8.15	0.22	0.84	0.1227	0.0032	0.979	0.013	0.31	14220	230	7097	26
	X402_13_20			4790	650	36.2	4.9	1.0	0.0276	0.0037	0.96	0.013	0.11	21200	610	8280	100
	X402_13_21			6280	690	47.9	5.1	1.0	0.0209	0.0017	0.947	0.014	0.17	23860	440	8665	65
	X402_13_22			540	21	4.06	0.16	0.95	0.2463	0.0095	0.96	0.011	0.17	10400	270	6371	40
	X402_13_23			2130	76	15.58	0.52	0.91	0.0642	0.0022	0.98	0.013	0.17	18070	270	7770	35
	X402_13_24			414.4	6.9	3.172	0.054	0.75	0.3153	0.0053	0.949	0.012	0.38	9205	180	6117	17
	X402_13_25			5220	290	39.6	2.3	0.98	0.0253	0.0014	0.971	0.013	0.20	23570	400	8650	56
	X402_13_27			695	46	5.29	0.35	0.98	0.1890	0.014	0.961	0.011	0.10	11600	400	6591	68
	X402_13_28			634	18	4.73	0.13	0.89	0.2114	0.0056	0.968	0.013	0.21	11250	230	6544	28
	X402_13_29			168.8	2.9	1.354	0.022	0.61	0.7386	0.012	0.916	0.014	0.43	5521	140	5212	17
	X402_13_30			7980	790	58.6	6.1	1.0	0.0171	0.0014	0.991	0.014	0.19	25350	470	8962	71
	X402_13_31			3260	340	24.6	2.6	1.0	0.0407	0.0026	0.97	0.011	0.13	19780	350	8039	56
	X402_13_32			11600	1200	88	9.5	0.99	0.0114	0.0014	0.965	0.015	0.14	27710	650	9330	97
	X402_13_33			652	21	4.96	0.15	0.96	0.2016	0.006	0.948	0.012	0.23	11430	240	6563	31
	X402_13_35			2990	220	22.5	1.6	0.98	0.0444	0.0042	0.965	0.013	0.02	20340	510	8126	77

Table 7: Zircon Sample Data (2014 Dredge Sample Analytical Run)

Identification		Location		Geochronological Data													
Sample	Sample Reference	Latitude	Longitude	$^{207}Pb/^{235}U$	2σ	$^{206}Pb/^{238}U$	2σ	Error Correlation	$^{207}Pb/^{206}Pb$	2σ	$^{207}Pb/^{235}U$ Age (Ma)	2σ	$^{206}Pb/^{238}U$ Age (Ma)	2σ	$^{207}Pb/^{206}Pb$ Age (Ma)	2σ
402-4	X402_4_1	53.95	-12.79	3.822	0.074	0.2806	0.0049	0.62	0.0987	0.0016	1599	15	1598	24	1595	30
	X402_4_2			3.906	0.084	0.2831	0.0060	0.72	0.1004	0.0016	1616	18	1610	30	1638	27
	X402_4_3			3.916	0.110	0.2868	0.0062	0.59	0.0986	0.0023	1616	23	1629	31	1591	44
	X402_4_4			3.926	0.120	0.2921	0.0079	0.72	0.0961	0.0021	1617	24	1655	39	1543	40
	X402_4_5			3.836	0.100	0.2809	0.0086	0.78	0.0985	0.0019	1599	22	1598	43	1602	36
	X402_4_6			4.086	0.110	0.2846	0.0071	0.75	0.103	0.0019	1648	23	1618	36	1678	34
	X402_4_7			3.333	0.093	0.2492	0.0086	0.93	0.0971	0.0013	1486	22	1436	44	1566	25
	X402_4_8			3.767	0.095	0.2783	0.0048	0.44	0.0978	0.0023	1587	21	1587	24	1581	44
	X402_4_9			3.863	0.077	0.2744	0.0053	0.69	0.1031	0.0016	1607	16	1566	27	1682	29
	X402_4_10			4.056	0.098	0.2847	0.0046	0.40	0.1042	0.0024	1646	20	1619	23	1699	41
	X402_4_11			3.899	0.067	0.2811	0.0050	0.52	0.0997	0.0017	1613	14	1601	25	1617	33
	X402_4_12			4.166	0.110	0.2916	0.0058	0.61	0.1037	0.0022	1674	20	1653	29	1684	39
	X402_4_13			3.476	0.093	0.2569	0.0065	0.62	0.0974	0.0022	1520	21	1477	33	1573	42
	X402_4_14			3.395	0.078	0.2502	0.0064	0.78	0.0993	0.0016	1502	18	1443	33	1606	30
	X402_4_15			3.971	0.078	0.2829	0.0065	0.62	0.101	0.0019	1627	16	1609	32	1642	34
	X402_4_16			3.929	0.093	0.2765	0.0053	0.56	0.1032	0.0021	1618	19	1577	27	1682	36
	X402_4_17			3.786	0.062	0.2744	0.0053	0.70	0.1003	0.0014	1589	13	1570	26	1626	26
	X402_4_18			3.425	0.086	0.2465	0.0060	0.79	0.1005	0.0016	1511	20	1424	31	1629	30
	X402_4_19			3.699	0.074	0.2700	0.0045	0.46	0.0989	0.0019	1573	16	1544	23	1603	37
	X402_4_20			4.116	0.120	0.2980	0.0074	0.90	0.0996	0.0013	1654	24	1684	37	1618	25
	X402_4_21			3.586	0.100	0.2611	0.0059	0.76	0.0989	0.0018	1543	22	1499	30	1597	35
	X402_4_22			3.917	0.078	0.2809	0.0063	0.64	0.0994	0.0018	1616	16	1599	32	1628	33
	X402_4_23			3.618	0.067	0.2610	0.0058	0.49	0.1011	0.0021	1553	15	1498	30	1648	37
	X402_4_24			3.766	0.070	0.2751	0.0049	0.54	0.0978	0.0017	1587	15	1574	24	1586	32
	X402_4_25			3.737	0.078	0.2679	0.0052	0.65	0.1006	0.0017	1578	17	1534	27	1630	32
	X402_4_26			3.896	0.120	0.2808	0.0072	0.71	0.1003	0.0022	1614	25	1598	36	1629	41
	X402_4_27			4.007	0.085	0.2907	0.0068	0.67	0.0987	0.0018	1635	17	1648	34	1595	33
	X402_4_28			3.546	0.120	0.2579	0.0077	0.75	0.1005	0.0023	1542	25	1482	39	1638	43
	X402_4_29			3.768	0.089	0.2785	0.0052	0.68	0.0972	0.0017	1590	19	1588	26	1577	33
	X402_4_30			3.612	0.086	0.2647	0.0057	0.84	0.0992	0.0013	1553	19	1517	29	1606	25
	X402_4_31			3.944	0.093	0.2868	0.0073	0.76	0.0998	0.0017	1625	18	1628	36	1630	32
	X402_4_32			3.543	0.072	0.2494	0.0058	0.68	0.1025	0.0018	1536	16	1438	30	1664	33
	X402_4_33			3.946	0.130	0.2889	0.0078	0.77	0.0995	0.0021	1623	25	1639	39	1608	39
	X402_4_34			3.646	0.110	0.2727	0.0060	0.77	0.0981	0.0019	1564	24	1557	30	1587	35
	X402_4_35			3.970	0.095	0.2859	0.0068	0.75	0.1008	0.0017	1626	19	1624	34	1641	30
	X402_4_36			4.066	0.120	0.2933	0.0081	0.75	0.0994	0.002	1645	23	1661	40	1613	36
	X402_4_37			4.166	0.100	0.3008	0.0069	0.67	0.1002	0.0019	1665	20	1699	34	1622	34
	X402_4_38			3.922	0.090	0.2827	0.0059	0.58	0.0997	0.002	1623	17	1608	30	1612	37
	X402_4_39			3.786	0.110	0.2761	0.0063	0.72	0.0984	0.002	1587	23	1575	32	1592	39
	X402_4_40			3.811	0.079	0.2800	0.0057	0.36	0.0991	0.0023	1594	17	1595	29	1604	42
	X402_4_41			3.904	0.095	0.2842	0.0064	0.43	0.1	0.0025	1616	19	1616	32	1615	46
	X402_4_42			3.808	0.079	0.2818	0.0057	0.60	0.0981	0.0018	1593	17	1608	29	1583	33

Table 7: Zircon Sample Data (2014 Dredge Sample Analytical Run)

Identification		Location		Geochronological Data													
Sample	Sample Reference	Latitude	Longitude	$^{207}Pb/^{235}U$	2σ	$^{206}Pb/^{238}U$	2σ	Error Correlation	$^{207}Pb/^{206}Pb$	2σ	$^{207}Pb/^{235}U$ Age (Ma)	2σ	$^{206}Pb/^{238}U$ Age (Ma)	2σ	$^{207}Pb/^{206}Pb$ Age (Ma)	2σ
	X402_4_43			3.896	0.120	0.2802	0.0062	0.77	0.1017	0.002	1615	26	1596	31	1649	37
	X402_4_44			3.696	0.092	0.2651	0.0048	0.68	0.0987	0.0018	1569	20	1519	24	1599	36
	X402_4_45			3.867	0.096	0.2812	0.0065	0.72	0.1005	0.0018	1605	20	1601	32	1629	34
	X402_4_46			3.956	0.130	0.2854	0.0065	0.86	0.1018	0.0018	1621	27	1622	32	1651	34
	X402_4_47			3.956	0.110	0.2775	0.0078	0.86	0.1026	0.0015	1623	22	1582	39	1669	28
	X402_4_48			3.840	0.091	0.2742	0.0060	0.70	0.1014	0.0018	1605	20	1565	30	1644	33
	X402_4_49			4.016	0.130	0.2863	0.0084	0.70	0.1001	0.0024	1634	26	1625	42	1616	45
	X402_4_50			3.886	0.110	0.2810	0.0084	0.73	0.0983	0.0021	1611	23	1599	42	1585	40
	X402_4_51			3.701	0.090	0.2723	0.0054	0.60	0.0996	0.002	1570	20	1556	27	1623	40
	X402_4_52			3.526	0.120	0.2500	0.0076	0.80	0.1007	0.0021	1530	26	1441	39	1642	39
	X402_4_53			3.607	0.099	0.2571	0.0066	0.80	0.1017	0.0017	1552	21	1483	33	1656	32
402-8	X402_8_2	53.95	-12.79	14.82	0.35	0.516	0.012	0.92	2878	15	2806	22	2697	51	2878	15
	X402_8_3			14.16	0.30	0.512	0.012	0.87	2827	19	2761	20	2669	51	2827	19
	X402_8_4			14.59	0.42	0.539	0.017	0.94	2805	18	2790	29	2795	74	2805	18
	X402_8_5			15.19	0.18	0.528	0.009	0.83	2892	16	2828	11	2739	39	2892	16
	X402_8_6			16.41	0.40	0.559	0.012	0.86	2920	20	2902	24	2877	52	2920	20
	X402_8_7			15.16	0.43	0.513	0.015	0.92	2902	19	2822	27	2692	63	2902	19
	X402_8_8			18.29	0.27	0.601	0.009	0.84	2986	13	3007	15	3039	34	2986	13
	X402_8_9			16.85	0.36	0.574	0.011	0.86	2922	18	2924	20	2930	46	2922	18
	X402_8_10			16.93	0.36	0.568	0.012	0.89	2949	15	2929	21	2912	51	2949	15
	X402_8_11			10.57	0.31	0.414	0.011	0.92	2714	19	2490	28	2235	50	2714	19
	X402_8_12			15.72	0.33	0.552	0.011	0.85	2880	18	2861	20	2841	45	2880	18
	X402_8_13			15.98	0.30	0.536	0.009	0.79	2945	18	2877	18	2773	38	2945	18
	X402_8_14			16.24	0.34	0.571	0.013	0.83	2871	20	2892	20	2927	54	2871	20
	X402_8_15			15.67	0.30	0.553	0.014	0.95	2859	15	2858	19	2843	59	2859	15
	X402_8_16			16.70	0.39	0.576	0.016	0.94	2904	16	2919	23	2934	66	2904	16
	X402_8_17			18.32	0.37	0.615	0.011	0.83	2943	18	3005	19	3095	44	2943	18
	X402_8_18			18.32	0.46	0.603	0.015	0.90	2980	18	3007	24	3044	61	2980	18
	X402_8_19			16.25	0.20	0.563	0.007	0.61	2888	18	2894	11	2885	27	2888	18
	X402_8_20			11.19	0.28	0.449	0.010	0.88	2632	20	2537	24	2404	43	2632	20
	X402_8_21			11.95	0.43	0.446	0.014	0.92	2772	23	2602	34	2380	60	2772	23
	X402_8_22			13.19	0.42	0.483	0.016	0.94	2812	19	2697	32	2540	69	2812	19
	X402_8_23			11.49	0.26	0.426	0.010	0.81	2785	23	2565	20	2291	45	2785	23
	X402_8_24			14.95	0.54	0.529	0.014	0.98	2872	19	2805	36	2741	59	2872	19
	X402_8_25			15.29	0.31	0.543	0.011	0.90	2854	15	2836	20	2800	47	2854	15
	X402_8_26			14.40	0.27	0.522	0.009	0.80	2827	20	2780	18	2720	36	2827	20
	X402_8_27			10.87	0.42	0.439	0.016	0.94	2654	22	2504	36	2345	71	2654	22
	X402_8_28			11.85	0.46	0.460	0.014	0.97	2731	19	2589	36	2439	62	2731	19
	X402_8_29			13.44	0.22	0.487	0.008	0.87	2820	14	2710	16	2563	37	2820	14
	X402_8_31			17.14	0.37	0.580	0.012	0.90	2956	16	2944	20	2954	48	2718	20
	X402_8_32			16.81	0.31	0.573	0.011	0.88	2928	16	2923	18	2928	45	2956	16
	X402_8_33			11.50	0.27	0.422	0.012	0.95	2808	16	2565	21	2272	54	2928	16
	X402_8_34			12.96	0.37	0.456	0.012	0.95	2868	15	2688	27	2425	55	2808	16

Table 7: Zircon Sample Data (2014 Dredge Sample Analytical Run)

Identification		Location		Geochronological Data													
Sample	Sample Reference	Latitude	Longitude	$^{207}Pb/^{235}U$	2σ	$^{206}Pb/^{238}U$	2σ	Error Correlation	$^{207}Pb/^{206}Pb$	2σ	$^{207}Pb/^{235}U$ Age (Ma)	2σ	$^{206}Pb/^{238}U$ Age (Ma)	2σ	$^{207}Pb/^{206}Pb$ Age (Ma)	2σ
	X402_8_36			15.46	0.59	0.536	0.020	0.95	2915	19	2858	36	2769	85	2868	15
	X402_8_37			15.97	0.44	0.553	0.015	0.94	2901	17	2884	27	2841	64	2918	19
	X402_8_38			11.14	0.44	0.438	0.014	0.93	2694	25	2532	36	2341	65	2915	19
	X402_8_39			10.51	0.36	0.424	0.014	0.90	2651	25	2486	32	2278	64	2901	17
	X402_8_40			14.26	0.29	0.505	0.011	0.89	2830	17	2769	21	2644	46	2694	25
	X402_8_41			11.62	0.36	0.440	0.011	0.88	2764	25	2570	28	2351	51	2651	25
	X402_8_42			12.09	0.42	0.436	0.013	0.98	2831	13	2614	32	2341	58	2830	17
	X402_8_43			17.12	0.38	0.577	0.016	0.96	2943	15	2940	21	2941	63	2764	25
	X402_8_44			16.95	0.56	0.587	0.020	0.95	2907	17	2941	31	2988	78	2831	13
	X402_8_45			15.28	0.21	0.549	0.009	0.83	2822	15	2833	13	2825	37	2943	15
	X402_8_46			15.57	0.33	0.522	0.013	0.87	2941	19	2849	20	2711	54	2907	17
	X402_8_47			18.35	0.33	0.619	0.008	0.82	2943	16	3007	17	3110	34	2822	15
	X402_8_48			17.98	0.35	0.599	0.011	0.89	2947	14	2987	19	3033	45	2941	19
	X402_8_49			18.29	0.34	0.602	0.011	0.86	2970	15	3007	17	3043	44	2943	16
	X402_8_50			16.47	0.34	0.569	0.013	0.87	2909	19	2906	20	2909	54	2947	14
	X402_8_51			14.05	0.29	0.512	0.012	0.91	2807	15	2754	20	2672	49	2970	15
	X402_8_52			18.25	0.25	0.593	0.008	0.71	3001	17	3003	13	3009	33	2909	19
	X402_8_53			17.45	0.31	0.586	0.013	0.88	2950	16	2959	17	2977	54	2807	15
	X402_8_54			14.93	0.31	0.518	0.010	0.79	2890	21	2813	19	2697	41	3001	17
402-11	X402_11_1	53.95	-12.79	15.90	0.22	0.579	0.007	0.71	15.92	0.22	2873	13	2950	29	2950	16
	X402_11_3			15.14	0.18	0.558	0.006	0.68	15.16	0.18	2824	11	2866	25	2890	21
	X402_11_4			10.03	0.33	0.360	0.014	0.91	10.04	0.33	2447	27	1983	67	2831	28
	X402_11_5			15.32	0.23	0.571	0.009	0.82	15.34	0.23	2840	14	2916	39	2803	16
	X402_11_6			15.68	0.27	0.577	0.009	0.85	15.7	0.27	2860	16	2948	41	2795	15
	X402_11_7			15.48	0.28	0.571	0.011	0.88	15.5	0.28	2845	17	2919	47	2780	15
	X402_11_8			14.67	0.20	0.543	0.006	0.77	14.68	0.2	2794	13	2802	24	2794	14
	X402_11_9			14.44	0.21	0.537	0.009	0.82	14.45	0.21	2781	15	2775	40	2797	17
	X402_11_10			13.81	0.32	0.503	0.013	0.91	13.82	0.32	2734	22	2631	56	2815	17
	X402_11_11			15.05	0.24	0.560	0.011	0.85	15.07	0.24	2818	15	2871	45	2784	17
	X402_11_12			15.02	0.22	0.551	0.008	0.72	15.04	0.22	2819	14	2833	35	2807	17
	X402_11_13			15.21	0.21	0.560	0.009	0.76	15.23	0.21	2833	13	2873	35	2808	17
	X402_11_14			15.95	0.27	0.559	0.009	0.77	15.97	0.27	2874	16	2870	37	2872	18
	X402_11_15			14.04	0.22	0.521	0.008	0.68	14.05	0.22	2752	15	2716	34	2791	21
	X402_11_17			14.84	0.24	0.542	0.010	0.77	14.86	0.24	2804	16	2798	40	2825	18
	X402_11_18			14.72	0.39	0.545	0.016	0.92	14.74	0.39	2795	26	2808	67	2803	18
	X402_11_19			15.25	0.17	0.562	0.006	0.71	15.27	0.17	2832	11	2883	27	2794	15
	X402_11_20			14.90	0.21	0.546	0.008	0.62	14.92	0.21	2811	14	2816	32	2795	20
	X402_11_21			15.07	0.21	0.549	0.007	0.90	15.09	0.21	2820	13	2826	30	2812	10
	X402_11_22			15.02	0.23	0.547	0.008	0.60	15.04	0.23	2817	15	2819	35	2820	22
	X402_11_23			14.55	0.19	0.538	0.007	0.73	14.56	0.19	2788	12	2783	30	2785	16
	X402_11_24			14.88	0.18	0.546	0.007	0.62	14.9	0.18	2808	11	2816	28	2797	18
	X402_11_25			14.59	0.20	0.542	0.008	0.79	14.6	0.2	2788	13	2796	33	2787	15
	X402_11_26			14.05	0.30	0.516	0.013	0.90	14.06	0.3	2751	21	2689	57	2781	18

Table 7: Zircon Sample Data (2014 Dredge Sample Analytical Run)

Identification		Location		Geochronological Data													
Sample	Sample Reference	Latitude	Longitude	$^{207}Pb/^{235}U$	2σ	$^{206}Pb/^{238}U$	2σ	Error Correlation	$^{207}Pb/^{206}Pb$	2σ	$^{207}Pb/^{235}U$ Age (Ma)	2σ	$^{206}Pb/^{238}U$ Age (Ma)	2σ	$^{207}Pb/^{206}Pb$ Age (Ma)	2σ
	X402_11_27			13.67	0.15	0.499	0.007	0.62	13.68	0.15	2729	11	2616	30	2804	18
	X402_11_28			14.83	0.14	0.550	0.007	0.48	14.85	0.14	2805.4	8.7	2832	27	2800	18
	X402_11_29			14.65	0.14	0.545	0.006	0.54	14.66	0.14	2792.7	8.9	2809	24	2789	16
	X402_11_30			14.72	0.19	0.544	0.008	0.75	14.74	0.19	2799	12	2812	33	2803	16
	X402_11_31			11.79	0.25	0.440	0.009	0.87	11.8	0.25	2593	20	2356	38	2776	17
	X402_11_32			13.67	0.30	0.503	0.012	0.91	13.68	0.3	2728	21	2631	49	2809	16
	X402_11_33			15.02	0.17	0.548	0.006	0.68	15.04	0.17	2817	11	2826	25	2824	15
	X402_11_34			13.41	0.28	0.500	0.010	0.88	13.42	0.28	2710	19	2619	41	2777	16
	X402_11_35			15.06	0.23	0.552	0.009	0.81	15.08	0.23	2819	15	2837	36	2813	16
	X402_11_36			15.26	0.31	0.570	0.012	0.87	15.28	0.31	2833	19	2912	47	2797	17
	X402_11_37			15.67	0.18	0.576	0.008	0.66	15.69	0.18	2857	11	2940	35	2796	18
	X402_11_38			14.76	0.43	0.542	0.015	0.95	14.78	0.43	2796	29	2796	62	2805	15
	X402_11_39			15.01	0.22	0.550	0.008	0.81	15.03	0.22	2818	14	2831	34	2798	15
	X402_11_40			14.95	0.19	0.552	0.007	0.66	14.97	0.19	2814	12	2841	27	2804	16
	X402_11_42			14.65	0.27	0.542	0.011	0.88	14.66	0.27	2791	17	2797	45	2791	16
	X402_11_43			14.29	0.14	0.524	0.007	0.80	14.3	0.14	2769.2	9.3	2722	28	2807	12
	X402_11_44			14.29	0.24	0.529	0.011	0.69	14.3	0.24	2769	16	2745	45	2794	25
	X402_11_46			14.76	0.22	0.541	0.008	0.83	14.78	0.22	2800	14	2795	32	2810	14
	X402_11_47			14.51	0.16	0.540	0.008	0.76	14.52	0.16	2784	10	2788	34	2789	16
	X402_11_48			14.75	0.18	0.538	0.007	0.60	14.77	0.18	2803	11	2781	31	2827	19
	X402_11_50			14.64	0.17	0.535	0.008	0.72	14.65	0.17	2795	11	2770	35	2816	17
	X402_11_51			15.00	0.47	0.546	0.017	0.94	15.02	0.47	2815	30	2810	72	2818	17
	X402_11_52			14.78	0.25	0.544	0.009	0.86	14.8	0.25	2804	17	2806	39	2801	15
402-13	X402_13_1	53.95	-12.79	6.56131	0.089	0.3720	0.0053	0.77	0.1279	0.0012	2056	12	2043	25	2070	17
	X402_13_2			5.684	0.110	0.3319	0.0053	0.63	0.1234	0.0019	1930	16	1852	26	2004	27
	X402_13_3			6.080	0.084	0.3503	0.0042	0.63	0.1253	0.0014	1991	12	1941	20	2031	20
	X402_13_4			6.478	0.090	0.3662	0.0050	0.77	0.1283	0.0012	2043	12	2016	24	2074	16
	X402_13_5			5.784	0.100	0.3399	0.0056	0.67	0.1242	0.0017	1944	15	1895	28	2015	25
	X402_13_6			6.423	0.100	0.3682	0.0058	0.75	0.1274	0.0014	2042	14	2026	27	2060	20
	X402_13_7			6.322	0.094	0.3618	0.0051	0.71	0.1268	0.0014	2021	13	1995	24	2058	20
	X402_13_8			6.415	0.083	0.3651	0.0050	0.71	0.1272	0.0013	2034	11	2011	24	2058	18
	X402_13_9			5.922	0.096	0.3499	0.0064	0.79	0.1227	0.0014	1964	14	1938	30	2000	20
	X402_13_10			5.914	0.110	0.3490	0.0065	0.84	0.124	0.0013	1962	17	1934	31	2017	18
	X402_13_11			5.895	0.087	0.3510	0.0046	0.61	0.1216	0.0015	1960	13	1944	22	1978	22
	X402_13_12			6.038	0.098	0.3516	0.0057	0.72	0.1248	0.0015	1981	14	1947	27	2027	21
	X402_13_13			6.044	0.100	0.3523	0.0053	0.74	0.1231	0.0014	1982	15	1950	25	2003	19
	X402_13_14			6.074	0.100	0.3475	0.0058	0.68	0.1281	0.0017	1989	15	1936	28	2070	23
	X402_13_15			5.624	0.150	0.3260	0.0098	0.89	0.1243	0.0017	1916	24	1821	48	2019	23
	X402_13_16			6.194	0.100	0.3552	0.0054	0.68	0.1279	0.0016	2006	14	1964	26	2067	22
	X402_13_17			6.493	0.120	0.3742	0.0079	0.78	0.1267	0.0017	2044	16	2059	36	2050	24
	X402_13_18			6.007	0.091	0.3539	0.0056	0.77	0.123	0.0013	1976	13	1958	26	1999	18
	X402_13_19			5.515	0.085	0.3227	0.0063	0.71	0.1237	0.0017	1903	13	1807	31	2008	24
	X402_13_20			5.564	0.120	0.3356	0.0077	0.87	0.1211	0.0014	1909	19	1869	37	1971	20

Table 7: Zircon Sample Data (2014 Dredge Sample Analytical Run)																
Identification		Location		Geochronological Data												
Sample	Sample Reference	Latitude	Longitude	$^{207}Pb/^{235}U$	2σ	$^{206}Pb/^{238}U$	2σ	Error Correlation	$^{207}Pb/^{206}Pb$	2σ	$^{207}Pb/^{235}U$ Age (Ma)	2σ	$^{206}Pb/^{238}U$ Age (Ma)	2σ	$^{207}Pb/^{206}Pb$ Age (Ma)	2σ
	X402_13_21			6.793	0.110	0.3857	0.0069	0.76	0.1273	0.0015	2084	15	2107	32	2063	21
	X402_13_22			5.305	0.130	0.3183	0.0059	0.79	0.1201	0.0018	1870	21	1785	29	1962	26
	X402_13_23			6.174	0.110	0.3634	0.0064	0.74	0.1253	0.0016	2002	16	2003	30	2035	23
	X402_13_24			6.234	0.160	0.3562	0.0091	0.85	0.128	0.0018	2007	22	1967	43	2068	25
	X402_13_25			6.104	0.180	0.3581	0.0094	0.77	0.1244	0.0024	1988	26	1976	44	2021	36
	X402_13_26			6.232	0.081	0.3654	0.0041	0.57	0.1232	0.0014	2009	11	2012	19	2001	20
	X402_13_27			6.104	0.110	0.3583	0.0063	0.83	0.1241	0.0013	1993	15	1978	30	2015	18
	X402_13_28			6.080	0.065	0.3500	0.0044	0.48	0.1255	0.0015	1987.8	9.3	1939	21	2039	21
	X402_13_29			6.034	0.100	0.3582	0.0054	0.74	0.1227	0.0014	1980	15	1978	26	1993	20
	X402_13_30			6.244	0.110	0.3598	0.0074	0.87	0.1272	0.0013	2010	16	1985	35	2058	18
	X402_13_31			6.694	0.086	0.3823	0.0058	0.66	0.1274	0.0015	2072	11	2092	27	2063	21
	X402_13_33			6.277	0.096	0.3683	0.0058	0.61	0.1246	0.0017	2015	13	2026	27	2025	24
	X402_13_34			6.253	0.082	0.3705	0.0064	0.71	0.1225	0.0015	2012	11	2036	30	1994	22
	X402_13_35			6.034	0.120	0.3480	0.0076	0.88	0.1263	0.0013	1980	17	1929	36	2046	19
	X402_13_36			6.018	0.090	0.3588	0.0049	0.72	0.1216	0.0013	1980	13	1981	23	1984	20
	X402_13_37			5.594	0.130	0.3234	0.0090	0.89	0.1248	0.0016	1919	19	1815	43	2024	23
	X402_13_38			6.443	0.160	0.3687	0.0074	0.88	0.1272	0.0015	2039	22	2033	36	2061	20
	X402_13_39			6.129	0.095	0.3588	0.0059	0.82	0.124	0.0012	1994	14	1988	28	2016	18
	X402_13_40			6.034	0.100	0.3463	0.0059	0.63	0.125	0.0018	1980	14	1921	28	2026	25
	X402_13_41			5.764	0.120	0.3404	0.0065	0.77	0.1239	0.0017	1940	18	1893	31	2011	24
	X402_13_42			6.334	0.110	0.3747	0.0058	0.72	0.1217	0.0015	2022	16	2056	27	1979	21
	X402_13_43			6.364	0.100	0.3805	0.0055	0.67	0.1224	0.0015	2030	14	2084	25	1989	22
	X402_13_44			6.423	0.110	0.3825	0.0067	0.64	0.122	0.0018	2037	15	2093	31	1983	27
	X402_13_45			5.824	0.120	0.3433	0.0063	0.72	0.1225	0.0018	1951	17	1907	30	1998	26
	X402_13_46			5.724	0.100	0.3351	0.0064	0.84	0.1233	0.0013	1934	15	1867	31	2003	19
	X402_13_47			6.341	0.082	0.3811	0.0060	0.85	0.1216	0.001	2028	12	2086	28	1978	15
	X402_13_48			6.294	0.130	0.3787	0.0074	0.78	0.121	0.0016	2021	19	2075	35	1970	23
	X402_13_49			6.274	0.100	0.3764	0.0052	0.79	0.1213	0.0012	2014	14	2065	25	1975	18
	X402_13_50			6.674	0.090	0.3848	0.0053	0.71	0.1252	0.0013	2069	12	2104	25	2032	18
	X402_13_51			5.703	0.085	0.3425	0.0049	0.77	0.1201	0.0012	1932	13	1903	24	1957	18
	X402_13_52			6.094	0.110	0.3576	0.0056	0.67	0.1231	0.0017	1989	15	1975	27	2003	24
	X402_13_53			6.493	0.100	0.3784	0.0067	0.74	0.1239	0.0015	2044	14	2078	31	2016	22
	X402_13_54			6.104	0.130	0.3588	0.0076	0.87	0.1217	0.0013	1989	19	1980	36	1982	20
	X402_13_55			6.024	0.130	0.3614	0.0075	0.78	0.1211	0.0017	1980	18	1992	36	1970	24
	X402_13_57			6.331	0.097	0.3769	0.0060	0.80	0.1224	0.0012	2022	13	2071	29	1996	18
	X402_13_58			5.872	0.088	0.3507	0.0053	0.78	0.121	0.0012	1957	13	1942	25	1969	18
	X402_13_59			6.219	0.071	0.3707	0.0049	0.57	0.122	0.0014	2007.4	9.9	2037	23	1987	20
	X402_13_60			6.341	0.090	0.3715	0.0067	0.74	0.1229	0.0015	2026	13	2045	32	2001	21
	X402_13_61			6.375	0.099	0.3710	0.0055	0.72	0.1237	0.0014	2028	14	2043	27	2008	20
302-1	X302_1_1	54.08	-11.97	10.91683	0.2	0.4264	0.0086	0.79	0.1844	0.0023	2520	18	2300	40	2691	21
	X302_1_2			9.720466	0.39	0.381	0.014	0.94	0.1848	0.0025	2401	40	2081	64	2695	22
	X302_1_3			12.83102	0.49	0.498	0.022	0.96	0.1864	0.0024	2668	37	2613	92	2708	22
	X302_1_4			14.66544	0.39	0.537	0.015	0.81	0.1954	0.0033	2792	25	2785	61	2784	27

Table 7: Zircon Sample Data (2014 Dredge Sample Analytical Run)

Identification		Location		Geochronological Data													
Sample	Sample Reference	Latitude	Longitude	$^{207}Pb/^{235}U$	2σ	$^{206}Pb/^{238}U$	2σ	Error Correlation	$^{207}Pb/^{206}Pb$	2σ	$^{207}Pb/^{235}U$ Age (Ma)	2σ	$^{206}Pb/^{238}U$ Age (Ma)	2σ	$^{207}Pb/^{206}Pb$ Age (Ma)	2σ
	X302_1_5			14.66544	0.27	0.5389	0.0097	0.82	0.2002	0.0022	2795	18	2783	41	2827	18
	X302_1_6			10.43829	0.37	0.409	0.016	0.91	0.1882	0.003	2470	33	2220	69	2727	26
	X302_1_7			10.04947	0.47	0.364	0.015	0.92	0.2024	0.0037	2431	48	2002	70	2842	30
	X302_1_8			11.31562	0.42	0.392	0.014	0.87	0.2086	0.0038	2548	37	2130	67	2900	29
	X302_1_9			2.768588	0.058	0.2278	0.0042	0.48	0.0896	0.0018	1348	15	1326	22	1424	35
	X302_1_10			3.240155	0.62	0.2300	0.0053	0.99	0.0966	0.0098	1380	49	1338	28	1439	87
	X302_1_11			2.651943	0.062	0.2226	0.0046	0.61	0.0874	0.0017	1315	17	1298	24	1364	37
	X302_1_12			2.233215	0.14	0.189	0.012	0.94	0.0855	0.0018	1181	44	1115	64	1337	40
	X302_1_13			1.958051	0.037	0.1876	0.0033	0.74	0.07561	0.00099	1104	13	1111	18	1082	26
	X302_1_14			1.915181	0.045	0.1923	0.0039	0.63	0.0739	0.0014	1089	16	1136	21	1043	39
	X302_1_15			1.961042	0.045	0.1911	0.0039	0.67	0.0738	0.0013	1103	15	1133	22	1042	36
	X302_1_16			1.468538	0.06	0.1456	0.0034	0.22	0.0734	0.0031	920	25	881	19	1028	80
	X302_1_17			1.470532	0.056	0.1526	0.0034	0.40	0.0704	0.0025	917	23	917	19	929	73
	X302_1_18			1.305035	0.037	0.1411	0.0031	0.01	0.0676	0.0024	853	16	856	17	868	70
	X302_1_19			1.483493	0.045	0.1485	0.0035	0.13	0.0737	0.003	929	20	894	20	1014	82
	X302_1_20			4.187278	0.15	0.3004	0.0078	0.28	0.1007	0.0038	1672	30	1696	39	1637	71
	X302_1_21			4.416581	0.12	0.2965	0.0077	0.60	0.1096	0.0026	1717	23	1676	39	1784	44
	X302_1_22			4.954945	0.16	0.334	0.011	0.14	0.1077	0.0046	1814	26	1857	54	1756	77
	X302_1_23			2.275088	0.07	0.2156	0.0052	0.43	0.0773	0.0023	1204	22	1261	27	1121	57
	X302_1_24			2.154454	0.05	0.2008	0.0036	0.53	0.0781	0.0016	1171	17	1183	20	1154	40
	X302_1_25			2.38276	0.076	0.2083	0.0064	0.45	0.0823	0.0027	1236	23	1222	34	1281	63
	X302_1_26			4.006826	0.096	0.291	0.0069	0.45	0.1005	0.0025	1645	20	1649	35	1630	48
	X302_1_27			3.759577	0.081	0.2815	0.0054	0.54	0.0974	0.0019	1593	17	1602	27	1569	37
	X302_1_28			1.835423	0.055	0.1749	0.0037	0.20	0.0758	0.0025	1061	19	1041	20	1109	62
	X302_1_29			17.92554	0.42	0.620	0.014	0.69	0.209	0.0038	2989	22	3116	54	2899	30
	X302_1_30			0.604164	0.027	0.0686	0.0015	0.03	0.0638	0.0032	479	17	428.7	8.9	710	110
	X302_1_31			0.591204	0.031	0.074	0.002	0.25	0.059	0.0031	473	21	463	12	530	110
	X302_1_32			12.68147	0.28	0.525	0.011	0.55	0.176	0.0036	2660	22	2721	48	2616	35
	X302_1_33			11.79417	0.22	0.5057	0.0079	0.40	0.1698	0.0032	2589	17	2643	34	2555	32
	X302_1_34			2.831397	0.14	0.2192	0.0095	0.95	0.0925	0.0014	1357	38	1285	51	1478	28
	X302_1_35			2.771579	0.1	0.2163	0.0066	0.89	0.0922	0.0015	1345	28	1270	36	1467	31
	X302_1_36			2.083669	0.16	0.179	0.011	0.97	0.0852	0.002	1140	56	1063	61	1315	45
	X302_1_37			10.18904	0.5	0.406	0.021	0.95	0.1794	0.0028	2441	48	2210	100	2649	24
	X302_1_38			10.8271	0.39	0.435	0.014	0.94	0.1833	0.0023	2504	35	2327	65	2681	21
	X302_1_39			1.663944	0.061	0.1421	0.0086	0.77	0.0875	0.0035	1001	21	857	49	1371	73
	X302_1_40			1.875302	0.051	0.174	0.004	0.60	0.0791	0.0018	1076	18	1034	22	1168	45
	X302_1_41			1.625063	0.13	0.131	0.0067	0.92	0.0876	0.0034	967	52	792	39	1365	77
	X302_1_42			1.867327	0.062	0.1519	0.0029	0.04	0.09	0.0035	1072	21	914	16	1437	72
	X302_1_43			1.923157	0.082	0.1467	0.0026	0.66	0.0954	0.0032	1090	27	885	15	1526	65
	X302_1_44			13.81802	0.27	0.507	0.01	0.81	0.1996	0.0024	2741	18	2647	43	2824	20
	X302_1_45			14.68538	0.33	0.528	0.011	0.83	0.1994	0.0025	2795	21	2746	46	2819	21
	X302_1_46			12.30262	0.24	0.4542	0.0099	0.85	0.1973	0.0023	2628	19	2418	44	2805	19
	X302_1_47			10.66759	1.3	0.360	0.046	1.00	0.2184	0.003	2420	110	1940	220	2966	22

Table 7: Zircon Sample Data (2014 Dredge Sample Analytical Run)

Identification		Location		Geochronological Data													
Sample	Sample Reference	Latitude	Longitude	$^{207}Pb/^{235}U$	2σ	$^{206}Pb/^{238}U$	2σ	Error Correlation	$^{207}Pb/^{206}Pb$	2σ	$^{207}Pb/^{235}U$ Age (Ma)	2σ	$^{206}Pb/^{238}U$ Age (Ma)	2σ	$^{207}Pb/^{206}Pb$ Age (Ma)	2σ
	X302_1_48			15.14399	0.77	0.517	0.023	0.95	0.2115	0.0035	2784	77	2680	100	2918	28
	X302_1_49			4.88117	0.093	0.3251	0.0053	0.62	0.1096	0.0017	1803	16	1819	26	1789	29
	X302_1_50			4.968903	0.076	0.3247	0.0053	0.53	0.1107	0.0017	1815	13	1816	26	1811	28
	X302_1_51			5.041682	0.081	0.3305	0.0049	0.62	0.111	0.0015	1828	14	1844	24	1813	24
	X302_1_52			9.072435	1.2	0.338	0.045	0.99	0.1951	0.0028	2310	160	1820	230	2783	24
	X302_1_53			4.599027	0.078	0.3155	0.0057	0.75	0.1059	0.0013	1750	14	1771	28	1730	23
	X302_1_54			4.644887	0.068	0.3165	0.0048	0.50	0.1073	0.0016	1759	12	1776	24	1751	28
	X302_1_56			18.94245	0.35	0.5776	0.0096	0.76	0.239	0.0029	3042	18	2944	39	3114	20
	X302_1_57			20.41796	0.23	0.622	0.011	0.67	0.2377	0.0031	3113	11	3131	46	3105	20
	X302_1_58			2.95901	0.068	0.201	0.012	0.89	0.1105	0.0089	1400	17	1181	67	1740	110
	X302_1_59			6.769433	0.73	0.287	0.028	0.98	0.1677	0.0039	2018	99	1630	140	2533	38
	X302_1_60			7.128342	0.77	0.300	0.029	0.99	0.1714	0.0035	2060	110	1670	150	2570	35
	X302_1_61			3.280034	0.14	0.2318	0.0086	0.92	0.1023	0.0017	1469	38	1346	45	1661	32
	X302_1_62			4.461445	0.077	0.3070	0.0051	0.65	0.1063	0.0015	1727	14	1730	25	1734	27
	X302_1_63			3.170368	0.27	0.235	0.016	0.90	0.0974	0.0037	1442	68	1359	86	1551	74
	X302_1_64			0.658998	0.028	0.0694	0.0014	0.36	0.0697	0.0037	513	17	433.8	8.4	900	110
	X302_1_65			0.517428	0.02	0.0681	0.0013	0.28	0.0554	0.0021	423	14	425.7	8.1	406	81
	X302_1_66			0.493501	0.015	0.0670	0.0012	0.20	0.0531	0.0017	408	10	419.5	7.1	350	71
	X302_1_67			10.84704	0.46	0.432	0.019	0.93	0.1835	0.0029	2502	40	2323	85	2685	25
	X302_1_68			12.21289	0.27	0.4757	0.0081	0.75	0.1855	0.0027	2621	21	2513	35	2708	24
303-1	303-1-1	54.07	-11.98	5.133	0.072	0.33	0.0038	0.73	0.113	0.0011	1838	12	1839	19	1843	17
	303-1-3			5.086	0.048	0.3286	0.0028	0.67	0.11221	0.00083	1832.4	8	1831	14	1833	13
	303-1-4			4.999	0.054	0.3267	0.0031	0.77	0.1109	0.00077	1817	9.2	1821	15	1813	12
	303-1-6			5.064	0.045	0.3298	0.0024	0.55	0.11152	0.00087	1829.3	7.6	1837	12	1822	14
	303-1-7			5.037	0.046	0.3285	0.0029	0.78	0.11118	0.00067	1824.2	7.9	1830	14	1816	11
	303-1-8			5.06	0.046	0.3282	0.0026	0.67	0.11177	0.00078	1828.1	7.7	1829	12	1825	13
	303-1-9			5.037	0.039	0.3256	0.0024	0.67	0.1123	0.00069	1824.2	6.6	1816	12	1835	11
	303-1-11			5.082	0.076	0.3259	0.0046	0.69	0.1133	0.0013	1832	13	1817	22	1849	20
	303-1-12			5.153	0.082	0.3272	0.0043	0.43	0.1145	0.0018	1843	13	1824	21	1866	28
	303-1-13			5.073	0.079	0.3264	0.0045	0.70	0.113	0.0013	1831	13	1820	22	1844	21
	303-1-14			5.042	0.074	0.3307	0.004	0.50	0.1108	0.0015	1826	12	1841	19	1810	25
	303-1-15			5.078	0.063	0.3303	0.0031	0.45	0.1114	0.0013	1832	10	1839	15	1818	21
	303-1-17			5.16	0.055	0.329	0.003	0.64	0.11393	0.00097	1845.6	9	1834	15	1861	15
	303-1-18			5.097	0.056	0.3292	0.0031	0.65	0.11264	0.00097	1834.3	9.3	1834	15	1840	16
	303-1-19			5.138	0.069	0.3325	0.0033	0.28	0.1122	0.0016	1841	12	1850	16	1830	25
	303-1-20			5.071	0.039	0.3292	0.0022	0.64	0.11194	0.00069	1829.8	6.5	1834	11	1828	11
	303-1-21			5.038	0.079	0.3276	0.0057	0.86	0.112	0.001	1822	13	1823	27	1828	16
	303-1-22			5.113	0.087	0.3297	0.0059	0.71	0.1127	0.0015	1841	15	1836	28	1839	24
	303-1-23			5.058	0.087	0.3278	0.0055	0.83	0.1118	0.0011	1825	15	1826	27	1827	18
	303-1-25			5.008	0.08	0.3275	0.0038	0.49	0.111	0.0016	1819	13	1826	18	1812	26
	303-1-27			5.057	0.054	0.3288	0.0033	0.65	0.11231	0.00097	1828	9	1831	16	1832	16
	303-1-28			5.068	0.041	0.3273	0.0025	0.60	0.11237	0.00079	1829.8	6.8	1825	12	1836	13
	303-1-29			5.18	0.11	0.3317	0.0067	0.74	0.1128	0.0017	1845	18	1845	32	1844	28

Table 7: Zircon Sample Data (2014 Dredge Sample Analytical Run)

Identification		Location		Geochronological Data													
Sample	Sample Reference	Latitude	Longitude	$^{207}Pb/^{235}U$	2σ	$^{206}Pb/^{238}U$	2σ	Error Correlation	$^{207}Pb/^{206}Pb$	2σ	$^{207}Pb/^{235}U$ Age (Ma)	2σ	$^{206}Pb/^{238}U$ Age (Ma)	2σ	$^{207}Pb/^{206}Pb$ Age (Ma)	2σ
	303-1-30			5.138	0.052	0.3302	0.0032	0.75	0.11296	0.00079	1840.7	8.4	1839	15	1846	13
402-1	P402_1_0	53.95	-12.79	16.58	0.15	0.5945	0.0051	0.60	0.202	0.0016	2912.7	9.1	3008	20	2845	13
	P402_1_1			16.21	0.32	0.5677	0.0092	0.90	0.2074	0.0018	2887	20	2896	38	2885	14
	P402_1_2			14.52	0.2	0.5400	0.0063	0.58	0.1939	0.0023	2784	13	2782	26	2779	19
	P402_1_3			14.73	0.33	0.543	0.010	0.87	0.1981	0.0022	2795	21	2795	43	2812	18
	P402_1_4			14.26	0.23	0.5368	0.0066	0.77	0.1932	0.002	2766	15	2769	28	2769	17
	P402_1_5			14.68	0.15	0.5455	0.0054	0.78	0.1948	0.0013	2794.3	9.5	2807	23	2784	11
	P402_1_6			14.81	0.34	0.545	0.014	0.66	0.1968	0.004	2801	22	2801	56	2802	35
	P402_1_7			16.24	0.28	0.5866	0.0086	0.57	0.2004	0.003	2891	16	2975	35	2828	25
	P402_1_8			15.63	0.1	0.5600	0.0039	0.67	0.2013	0.0011	2855.5	6.1	2866	16	2837.9	9.2
	P402_1_9			15.5	0.19	0.5773	0.0064	0.81	0.1935	0.0014	2847	11	2936	26	2773	12
	P402_1_10			15.28	0.2	0.5607	0.0071	0.75	0.1984	0.0018	2831	12	2871	29	2814	15
	P402_1_11			14.4	0.24	0.5396	0.0091	0.88	0.1949	0.0016	2777	16	2779	38	2784	14
	P402_1_12			16.44	0.23	0.5682	0.0069	0.56	0.2113	0.0026	2904	13	2899	28	2913	20
	P402_1_13			14.76	0.19	0.5427	0.0063	0.67	0.199	0.002	2797	12	2789	26	2812	17
	P402_1_14			16.01	0.26	0.5657	0.0081	0.49	0.207	0.0032	2875	16	2888	33	2878	25
	P402_1_15			17.52	0.54	0.663	0.022	0.83	0.1946	0.0037	2961	30	3273	85	2778	32
	P402_1_16			16.32	0.16	0.5678	0.0058	0.78	0.2101	0.0014	2895.6	9.2	2896	24	2905	11
	P402_1_17			15.97	0.32	0.565	0.010	0.76	0.2055	0.0027	2872	19	2886	41	2870	21
	P402_1_18			14.36	0.12	0.5413	0.0048	0.60	0.1948	0.0015	2773.7	8.3	2791	20	2784	12
	P402_1_19			14.24	0.16	0.5401	0.0054	0.70	0.1916	0.0016	2768	11	2782	23	2757	14
	P402_1_20			17.68	0.51	0.656	0.014	0.84	0.1969	0.0031	2969	27	3245	55	2794	26
	P402_1_21			14.64	0.2	0.5074	0.0075	0.71	0.2103	0.0023	2791	13	2644	32	2905	18
	P402_1_22			15.74	0.21	0.5585	0.0068	0.55	0.2068	0.0025	2862	13	2862	28	2881	20
	P402_1_23			16.9	0.37	0.627	0.011	0.90	0.1941	0.0019	2924	21	3135	45	2780	16
	P402_1_24			16.01	0.13	0.5644	0.0044	0.69	0.2079	0.0013	2876.5	7.7	2884	18	2888	10
	P402_1_25			15.77	0.28	0.5774	0.0091	0.91	0.1996	0.0015	2863	17	2937	37	2823	12
	P402_1_26			14.9	0.16	0.5474	0.006	0.72	0.1986	0.0016	2810.8	9.8	2813	25	2814	13
	P402_1_28			16.63	0.12	0.5712	0.0038	0.67	0.2119	0.0012	2912.5	7	2912	16	2918.8	9
	P402_1_29			15.04	0.24	0.5300	0.0077	0.72	0.2072	0.0024	2821	14	2741	32	2883	19
402-2	402-2-1	53.95	-12.79	15.78	0.31	0.575	0.011	0.93	0.2	0.0015	2859	19	2926	44	2825	13
	402-2-2			15.39	0.31	0.569	0.0098	0.88	0.1973	0.0019	2835	19	2901	40	2804	15
	402-2-3			14.72	0.43	0.544	0.015	0.98	0.1964	0.0012	2781	29	2790	63	2796.6	9.9
	402-2-4			14.88	0.2	0.5516	0.0068	0.80	0.1959	0.0016	2806	13	2831	28	2791	13
	402-2-5			14.48	0.27	0.5386	0.0095	0.96	0.1954	0.001	2773	18	2771	40	2786.5	8.4
	402-2-7			14.86	0.19	0.5442	0.0067	0.84	0.1981	0.0014	2804	13	2807	26	2809	12
	402-2-8			14.55	0.31	0.542	0.011	0.96	0.1955	0.0011	2778	20	2784	44	2788.2	9.2
	402-2-9			15.37	0.25	0.5665	0.0097	0.91	0.197	0.0014	2835	16	2890	40	2802	11
	402-2-10			16.1	0.28	0.589	0.01	0.92	0.1989	0.0014	2879	17	2980	41	2816	11
	402-2-11			14.96	0.23	0.5466	0.0077	0.92	0.1986	0.0012	2808	15	2807	32	2813.4	9.6
	402-2-12			15	0.19	0.5454	0.0066	0.86	0.1994	0.0013	2811	12	2803	28	2819	11
	402-2-13			14.71	0.25	0.5436	0.0088	0.94	0.1958	0.0011	2788	17	2792	37	2789.5	9.5
	402-2-14			14.64	0.35	0.542	0.012	0.88	0.1955	0.0022	2790	23	2791	51	2788	18

Table 7: Zircon Sample Data (2014 Dredge Sample Analytical Run)

Identification		Location		Geochronological Data													
Sample	Sample Reference	Latitude	Longitude	$^{207}Pb/^{235}U$	2σ	$^{206}Pb/^{238}U$	2σ	Error Correlation	$^{207}Pb/^{206}Pb$	2σ	$^{207}Pb/^{235}U$ Age (Ma)	2σ	$^{206}Pb/^{238}U$ Age (Ma)	2σ	$^{207}Pb/^{206}Pb$ Age (Ma)	2σ
	402-2-16			16.53	0.29	0.597	0.01	0.91	0.2016	0.0015	2906	16	3013	41	2838	13
	402-2-17			15.38	0.27	0.5722	0.0097	0.86	0.1956	0.0018	2836	18	2914	40	2791	15
	402-2-19			16.2	0.19	0.5904	0.0068	0.82	0.2006	0.0014	2886	11	2989	28	2829	11
	402-2-20			15.72	0.37	0.57	0.014	0.94	0.2023	0.0017	2854	22	2904	56	2844	14
	402-2-21			14.61	0.26	0.5409	0.0088	0.83	0.1974	0.002	2787	16	2785	37	2803	17
	402-2-22			16.22	0.29	0.606	0.01	0.89	0.1974	0.0016	2886	17	3049	42	2803	13
	402-2-23			14.77	0.28	0.547	0.01	0.91	0.1998	0.0016	2797	18	2808	42	2823	13
	402-2-24			16.59	0.19	0.6063	0.0088	0.86	0.2025	0.0015	2909	11	3050	35	2844	12
	402-2-25			14.46	0.34	0.544	0.012	0.97	0.1964	0.0011	2766	24	2788	51	2795.4	9.2
	402-2-26			14.65	0.22	0.546	0.0084	0.80	0.1998	0.0019	2791	15	2807	35	2822	16
	402-2-27			14.83	0.25	0.5549	0.0095	0.71	0.1994	0.0026	2803	17	2843	39	2819	21
	402-2-28			14.85	0.2	0.5457	0.007	0.88	0.2013	0.0013	2805	13	2807	29	2835	10
	402-2-29			15.55	0.4	0.577	0.015	0.93	0.2008	0.002	2845	25	2932	61	2831	16
	402-2-30			15.85	0.45	0.593	0.016	0.96	0.1981	0.0015	2857	28	2992	66	2809	12
402-3	402-3-1	53.95	-12.79	5.853	0.092	0.355	0.0055	0.86	0.12082	0.00099	1950	14	1955	26	1964	15
	402-3-3			6.97	0.11	0.4264	0.0057	0.48	0.1194	0.0018	2107	15	2289	26	1951	25
	402-3-5			6.54	0.16	0.398	0.0083	0.86	0.1205	0.0015	2045	22	2157	39	1959	23
	402-3-6			6.589	0.056	0.4104	0.0034	0.61	0.1176	0.00087	2056.6	7.6	2216	16	1919	13
	402-3-8			6.36	0.11	0.3849	0.0069	0.69	0.1219	0.0017	2024	16	2097	32	1979	25
	402-3-9			6.21	0.12	0.3766	0.0077	0.72	0.1217	0.0018	2003	17	2059	36	1976	27
	402-3-10			5.73	0.18	0.354	0.013	0.92	0.1197	0.0017	1931	28	1949	61	1949	25
	402-3-11			6.52	0.14	0.4012	0.0081	0.82	0.1194	0.0015	2044	19	2178	36	1947	23
	402-3-12			6.771	0.095	0.416	0.0044	0.75	0.1193	0.0011	2078	12	2241	20	1941	17
	402-3-13			6.671	0.089	0.4129	0.006	0.64	0.1184	0.0014	2066	12	2226	27	1926	21
	402-3-14			5.8	0.11	0.3543	0.0067	0.88	0.1201	0.0011	1944	17	1953	32	1956	16
	402-3-17			6.19	0.11	0.3884	0.0063	0.85	0.1162	0.0011	1998	16	2117	29	1898	16
	402-3-18			5.923	0.098	0.3566	0.0065	0.64	0.1212	0.0018	1963	14	1965	31	1970	25
	402-3-19			6.419	0.08	0.3875	0.0044	0.80	0.12048	0.00092	2033	11	2110	21	1960	14
	402-3-20			5.68	0.13	0.3516	0.0099	0.72	0.1164	0.0023	1926	20	1940	47	1896	36
	402-3-21			5.951	0.097	0.3666	0.0061	0.70	0.117	0.0015	1966	14	2012	29	1907	22
	402-3-22			5.7	0.14	0.3487	0.0072	0.57	0.1177	0.0025	1928	21	1933	36	1913	37
	402-3-23			5.7	0.11	0.3488	0.0065	0.68	0.1181	0.0018	1929	16	1927	31	1924	27
	402-3-24			5.82	0.16	0.3506	0.0098	0.83	0.1192	0.0019	1946	24	1936	47	1942	29
	402-3-25			5.82	0.11	0.3583	0.0072	0.69	0.1175	0.0018	1946	17	1972	34	1913	27
	402-3-26			5.72	0.19	0.348	0.01	0.97	0.11813	0.00098	1922	29	1921	48	1928	15
	402-3-27			6.04	0.12	0.3748	0.0080	0.81	0.1169	0.0015	1978	18	2049	38	1905	23
	402-3-28			5.72	0.14	0.3516	0.0075	0.74	0.1182	0.002	1931	21	1941	36	1925	30
	402-3-29			6.12	0.12	0.369	0.0067	0.79	0.1206	0.0015	1990	18	2028	30	1962	22
	402-3-30			5.83	0.12	0.363	0.0077	0.76	0.1167	0.0017	1952	18	2001	39	1901	27
402-9	402-9-1	53.95	-12.79	3.590	0.091	0.2694	0.0087	0.77	0.0976	0.002	1543	21	1534	45	1568	37
	402-9-2			3.983	0.087	0.3078	0.0065	0.64	0.0938	0.0017	1627	18	1728	32	1501	36
	402-9-3			4.005	0.051	0.3110	0.0035	0.74	0.09319	0.00081	1634	10	1744	17	1487	16
	402-9-7			3.662	0.080	0.2751	0.0045	0.64	0.0948	0.0016	1559	17	1565	23	1517	34

Table 7: Zircon Sample Data (2014 Dredge Sample Analytical Run)

Identification		Location		Geochronological Data													
Sample	Sample Reference	Latitude	Longitude	$^{207}Pb/^{235}U$	2σ	$^{206}Pb/^{238}U$	2σ	Error Correlation	$^{207}Pb/^{206}Pb$	2σ	$^{207}Pb/^{235}U$ Age (Ma)	2σ	$^{206}Pb/^{238}U$ Age (Ma)	2σ	$^{207}Pb/^{206}P$ b Age (Ma)	2σ
	402-9-8			3.835	0.087	0.2925	0.0043	0.59	0.093	0.0017	1598	19	1653	21	1476	35
	402-9-9			3.620	0.070	0.2729	0.0039	0.52	0.0941	0.0016	1551	15	1555	20	1503	32
	402-9-10			3.827	0.077	0.2868	0.0037	0.57	0.0962	0.0016	1593	16	1625	19	1546	32
	402-9-12			3.580	0.050	0.2682	0.0028	0.50	0.0953	0.0012	1543	11	1533	14	1532	24
	402-9-13			3.801	0.062	0.2941	0.0043	0.61	0.0943	0.0013	1591	13	1660	21	1504	26
	402-9-14			3.669	0.081	0.2739	0.0049	0.75	0.0954	0.0014	1559	18	1559	25	1526	29
	402-9-15			3.762	0.042	0.291	0.0025	0.43	0.0932	0.001	1583.1	9.1	1646	13	1483	21
	402-9-16			4.053	0.072	0.3067	0.0037	0.49	0.0949	0.0015	1642	14	1724	18	1522	30
	402-9-17			3.971	0.099	0.3068	0.006	0.60	0.0929	0.0019	1625	20	1724	30	1479	40
	402-9-18			4.214	0.054	0.3175	0.0035	0.68	0.09545	0.00093	1673	11	1776	17	1533	18
	402-9-19			3.865	0.076	0.2922	0.0038	0.45	0.0942	0.0017	1602	16	1652	19	1498	35
	402-9-20			3.579	0.069	0.2675	0.0039	0.66	0.0954	0.0014	1542	15	1527	20	1530	28
	402-9-21			3.765	0.077	0.2831	0.0043	0.52	0.0943	0.0017	1582	16	1606	21	1504	34
	402-9-22			3.966	0.051	0.2999	0.0028	0.49	0.0948	0.0011	1624	10	1690	14	1516	21
	402-9-23			3.825	0.056	0.2894	0.0034	0.56	0.0950	0.0012	1593	12	1637	17	1516	24
	402-9-24			3.609	0.086	0.2761	0.0049	0.82	0.0943	0.0013	1544	19	1570	25	1507	24
	402-9-25			3.93	0.049	0.301	0.0029	0.65	0.09437	0.00091	1618	10	1695	14	1509	18
	402-9-26			3.691	0.036	0.283	0.0025	0.68	0.09378	0.0007	1567.4	7.9	1608	12	1501	14
	402-9-28			3.744	0.051	0.2794	0.0033	0.61	0.0968	0.0011	1579	11	1589	17	1555	21
	402-9-30			3.873	0.092	0.2954	0.0059	0.93	0.0942	0.00087	1603	20	1667	30	1511	17
204-1	P204_1_0	54.22	-11.63	2.173	0.052	0.202	0.0046	0.68	0.0802	0.0015	1171	17	1186	25	1199	35
	P204_1_1			2.043	0.039	0.1921	0.0023	0.19	0.0782	0.0016	1130	13	1132	13	1138	40
	P204_1_2			4.11	0.12	0.2953	0.004	0.48	0.1017	0.0026	1650	25	1668	20	1657	49
	P204_1_3			2.512	0.029	0.2222	0.0014	0.53	0.08184	0.0008	1274.2	8.4	1293.2	7.3	1234	19
	P204_1_4			1.74	0.053	0.1698	0.002	0.07	0.0752	0.0024	1015	21	1010	11	1011	67
	P204_1_5			1.747	0.040	0.1715	0.0016	0.19	0.0739	0.0017	1019	15	1020.3	8.6	997	48
	P204_1_6			1.649	0.027	0.166	0.0013	0.22	0.0725	0.0012	987	10	989.8	7.2	990	33
	P204_1_8			3.411	0.043	0.2656	0.0022	0.31	0.0939	0.0012	1505.4	9.8	1518	11	1503	23
	P204_1_9			2.259	0.020	0.2055	0.0011	0.47	0.0794	0.00063	1198.5	6.1	1204.7	5.9	1177	16
	P204_1_10			3.962	0.062	0.2918	0.0027	0.55	0.0993	0.0013	1626	13	1652	14	1609	25
	P204_1_11			3.329	0.057	0.2577	0.0028	0.57	0.0924	0.0013	1487	13	1478	14	1473	27
	P204_1_12			3.217	0.061	0.2464	0.0029	0.39	0.0946	0.0017	1458	15	1420	15	1516	35
	P204_1_13			3.934	0.099	0.2884	0.0046	0.63	0.0975	0.0019	1618	20	1633	23	1572	35
	P204_1_14			2.984	0.043	0.2437	0.0016	0.19	0.0886	0.0013	1401	11	1405.6	8.4	1380	28
	P204_1_15			3.79	0.07	0.2825	0.0034	0.42	0.0984	0.0017	1590	14	1604	17	1586	32
	P204_1_16			3.255	0.064	0.2575	0.003	0.32	0.0928	0.0018	1466	15	1476	15	1468	38
	P204_1_17			3.380	0.055	0.2624	0.0032	0.37	0.0922	0.0015	1499	13	1502	16	1467	32
	P204_1_18			4.271	0.08	0.2998	0.0036	0.48	0.1018	0.0017	1686	16	1690	18	1654	30
	P204_1_19			3.009	0.092	0.2419	0.0035	0.18	0.0894	0.0028	1408	23	1396	18	1407	59
	P204_1_20			1.721	0.032	0.1638	0.0014	0.22	0.0751	0.0014	1014	12	977.8	7.9	1068	39
	P204_1_21			4.081	0.064	0.2902	0.0034	0.36	0.1008	0.0016	1651	13	1642	17	1638	28
	P204_1_22			2.848	0.059	0.2367	0.0032	0.50	0.0882	0.0016	1365	16	1369	16	1375	36
	P204_1_23			2.875	0.079	0.2379	0.0069	0.77	0.0889	0.0017	1379	23	1375	36	1397	38

Table 7: Zircon Sample Data (2014 Dredge Sample Analytical Run)

Identification		Location		Geochronological Data													
Sample	Sample Reference	Latitude	Longitude	$^{207}Pb/^{235}U$	2σ	$^{206}Pb/^{238}U$	2σ	Error Correlation	$^{207}Pb/^{206}Pb$	2σ	$^{207}Pb/^{235}U$ Age (Ma)	2σ	$^{206}Pb/^{238}U$ Age (Ma)	2σ	$^{207}Pb/^{206}Pb$ Age (Ma)	2σ
	P204_1_24			3.507	0.026	0.2738	0.0018	0.63	0.09289	0.00056	1527.7	6	1559.6	9.1	1484	11
	P204_1_25			3.461	0.055	0.2686	0.0021	0.22	0.0934	0.0015	1515	13	1533	11	1484	31
	P204_1_26			1.768	0.031	0.174	0.0012	0.37	0.0735	0.0012	1030	11	1033.7	6.4	1021	35
	P204_1_27			2.924	0.050	0.2404	0.0023	0.01	0.0872	0.0017	1386	13	1388	12	1356	36
	P204_1_29			2.869	0.066	0.2375	0.003	0.45	0.0871	0.0018	1373	18	1373	16	1350	40
	P204_1_30			3.290	0.046	0.2578	0.002	0.26	0.0923	0.0013	1479	11	1478	10	1464	26
	P204_1_31			1.562	0.017	0.1592	0.001	0.31	0.07087	0.00076	953.8	6.8	952.4	5.6	944	22
	P204_1_32			3.46	0.075	0.2671	0.003	0.22	0.0948	0.0021	1514	17	1525	15	1510	43
	P204_1_33			4.057	0.052	0.2935	0.0032	0.59	0.1008	0.0011	1644	11	1658	16	1638	21
	P204_1_34			2.898	0.046	0.2399	0.003	0.74	0.08666	0.00092	1379	12	1385	16	1351	20
	P204_1_35			3.287	0.067	0.2568	0.0028	0.35	0.0926	0.0018	1471	16	1473	14	1461	37
	P204_1_36			4.331	0.045	0.3034	0.0026	0.62	0.10343	0.00087	1698.5	8.4	1707	13	1684	15
	P204_1_37			4.041	0.086	0.2880	0.0042	0.50	0.1011	0.0019	1641	17	1631	21	1641	34
	P204_1_38			3.377	0.054	0.2634	0.0033	0.39	0.0937	0.0015	1497	13	1509	17	1497	30
	P204_1_40			2.719	0.060	0.2276	0.0022	0.23	0.0865	0.0019	1331	17	1322	11	1336	43
	P204_1_41			4.138	0.093	0.2955	0.0045	0.52	0.1028	0.002	1658	19	1668	23	1672	38
	P204_1_42			4.065	0.063	0.2910	0.0022	0.21	0.1015	0.0016	1644	13	1646	11	1645	29
	P204_1_43			4.305	0.090	0.3027	0.0038	0.36	0.1045	0.0021	1691	17	1704	19	1697	36
	P204_1_45			3.971	0.063	0.2892	0.0032	0.66	0.1008	0.0012	1628	13	1640	15	1641	23
	P204_1_46			3.875	0.094	0.2730	0.0032	0.32	0.1031	0.0024	1602	19	1555	16	1663	42
	P204_1_47			1.804	0.072	0.1757	0.0029	0.06	0.0733	0.0031	1043	25	1043	16	1008	84
	P204_1_48			3.949	0.065	0.2842	0.0025	0.44	0.1006	0.0015	1621	13	1612	12	1627	28
	P204_1_49			3.316	0.049	0.2587	0.0019	0.34	0.0925	0.0013	1481	12	1482.6	9.7	1468	26
	P204_1_50			2.871	0.06	0.2370	0.0030	0.51	0.0887	0.0016	1372	16	1371	16	1389	35
	P204_1_51			3.222	0.034	0.2561	0.0020	0.46	0.09149	0.0009	1462.5	7.9	1470	10	1455	19
	P204_1_52			3.932	0.046	0.2849	0.0022	0.52	0.0987	0.001	1619.5	9.6	1616	11	1597	19
	P204_1_53			3.414	0.036	0.264	0.0025	0.75	0.09424	0.00068	1508.3	8	1510	13	1510	13
	P204_1_54			1.681	0.048	0.1679	0.0022	0.42	0.0732	0.0019	998	19	1000	12	988	55
	P204_1_55			1.760	0.043	0.172	0.0016	0.34	0.0739	0.0017	1028	17	1022.7	9	1014	49
	P204_1_56			1.727	0.04	0.1717	0.0018	0.10	0.0735	0.0018	1016	15	1021	10	1016	51
	P204_1_57			3.422	0.078	0.2628	0.0031	0.23	0.095	0.0022	1504	18	1503	16	1506	45
	P204_1_58			4.038	0.094	0.2939	0.0083	0.73	0.1021	0.002	1640	19	1660	42	1659	36
	P204_1_59			3.417	0.057	0.2645	0.0037	0.55	0.0949	0.0014	1507	13	1512	19	1521	27
	P204_1_60			4.031	0.068	0.2915	0.004	0.48	0.1008	0.0016	1640	14	1648	20	1634	30
	P204_1_61			1.670	0.079	0.1662	0.0032	0.33	0.0735	0.0033	988	30	990	18	982	99
	P204_1_62			3.185	0.055	0.2524	0.0035	0.60	0.0911	0.0013	1449	13	1450	18	1441	27
	P204_1_63			3.338	0.057	0.2591	0.0047	0.69	0.093	0.0013	1488	14	1483	24	1481	27
	P204_1_64			3.356	0.061	0.2606	0.0035	0.37	0.0937	0.0017	1490	14	1497	18	1486	36
	P204_1_65			3.942	0.046	0.2845	0.0029	0.50	0.1	0.0011	1620.1	9.5	1613	14	1618	20
	P204_1_66			4.198	0.058	0.2978	0.0037	0.72	0.1018	0.001	1670	11	1680	19	1654	19
	P204_1_67			3.368	0.055	0.2598	0.0041	0.57	0.094	0.0014	1496	13	1487	21	1498	27
	P204_1_68			1.917	0.051	0.1821	0.0031	0.48	0.0756	0.0018	1085	17	1078	17	1066	48
	P204_1_69			2.541	0.050	0.2092	0.0031	0.41	0.0887	0.0017	1282	14	1227	18	1397	36

Table 7: Zircon Sample Data (2014 Dredge Sample Analytical Run)

Identification		Location		Geochronological Data													
Sample	Sample Reference	Latitude	Longitude	$^{207}Pb/^{235}U$	2σ	$^{206}Pb/^{238}U$	2σ	Error Correlation	$^{207}Pb/^{206}Pb$	2σ	$^{207}Pb/^{235}U$ Age (Ma)	2σ	$^{206}Pb/^{238}U$ Age (Ma)	2σ	$^{207}Pb/^{206}Pb$ Age (Ma)	2σ
	P204_1_70			3.06	0.036	0.2404	0.0028	0.57	0.0925	0.0010	1421.8	9.2	1388	14	1476	21
	P204_1_71			3.916	0.075	0.2759	0.0046	0.62	0.1019	0.0016	1613	15	1570	23	1650	30
	P204_1_72			2.849	0.066	0.2351	0.0036	0.42	0.0876	0.0019	1360	17	1361	19	1340	42
	P204_1_73			3.039	0.069	0.2444	0.0036	0.43	0.0902	0.0019	1412	18	1408	19	1411	39
	P204_1_74			3.324	0.072	0.2585	0.0042	0.56	0.0923	0.0017	1482	17	1481	21	1460	36
	P204_1_75			4.079	0.094	0.2946	0.0068	0.77	0.1015	0.0016	1647	18	1663	33	1656	33
	P204_1_76			4.289	0.083	0.3016	0.0056	0.63	0.1041	0.0017	1687	16	1701	27	1693	29
	P204_1_77			3.982	0.058	0.2857	0.0039	0.70	0.0996	0.0011	1629	12	1619	19	1614	20
	P204_1_79			1.727	0.047	0.1713	0.0024	0.27	0.0738	0.002	1016	18	1019	13	1030	53
	P204_1_81			4.122	0.081	0.2948	0.0041	0.36	0.1022	0.002	1656	16	1665	20	1663	37
	P204_1_82			4.244	0.080	0.2991	0.004	0.53	0.1043	0.0017	1679	16	1686	20	1695	29
	P204_1_83			4.049	0.057	0.2886	0.0028	0.47	0.1013	0.0013	1643	11	1634	14	1649	25
	P204_1_84			5.087	0.067	0.3299	0.004	0.58	0.1123	0.0013	1832	11	1837	19	1836	21
	P204_1_85			3.982	0.046	0.2874	0.0023	0.56	0.10000	0.00097	1629.1	9.1	1628	11	1618	18
	P204_1_86			3.765	0.064	0.2697	0.0028	0.42	0.1018	0.0016	1583	14	1539	14	1653	28
	P204_1_87			2.047	0.050	0.1840	0.0019	0.16	0.0802	0.002	1123	17	1089	10	1156	50
	P204_1_88			3.433	0.060	0.2616	0.0030	0.38	0.0949	0.0016	1507	14	1497	15	1516	32
	P204_1_89			14.69	0.19	0.5405	0.0053	0.54	0.1951	0.0022	2792	12	2784	22	2780	19
	P204_1_90			4.198	0.047	0.2973	0.0024	0.41	0.1023	0.0011	1672.6	9.2	1678	12	1663	19
	P204_1_91			3.667	0.044	0.2685	0.0032	0.49	0.0998	0.0012	1562.8	9.6	1533	16	1615	22
	P204_1_92			3.409	0.065	0.2619	0.0034	0.47	0.0927	0.0016	1504	15	1499	17	1484	34
	P204_1_93			4.044	0.066	0.2912	0.0034	0.56	0.1019	0.0014	1641	13	1647	17	1652	26
	P204_1_94			1.774	0.056	0.1741	0.0026	0.29	0.0748	0.0023	1032	21	1035	14	1040	61
	P204_1_95			2.84	0.034	0.2300	0.0017	0.40	0.0887	0.001	1365.9	9.2	1334.1	9	1392	22
	P204_1_96			1.682	0.054	0.1662	0.0028	0.36	0.0722	0.0022	999	20	991	15	974	62
	P204_1_97			3.384	0.072	0.2632	0.0033	0.53	0.094	0.0017	1498	17	1506	17	1500	33
	P204_1_98			4.068	0.049	0.2940	0.0025	0.48	0.1007	0.0011	1646.6	9.9	1661	12	1636	22

Appendix B: Individual U-Pb zircon age probability density diagrams of data used to contrsuct Figure 7 in Chapter 4.

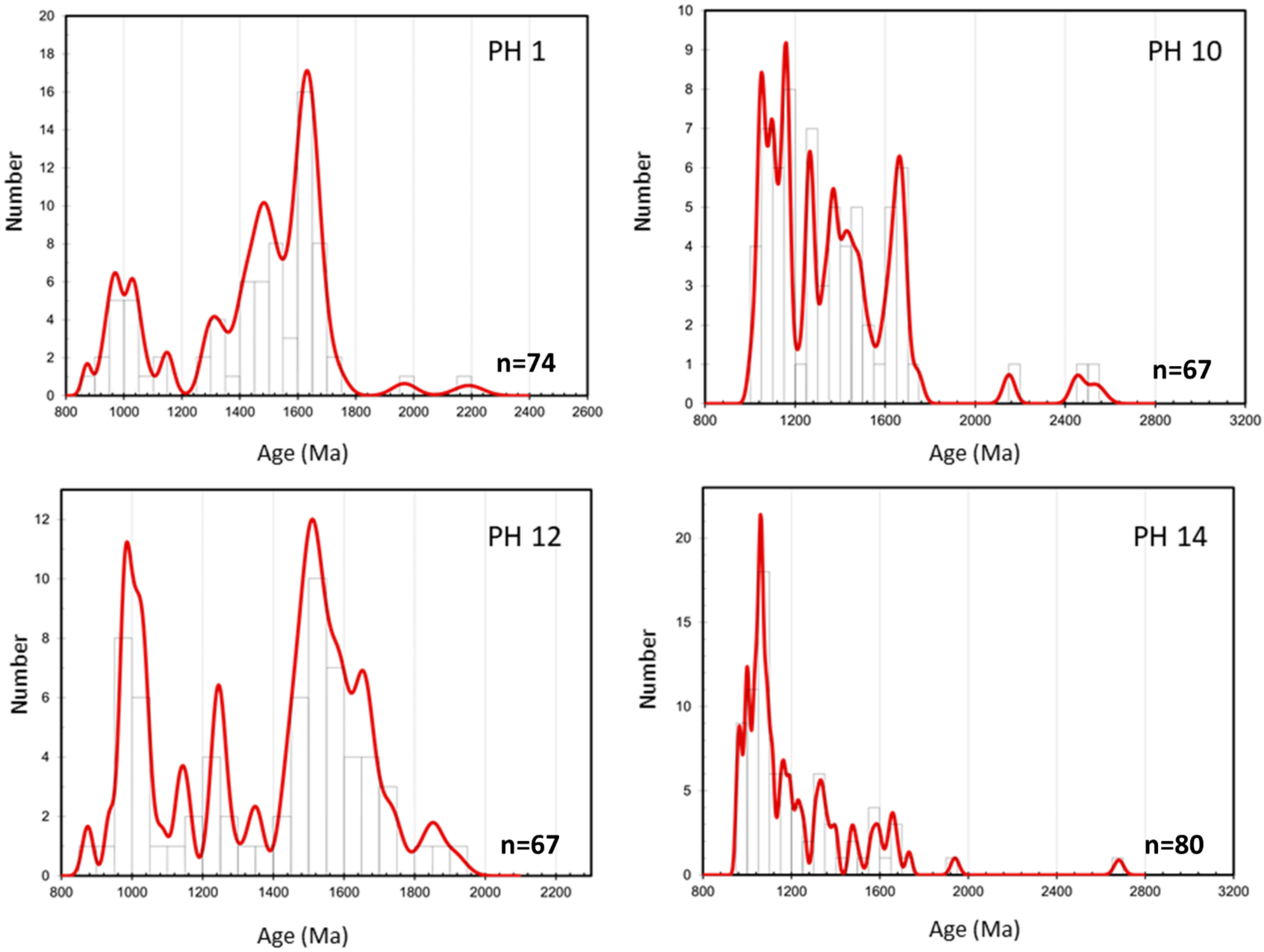

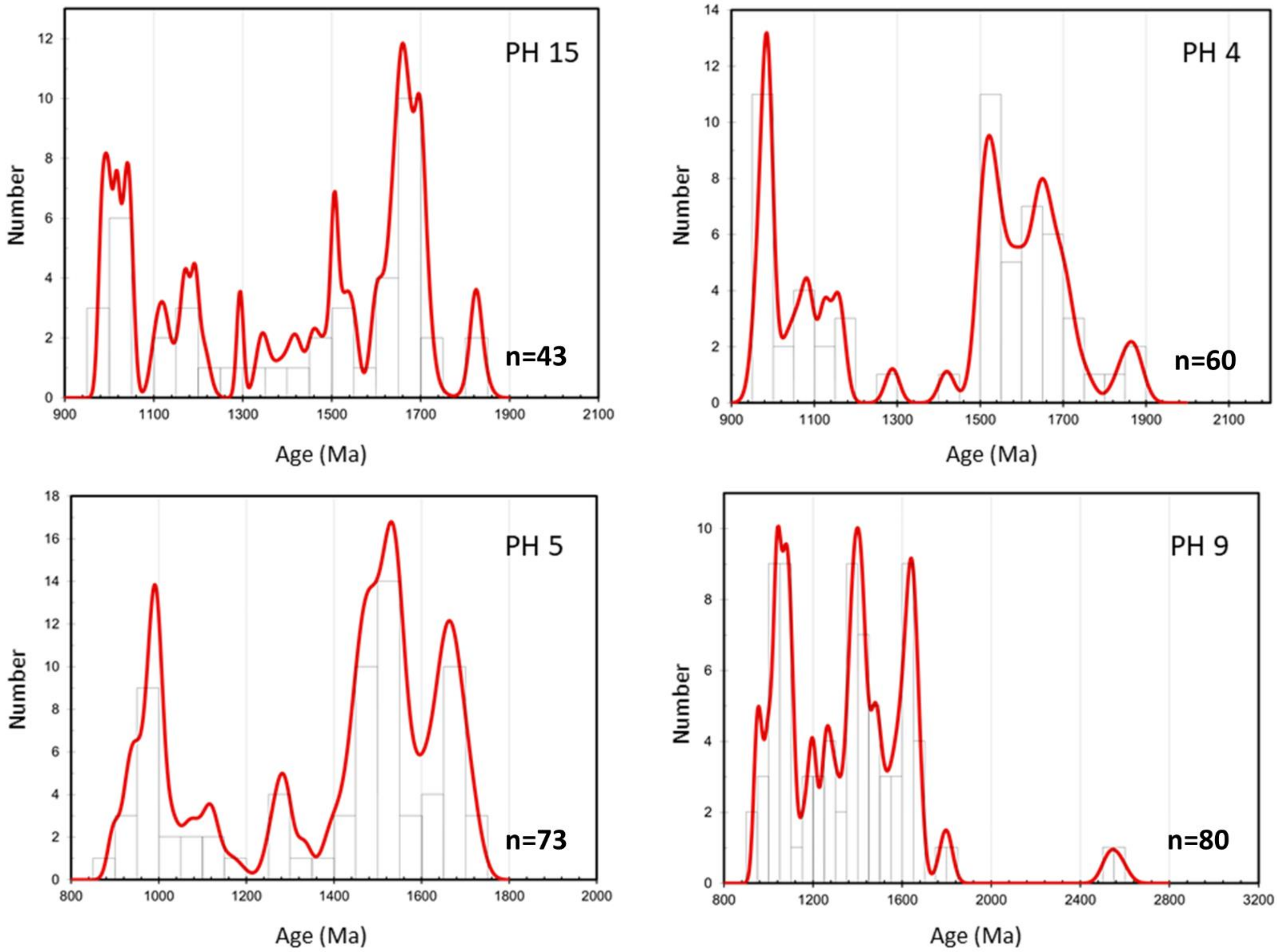
PH 15
n=43
PH 4
n=60
PH 5
n=73
PH 9
n=80
Number
Age (Ma)

Appendix C: Color CL images of the 2011 dredge samples. A and B) Representative zircons of sample 302-1 (psammite) with a U-Pb zircon age spectra of 450 – 3200 Ma, C) Representative zircons of sample 303-1 (amphibolite) with a U-Pb zircon age of 1831.5 ± 6 Ma, D) Representative zircons of sample 402-4 (banded pink gneiss) with a U-Pb zircon age of 1635 ± 11 Ma, E and F) Representative zircons of sample 402-11 (gneiss) with a U-Pb zircon age of 2804.2 ± 6.7 Ma.